SAMPLING MADE SIMPLE:

TOWARDS A FULLY INTEGRATED, LOW-COST AND WEARABLE DIAGNOSTIC TECHNOLOGY

Lorenz VAN HILEGHEM

Supervisors:
Prof. J. Lammertyn
Dr. F. Dal Dosso

Members of the Examination Committee:
Prof. D. De Vos (chair)
Prof. J. Lammertyn (promotor)
Dr. F. Dal Dosso (co-supervisor)
Prof. M. Kraft
Prof. R. Ameloot
Prof. J. Verbakel
Prof. C. Stove
Dr. K. Bloem

Dissertation presented in partial fulfilment of the requirements for the degree of Doctor of Bioscience Engineering.

Doctoraatsproefschrift nr. 1862 aan de faculteit Bio-ingenieurswetenschappen van de KU Leuven

©2023 Lorenz Van Hileghem

Uitgegeven in eigen beheer, Lorenz Van Hileghem, Willebringsestraat 54A, 3370 Boutersem

Alle rechten voorbehouden. Niets uit deze uitgave mag worden vermenigvuldigd en/of openbaar gemaakt worden door middel van druk, fotokopie, microfilm, elektronisch of op welke andere wijze ook zonder voorafgaandelijke schriftelijke toestemming van de uitgever.

All rights reserved. No part of the publication may be reproduced in any form by print, photoprint, microfilm, electronic or any other means without written permission from the publisher.

Preface

Almost 5 years ago, I embarked on a journey that would forever shape me as a person. What a time it has been! Even though it feels like I just started my PhD, writing these words made me realize more than ever that I am close to the end of what has been maybe the most intense period of my entire life. Every day was educational, both on a professional and personal level, filled with little triumphs, but also with many humbling lessons. Luckily, I was never alone during this journey. This preface serves as a heartfelt acknowledgment of all the people that played an important role, in one way or another, during this journey.

First and foremost, I would like to start by thanking my promotor, Jeroen, for granting me the opportunity to embark on this PhD journey within the Biosensors Group. It all started with a master thesis, which served as an ideal introduction to the fascinating and diverse research topics explored within the unique team you have brought together. I also got to know you as a very passionate scientist, engineer, manager, and as a credible person. Despite your continuously demanding schedule, your door was always open, even literally, to provide the right insights and advice whenever it was needed. Thank you!

Secondly, I would like to express my deepest appreciation to Francesco. I was very happy when you accepted, along the course of my PhD journey, to become my co-promotor. Your pioneering research on (i)SIMPLE technology was the fundamental basis of all the work I was able to do and your passion for this project was reflected in all the time you invested in discussing the experiments, answering my many questions and revising my manuscripts. This might be even the first piece of text you did not read before it was published. But, your impact extended far beyond your technical

guidance, as your mentorship played an integral role in shaping my professional growth and development. Thank you!

Next, I would like to thank all my colleagues for always creating such a pleasant working environment. Whether it was during work in the lab or during casual lunch breaks, there was always a reason for laughter. I genuinely believe that the unique combination of joy, work ethics and positive spirit in our group is something truly precious and worth to cherish.

In particular, I want to acknowledge my initial office mates Annelies, Jolien, Jiahuan, Ruben and Dries. It was an absolute delight to share room 04.30 with each of you. After the COVID-19 lockdown, office dynamics became more flexible. Still, some key individuals made work an absolute blast. Wouter, thank you for your punctual reminders about lunch time, which served as little anchors throughout the day. Claudia, thank you for always being such a pleasant company as office neighbour, whether it was sharing jokes or sympathizing my occasional frustrations during the slow writing process. Ruben, thank you for bringing so much joy with your humorous memes and for allowing us to try all your homemade beers (except for the one with the gray cap, truly unforgettable!). Wannes, Henry, Dries and Simao, thank you for making the (i)SIMPLE squad such a remarkable team. Henry and Simao, a special thanks for the delightful after-work drinks and the incredible red velvet cake we savored in Luxembourg. Lastly, I must extend a heartfelt word of appreciation to Dries. We have spent so many long days together in the lab fabricating chips, discussing new microfluidic concepts, sharing both the frustrations as the passion for our research. Collaborating with you was always a pleasure and I have learned a lot from our partnership. Thank you!

Also besides work, there have been many people who steadfastly stood by my side. I am grateful to be surrounded by an incredible circle of genuine friends upon whom I can always rely. The epic meme wars, legendary ‘Bwatweekends’,

fateful encounters with the bottle of Kraken and the awe-inspiring Boar Vessel 600-500 BC Etruscan ceramic – these are just a glimpse into the many joyful moments that served as lovely distractions along the way. 'Dees ist leven!' I also have to thank the incredible musicians of The Pixels, who provided an outlet for me every Wednesday, allowing me to release stress and momentarily forget about work while doing what I love to do, which is playing music together. Thank you!

Natuurlijk wil ik ook graag mijn ouders en mijn broer van harte bedanken. Ik besef dat het voor jullie niet altijd eenvoudig was om mijn doctoraatstraject te volgen en dat het wellicht een wereld was die ver van jullie dagelijkse realiteit stond. Desondanks zijn jullie er telkens in geslaagd om op de juiste momenten de steun en het vertrouwen te bieden die ik nodig had. Ik kon altijd bij jullie terecht om mijn hart te luchten, om rust te vinden, maar ook om samen mijn successen te vieren. Ik ben ontzettend dankbaar voor de geborgenheid en steun die jullie mij bieden als thuisbasis. Bedankt!

I would like to dedicate my final words to the most important person in my life, my fiancé, my love and my dearest friend, Tine. Over the course of the past six years, we have traversed numerous experiences together, both the beautiful moments and the challenges that life brought to us. A significant portion of this shared journey was during my PhD, and I really can say we tackled it together. Whether you had to patiently listen to the stories I brought home from work, whether you had to cheer me up if things did not go as planned, or whether you had to wait for that elusive period I promised you things would be calmer (which, I confess, you are still waiting for). You have always been there, supporting me unconditionally in every aspect of my life. I really look forward to all the beautiful things life yet has to unveil for us!

Lorenz

Abstract

Globally, millions of blood samples are collected daily for diagnostic purposes. In current medical practice, venous blood is obtained using an invasive hypodermic needle. This procedure is, besides evoking needle phobia, time-consuming for both patient and medical personnel as it requires a visit to the doctor's office or clinic. This is inconvenient for e.g. chronically ill patients that require frequent blood draws for (tele)monitoring their disease and treatment statuses. Next, once venous blood is extracted from a patient, it is stabilized and transferred to a highly-equipped and well-automated analytical lab. This centralized approach requires resources and a proper logistic network, which is especially critical in low- to middle-income countries due to the lack of trained personnel, financial resources and infrastructure. In these remote settings, the risk of infection for both the patient and healthcare workers is significantly higher through needle re-use and needle-stick injuries. In fact, according to the World Health Organization, in the developing world, up to 50% of needle use is regarded as unsafe. Furthermore, people living in rural areas must travel long distances and too often, a proper follow-up is not guaranteed.

These challenges highlight the need for a worldwide decentralization of the healthcare system toward the point-of-care (POC). To achieve this, a crucial aspect is empowering patients to self-collect blood samples and send them to the central laboratory by regular distribution services. In this context, dried blood spot (DBS) sampling is gaining clinical acceptance. However, the preparation of DBS from capillary blood suffers from sample heterogeneity, which is primarily due to manual handling errors and highly varying blood hematocrit levels.

The global aim of this thesis was to exploit and further develop microfluidic solutions to allow the self-powered collection, processing and storage of capillary blood upon a

single finger-activation. This was done in two main parts. In the first part of this dissertation, a passive, low-cost and user-friendly microfluidic sampling device was developed for the collection of high-quality DBS. Hereto, innovative hydrophobic burst valves with configurable burst pressures were exploited to enable parallel metering of predefined blood volumes starting from an unknown sample volume. To bring this concept at the POC in a portable and autonomous device, the metering system was integrated with our established self-powered microfluidic pump by liquid encapsulation (SIMPLE) and pre-cut DBS papers. Initially, a device to collect a single metered DBS was validated in the context of therapeutic drug monitoring of biological drugs using venous blood samples spiked with adalimumab. Subsequently, the microfluidic solution to enable parallel DBS loading was introduced as a split-pump SIMPLE system and a user-friendly interface was developed to make the device also field-ready. The functionality was again validated for adalimumab.

The second part of the thesis focused on improving the collection of capillary blood. On the one hand, a new finger-pricking procedure was proposed to increase the obtained volumes to comply with the broadly varying requirements of POC devices. On the other hand, as finger-pricking is still relatively invasive, especially for chronic patients and others that frequently sample, this work looked into hollow microneedle arrays (HMNA) to replace the lancets on the longer term. Hereto, we developed and characterized a novel two-step fabrication protocol for stainless steel HMNAs. The obtained HMNAs were then integrated in a self-powered microfluidic sampling patch, driven by SIMPLE. Finally, injection molding was considered for polymer HMNA microfabrication technique to improve the production scalability.

We believe that combining the different elements developed in this work is a starting point into the direction of more sophisticated all-in-one blood sampling and POC testing systems that, on the one hand, can work passively with a

single activation and, on the other hand, integrates well in today’s healthcare workflow.

Samenvatting

Wereldwijd worden dagelijks miljoenen bloedstalen verzameld voor diagnostische doeleinden. In de huidige medische praktijk wordt veneus bloed verkregen door middel van een invasieve injectienaald. Deze methode is niet alleen een mogelijke trigger voor naaldenfobie, maar is ook tijdrovend voor zowel de patiënt als het medisch personeel aangezien een bezoek aan een dokterspraktijk of ziekenhuis hiervoor nodig is. Dit is moeilijk voor bijvoorbeeld chronisch zieken die op regelmatige basis bloedstalen nodig hebben om de progressie van hun ziekte en behandeling nauwlettend op te volgen. Nadat het bloed afgenomen werd van de patiënt wordt het gestabiliseerd en overgebracht naar een goed uitgerust en geautomatiseerd analytisch laboratorium. Dit alles vereist heel wat werkmiddelen en een degelijk logistiek netwerk, wat niet vanzelfsprekend is in landen met een laag inkomen door het gebrek aan opgeleid personeel, financiële middelen en infrastructuur. In dit soort omstandigheden is het risico op infecties bij zowel de patiënt als het medisch personeel beduidend hoger, bijvoorbeeld door het hergebruiken van naalden of door prikaccidenten. Volgens de Wereldgezondheidsorganisatie is zelfs tot 50% van het naaldengebruik in ontwikkelingslanden onveilig. Daarenboven dienen patiënten die in afgelegen gebieden wonen vaak lange afstanden te overbruggen waardoor een degelijke opvolging niet gegarandeerd kan worden.

Deze uitdagingen benadrukken de wereldwijde nood aan een decentralisatie van het gezondheidssysteem richting de zogenaamde point-of-care (POC). Om dit te kunnen bewerkstelligen, is het belangrijk dat patiënten bij zichzelf betrouwbare bloedstalen kunnen afnemen en deze kunnen opsturen naar een centraal laboratorium via reguliere distributiediensten zoals de post. In die context worden gedroogde bloedvlekken (GBV) klinisch gezien steeds relevanter. De kwaliteit van die GBV uit capillair bloed kan echter sterk verschillen door de heterogeniteit van de stalen,

wat voornamelijk te wijten is aan menselijke fouten bij de verwerking en sterk variërende hematocrietwaarden van het bloed.

Het algemene doel van deze thesis was om met behulp van microfluïdica een oplossing te vinden waarmee de patiënt in staat is om capillaire bloedstalen bij zichzelf af te nemen. Dit werd gedaan in twee grote delen. In het eerste deel van de thesis werd een passief, goedkoop en gebruiksvriendelijk microfluïdisch hulpmiddel ontwikkeld om kwalitatieve GBV te verzamelen. Hiervoor werden innovatieve hydrofobe barstkleppen ontwikkeld om precieze volumes capillair bloed te verzamelen vanaf een compleet ongekend staalvolume. Om dit een draagbaar en autonoom werkend concept voor de POC te maken, werd het geïntegreerd met de zogenaamde 'self-powered microfluidic pump by liquid encapsulation' (SIMPLE) die werd ontwikkeld in onze onderzoeksgroep. Eerst en vooral werd een hulpmiddel dat een voorgesneden GBV verzamelt, gevalideerd voor het opvolgen van biologische geneesmiddelen door middel van veneus bloed met een gekende hoeveelheid adalimumab. Vervolgens werd een microfluïdische oplossing om parallel meerdere GBV te verzamelen voorgesteld door middel van een gesplitste-pomp systeem en een gebruiksvriendelijke interface om het hulpmiddel klaar te maken voor meer realistische scenario's. De functionaliteit hiervan werd opnieuw voor adalimumab gevalideerd.

Het tweede deel van de thesis focuste voornamelijk op het verbeteren van die capillaire bloedafname. Zo werd er enerzijds een nieuwe vingerprikprocedure voorgesteld om het verkregen bloedvolume te verhogen zodat deze techniek voor meerdere toepassingen kan ingezet worden. Anderzijds werd ook gewerkt aan het minder invasief maken van staalname voor chronisch zieken of andere patiënten die regelmatig een bloedstaal afnemen. Hiervoor werd gekeken naar holle micronaalden die mogelijks de vingerprikkers in de toekomst zouden kunnen vervangen. Een vernieuwende methode bestaande uit twee stappen werd ontwikkeld om holle

micronaalden uit roestvrij staal te fabriceren. Deze micronaalden werden geïntegreerd in een autonoom microfluïdisch hulpmiddel voor staalname. Als laatste werd ook gekeken naar het spuitgieten van polymeren voor de productie van zulke micronaalden om zo naar een meer opschaalbare techniek te kunnen toewerken.

We zijn ervan overtuigd dat de verschillende elementen aangereikt in deze thesis een startpunt kunnen zijn naar alles-in-een staalname en POC-test hulpmiddelen die volledig autonoom werken en vlot geïntegreerd kunnen worden in de huidige medische praktijk.

List of abbreviations

ADM	Adalimumab
AR	Aspect ratio
ASSURED	Affordable, sensitive, specific, user-friendly, robust, equipment-free and deliverable
BF	Brightfield
CA	(water) contact angle
CNC	Computer numerical control
CV	Coefficient of variation
DBS	Dried blood spot
dc HBV	Double-coated hydrophobic burst valve
DPS	Dried plasma spot
EDM	Electrical discharge machining
ELISA	Enzyme-linked immunosorbent assay
GLM	Generalized linear model
HB	Hydrophobic barrier
HBV	Hydrophobic burst valve
Hct	Haematocrit
HIV	Human immunodeficiency virus
HMN	Hollow microneedle

HMNA	Hollow microneedles array
HRP	Horseradish peroxidase
HSV	Hydrophobic stop valve
iSIMPLE	Infusion self-powered imbibing microfluidic pump by liquid encapsulation
IVD	*In vitro* diagnostics
LFA	Lateral flow assay
LOC	Lab-on-a-chip
MN	Microneedle
MW	Molecular weight
NAAT	Nucleic acid amplification test
PBS	Phosphate buffer saline
PDMS	Polydimethyl siloxane
PEGDA	Polyethylene glycol diacrylate
PMMA	Polymethyl metacrylate
POC	Point-of-care
POCS	Point-of-care sampling
POCT	Point-of-care testing
PSA	Pressure-sensitive adhesive
PVC	Polyvinyl chloride
RBC	Red blood cell
RCF	Relative centrifugal force

REASSURED	Real-time connected, easy sample collection, affordable, sensitive, specific, user-friendly, robust, equipment-free, and environment-friendly and deliverable
sc HBV	Single-coated hydrophobic burst valve
SIMPLE	Self-powered imbibing microfluidic pump by liquid encapsulation
TDM	Therapeutic drug monitoring
UV	Ultraviolet
VAMS	Volumetric absorptive micro samplers
VPAD	Volumetric paper absorptive disc
v/v	Volume/volume
WHO	World health organization
w/v	Weight/volume
µCT	X-ray micro-computed tomography

List of symbols

A	m^2	Cross-sectional area
C	/	Circularity
D	m	Diameter
ED	m	Equivalent diameter
g	$m \cdot s^{-2}$	Gravitational acceleration
h	m	Channel height
L	m	Length
P	m	Perimeter
P	Pa	Pressure
P_{atm}	Pa	Atmospheric pressure
P_c	Pa	Capillary pressure
P_{fin}	Pa	Final pressure
P_{in}	Pa	Initial pressure
Q	$m^3 \cdot s^{-1}$	Volumetric flow rate
t	s	Time
V	m^3	Volume
V_{fin}	m^3	Final volume
V_{in}	m^3	Initial volume
w	m	Channel width
γ	$N \cdot m^{-1}$	Surface tension
ΔP	Pa	Pressure gradient/drop
ΔP_b	Pa	Burst pressure
θ	°	Contact angle
θt	°	Top contact angle
θb	°	Bottom contact angle
θl	°	Left contact angle

θr	°	Right contact angle
μ	Pa·s	Dynamic viscosity
τ	ms	Laser pulse duration

Table of contents

Preface *I*
Abstract *V*
Samenvatting *IX*
List of abbreviations *XIII*
List of symbols *XVII*

Chapter 1 General introduction **1**
1.1 The healthcare system today 2
1.2 The need for decentralization 3
1.2.1 Two complementary decentralization approaches 3
1.2.2 Decentralization of therapeutic drug monitoring 4
1.3 Key elements towards decentralization 5
1.3.1 Minimally invasive body fluid collection 6
1.3.1.1 Overview of easy-to-sample body fluids *7*
1.3.1.2 Capillary blood microsampling *8*
1.3.1.3 Microneedle-based microsampling *9*
1.3.2 Self-powered solutions without manual handling 10
1.3.2.1 Microfluidics for automating fluid handling *10*
1.3.2.2 Capillary-driven passive microfluidics *11*
1.4 Objectives and outline of the thesis 14
1.5 References 17

Chapter 2: State-of-the-art methods in capillary blood sampling **21**
2.1 Remote capillary blood collection 22
2.1.1 DBS sampling: essential but challenging 22
2.1.2 Microfluidic solutions for DBS collection 25
2.1.3 Alternatives for dealing with Hct variability in DBS 31
2.1.4 Liquid capillary blood storage 34
2.1.5 Precise capillary blood collection for POCT 35
2.2 Microneedles for microsampling 37
2.2.1 Different types of microneedles 38
2.2.2 Microneedle-based sample collection 39
2.2.3 Towards sample in – result out systems 42
2.3 References 44

Chapter 3 Precise sample metering method by coordinated burst action of hydrophobic burst valves applied to dried blood spot collection **49**
3.1 Introduction 50
3.2 Materials and methods 52
3.2.1 Reagents and materials 52
3.2.2 Microfluidic device fabrication 52
3.2.3 HBV fabrication 53
3.2.4 HBV characterization 54
3.2.5 Sample metering system characterization 56
3.2.6 Validation of the SIMPLE-DBS sampling device 57
3.3 Results and discussion 58
3.3.1 HBV characterization 58
3.3.2 Sample metering system 60
3.3.3 Parallel sample metering on SIMPLE 64
3.3.4 Integrated volumetric SIMPLE-DBS sampling device 66
3.3.5 Device validation with adalimumab-spiked blood samples 68
3.4 Conclusions 70
3.5 Supporting information 72
3.5.1 Burst pressure calculation and experimental setup 72
3.5.2 Gravimetric methodology for the volumetric performance characterizations 73
3.5.3 Characterization of the burst pressures for different HBV types 75
3.5.4 Influence of microchannel dimensions on HBV burst pressure 76
3.5.5 Volumetric characterization of the metering system by a gravimetric method 80
3.5.6 Multilayer configuration of SIMPLE-DBS sampling device, DBS loading, drying and removal 81
3.5.7 ELISA measurements on extracted DBS samples 82
3.6 References 82

Chapter 4 Multiple dried blood spot sampling device for therapeutic drug monitoring of biologicals **87**
4.1. Introduction 88
4.2. Materials and methods 90
4.2.1 Reagents and material 90
4.2.2 Hydrophilic PVC treatment 91
4.2.3 Fabrication and testing of the sample inlet system 91

4.2.4 Finger-prick blood sample acquisition 92
4.2.5 Fabrication and testing of SIMPLE-DBS cartridges 93
4.2.6 Preparation of spiked blood samples 95
4.2.7 Loading, extraction and analysis of DBS samples 95
4.3. Results and discussion 97
4.3.1 User-friendly sample inlet system 97
4.3.2 SIMPLE-DBS cartridge working principle 100
4.3.3 Analytical performance of the SIMPLE-DBS sampling device 102
4.3.3.1. Validation for different ADM concentrations 102
4.3.3.2. Validation for different haematocrit levels 104
4.4. Conclusion 106
4.5. Supporting information 107
4.5.1. Overview of the DBS sample types for *in vitro* validations 107
4.5.2. Influence of DBS drying time 107
4.5.3. Device failure upon addition of insufficient or excess sample volume 108
4.5.4. Characterization of hydrophilic coating strategies 110
4.5.5. Volumetric inlet independency from Hct level 112
4.5.6. Device engineering and design choices 112
4.5.7. Influence of the hydrophilic coating of the inlet 114
4.6. References 115

Chapter 5 An improved finger-prick procedure for capillary blood self-sampling 119
5.1. Introduction 120
5.2. Materials and methods 121
5.2.1. Reagents and materials 121
5.2.2. Metering tool fabrication and characterization 122
5.2.3. Finger-prick procedure 123
5.2.4. Study design with participants 125
5.3. Results and discussion 126
5.3.1. Characterization of an accurate volume metering tool 126
5.3.2. Validation of the obtained sample volume by the finger-tourniquet procedure 129
5.4. Conclusion 132
5.5. References 133

Chapter 6 Innovative fabrication of hollow microneedle arrays enabling blood sampling with a self-powered microfluidic patch **137**
6.1. Introduction 138
6.2. Materials and methods 140
6.2.1 Reagents and materials 140
6.2.2 Hollow microneedle fabrication process 141
6.2.3 Microscopic and tomographic inspections 143
6.2.4 Microfluidic chip fabrication 144
6.2.5 Flow characterization of the HMNAs 145
6.2.6 SIMPLE pressure generation 145
6.2.7 Validation of a self-powered biofluid sampling patch with in vitro models 147
6.3. Results and discussion 147
6.3.1 HMNA fabrication 147
6.3.2 Flow characterization of the HMNAs 151
6.3.3 Characterization of SIMPLE pressure generation 153
6.3.4 Validation of self-powered microsampling patch with *in vitro* models 154
6.4. Conclusions 156
6.5. Supporting information 157
6.5.1 Micro-milling tool list 157
6.5.2 Flow characterization of the HMNAs 157
6.5.3 SIMPLE pressure generation measurement 159
6.5.4 Laser drilling settings characterization 161
6.5.5 Assessment of the HMNA sharpness 162
6.5.6 Flow characterization of the fabricated HMNAs 163
6.5.7 Machining artefacts 164
6.5.8 Optimization of SIMPLE fabrication 165
6.5.9 Proof-of-concept sampling patch: flow rates 166
6.6. References 168

Chapter 7 Producing hollow polymer microneedles using laser ablated molds in an injection molding process **173**
7.1 Introduction 174
7.2 Materials and methods 178
7.2.1 Reagents and materials 178
7.2.2 Representation of the process chain 178
7.2.3 Laser machining 179
7.2.4 Polymer injection molding 181
7.2.5 Micro drilling 182
7.2.6 Topography characterization 182

7.2.7 Preparation of a skin-mimicking substrate 183
7.2.8 Validation of single-needle injections 183
7.3 Results and discussion 185
7.3.1 Laser ablation 185
7.3.2 Replication through injection molding 187
7.3.3 Validation on skin-mimicking substrate 192
7.4. Conclusion 193
7.5. References 194

Chapter 8 Conclusions and future perspectives 197
8.1 Conclusions 198
8.2 Future perspectives 201
8.2.1 Further development of the microfluidics 202
8.2.1.1 Integration of multiple microfluidic modules 202
8.2.1.2 Plasma separation 203
8.2.1.3 Sample stabilization 204
8.2.1.4 Towards sample-in-result-out systems 205
8.2.1.5 External liquid storage 205
8.2.1.6 Alternative body fluids 206
8.2.2 From laboratory to field validation 207
8.2.2.1 In-field validation of the SIMPLE-DBS device 207
8.2.2.2 Evaluation of the tourniquet finger-prick procedure 207
8.2.2.3 Microneedle-based capillary blood sampling 209
8.2.3 Regulatory aspects toward the industry 209
8.3 References 211

Publication list 213

Chapter 1

General introduction

1.1. The healthcare system today

Since time immemorial, blood drawing is one of the most common medicinal activities, with the earliest documents even going back to ca. 1550 BC[1]. Since then, for a very long time, bloodletting had the therapeutic aim to remove 'bad humours'[1,2]. However, from the late 1800s onwards, it became clear that blood is a treasure throve of information that can be used for monitoring human health. As a consequence, millions of blood samples are daily collected worldwide for clinical testing. In the current medical practice, venous blood is drawn by trained phlebotomists with a hypodermic needle and transported by cooled transport to an analytical laboratory where an *in vitro* diagnostic (IVD) test is performed. This centralized diagnostic workflow is also depicted in **Figure 1.1**.

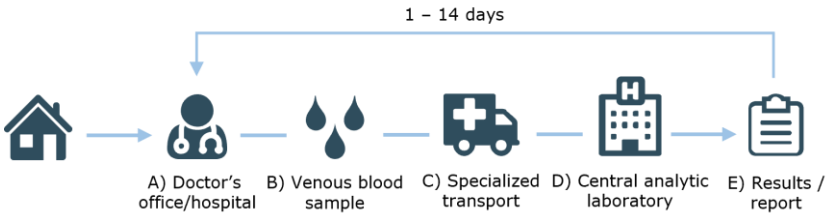

Figure 1.1: *Simplified representation of the centralized IVD workflow. A) Patient visits doctor's office or hospital. B) Invasive venous blood draw is performed. C) Rapid transportation to the analytic laboratory. This requires an efficient logistic system to avoid deterioration. D) Time-consuming and infrastructure-intensive diagnostic assays carried out. E) Results communicated to attending doctor for further follow-up. This often results in an extra patient appointment.*

However, the procedure of venous blood draw, called venipuncture, is time-consuming for both healthcare workers and patients as it requires a visit to the doctor's office or clinic[3]. This is problematic in today's context where a worldwide shortage of healthcare workers is expected in countries of all socioeconomic levels[4]. Moreover, it is often not taken into account that venipuncture evokes needle phobia in approximately 10% of the population, eventually leading to avoidance of medical settings[5,6]. Furthermore, blood is

typically collected in volumes of several milliliters but the majority of it is wasted since modern clinical IVD systems require only microliter volumes for analysis[7].

So far, most challenges of this demanding centralized workflow can be overcome in high-income countries that have access to expensive fully- or semi-automated devices, highly-trained personnel and a robust healthcare and social security system. For the majority of the world population, however, still too many people do not have access to proper healthcare due to the lack of financial and infrastructural resources[8–10]. In the developing world, up to 50% of the needle use is regarded as unsafe with serious risks of infection, both to the patient and healthcare workers through needle re-use and needle-stick injuries[11,12]. Furthermore, people often simply live too far away from the already low-abundant medical settings due to which their test results do not get followed-up.

1.2. The need for decentralization

1.2.1 Two complementary decentralization approaches

To relieve the burden of the medical staff and to offer more comfort to the patient while reducing the overall healthcare costs, decentralized approaches are seen as possible solutions[13,14]. Two possible approaches can bring diagnostics closer to the point-of-care (POC), i.e. at the time and location (e.g. patient's homes, schools, community centers) of need[15]. The first approach, POC sampling (POCS), consists in empowering patients to take their own sample and send it directly to the centralized lab without the intervention of a healthcare worker (**Figure 1.2A**). The second approach, POC testing (POCT), aims to bring the complete IVD test to the POC (**Figure 1.2B**).

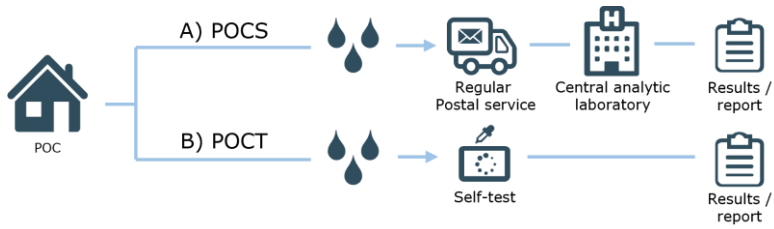

Figure 1.2: *Simplified representation of decentralized diagnostic workflows by A) bringing the sample collection to the POC or B) bringing also the IVD test to the POC.*

POCT is beneficial in situations where rapid answers are required (e.g. blood type check before transfusion), discretion is desired (e.g. pregnancy tests or syphilis tests) or isolation of the patient improves confining of contagious infectious diseases (e.g. SARS-CoV-2 rapid antigen tests). However, POCT often comes with qualitative to semi-quantitative results, which might not be sufficient in some cases. Also, if rapid answers are not key, the POCS approach can be seen as a hybrid between decentralized sample collection while the IVD tests are still centralized. This is beneficial since analytic laboratories offer a great advantage in terms of sensitivity, accuracy and throughput. For this reason, the hybrid POCS approach with central testing can be seen as the more economic model by exploiting the economies of scale[3]. Depending on the application, either one or the other approach will be profitable, making them complementary to each other.

1.2.2 Decentralization of therapeutic drug monitoring

An application that would especially benefit from POCS is therapeutic drug monitoring (TDM)[16]. As nowadays, drugs are mostly administered in a one-size-fits-all approach, the variable pharmacokinetic responses by different patients lead to sub- or supra-therapeutic drug concentrations in the blood, either leading to reduced clinical effects or even toxic concentrations, respectively (**Figure 1.3A**). A specific class suffering from such a response variability is biological drugs. Although they are expected to dominate the market in the future, their complex manufacturing processes and the

governmental policies render them more expensive than chemicals. Furthermore, they can trigger immune reactions of the body leading to a reduction or complete loss of the clinical effect. To avoid ineffective but costly treatments, the goal of TDM is to adjust the administered dose according to frequent blood concentration checks (**Figure 1.3B**). This practice could lead to a reduction in clinical costs by 50%[17]. Despite its potential to improve the clinical outcome for the patient on the long-term, TDM is also highly demanding as a result of the frequently required hospital visits. For this reason, remote self-sampling of blood is not only more convenient for the patient as it reduces the number of hospital visits, but also offers an increased access to longitudinal patient data.

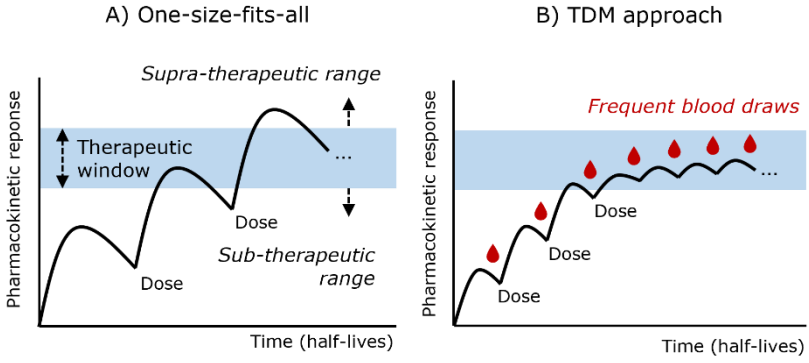

Figure 1.3: *Theoretical pharmacokinetic response curves during start-up of a treatment with biological drugs by A) a one-size-fits-all approach whereby administered dosage is constant in time, and by B) the proactive TDM approach in which the dosage is varied over time according to the predicted pharmacokinetic response of the patient.*

1.3. Key elements towards decentralization

Remote self-sampling has to be safe and easy to perform by untrained persons. To guide the development of such POC solutions, the World Health Organization published in 2003 the ASSURED criteria, an acronym referring to the requirements that the devices have to be affordable, sensitive, specific, user-friendly, rapid and robust, equipment-free and deliverable to the end-user[8,18]. More recently, these guidelines

were extended by real-time connectivity and ease of specimen collection, leading to the new acronym REASSURED[19]. Although introduced specifically in the context of POCT, most of the guidelines are applicable to POCS as well. Overall, the solutions need to be minimally invasive and fully-integrated, two key features which are further introduced in the following sections.

1.3.1 Minimally invasive body fluid collection

As already made clear, blood is the standard collected body fluid for clinical investigation. It is a highly complex mixture of many different components (**Figure 1.4**)[20,21].

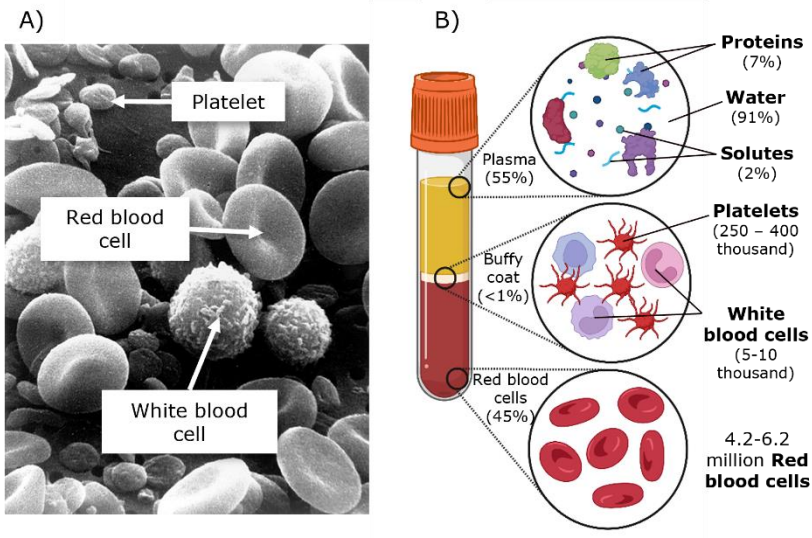

Figure 1.4: *A) Image obtained by scanning electron microscopy showing the different components contained in circulating blood. [Image adapted from ©National Cancer Institute] B) Summary of the average composition of human blood, including plasma, red and white blood cells, and platelets (not drawn on scale). Inside the plasma fraction, many components like proteins, ions, nutrients and gasses are dissolved [Image created with Biorender.com].*

Still, many of these components also end up in other body fluids through the circulatory system. Cerebrospinal fluid, for instance, is relevant to measure infections like meningitis or encephalitis, however, sampling is even more invasive and requires specifically trained doctors. For remote POCS,

alternative body fluids like urine, saliva, sweat or tears are more interesting and easy to self-sample by the patient.

1.3.1.1 Overview of easy-to-sample body fluids

Urine can easily be sampled by dipsticks or collection tubes, e.g. Colli-Pee® (Novosanis, **Figure 1.5A**), and is traditionally used for pregnancy tests or anti-doping controls[22]. For the latter, urine is, however, more and more being replaced by saliva as this is more difficult to adulterate[23]. Saliva can be obtained by spitting, passive drooling (**Figure 1.5B**) or oral swabs, making it also interesting for other applications including the detection/monitoring of infectious, systemic and metabolic diseases[24]. Next, sweat is regularly sampled for sports monitoring (e.g. electrolytes and metabolites) as it is excessively excreted in this context (**Figure 1.5C**). However, efforts have been made to also sample sweat without exercising, with applications in e.g. stress monitoring (e.g. cortisol) or the detection of cystic fibrosis[25–27]. Furthermore, interstitial fluid (ISF) from the skin tissue can be obtained with a needle from suction blisters (**Figure 1.5D**) induced by applying a vacuum[28]. ISF is an interesting derivative of blood plasma that also contains unique biomarkers. To replace the cumbersome blister collection method, mainly microneedles (see further) are under investigation[29].



Figure 1.5: *Overview of the different easy-to-sample body fluids. [Images adopted with permission from[33,34], other copyrights belong to ©Novosanis[35], ©Salimetrics[36], ©PharmChek[37]]*

Nowadays, tears are also becoming an accepted body fluid for minimally invasive sampling by sponges or so-called Schirmer strips (**Figure 1.5E**)[30]. Due to its functions of lubricating, cleaning and immunizing the eyes, it is a highly

stable sample type. Glucose was for long the only targeted analyte from tear fluid, but recently, the focus is shifting towards measuring hormones (e.g. cortisol) and proteins (e.g. TNF-α)[31,32].

Although easy to sample with non-invasive methods, the discussed body fluids still have complex biochemical and physical fluid properties, unknown analyte stability and low or highly variable concentrations[38]. This requires application-specific research before they can really impact the medical world. To replace the gold standard (i.e. venous blood) capillary blood is being looked at as primary alternative as (1) it is accessible from the skin's superficial layers, (2) it has a rich proteome, genome and metabolome, thereby offering a possibility to detect disease-specific analytes as early as possible even with low-abundant proteins and nucleic acids, and (3) major steps have been already taken in the high-quality capillary blood collection at the POC.

1.3.1.2 Capillary blood microsampling

Capillary blood can easily be reached by a finger- or heel-prick using a lancet[39]. This way, multiple capillaries in the dermal layer of the finger-tip skin, which has a density of 14-30 capillary loops per mm^2, are ruptured, subsequently releasing the blood (**Figure 1.6A-B**)[40]. Guthrie and Susi described this procedure for the first time to sample minute volumes of capillary blood by puncturing the heel of newborns, drying the collected blood on a filter paper, resuspending and analyzing the retrieved samples. This method is nowadays known as dried blood spot (DBS) sampling, which was first performed in the context of newborn screening for the early detection of phenylketonuria, an inherited genetic disorder. In the meantime, the so-called Guthrie test (**Figure 1.6B**) is standardly performed after birth to screen for a multitude of disorders. However, nowadays, finger-pricking is gaining interest for other applications requiring regular blood checks, like TDM, pharmacokinetic studies, or population health screening[41–43]. Furthermore, it offers a solution to the current

issue of needle reuse and lack of medical trained personnel in the developing world (e.g., for HIV viral load monitoring)[44,45].

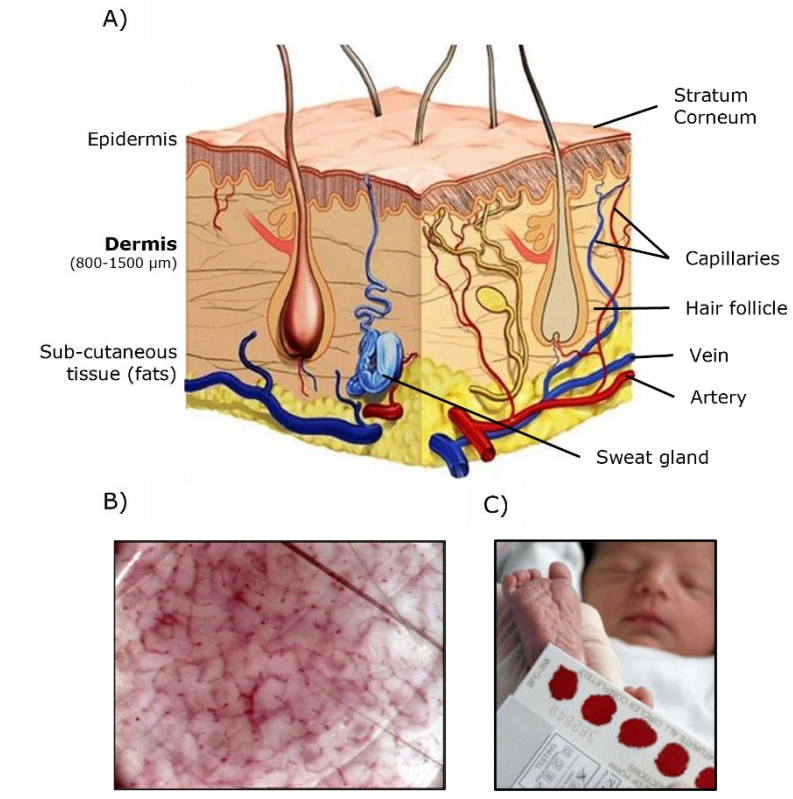

Figure 1.6: *A) The (simplified) anatomy of the human skin. The blood capillaries are located in the dermis layer. The other layers on top of the dermis, which have to be surpassed for capillary blood microsampling, are the stratum corneum and epidermis. B) Capillaries network obtained by video-capillaroscopy showing perpendicularly arranged loops in the dermis layer as dark red dots (magnification x100). C) Guthrie test for newborn screening for which blood released after a heel prick is collected on a DBS filter paper card. [Images adopted with permissions from*[46,34,40]*]*

1.3.1.3 Microneedle-based microsampling

Despite the reduced invasiveness compared to hypodermic needles, lancets still trigger significant pain perception and needle phobia. For microsampling applications, it has to be taken into account that sufficient capillary blood volumes can only be reached when the size of the injury after the puncture is adequately large and that the caused pain is directly

proportional to the lancet length[47]. This holds the risk that consent from patients for regular health monitoring gets lost[48]. Also, the regular use of lancets holds the risk of inducing disturbed microcirculation, scarring, nerve damage, haematoma forming or even local necrosis[49]. As an alternative, miniaturized needles with a micrometer-sized diameter, called microneedles, have been gaining a lot of interest in the latest decades by further reducing invasiveness, being easier for use and getting much higher patient acceptance[50,51].

1.3.2 Self-powered solutions without manual handling

Next to the accessibility of the body fluid sample, the POC device should allow an inexperienced user to perform the sampling and further processing in a simple and intuitive way. Ideally, all liquid manipulations performed in the analytical laboratory to prepare the sample for an IVD test (e.g. metering, plasma separation, dilution, etc.) are performed on the POCS device. This can be made possible by microfluidic technology.

1.3.2.1 Microfluidics for automating fluid handling

Microfluidics as defined by Whitesides is: *the science and technology of systems that process or manipulate small (10^{-9} to 10^{-18} L) amounts of fluids using channels with dimensions of tens to hundreds of micrometers*[52]. The two main types of microfluidics are sub-divided based on their actuation: active and passive. Active microfluidics often rely on external equipment like pumps or rotators for the propulsion of liquids through the microchannel network[53]. However, to enable microfluidic platforms at the POC complying with the ASSURED criteria, it is key to decouple them from laboratory equipment, the electricity network and even integrated power-sources. For this, passive liquid propulsion concepts (e.g. capillary action, finger-actuation, osmosis) have been developed to make a microfluidic device self-powered[54,55].

1.3.2.2 Capillary-driven passive microfluidics

The most successful propulsion mechanism in passive microfluidics is capillary action[55]. This phenomenon can be explained by the intermolecular forces that dominate bulk forces like gravity when dimensions reach the microfluidic size range. On the one hand, aqueous liquids tend to minimize their surface area by the cohesion of the liquid molecules, which results in a large surface tension (**Figure 1.7A**).

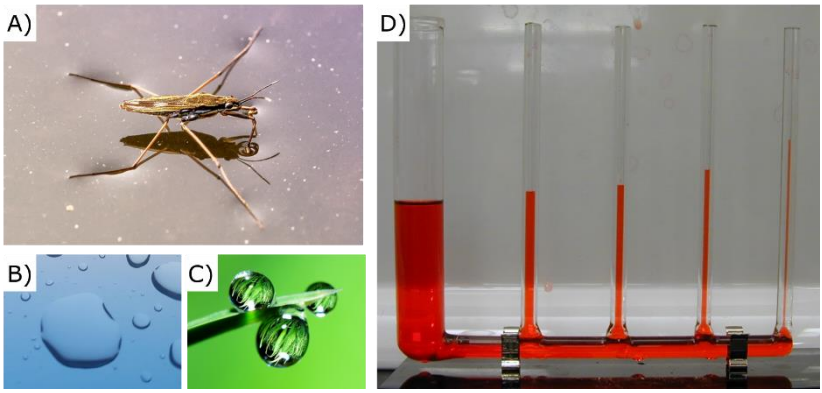

Figure 1.7: *Representation of intermolecular forces acting on water molecules. A) Water striders can walk on water due to the high surface tension. B) Hydrophilic surface showing adhered water droplets. C) Hydrophobic plant leaf surface repelling the water droplets. D) Capillary filling in narrow tubes. [Surface tension, hydrophilicity and hydrophobicity images used under license from Pixabay.com, capillarity image adopted from MIT.edu[56]]*

On the other hand, the attractive forces between the liquid molecules and solid surfaces lead to a certain degree of wettability or hydrophilicity (**Figure 1.7B**) as opposed to hydrophobicity (**Figure 1.7C**). Together, the surface tension of the liquid and hydrophilicity of the surface result in passive capillary wicking into tubes with small radii. This wicking is represented by the experimental setup in **Figure 1.7D**.

This principle has been used to propel liquids in passive microfluidics. Three types of capillary microfluidics exist: channel-based, paper-based and hybrid capillary microfluidics (see overview in **Figure 1.8**). In channel-based capillary microfluidics, the liquids are propelled by their interaction with

the (hydrophilic) microfluidic channels. Besides microchannels, also porous materials like paper can passively wick liquids, which led to the development of paper-based microfluidics. To combine best of both worlds, hybrid capillary microfluidic systems have been proposed, in which closed microchannels are used to take advantage of reduced sample-matrix interferences and lower sample-volume requirements, whereas porous materials increase the liquid absorption capacity and thus pumping duration.

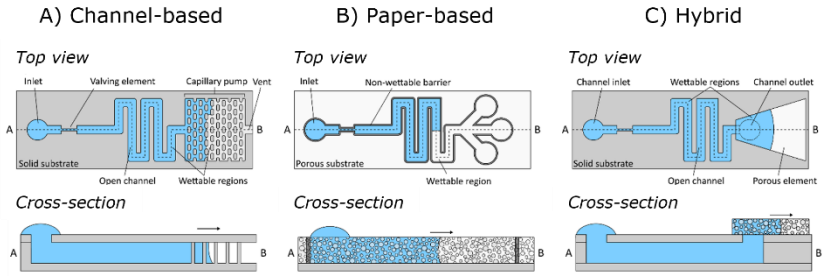

Figure 1.8: *Schematic top view and cross-section representations of the microfluidic propulsion types based on capillarity: A) channel-based, B) paper-based and C) hybrid capillary microfluidic systems.*

The (i)SIMPLE – (infusion) self-powered microfluidic pump by liquid manipulation – technology was mainly developed by the MeBioS-Biosensors group at KU Leuven to propel liquids through microchannels by the passive wicking action of a porous material[57,58]. By bringing a sacrificial working liquid into contact with the tip of the fan-shaped paper by a single finger-press, liquids can either be pulled (SIMPLE, **Figure 1.9A**) or pushed (iSIMPLE, **Figure 1.9B**), depending on the configuration.

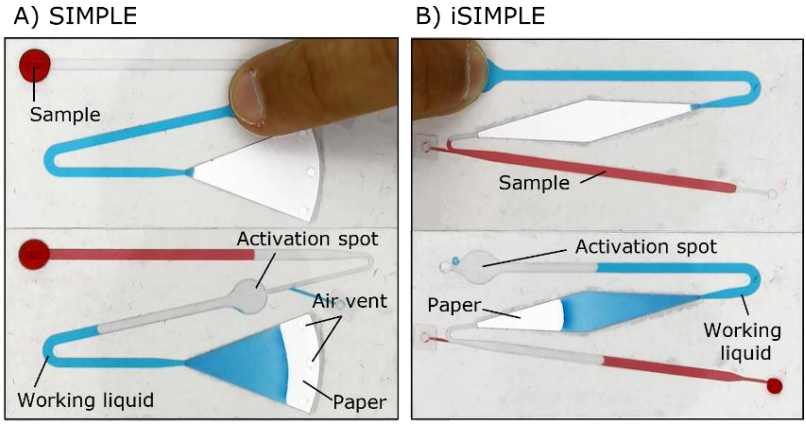

Figure 1.9: *Hybrid channel- and paper-based microfluidic platform for A) pulling (SIMPLE) and B) pushing (iSIMPLE) samples (red) upon wicking of sacrificial working liquid (blue).*

Combining the 2 pumping modes and different valving systems, complex liquid manipulations can be achieved, such as all the steps for a complex immunoassay (e.g. ELISA) on-chip, as shown in **Figure 1.10**[59].

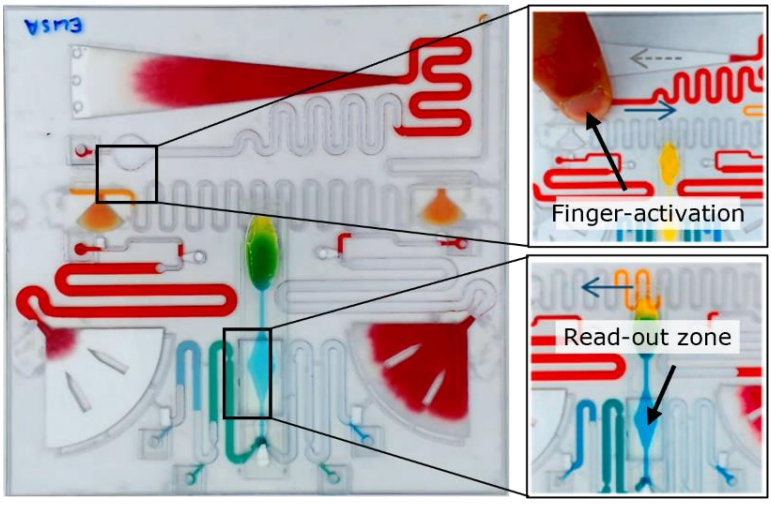

Figure 1.10: *Implementation of a full ELISA assay on-chip by combining SIMPLE and iSIMPLE, showing the high complexity that can be reached by hybrid capillary microfluidics. [Images adopted with permission from*[59]*]*

1.4. Objectives and outline of the thesis

To decentralize healthcare, minimally invasive micro-sampling tools that can be used by anyone in resource-limited settings (e.g. patient's home) are key. To achieve this, the (i)SIMPLE technology has matured to perform various complex liquid manipulation steps on-chip. Building further on this, **the general objective of this dissertation is to exploit and further develop (i)SIMPLE-based microfluidic elements toward next-generation tools for the collection, processing and storage of capillary blood upon a single finger-activation.** This is done by focusing on two sub-objectives:

- the development, characterization (Chapter 3) and validation (Chapter 4) of a self-powered, low-cost and user-friendly microfluidic DBS microsampling device.
- the improvement of the efficacy and invasiveness of capillary blood collection procedures, such as novel finger-prick protocol (Chapter 5), HMN-mediated sampling patch (Chapter 6) and HMN scalable fabrication (Chapter 7).

The different chapters that comprise this dissertation and how they link to each other are schematically represented in **Figure 1.11**.

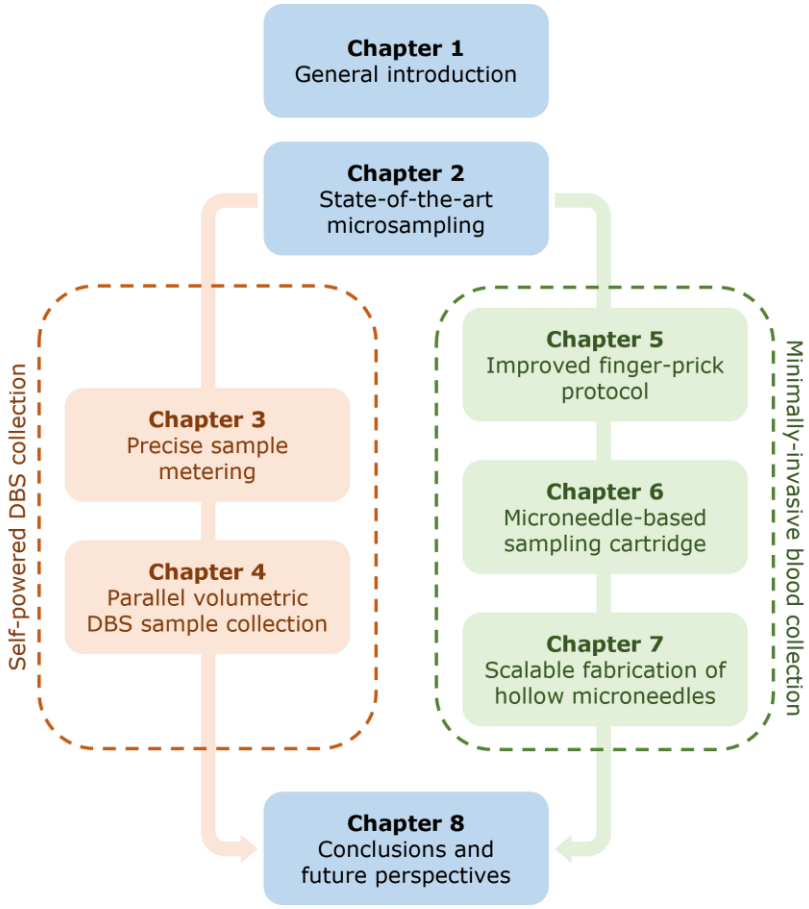

Figure 1.11: *Schematic overview of the different chapters of this thesis.*

Following this introductory chapter, **Chapter 2** provides the reader with an overview of the current state-of-the-art in capillary blood microsampling solutions for use at the POC. More specifically, the chapter presents the current gold standard procedure of DBS and its drawbacks. This is followed by an overview of currently existing (non-)microfluidic solutions to enable high-quality, user-friendly and robust capillary blood collection. Next, the chapter further elaborates on microneedles-based solutions for minimally invasive capillary blood collection and their importance towards sample in-result out devices.

In **Chapter 3**, a SIMPLE-based microfluidic device is developed and characterized to split-off precisely metered volumes from a single drop of blood. This metering concept is then integrated with SIMPLE to collect a single, precisely metered DBS. In the continuation of this work, the DBS device is further developed in **Chapter 4** to collect multiple DBS samples in parallel in a user-friendly format. Hereto, a volumetric sample inlet is demonstrated to facilitate correct application of the finger-prick capillary blood. The analytical performance of the device was then validated in the context of TDM.

As finger-pricks often fail to yield enough blood for various POC applications, **Chapter 5** deals with an improved pricking procedure aimed at increasing the bleeding intensity. This procedure involves the application of a tourniquet to strain the finger-tip before lancing. To enable even less invasive microsampling, a novel technique for fabricating stainless steel high aspect ratio hollow microneedle arrays is shown in **Chapter 6**. The resulting microneedle arrays are then integrated with SIMPLE to validate a proof-of-concept self-powered microfluidic device on an *in vitro* skin-mimicking model. Next, **Chapter 7** introduces an alternative fabrication technique by laser micro structuring and micro-injection molding to enable mass-fabrication of polymer HMNAs.

Finally, **Chapter 8** summarizes the main results and formulates the general conclusion of this dissertation. Additionally, insights regarding the further development of the technology towards fully-integrated POCS and POCT devices are presented.

1.5. References

1. Parapia, L. A. History of bloodletting by phlebotomy. *British Journal of Haematology* 143, 490–495 (2008).
2. Zubieta-Calleja, G. R. Bloodletting: a medical resource since the stone age. *Journal of Qinghai Medical College* 25, 273–275 (2004).
3. Lei, B. U. W. & Prow, T. W. A review of microsampling techniques and their social impact. *Biomedical Microdevices* 21, 1–30 (2019).
4. World Health Organisation (WHO). Working for Health 2022-2030 action plan. Preprint at https://doi.org/10.1136/bmj.4.5779.63 (2022).
5. Jenkins, K. Needle phobia: A psychological perspective. *British Journal of Anaesthesia* 113, 4–6 (2014).
6. Cook, L. S. Needle phobia. *Journal of Infusion Nursing* 39, 273–279 (2016).
7. Blicharz, T. M. *et al.* Microneedle-based device for the one-step painless collection of capillary blood samples. *Nat Biomed Eng* 2, 151–157 (2018).
8. Mabey, D., Peeling, R. W., Ustianowski, A. & Perkins, M. D. Diagnostics for the developing world. *Nature Reviews Microbiology* 2, 231–240 (2004).
9. Yager, P., Domingo, G. J. & Gerdes, J. Point-of-care diagnostics for global health. *Annual Review of Biomedical Engineering* 10, 107–144 (2008).
10. Peeling, R. W. & Mabey, D. Point-of-care tests for diagnosing infections in the developing world. *Clinical Microbiology and Infection* 16, 1062–1069 (2010).
11. Simonsen, L., Kane, A., Lloyd, J., Zaffran, M. & Kane, M. Unsafe injections in the developing world and transmission of bloodborne pathogens: A review. *Bulletin of the World Health Organization* 77, 789–800 (1999).
12. Mengistu, D. A. & Tolera, S. T. Prevalence of occupational exposure to needle-stick injury and associated factors among healthcare workers of developing countries: Systematic review. *Journal of Occupational Health* 62, 1–9 (2020).
13. St John, A. & Price, C. P. Existing and Emerging Technologies for Point-of-Care Testing. *The Clinical biochemist. Reviews / Australian Association of Clinical Biochemists* 35, 155–67 (2014).
14. Abimbola, S., Baatiema, L. & Bigdeli, M. The impacts of decentralization on health system equity, efficiency and resilience: A realist synthesis of the evidence. *Health Policy and Planning* 34, 605–617 (2019).
15. Larsson, A., Greig-Pylypczuk, R. & Huisman, A. The state of point-of-care testing: A european perspective. *Upsala Journal of Medical Sciences* 120, 1–10 (2015).
16. Velghe, S., De Troyer, R. & Stove, C. Dried blood spots in therapeutic drug monitoring and toxicology. *Expert Opinion on Drug Metabolism and Toxicology* 14, 1–3 (2018).
17. McNeill, R. P. & Barclay, M. L. Cost-effectiveness of therapeutic drug monitoring in inflammatory bowel disease. *Current Opinion in Pharmacology* 55, 41–46 (2020).
18. Kettler, H., White, K. & Hawkes, S. *Mapping the landscape of diagnostics for sexually transmitted infections: Key findings and recommendations*. *Unicef/Undp/World Bank/Who* (2004).

19. Land, K. J., Boeras, D. I., Chen, X. S., Ramsay, A. R. & Peeling, R. W. REASSURED diagnostics to inform disease control strategies, strengthen health systems and improve patient outcomes. *Nature Microbiology* 4, 46–54 (2019).
20. Heikenfeld, J. *et al.* Accessing analytes in biofluids for peripheral biochemical monitoring. *Nature Biotechnology* 37, 407–419 (2019).
21. Lippi, G. & Plebani, M. Opportunities and drawbacks of nonstandard body fluid analysis. *Clinical Chemistry and Laboratory Medicine* 55, 907–909 (2017).
22. Gubala, V., Harris, L. F., Ricco, A. J., Tan, M. X. & Williams, D. E. Point of care diagnostics: Status and future. *Analytical Chemistry* 84, 487–515 (2012).
23. Anizan, S. & Huestis, M. A. The potential role of oral fluid in antidoping testing. *Clinical Chemistry* 60, 307–322 (2014).
24. García-Carmona, L. *et al.* Pacifier Biosensor: Toward Noninvasive Saliva Biomarker Monitoring. *Analytical Chemistry* 91, 13883–13891 (2019).
25. Emaminejad, S. *et al.* Autonomous sweat extraction and analysis applied to cystic fibrosis and glucose monitoring using a fully integrated wearable platform. *Proceedings of the National Academy of Sciences of the United States of America* 114, 4625–4630 (2017).
26. Bariya, M., Nyein, H. Y. Y. & Javey, A. Wearable sweat sensors. *Nature Electronics* 1, 160–171 (2018).
27. Torrente-Rodríguez, R. M. *et al.* Investigation of Cortisol Dynamics in Human Sweat Using a Graphene-Based Wireless mHealth System. *Matter* 2, 921–937 (2020).
28. Niedzwiecki, M. M. *et al.* Human Suction Blister Fluid Composition Determined Using High-Resolution Metabolomics. *Analytical Chemistry* 90, 3786–3792 (2018).
29. Samant, P. P. & Prausnitz, M. R. Mechanisms of sampling interstitial fluid from skin using a microneedle patch. *PNAS* 95, 1, 515-534 (2018) doi:10.1073/pnas.1716772115.
30. Posa, A. *et al.* Schirmer strip vs. capillary tube method: Non-invasive methods of obtaining proteins from tear fluid. *Annals of Anatomy* 195, 137–142 (2013).
31. Sempionatto, J. R. *et al.* Eyeglasses-based tear biosensing system: Non-invasive detection of alcohol, vitamins and glucose. *Biosensors and Bioelectronics* 137, 161–170 (2019).
32. Moreddu, R. *et al.* Integration of paper microfluidic sensors into contact lenses for tear fluid analysis. *Lab on a Chip* 20, 3970–3979 (2020).
33. Samant, P. P. & Prausnitz, M. R. Mechanisms of sampling interstitial fluid from skin using a microneedle patch. *Proceedings of the National Academy of Sciences of the United States of America* 115, 4583–4588 (2018).
34. Lei, B. U. W. & Prow, T. W. A review of microsampling techniques and their social impact. *Biomedical Microdevices* 21, (2019).
35. Novosanis. Colli-Pee. *https://novosanis.com/our-products*.
36. Salimetrics. SalivaBio Oral Swab (SOS). *https://salimetrics.com/collection-method/oral-swab-saliva-collection-device/*.
37. PharmChek. PharmChek® Sweat Patch. *https://www.pharmchek.com/products/pharmchek-patch*.
38. Ates, H. C. *et al.* Integrated devices for non-invasive diagnostics. *Advanced Functional Materials* 31 (2021).

39. Guthrie, R. & Susi, A. A simple phenylalanine method for detecting phenylketonuria in large populations of newborn infants. *Pediatrics* 32 (3), 338–343 (1963).
40. Humbert, P. *et al.* Skin Capillaroscopy. in *Agache's Measuring the Skin* 549–562 (2000).
41. Bian, S. *et al.* Evaluating an easy sampling method using dried blood spots to determine vedolizumab concentrations. *Journal of Pharmaceutical and Biomedical Analysis* 185 (2020).
42. Sciberras, D. *et al.* A pharmacokinetic study of radiprodil oral suspension in healthy adults comparing conventional venous blood sampling with two microsampling techniques. *Pharmacology Research and Perspectives* 7, 1–8 (2019).
43. Karp, D. G. *et al.* A serological assay to detect SARS-CoV-2 antibodies in at-home collected finger-prick dried blood spots. *Scientific Reports* 10, 1–7 (2020).
44. Popp, W. *et al.* What is the use? An international look at reuse of single-use medical devices. *International Journal of Hygiene and Environmental Health* 213, 302–307 (2010).
45. Smit, P. W. *et al.* Systematic review of the use of dried blood spots for monitoring HIV viral load and for early infant diagnosis. *PLOS One* 9 (2014), doi:10.1371/journal.pone.0086461.
46. Al-Kaf, A. A review on needle free injections. *Universal Journal of Pharmaceutical Research* 2 (2017).
47. Fruhstorfer, H. Capillary blood sampling: The pain of single-use lancing devices. *European Journal of Pain* 4, 301–305 (2000).
48. Tsai, C. W., Li, C. H., Lam, R. W. K., Li, C. K. & Ho, S. Diabetes care in motion: blood glucose estimation using wearable devices. *IEEE Consumer Electronics Magazine* 9, 30–34 (2020).
49. Monica Cheesbrough. *WHO guidelines on drawing blood : best practices in phlebotomy*. *World Health Organization* (2010).
50. Dixon, R. V., Lau, W. M., Moghimi, S. M. & Ng, K. W. The diagnostic potential of microneedles in infectious diseases. *Precision Nanomedicine* **3**, 629–640 (2020).
51. Dixon, R. V. *et al.* Microneedle-based devices for point-of-care infectious disease diagnostics. *Acta Pharmaceutica Sinica B* 11, 2344–2361 (2021).
52. Whitesides, G. M. The origins and the future of microfluidics. *Nature* 442, 368–373 (2006).
53. Mohammed, M. I., Haswell, S. & Gibson, I. Lab-on-a-chip or chip-in-a-lab: challenges of commercialization lost in translation. *Procedia Technology* 20, 54–59 (2015).
54. Xu, L., Wang, A., Li, X. & Oh, K. W. Passive micropumping in microfluidics for point-of-care testing. *Biomicrofluidics* 14 (2020).
55. Narayanamurthy, V. *et al.* Advances in passively driven microfluidics and lab-on-chip devices: A comprehensive literature review and patent analysis. *RSC Advances* 10, 11652–11680 (2020).
56. MIT. Capillarity and Gravity. *https://web.mit.edu/nnf/education/wettability/gravity.html.*
57. Dal Dosso, F., Kokalj, T., Belotserkovsky, J., Spasic, D. & Lammertyn, J. Self-powered infusion microfluidic pump for ex vivo drug delivery. *Biomedical Microdevices* 20, 44 (2018).
58. Kokalj, T., Park, Y., Vencelj, M., Jenko, M. & Lee, L. P. Self-powered imbibing microfluidic pump by liquid encapsulation: SIMPLE. *Lab on a Chip* 14, 4329–4333 (2014).

59. Ordutowski, H. *et al.* Next generation point-of-care test for therapeutic drug monitoring of adalimumab in patients diagnosed with autoimmune diseases. *Biosens Bioelectron* 208, 114189 (2022).

Chapter 2

State-of-the-art methods in capillary blood sampling

The work reported in this chapter is adapted from:

Vloemans, D.*, **Van Hileghem, L.***, Ordutowski, H.*, Dal Dosso, F., Spasic, D., Lammertyn, J. (2023). Self-powered microfluidics for point-of-care solutions: from sampling to detection of proteins and nucleic acids. (Submitted as a book chapter in *Methods in Molecular Biology*)

*Equal contributions

Van Hileghem L. contributed to this manuscript in terms of structuring, collection and analysis of the part of the literature on microsampling technologies, next to writing and editing of the text.

2.1. Remote capillary blood collection

An often overlooked challenge in bringing diagnostics to the POC is the collection of the sample. The latter is, however, critical because the accuracy of the test is directly dependent on the quality of the sample, which is either received by the analytical laboratory or applied onto a POCT device. Over the years, numerous methods have been investigated with the aim of solving the main problems from collecting the sample to preparing it for analysis. This section gives an overview of the main approaches for high-quality capillary blood sample collection and preparation.

2.1.1 DBS sampling: essential but challenging

If direct analysis is not intended, the collected blood sample should immediately be stabilized to maintain its quality during storage or transport to the analytical laboratory. DBS collection, as initially proposed by Guthrie and colleagues, offers a valuable solution by drying the sample on absorbent filter paper. This approach allows the storage at room temperature for weeks, months or even years, depending on the analyte characteristics[1]. Today's growing clinical importance of DBS is mainly thanks to this increased stability during transport, but also the logistical convenience and overall reduced cost[2]. Furthermore, regarding centralized laboratories, DBS sampling allows for automated sample preparation and subsequent analysis.

In the standard workflow of DBS collection (see overview in **Figure 2.1**), a single drop of finger-prick blood with a volume ideally between 35-75 µL is deposited onto the pre-printed zones of a commercially available protein saver card. Next, the blood is air-dried at room temperature for several hours before storage or shipment. Once the sample arrives in the analytical lab, one or multiple sub-punches with a diameter of typically 6 mm are taken from the DBS and transferred into an extraction solvent to reconstitute the analytes. If the nature of the analyte allows, e.g. in case of robust, small molecules, the extraction can be

stimulated by vortexing or sonicating. Next, the extract is centrifuged and the supernatant is analyzed.

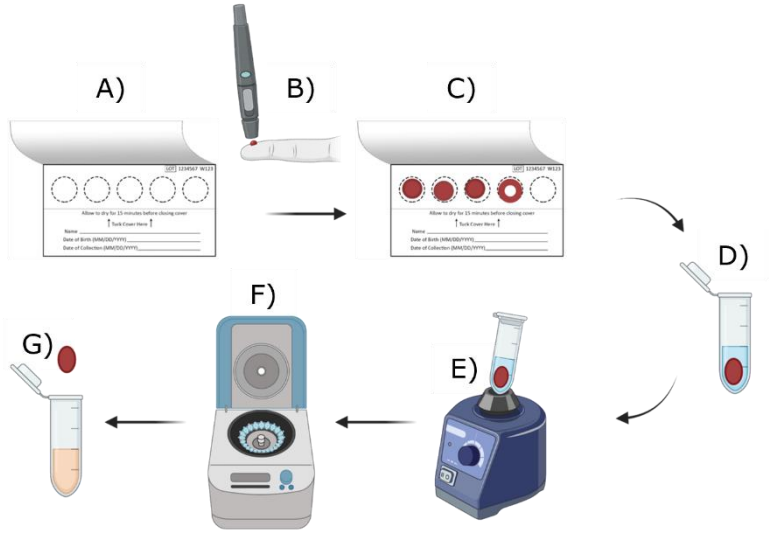

Figure 2.1: *Current gold standard workflow for DBS preparation [figure created with Biorender.com based on Ramesh et al. 2016[3]]. A) Pre-printed protein saver card for the collection of 5 DBS samples. B) Finger-prick blood collection by the deposition of a single and adequately large blood drop within the indicated zone. C) A sub-punch with a fixed diameter is taken from each DBS sample. D) The sub-punch is immersed in a fixed volume of extraction solvent. E) If the analyte's stability allows, the sample is vortexed. F) Afterwards, the sample is also centrifuged. G) Next, the supernatant is collected for subsequent analysis.*

Despite the advantages, some critical limitations form the basis for a relatively high variability in the analysis results, detaining DBS sampling from reaching its full potential. Firstly, operator errors often result in inadequate DBS samples by e.g., spotting insufficient volumes, depositing the blood on the wrong location or overlapping spots, contaminating after direct finger contact or sending insufficiently dried samples (**Figure 2.2A**). Secondly, factors like the temperature, humidity and batch-to-batch variability of the filter paper cause inconsistencies in the drying process[4,5]. This leads to two possible chromatographic effects, the 'volcano effect' and the 'coffee stain effect', which cause a local increase in amount of RBC and analyte concentrations, respectively, at the perimeter of the DBS (**Figure**

2.2B). Thirdly, the high inter- and intra-person variation in blood Hct level (i.e., volumetric percentage of RBCs) causes analytical bias due to altered extraction efficiencies (**Figure 2.2C**)[6].

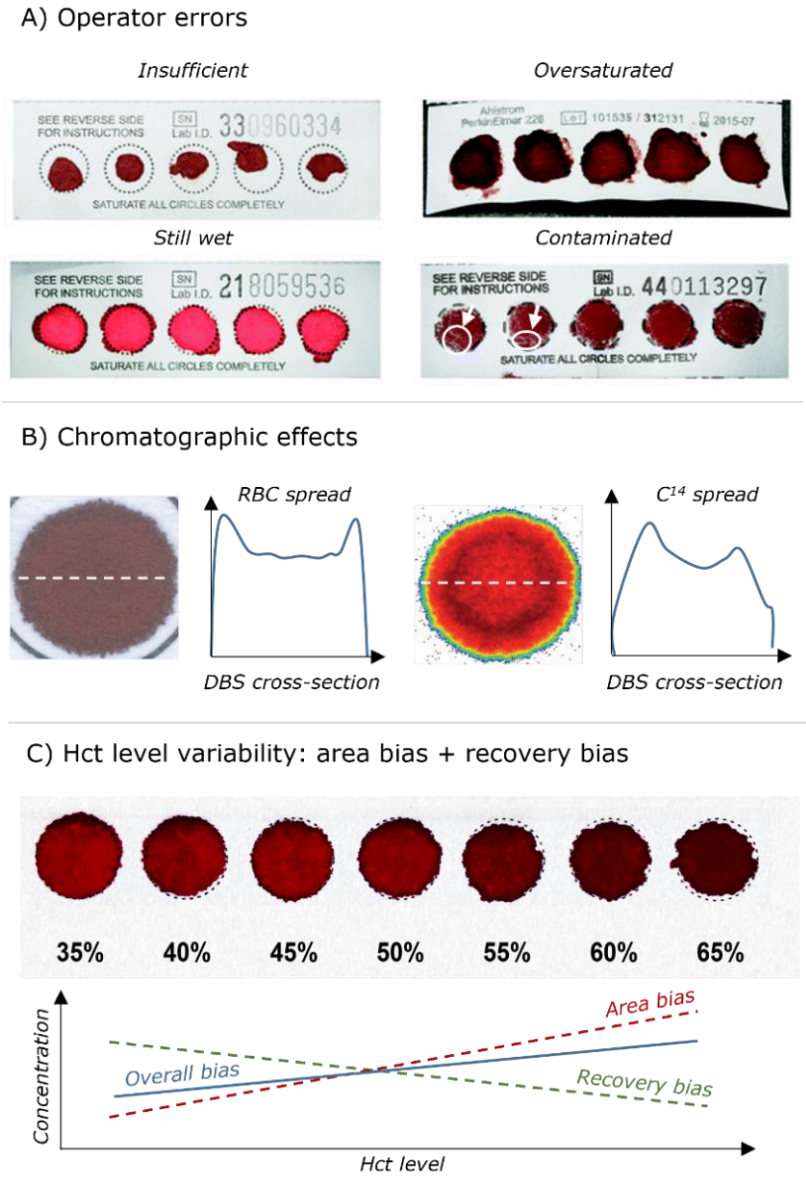

Figure 2.2: *Overview of different sources of variabilities leading to inaccuracies. [Figures adapted with permissions from*[7,4,5,8,6]*]*

The higher the haematocrit (Hct) level, the lower the diffusion through the filter paper leading to smaller spot areas. Hence, these sub-punches contain proportionally more analyte compared to the DBS sub-punch with a low Hct level, which can be referred to as the Hct-based area bias. Fourthly, variable Hct levels may lead to a recovery bias, caused by the red blood cells (RBCs) hampering the efficiency of analyte extraction, and a matrix bias, where remnants of the whole blood matrix (e.g. haemoglobin) interfere with the analysis itself.

2.1.2 Microfluidic solutions for DBS collection

Among above-mentioned challenges, the major source of analytic bias is related to the Hct variability. The easiest way to solve the Hct-based area bias is to avoid the sub-punching practice by applying a precise volume of blood on the filter paper and extract the whole spot. In research settings, this has been done using capillary tubes or even pipettes. However, this would introduce an extra manual handling step to be performed, which does not comply with the requirements for the POC settings. An important solution to this issue came from Denniff and Spooner[9], who introduced a sampler which was later branded as the 'Volumetric Absorptive Micro Sampler' (VAMS®, see **Figure 2.3**). It consists of a plastic handle and a hydrophilic porous tip to rapidly absorb and dry precisely 10, 20 or 30 µL of blood. In essence, this tip is extracted as a whole to avoid Hct bias upon extraction. After lancing, the porous tip is brought into contact with the blood under an angle of about 45° until the complete tip has turned red[10]. After an additional two seconds, to assure complete saturation, the tip is removed and air-dried. Next, upon shipping to the central laboratory, VAMS® are placed in a clamshell for protection to the environment. Studies comparing VAMS® against traditional DBS and pipetted reference show high reproducibility with CV-values between 3.9-4.3%[11,12]. However, patient self-sampling validation revealed that VAMS® is still prone to user-dependent variability by over- or undersampling, contamination due to direct finger contact or the blood drop touching the sample holder[13]. Hence, obtaining high quality samples using VAMS® can only be assured when following the instructions carefully.

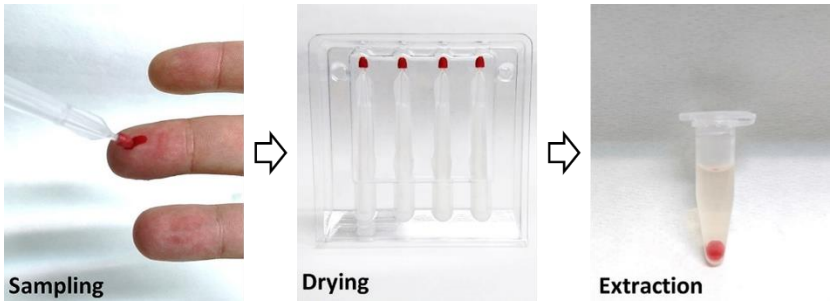

Figure 2.3: *The VAMS® sampling procedure [Figure adopted with permission from[10]]*

User dependency can be minimized by physically decoupling sample application from DBS loading. The company Spot On Sciences developed a sealed cartridge named HemaSpot HF which contains a fan-shaped filter paper with 8 wedges that load simultaneously starting from the center (see **Figure 2.4A**). The cartridge also contains a desiccant to improve the drying process. Immediately after loading the wedges, the lid of the cartridge has to be closed. Once arrived in the laboratory, the wedges are removed using scissors to obtain DBS samples containing 18.7 µL of dried blood. Studies showed improved extraction efficiencies and consistencies, however, data on Hct variability are not available[14,15]. Furthermore, the total requirement of 150 µL to fill all 8 wedges is relatively large compared to what can be reached by finger-pricking[16]. This holds the risk of undersaturation of the filter paper, as shown in **Figure 2.4B**, which affects all DBS samples[17]. Oversaturation, on the other hand, is less likely by the removal of sample excess by an outer filter ring (**Figure 2.4C**).

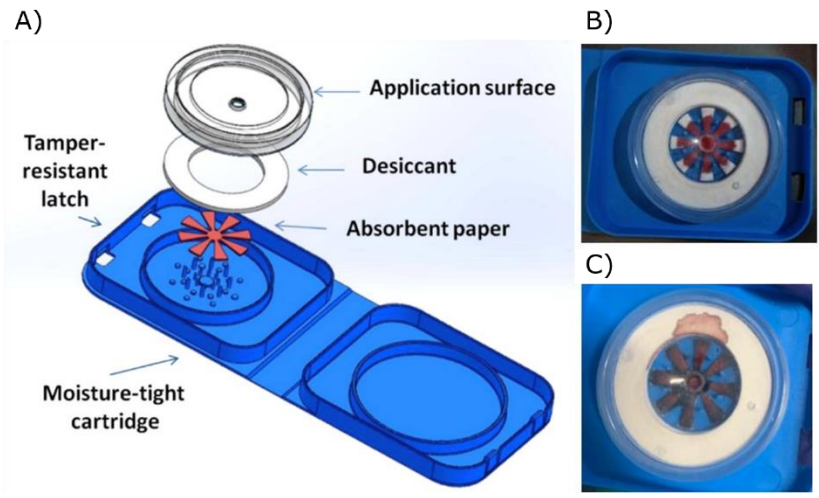

Figure 2.4: *HemaSpot HF by the company Spot On Sciences[18] [Figures adopted with permissions from[19,20]]. A) Schematic representation of the elements inside the sealable cartridge. B) Undersaturation of the wedges. C) Oversaturation of the wedges, showing the excess removal by the outer filter ring.*

To gain precise control over the capillary blood collection, passive microfluidic solutions have been developed in the latest decennia to separately perform an accurate metering step before DBS loading. This also provides a visible proof of both successful sample metering and DBS loading by checking if the metering channel has completely filled and emptied, respectively. Hereto, HemaXis™ DBS10 (**Figure 2.5**) combines a self-filling capillary metering channel with a traditional DBS card[21]. Upon loading a 10 µL blood sample, the blood drop after finger-pricking has to be brought in contact with the capillary inlet. After completely filling the capillary channel, closing the cartridge brings the filter paper into contact with the channel outlet to generate the DBS. By repeating this process, up to 4 DBS samples can be generated per cartridge. As a single DBS sample at a time has to be generated according to the user instructions, multiple finger-pricks may be required to produce enough blood throughout this entire process. Furthermore, the small, side-located sample inlets may reduce the usability for individuals with impaired vision or tremors, potentially leading to unwanted sample losses.

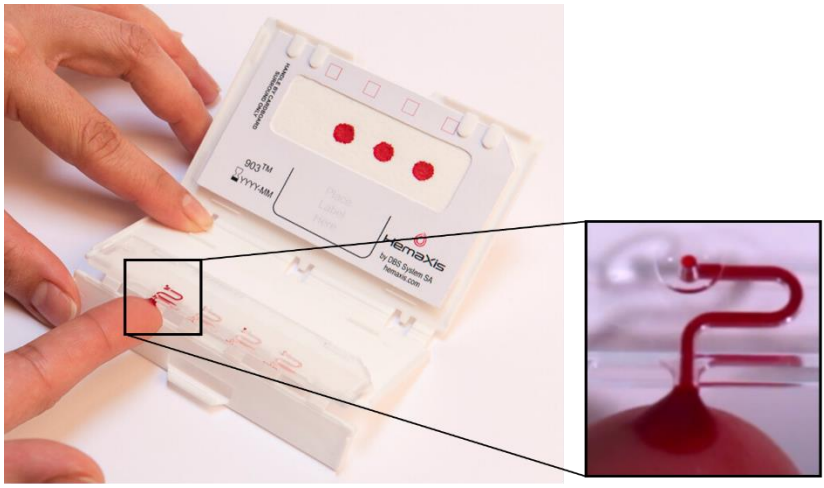

Figure 2.5: *HemaXis™ DBS10 generating up to 4 metered DBS by loading blood samples in the self-filling capillaries and closing the cartridge [©HemaXis[22]].*

Capitainer® is another example based on a self-filling capillary channel, which loads automatically a pre-cut DBS, further avoiding manual handling steps (**Figure 2.6A**)[23]. Significantly large blood drops (e.g. > 18 µL to obtain 10 µL DBS) have to be applied at once on the sample inlet hole with hydrophobic surroundings. The excess blood is removed from the inlet before loading the DBS by the timely disintegration of a dissolvable polyvinyl alcohol film on top of the waste and DBS filter papers. **Figures 2.6 A-B** show Capitainer® devices for the collection of 10 µL and 50 µL DBS, respectively.

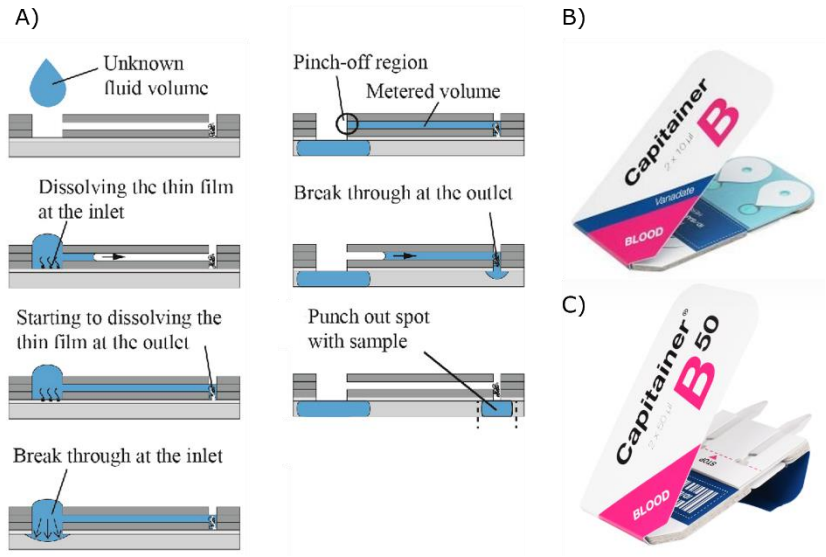

Figure 2.6: *Capitainer® using a self-filling capillary channel in combination with a pre-cut DBS and automated sample excess removal. A) Working principle explained schematically. First, a sample with unknown volume is deposited into the inlet, upon which the capillary channel fills. The polyvinyl alcohol film dissolve upon contact with blood, removing the excess below the inlet and, afterward, loading the pre-cut DBS [Adopted with permission from[24]]. B-C) Images of the commercial product for 10 and 50 µL DBS, respectively. [©Capitainer[25,26]]*

Both the HemaXis™ DBS10 and Capitainer® devices are similar in the sense that multiple samples have to be applied for generating multiple DBS on a single cartridge. Contrarily, hemaPEN® (**Figure 2.7**) meters 4 parallel samples from the same drop in a pen format device[27]. However, designed sample volumes are only 2.7 µL, limiting their applicability. Furthermore, the device is still prone to user mistakes. Indeed, the pen tip has to be positioned correctly and adequately long into the blood droplet, while DBS loading is based on gravitational force by turning the pen upside down.



Figure 2.7: *hemaPEN® allowing for parallel sampling of 4 DBS in a pen format. After filling all the capillary channels (visual proof), the pen has to be turned upside down to load the pre-cut DBS [©Trajan Scientific and Medical[28]].*

Although the discussed microfluidic solutions (semi) automate sample metering and subsequent DBS loading, sample collection is still done by finger-pricking. This potentially suffers from problems like insufficient hand washing, failing to drop the capillary blood into the inlet or not maintaining contact with the blood droplet as long as needed. Indeed, pre-analytical operator errors still remain the largest source of inaccuracies nowadays[29,30]. Furthermore, adequate volumes can often only be achieved by squeezing the finger-tips[16,31], which increases the risk of haemolysis, coagulation and might dilute the sample with intra- and intercellular fluid biasing the analysis results[32,33]. To standardize capillary blood collection, Tasso developed an integrated DBS sampling device, i.e. Tasso-M20 (**Figure 2.8**). The device has to be applied on the upper arm and upon one finger-push, a lancet is released and retracted, while blood starts flowing by the generation of a vacuum. In the attached sampling unit, 4 precisely metered DBS samples with a CV of < 5% are loaded. However, the user-friendliness for lab-workers is below expectations as it is difficult to label and retrieve the DBS samples. Furthermore, the device is relatively bulky, taking up too much space in analytical laboratory and too costly for frequent sample collection.

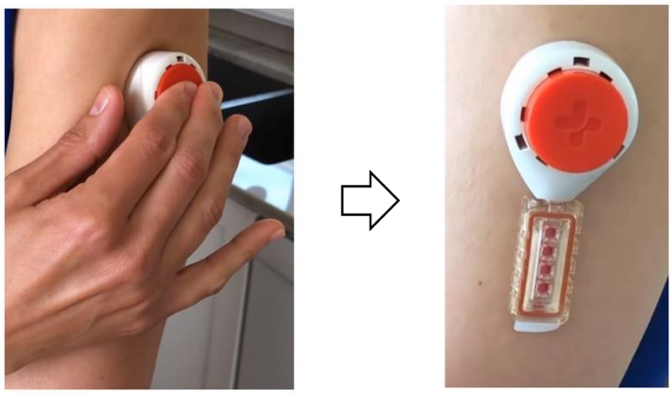

Figure 2.8: *Tasso-M20 integrating capillary blood collection with volumetric DBS sampling upon single press on a button [©Tasso[34]].*

2.1.3 Alternatives for dealing with Hct variability in DBS

Next to the Hct-based sampling bias, which can be solved by the shown (microfluidic) devices, highly varying Hct levels also have effect on the next steps in the DBS analysis workflow. The remainders of the RBCs can for some analytes hamper the release upon submerging the DBS in the extraction solvent. This extraction can be improved by factors like temperature, extraction time, the solvent or physical stimuli like shaking or sonicating[35]. However, options might be limited in the context of larger analytes, like proteins or nucleic acids, when trying to avoid damage. In some cases, the extraction bias can be corrected by the addition of an isotopically labelled internal standard (IS). Ideally, the sample is co-spiked with this IS before DBS loading as it would be subjected to the same extraction process and, hence, nullify all biases caused during the downstream processes. However, this is not a feasible approach at the POC. Alternatively, the *post forma* addition of the IS on top of the DBS samples by spraying can be integrated in a fully-automated laboratory workflow (see **Figure 2.9**)[6]. However, it must be noted that the addition of an IS is only applicable for LC-MS analyses.

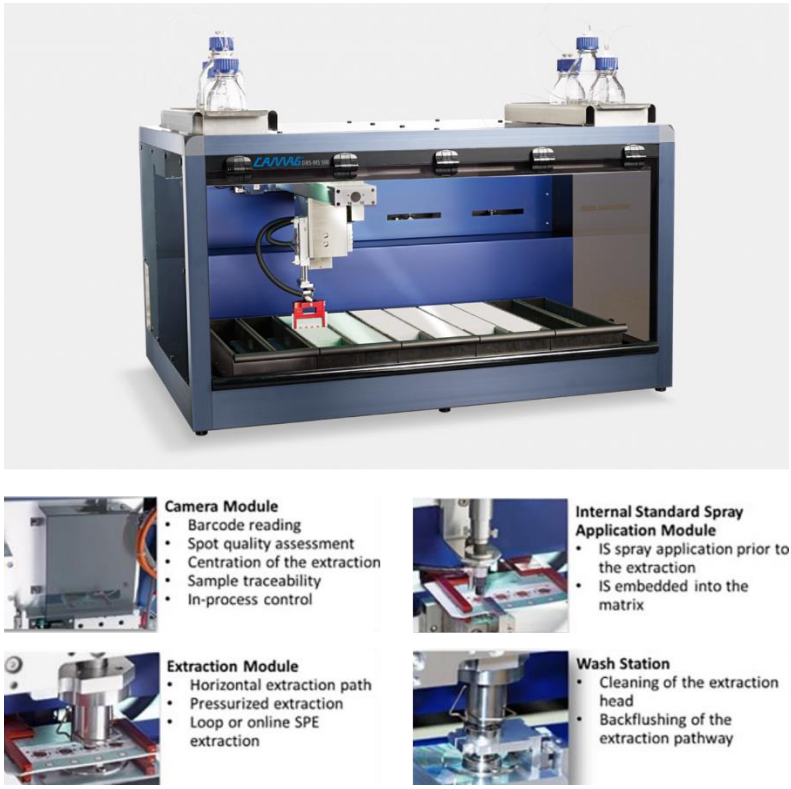

Figure 2.9: *The CAMAG® DBS-MS 500 system (Muttenz, Switzerland), a fully-automated DBS analysis system for the analytical laboratory, including an integrated IS spray. [Figures adopted with permission from*[36]*]*

When the extraction bias is directly proportional to the Hct level of the blood, it is also an option to predict the Hct levels *post forma* from the DBS samples. Such an Hct level prediction is in any case important for the correct interpretation of the analysis results. Therefore, methods have been developed, for instance, by measuring potassium (K^+) as its intracellular concentration is a factor 35 higher than its extracellular concentration. The more RBCs lyse, the higher the K^+-concentration becomes, which relates well to the Hct level. Alternatively, near-infrared (NIR) and ultra-violet/visible (UV/VIS) spectroscopy in combination with a correction algorithm have paved the way towards non-contact Hct measurements from DBS samples[37–39].

Finally, the presence of a varying amount of RBC remnants, e.g. haemoglobin, in the matrix also leads to an altered response by interfering with the signal detection or the assay elements. Besides, measuring analytes directly from a complex matrix is usually subject to a response suppression or interference. Therefore, in case whole blood samples are not essential, plasma separation and, hence, loading dried plasma spots can circumvent Hct-based issues. Membrane-based plasmapheresis has been used by Hauser et al. (**Figure 2.10A**), Spot On Sciences (**Figure 2.10B**), Telimmune™ (previously Noviplex™, **Figure 2.10C**) and Ordutowski et al. (**Figure 2.10D**)[40–43].

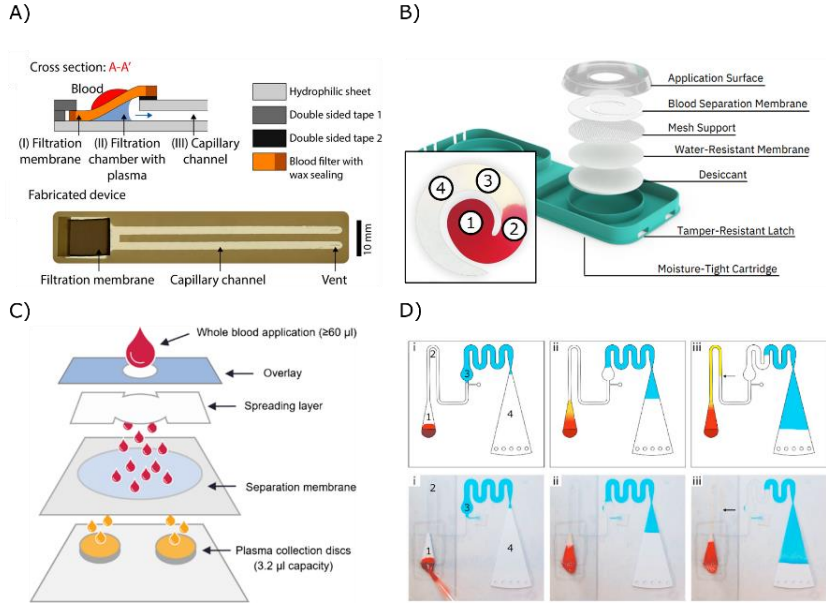

Figure 2.10: *A) The concept from the previously shown Capitainer® DBS cardridge, but adapted to filter the plasma using a membrane (blue) right below the sample inlet. B) HemaSpot SE contains a spiral-shaped filter membrane for filtration of the whole blood. By punching at the 4 different locations (indicated by 1, 2, 3, 4), different sample types can be extracted as a result of the 4 different levels of filtration. C) Schematic representation of the Noviplex™ card by Telimmune. D) Steps of the plasmapheresis process by integrating a commercial filtering membrane into a SIMPLE cartridge. After application of whole blood on top of the membrane (1), the SIMPLE paper pump (4) wicks in the working liquid (3), subsequently drawing the separated plasma into the downstream channel (2). [Figures adopted with permissions from[41,42,44], other copyrights belong to ©Telimmune and ©Spot On Sciences]*

Among these examples, only the last one provides a microfluidic solution for further on-chip sample processing by combining paper-based and channel-based microfluidics. This is a technological advantage which will be further exploited throughout the work presented in this dissertation (see Chapters 3 and 4).

2.1.4 Liquid capillary blood storage

Although DBS sampling is highly advantageous for decentralized sampling solutions, with many applications of interest, some applications would benefit from the collection and storage of a liquid blood sample. This is relevant for applications in haematology where RBCs should remain intact[45]. Moreover, applications targeting non-abundant analytes might not be compatible with dried storage due to the intrinsic dilution ratio caused by extraction of the DBS sample. For this reason, Stuart and colleagues proposed in 1974 to simply drip obtained capillary blood from finger- or heel-pricks directly into a 1 mL collection tube[46]. This tube contained 50 µL of the 1.8% (w/v) anti-coagulating agent ethylenediamine tetra-acetic acid (EDTA) to stabilize the blood upon storage or transport. This simplified technique was proposed as an alternative to pipetting and diluting the samples on the spot. However, a possible problem is that the anti-coagulant concentration might change significantly when collected volumes are too low, resulting in an additional variability. Furthermore, the tendency of scooping the blood from the finger increases the risk of haemolysis and clot formation[47]. This is usually solved by plastic or glass capillary tubes to collect a precise volume of blood by a finger-prick (**Figure 2.11A**). After sample collection, the blood can immediately be released into a collection tube containing an anti-coagulant. Alternatively, many capillary tubes available are pre-coated with an anti-coagulant, e.g. Sarstedt capillaries (K_2EDTA, citrate, Lithium Heparin, etc.). Furthermore, if plasma is the preferred sample matrix for analysis, for the reasons previously stated, capillary tubes can also be used to facilitate plasma separation once arrived in the lab (**Figure 2.11B**). However, this requires an extra centrifugation step in the laboratory, as well as a manual plunger

to release the obtained plasma afterwards[48]. Additional disadvantages with capillary tubes is that the accuracy is user-dependent, both on the side of the self-sampling patient (e.g. by altered capillary interaction due to Hct variability) as the analytical laboratory[48–50]. To replace manual handling, and thus standardize liquid capillary blood sampling, Tasso developed an integrated device for the collection of 200-600 µL of capillary blood (**Figure 2.11C**). Depending on the envisioned application, different collection tubes are available, containing different or no anti-coagulants.

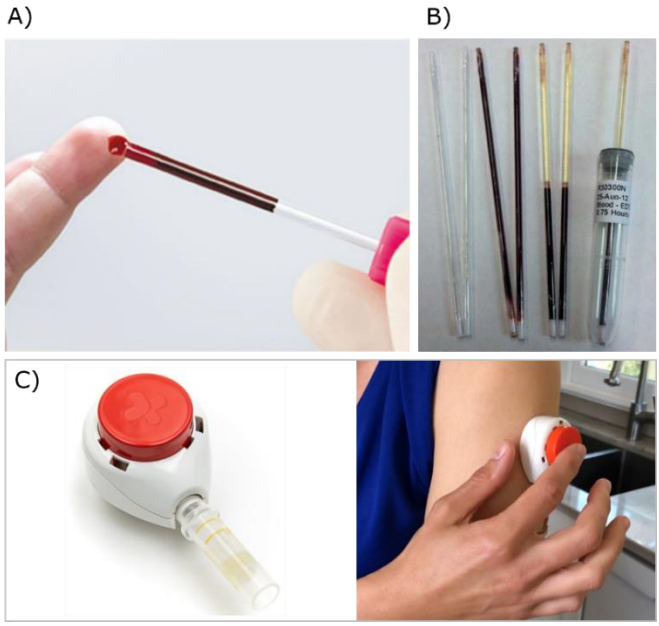

Figure 2.11: *A) Collection of blood using a Sarstedt end-to-end capillary tube [©Sarstedt[51]]. B) Drummond capillary tubes containing a gel for the separation of the plasma and RBC fractions upon centrifugation [Figure adopted with permission from[49]]. C) Integrated device named Tasso+ for standardized capillary blood collection using the lancet poke-and-release principle. [©Tasso[52]]*

2.1.5 Precise capillary blood collection for POCT

Some applications require not only the samples to be collected but also the tests to be carried out on the spot. However, the sensitivity and accuracy of a POCT are significantly dependent on the applied sample volume and correct handling. For capillary

blood, pipettes for sample collection and serial dispensing for POCT have been developed (**Figure 2.12A**), reaching an accuracy and precision close to commercial pipettes. However, they were not meant for self-sampling and suffered from high systematic (12%) and random errors (13%)[53]. As an alternative, the single-use tools shown in **Figure 2.12B** have been developed for capillary blood collection and subsequent deposition on a POCT. Among these, the inverted cup was selected to be the easiest, safest and most accurate blood transfer tool[54]. For example, **Figure 2.13C** shows the working principle of an inverted cup that was designed for a malaria self-test[55].

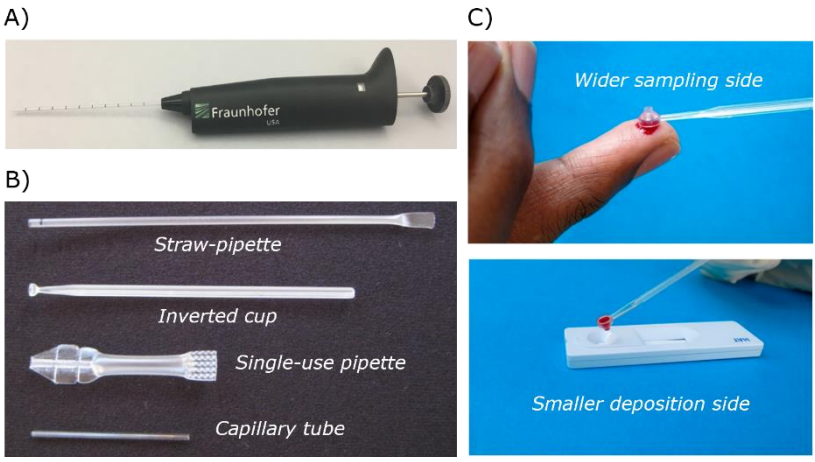

Figure 2.12: *A) Commercial pipette with disposable capillary for the uptake of 100 µL and serial disposal of precise volumes of a few µL for use at the POC. B) Single-use blood collection and deposition tools for use with POCT C) Alternative design for the inverted cup to increase the volume that can be collected and deposited with greater precision. [Figures adopted with permissions from*[53–55]*]*

In a field study of the main blood transfer tools, a high variability in delivered volumes was obtained and one of the main factors was the level of experience of the user[56]. Furthermore, the need for integrating the test components and procedures has been shown in context of a sample-to-answer HIV self-testing[57] (see also Section 2.2.3). As an intermediate step, the AtomoRapid™ device (**Figure 2.13**) has an integrated safety lancet and integrated capillary tube to facilitate HIV self-testing. Despite of its promising innovation, though, the device still does

not allow self-testing by lay users without previously obtaining minimal training[58].

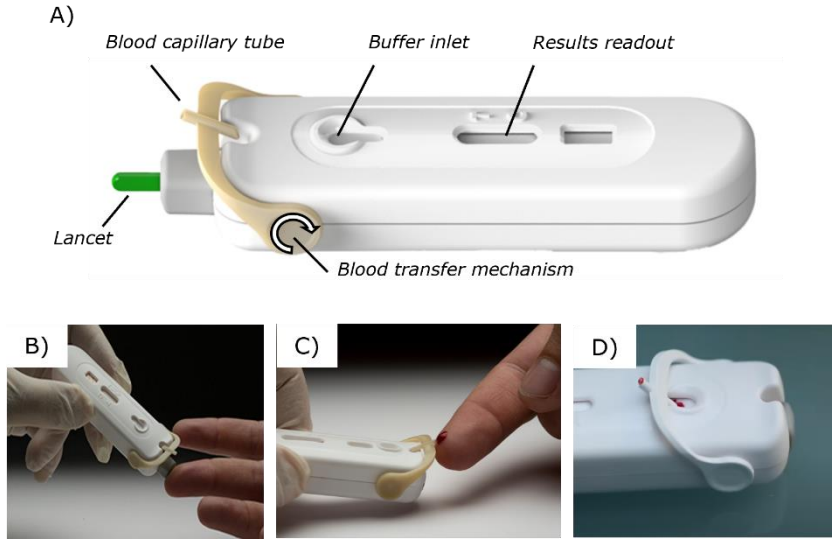

Figure 2.13: *A) Overview of the components of the AtomoRapid device, which integrates the finger-prick lancet, capillary tube for collection with a lateral flow strip. The steps to be taken by the user are lancet activation (B), filling of the capillary tube (C), turning the capillary tube towards the inlet using the blood transfer mechanism (D), and adding the co-delivered buffer in the same inlet [©Atomo Diagnostics[59]].*

2.2. Microneedles for microsampling

The solutions for capillary blood POCS and POCT discussed until here rely on the use of lancets to collect blood from the finger-tips or the arm. Despite the advantages of lancets over hypodermic needles, their regular use holds several risks and is still quite painful, as already indicated in Chapter 1. To serve as an alternative, microneedles (MNs) induce significantly less pain than both lancets and hypodermic needles[60–62]. MNs are miniaturized, needle-like projections, either configured in-plane or out-of-plane, with a diameter in the micrometer range. They were first invented in 1971 to improve drug uptake through the skin by the creation of micropores through the *stratum corneum*, the outermost protective layer of the skin[63]. Nowadays, MNs are employed both for extracting body fluids (capillary blood and ISF)

and to inject medicine into the skin. In this section, a brief overview of MNs is given after which some examples of capillary blood and ISF collection by MNs are highlighted.

2.2.1 Different types of microneedles

MNs can be categorized in different ways. Firstly, they can be sub-divided by the materials they have been made of: silicon, glass, ceramic, metals, alloys, polymers and hydrogels[64–70]. Initially, MN development was mainly focused on the processing of silicon using techniques like dried reactive-ion etching. However, materials preferably have good mechanical properties, without breaking or buckling, and are also biocompatible. Therefore, medical-grade metals and polymers became more accepted.

Secondly, MNs can exist either as a single MN or as an array. Both 1-dimensional (1×n MNs) and 2-dimensional (n×n MNs) arrays have been reported, the latter often being referred to as a patch. The difference between an array and a single MN is identical for delivery and sampling, i.e. the improved efficiency by an increased total contact area or decreased required flow pressure. However, it must be noted that choosing the right design (e.g. size of the patch, inter-needle density, shaft length, etc.) of MN arrays is also challenging as the interaction with the viscoelastic skin is difficult to predict. Poorly designed patches might, for instance, encounter a substantially large 'bed-of-nails' effect, preventing their penetration, even for very sharp needle tips.

Thirdly, MNs can be classified according to their *modus operandi*. Six different types of MNs have been reported in the literature so far: solid, hollow, porous, pre-coated, dissolving and swelling MNs[71–74]. The solid, hollow and swelling MN types have been used both for delivery and sampling applications. Pre-coated and dissolving MNs can only be used to discharge substances into the skin tissue while porous MNs can only take up body fluids. As this chapter focuses only on sample collection, the state-of-the-art of MN-based drug and vaccine delivery is not covered here. For a more detailed overview on this, the reader is

recommended to read the reviews by Waghule et al.[75] and Woo Lee & Prausnitz[76].

2.2.2 Microneedle-based sample collection

The different types of MNs that are interesting for capillary blood and ISF sampling are solid, hollow, porous and swelling MNs. Solid MNs are mostly used in a poke-and-release methodology (**Figure 2.14A**), similarly to the previously discussed lancing devices. YourBio Health's TAP II device has an integrated array of solid MNs to puncture skin capillaries (see **Figure 2.14B**) and collect the blood similarly to the previously discussed Tasso devices[77].

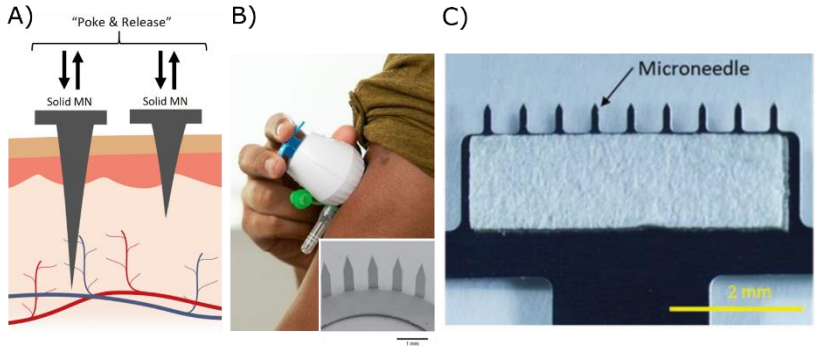

Figure 2.14: *A) Schematic representation of the poke-and-release approach by long or short solid MNs, either to reach the skin capillaries or to avoid them, respectively. B) Commercially available TAP II integrated capillary blood sampling system. The inset shows a solid MN array used by the initial device during development of the system. The microscopy image was taken by Scanning Electron Microscopy. C) Short solid MNs combined with a filter paper patch for the collection of 2 µL ISF within 1 minute. [Figures adapted with permission from[77,79], other copyrights belong to ©YourBio Health[78]]*

A similar poke-and-release approach has been used by the group of Mark R. Prausnitz for collecting up to 2 µL of ISF within 1 minute. Hereto, out-of-plane configured solid MNs with a length of 650 µm with attached filter paper pads (**Figure 2.14C**) were inserted 10-12 times (with a frequency of 1 insertion per second) into hairless rat skin while pinching the skin with a relatively large force (20-40 N)[79,80]. As a result, the gap between the MN shafts and the skin tissue allowed the ISF to flow by capillarity into a piece of filter paper attached to the handler. However, the need

to retract them again after piercing is a disadvantage inherent to solid MNs.

Hollow MNs, instead, create a transdermal duct through which the released sample can be withdrawn, referred to as a poke-and-flow approach. By inserting a wick, reducing the lumen diameter or making the material's surface hydrophilic, capillarity can be used to passively retract the released body fluid[81–83]. However, in general, sample volumes obtained by capillary suction are small and in the range of a few microliters per needle[84]. To illustrate this, for ISF sampling, a one-dimensional hollow MN array proof-of-concept (**Figure 2.15**) was fabricated by combining 32G pen needles in a plastic holder, collecting 16 µL after 1-2 hours of sampling[85].

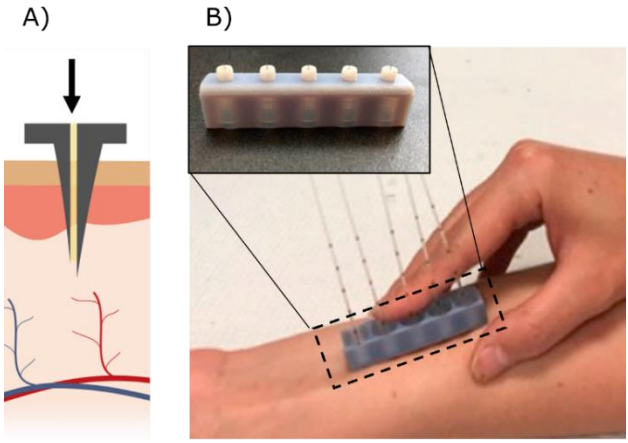

Figure 2.15: *A) Schematic representation of the poke-and-flow approach by short, hollow MNs to avoid piercing capillaries. B) Hollow MNs proof-of-concept combined as a 1-dimensional array into a 3D-printed holder to sample ISF upon capillary filling of the lumen [Figure adopted with permission from[86]].*

Sampling flow rates are often increased by combining multiple MNs in arrays and/or creating an external vacuum. Hereto, Li and colleagues used a pre-stored vacuum inside a PDMS chamber to integrate a negative pressure gradient source with a single MN (**Figure 2.16**)[87]. The latter was fabricated by their novel technique for fabricating sharp SU-8 pillars, i.e. drawing lithography, followed by nickel electroplating and laser cutting.

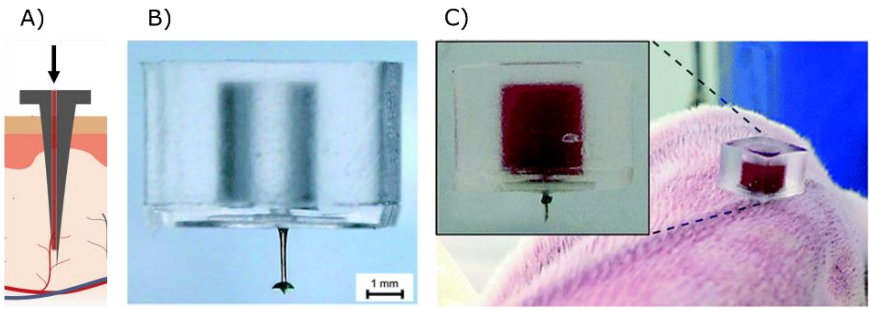

Figure 2.16: *A) Schematic representation of the poke-and-flow approach by a long, hollow MN. B) MN integrated with a PDMS chamber pre-storing a vacuum, which is kept by the sealing at the tip of the MN. C) Upon insertion of the MN into the skin, the sealing is retracted and vacuum is released, withdrawing the blood directly into the PDMS chamber [Figures adopted with permission from*[87]*].*

Hollow MNs are, despite their functional advantage, more challenging to fabricate with a scalable production technology without jeopardizing their strength which is needed to avoid rupture or buckling upon insertion. For example, small-scale 3D-printing has been used but an extra micromachining step was needed to make the fluidic connection through the base plane[88]. Furthermore, shaft lengths above 1500 µm are required to reach capillary blood vessels in the skin, which is even more challenging to achieve without losing aspect ratio and/or out-of-plane configuration for easy integration with a sampling platform[84,89]. The fabrication of such hollow MNs is discussed in detail in the introductory section of Chapter 6.

Finally, porous and swelling MNs are often used for passive ISF sampling. Porous MNs (**Figure 2.17A**) have been fabricated both in metals (e.g. stainless steel or alumina) and polymers (e.g. PDMS or cellulose acetate) by various techniques which are often rather complex to carry out or contain toxic porogens and solvents[74]. A scalable technique using emulsification was proposed by Bao and colleagues to produce biocompatible porous MNs from polylactic acid for ISF sampling[74]. Furthermore, swelling MNs (**Figure 2.17B**) exist of a hydrogel or polymer that swells upon insertion by the uptake of body fluid. However, these are less interesting towards integration with laboratory practices

as bench-top devices such as centrifuges are required for reconstituting the analytes[90,91].

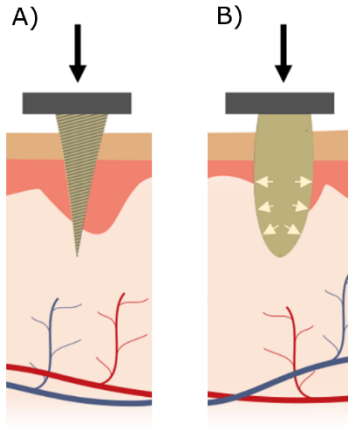

Figure 2.17: *Schematic representations of additional MN types that can be used in a poke-and-flow approach, i.e. A) porous MNs and B) hydrogel-forming or swelling MNs.*

2.2.3 Towards sample in – result out systems

If rapid answers are essential, the ideal solution is the full integration of hollow MNs (arrays) with a POCT microfluidic device, thus providing sample collection, processing and analysis[90]. However, integrated solutions without the need for external syringe pumps or manual handling steps barely exist nowadays. The few examples that combine MNs with paper-based biosensors by direct contact are discussed below.

Firstly, porous MNs are interesting to integrate with paper-based microfluidic platforms because the latter can be just attached as an extension to the sample collection. This way, Lee and co-workers connected porous PDMS MNs for sample collection from a skin-mimicking agarose gel to filter paper for glucose detection by an enzymatic colorimetric reaction (**Figure 2.18A**)[92]. Porous PDMS MNs were integrated with an open capillary pump via microchannels to ensure a continuous flow over an assay chamber for glucose monitoring (**Figure 2.18B**), however, this proof-of-concept only validated the fluidic connection and no on-chip analysis[93]. Furthermore, Jiang and

Lillehoj connected a hollow MN array, consisting of SU-8 MNs polymerized on a PET-substrate, with a test strip for the detection of a malaria biomarker, namely Plasmodium falciparum histidine-rich protein 2 (PfHRP2) (**Figure 2.18C**)[83]. Here, by affixing a hydrophilic membrane between the backside of the hollow MN array and the sample pad, the ISF is transferred from the micro-lumens onto the test strip.

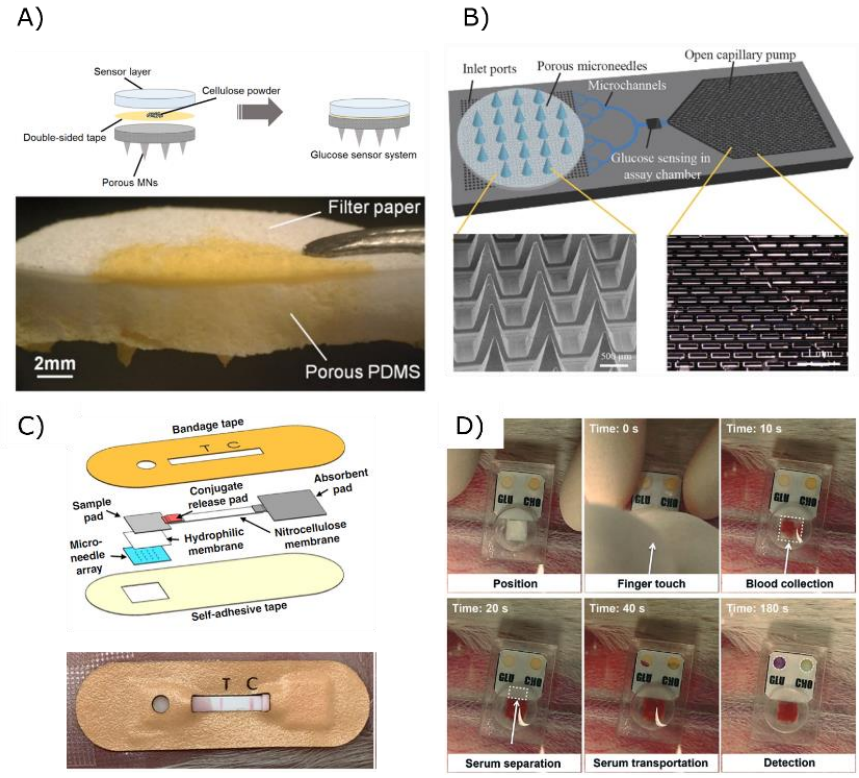

Figure 2.18: *Platforms integrating MN-based sample collection and paper-based testing by direct contact. A) Porous PDMS MNs affixed to a filter paper for single-step enzymatic colorimetric glucose testing. B) Porous PDMS MNs connected to an open capillary pump through microchannels to show the fluidic connection for continuous glucose monitoring. C) Hollow MN array connected to a lateral flow test for PfHRP2 detection. The proof-of-concept was validated on piglet cadaver skin which was previously spiked with PfHRP2. D) Single hollow MN for sampling blood actuated by a PDMS touch-switch and connected to a paper-based platform. The latter filtrated serum from whole blood in advance of loading detection pads for simultaneous glucose and cholesterol measurement. This device was tested on an in vivo rat model by sampling blood from the ear vein. [Figures adopted with permissions from*[92,93,83,94]*]*

Lastly, the single existing proof-of-concept working with extracted blood was shown by Li and colleagues (**Figure 2.18D**). They used a PDMS touch-switch, which had advanced from the previously mentioned PDMS vacuum chamber to a single hollow MN to pull 30 µL blood onto a polysulfone membrane for blood-serum separation. After filtration, the serum sample was drawn further through the filter paper until it reached 2 detection pads for simultaneous glucose and cholesterol measurement.

2.3. References

1. Jurado, C. Toxicology/Drugs of Abuse. in *Encyclopedia of Forensic Sciences* 336–342 (2013).
2. Martial, L. C. *et al.* Cost evaluation of dried blood spot home sampling as compared to conventional sampling for therapeutic drug monitoring in children. *PLoS One* 11, (2016).
3. Ramesh, B. *et al.* LC-HRMS determination of piperine on rat dried blood spots: A pharmacokinetic study. *J Pharm Anal* 6, 18–23 (2016).
4. Ren, X. *et al.* Impact of various factors on radioactivity distribution in different DBS papers. *Bioanalysis* 2, 1469–1475 (2010).
5. Lenk, G., Hansson, J., Beck, O. & Roxhed, N. The effect of drying on the homogeneity of DBS. *Bioanalysis* 7 (2015).
6. Abu-Rabie, P., Denniff, P., Spooner, N., Chowdhry, B. Z. & Pullen, F. S. Investigation of different approaches to incorporating internal standard in DBS quantitative bioanalytical workflows and their effect on nullifying hematocrit-based assay bias. *Anal Chem* 87, 4996–5003 (2015).
7. Parsons, P. J. *et al.* A critical review of the analysis of dried blood spots for characterizing human exposure to inorganic targets using methods based on analytical atomic spectrometry. *J Anal At Spectrom* 35, 2092–2112 (2020).
8. Butler, A. M. *et al.* Newborn thyroid screening: influence of pre-analytic variables on dried blood spot thyrotropin measurement. *Thyroid* 27, 1128–1134 (2017).
9. Denniff, P. & Spooner, N. The effect of hematocrit on assay bias when using DBS samples for the quantitative bioanalysis of drugs. *Bioanalysis* 2, 1385–1395 (2010).
10. Protti, M., Mandrioli, R. & Mercolini, L. Tutorial: Volumetric absorptive microsampling (VAMS). *Analytica Chimica Acta* 1046, 32–47 Preprint at https://doi.org/10.1016/j.aca.2018.09.004 (2019).
11. Jones, C., Dunseath, G. J., Lemon, J. & Luzio, S. D. Microsampling collection methods for measurement of C-peptide in whole blood. *J Diabetes Sci Technol* 12, 1024–1028 (2018).
12. Bloem, K. *et al.* Capillary blood microsampling to determine serum biopharmaceutical concentration: Mitra® microsampler vs dried blood spot. *Bioanalysis* 10, 815–823 (2018).
13. Veenhof, H. *et al.* Volumetric absorptive microsampling and dried blood spot microsampling vs. Conventional venous sampling for tacrolimus trough concentration monitoring. *Clin Chem Lab Med* 58, 1687–1695 (2020).

14. Brooks, K. *et al.* HemaSpot, a novel blood storage device for HIV-1 drug resistance testing. *J Clin Microbiol* 54, 223–225 (2016).
15. Manak, M. M. *et al.* Stability of human immunodeficiency virus serological markers in samples collected as hemaspot and whatman 903 dried blood spots. *J Clin Microbiol* 56, (2018).
16. Serafin, A., Malinowski, M. & Prażmowska-Wilanowska, A. Blood volume and pain perception during finger prick capillary blood sampling: are all safety lancets equal? *Postgrad Med* 132, 288–295 (2020).
17. Kaduskar, O. *et al.* Optimization and stability testing of four commercially available dried blood spot devices for estimating measles and Rubella IgG antibodies. *mSphere* 6, (2021).
18. Spot On Sciences. HemaSpot HF. *https://www.spotonsciences.com/hemaspot-hf/*.
19. Hall, J. M. *et al.* HbA1c determination from HemaSpot™ blood collection devices: comparison of home prepared dried blood spots with standard venous blood analysis. *Diabetic Medicine* 37, 1463–1470 (2020).
20. Prosperi, C. *et al.* Diagnostic accuracy of dried blood spots collected on HemaSpot HF devices compared to venous blood specimens to estimate measles and Rubella seroprevalence. *mSphere* 6, 1–10 (2021).
21. Leuthold, L. A. *et al.* New microfluidic-based sampling procedure for overcoming the hematocrit problem associated with dried blood spot analysis. *Anal Chem* 87, 2068–2071 (2015).
22. HemaXis. HemaXis DB10. *https://hemaxis.com/*.
23. Lenk, G. *et al.* A disposable sampling device to collect volume-measured DBS directly from a fingerprick onto DBS paper. *Bioanalysis* 7, 2085–2094 (2015).
24. Lenk, G., Pohanka, A., Stemme, G., Beck, O. & Roxhed, N. A Disposable chip enabling metering in dried blood spot sampling. in *17th International Conference on Miniaturized Systems for Chemistry and Life Sciences, MicroTAS 2013* 281–283 (2013).
25. Capitainer. Capitainer B. *https://capitainer.se/capitainerb/*.
26. Capitainer. Capitainer B50. *https://capitainer.se/capitainerb50/*.
27. Neto, R., Gooley, A., Breadmore, M. C., Hilder, E. F. & Lapierre, F. Precise, accurate and user-independent blood collection system for dried blood spot sample preparation. *Anal Bioanal Chem* 410, 3315–3323 (2018).
28. Trajan Scientific & Medical. hemaPEN. *https://www.trajanscimed.com/pages/hemapen*.
29. Dungan, K., Chapman, J., Braithwaite, S. S. & Buse, J. Glucose measurement: confounding issues in setting targets for inpatient management. *Diabetes Care* 30, 403–409 (2007).
30. Erbach, M. *et al.* Interferences and limitations in blood glucose self-testing: An overview of the current knowledge. *J Diabetes Sci Technol* 10, 1161–1168 (2016).
31. Morgan, P. E. Microsampling devices for routine therapeutic drug monitoring-are we there yet? *Ther Drug Monit* 43, 322–334 (2021).
32. Chan, P. C. R., Rozmanc, M., Seiden-Long, I. & Kwan, J. Evaluation of a point-of-care glucose meter for general use in complex tertiary care facilities. *Clin Biochem* 42, 1104–1112 (2009).
33. Lenicek Krleza, J., Dorotic, A., Grzunov, A. & Maradin, M. Capillary blood sampling: National recommendations on behalf of the Croatian society of medical biochemistry and laboratory medicine. *Biochem Med (Zagreb)* 25, 335–358 (2015).
34. Tasso. Tasso-M20. *https://www.tassoinc.com/tasso-m20*.
35. Clavijo, C. F. *et al.* A sensitive assay for the quantification of morphine and its active metabolites in human plasma and dried blood spots using

high-performance liquid chromatography-tandem mass spectrometry. *Anal Bioanal Chem* 400, 715–728 (2011).
36. Luginbühl, M. & Gaugler, S. The application of fully automated dried blood spot analysis for liquid chromatography-tandem mass spectrometry using the CAMAG DBS-MS 500 autosampler. *Clin Biochem* 82, 33–39 (2020).
37. Van Holten, T. C., Van Der Horst, F. A. L., Huisman, S. J. & Loupatty, F. J. Formulas for calculating calcium values underestimate hypocalcemia in hemodialysis patients. *Clin Chem* 62, 1533–1534 (2016).
38. van de Velde, D. *et al.* Development and validation of hematocrit level measurement in dried blood spots using near-infrared spectroscopy. *Ther Drug Monit* 43, 351–357 (2021).
39. Deprez, S., Heughebaert, L., Boffel, L. & Stove, C. P. Application of non-contact hematocrit prediction technologies to overcome hematocrit effects on immunosuppressants quantification from dried blood spots. *Talanta* 254, 124111 (2022).
40. Hauser, J. *et al.* High-yield passive plasma filtration from human finger prick blood. *Anal Chem* 90, 13393–13399 (2018).
41. Hauser, J. *et al.* An autonomous microfluidic device for generating volume-defined dried plasma spots. *Anal Chem* 91, 7125–7130 (2019).
42. Kim, J.-H., Woenker, T., Adamec, J. & Regnier, F. E. Simple, miniaturized blood plasma extraction method. *Anal Chem* 85, 11501-11508 (2013).
43. Ordutowski, H. *et al.* Next generation point-of-care test for therapeutic drug monitoring of adalimumab in patients diagnosed with autoimmune diseases. *Biosens Bioelectron* 208 (2022).
44. Ordutowski, H. *et al.* Next generation point-of-care test for therapeutic drug monitoring of adalimumab in patients diagnosed with autoimmune diseases. *Biosens Bioelectron* 208, 114189 (2022).
45. Bransky, A., Larsson, A., Aardal, E., Ben-Yosef, Y. & Christenson, R. H. A novel approach to hematology testing at the point of care. *J Appl Lab Med* 6, 532–542 (2021).
46. Stuart, J., Barrett, B. A. & Prangnell, D. R. Capillary blood collection in haematology. *J Clin Pathol* 27, 869–874 (1974).
47. Folk, L. A. Guide to capillary heelstick blood sampling in infants. *Advances in Neonatal Care* 7, 171–178 (2007).
48. Cobb, Z. *et al.* Feedback from the European Bioanalysis Forum liquid microsampling consortium: Capillary liquid microsampling and assessment of homogeneity of the resultant samples. *Bioanalysis* 11, 525–532 (2019).
49. Bowen, C. L. *et al.* A novel approach to capillary plasma microsampling for quantitative bioanalysis. *Bioanalysis* 5, 1131–1135 (2013).
50. Lapierre, F., Gooley, A. & Breadmore, M. Principles around accurate blood volume collection using capillary action. *Langmuir* 33, 14220–14225 (2017).
51. Sarstedt. Microvette. *https://www.sarstedt.com/en/products/diagnostic/capillary-blood/tubes/*.
52. Tasso. Tasso Plus. *https://www.tassoinc.com/tasso-plus-kit*.
53. Sauer-Budge, A. F. *et al.* A novel device for collecting and dispensing fingerstick blood for point of care testing. *PLoS One* 12, 1–13 (2017).
54. Hopkins, H. *et al.* Blood transfer devices for malaria rapid diagnostic tests: Evaluation of accuracy, safety and ease of use. *Malar J* 10, 1–9 (2011).
55. Incardona, S. *et al.* Accuracy, ease of use, safety, and acceptability of a 23-µL conical cup blood transfer device for use with rapid diagnostic tests. *American Journal of Tropical Medicine and Hygiene* 99, 797–804 (2018).

56. Luchavez, J., Lintag, M. E., Coll-Black, M., Baik, F. & Bell, D. An assessment of various blood collection and transfer methods used for malaria rapid diagnostic tests. *Malar J* 6, 1–5 (2007).
57. Peck, R. B. *et al.* What Should the IDEAL HIV self-test look like? A usability study of test prototypes in unsupervised HIV self-testing in Kenya, Malawi, and South Africa. *AIDS Behav* 18, 422–432 (2014).
58. Smith, S., Korvink, J. G., Mager, D. & Land, K. The potential of paper-based diagnostics to meet the ASSURED criteria. *RSC Adv* 8, 34012–34034 (2018).
59. Atomo Diagnostics. AtomoRapid™ HIV 1&2. *https://www.atomodiagnostics.com/products/hiv_tests/*.
60. Gill, H. S., Denson, D. D., Burris, B. A. & Prausnitz, M. R. Effect of microneedle design on pain in human volunteers. *Clinical Journal of Pain* 24, 585–594 (2008).
61. Ebrahiminejad, V., Prewett, P. D., Davies, G. J. & Faraji Rad, Z. Microneedle arrays for drug delivery and diagnostics: toward an optimized design, reliable insertion, and penetration. *Adv Mater Interfaces* 9, 1–26 (2022).
62. Smart, W. H. & Subramanian, K. The use of silicon microfabrication technology in painless blood glucose monitoring. *Diabetes Technol Ther* 2, 549–559 (2000).
63. Gerstel, M. S. & Place, V. A. Drug delivery device - US 3964482 A. *U. S. Patent* 482, (1976).
64. Roxhed, N., Gasser, T. C., Griss, P., Holzapfel, G. A. & Stemme, G. Penetration-enhanced ultrasharp microneedles and prediction on skin interaction for efficient transdermal drug delivery. *Journal of Microelectromechanical Systems* 16, 1429–1440 (2007).
65. Lee, S., Jeong, W. & Beebe, D. J. Microfluidic valve with cored glass microneedle for microinjection. *Lab Chip* 3, 164–167 (2003).
66. Ita, K. Transdermal delivery of drugs with microneedles—potential and challenges. *Pharmaceutics* 7, 90–105 (2015).
67. Tsuchiya, K., Jinnin, S., Yamamoto, H., Uetsuji, Y. & Nakamachi, E. Design and development of a biocompatible painless microneedle by the ion sputtering deposition method. *Precis Eng* 34, 461–466 (2010).
68. García-López, E., Siller, H. R. & Rodríguez, C. A. Study of the fabrication of AISI 316L microneedle arrays. in *46th SME North American Manufacturing Research Conference* 26, 117–124 (2018).
69. Juster, H., van der Aar, B. & de Brouwer, H. A review on microfabrication of thermoplastic polymer-based microneedle arrays. *Polym Eng Sci* 264, 125521 (2019).
70. Olatunji, O. & Denloye, A. Production of hydrogel microneedles from fish scale biopolymer. *J Polym Environ* 27, 1252–1258 (2019).
71. Tariq, N., Ashraf, M. W. & Tayyaba, S. A review on solid microneedles for biomedical applications. *J Pharm Innov* 17, 1464–1483 (2021).
72. Cárcamo-Martínez, Á. *et al.* Hollow microneedles: a perspective in biomedical applications. *Int J Pharm* 599, (2021).
73. Turner, J. G., White, L. R., Estrela, P. & Leese, H. S. Hydrogel-forming microneedles: current advancements and future trends. *Macromol Biosci* 21, 1–18 (2021).
74. Bao, L., Park, J., Bonfante, G. & Kim, B. Recent advances in porous microneedles: materials, fabrication, and transdermal applications. *Drug Deliv Transl Res* 12, 395–414 (2022).
75. Waghule, T. *et al.* Microneedles: A smart approach and increasing potential for transdermal drug delivery system. *Biomedicine and Pharmacotherapy* 109, 1249–1258 (2019).

76. Lee, J. W. & Prausnitz, M. R. Drug delivery using microneedle patches: not just for skin. *Expert Opin Drug Deliv* 15, 541–543 (2018).
77. Blicharz, T. M. *et al.* Microneedle-based device for the one-step painless collection of capillary blood samples. *Nat Biomed Eng* 2, 151–157 (2018).
78. YourBio Health. TAP® II. *https://yourbiohealth.com/en-us/virtually-painless-blood-collection-devices-for-clinical-trials-and-wellness-testing*.
79. Kolluru, C. *et al.* Plasmonic paper microneedle patch for on-patch detection of molecules in dermal interstitial fluid. 4, 6, 1569–1576 (2019).
80. Kolluru, C., Williams, M., Chae, J. & Prausnitz, M. R. Recruitment and collection of dermal interstitial fluid using a microneedle patch. *Adv Healthc Mater* 453, 139902 (2019).
81. Li, T., Barnett, A., Rogers, K. L. & Gianchandani, Y. B. A blood sampling microsystem for pharmacokinetic applications: design, fabrication, and initial results. *Lab Chip* (2009).
82. Strambini, L. M. *et al.* Self-powered microneedle-based biosensors for pain-free high-accuracy measurement of glycaemia in interstitial fluid. *Biosens Bioelectron* 66, 162–168 (2015).
83. Jiang, X. & Lillehoj, P. B. Microneedle-based skin patch for blood-free rapid diagnostic testing. *Microsyst Nanoeng* 6 (2020).
84. Liu, L., Wang, Y., Yao, J., Yang, C. & Ding, G. A minimally invasive micro sampler for quantitative sampling with an ultrahigh-aspect-ratio microneedle and a PDMS actuator. *Biomed Microdevices* 18 (2016).
85. Miller, P. R. *et al.* Extraction and biomolecular analysis of dermal interstitial fluid collected with hollow microneedles. *Commun Biol* 1, (2018).
86. Tran, B. Q. *et al.* Proteomic characterization of dermal interstitial fluid extracted using a novel microneedle-assisted technique. *J Proteome Res* 17, 479–485 (2018).
87. Li, C. G., Lee, C. Y., Lee, K. & Jung, H. An optimized hollow microneedle for minimally invasive blood extraction. *Biomed Microdevices* 15, 17–25 (2013).
88. Miller, P. R. *et al.* Microneedle-based transdermal sensor for on-chip potentiometric determination of K+. *Adv Healthc Mater* **3**, 876–881 (2014).
89. Chaudhri, B. P., Ceyssens, F., De Moor, P., Van Hoof, C. & Puers, R. A high aspect ratio SU-8 fabrication technique for hollow microneedles for transdermal drug delivery and blood extraction. *Journal of Micromechanics and Microengineering* 20, (2010).
90. Romanyuk, A. V. *et al.* Collection of analytes from microneedle patches. *Anal Chem* 86, 10520–10523 (2014).
91. O'Farrell, B. Lateral flow technology for field-based applications-basics and advanced developments. *Top Companion Anim Med* 30, 139–147 (2015).
92. Lee, H. *et al.* Porous microneedle integrated in paper based glucose sensor for fluid channel interface. *2019 IEEE CPMT Symposium Japan, ICSJ 2019* 39–42 (2019).
93. Takeuchi, K. *et al.* Microfluidic chip connected to porous microneedle array for continuous ISF sampling. *Drug Deliv Transl Res* 12, 435–443 (2021).
94. Li, C. G. *et al.* One-touch-activated blood multidiagnostic system using a minimally invasive hollow microneedle integrated with a paper-based sensor. *Lab Chip* 15, 3286–3292 (2015).

Chapter 3

Precise sample metering method by coordinated burst action of hydrophobic burst valves applied to dried blood spot collection

The work reported in this chapter is adapted from:

Vloemans D.*, **Van Hileghem L.***, Verbist W., Thomas D., Dal Dosso F. and Lammertyn J. (2021). Precise sample metering method by coordinated burst action of hydrophobic burst valves applied to dried blood spot collection. Lab Chip, 21, 4445-4454.

*Equal contributions.

Van Hileghem L. contributed to this work in terms of conceptualization, experimental design, planning and execution of the experiments, next to writing and editing of the text.

3.1. Introduction

Dried blood spot (DBS) sampling of capillary blood is a promising minimally invasive alternative to conventional venipuncture[1]. DBS sampling, exploited for the first time for new-born screening in the 1960s[2,3], has now shown its applicability in a multitude of areas like therapeutic drug monitoring (TDM)[4,5], pharmacokinetics[6] and diagnosis of infectious diseases (e.g. HIV)[7]. These applications take advantage of improved logistical convenience, reduced cost, automatable processing and analysis, and increased analyte stability[8,9].

Despite the advantages, the high variability in blood sample hematocrit (Hct) levels (ranging between 23 and 67%) among different groups of patients[4,10–12] induces biases in quantitative bioanalyses. In fact, as blood with different Hct levels spreads differently through filter paper as a direct consequence of its different viscosity[13–15], DBS sub-punches with the same area contain different blood volumes linked to the respective Hct levels. Denniff and Spooner characterized a difference in blood volume of 35% across a Hct range of 0.2-0.8[12]. Additionally, since red blood cells (RBCs) tend to accumulate at the edges of the DBS (14% higher RBC concentration at edges compared to center)[16], referred to as the volcano effect, applying larger blood volumes or taking sub-punches in the central versus peripheral area of the DBS will lead to different assay data[17,18]. Furthermore, the susceptibility of the DBS method to contamination is a frequently reported problem due to, for instance, impurities and cell debris from the finger and imperfect sealing from the environment[19].

Different approaches to overcome the Hct-dependent spreading issue were reported. The first solutions, including pre-cut DBS papers[20] or perforated DBS papers in combination with micropipettes or microcapillaries[21], lack control over precise volume application and user-friendliness, respectively. Volumetric absorptive micro samplers (VAMS®)[22] form an interesting solution in this direction, however, trials indicated that the tool is still relatively fallible for poor sample loading,

significantly altering the absorbed blood volume[23,24]. Another approach, the volumetric absorptive paper disc (VAPD) and its downscaled version (VAPD-mini), sought to tackle the Hct effect by combining the VAMS principle with traditional DBS[25]. However, to circumvent user-dependency, direct finger contact during sample loading must be avoided. Therefore, improved strategies combine a microfluidic metering concept with the capillary action of a collection channel, allowing whole-spot analysis. The HemaXis DB device[26] and the Capitainer qDBS card[27] are important examples here, showing volumetric loading of capillary blood in the range of 5-13.5 µL. Possible disadvantages in terms of contamination are conceivably improved by Neto et al. as they combined glass capillaries with pre-punched filter papers in a closed, pen-like handler, the HemaPEN[28]. Though, it only allows for sampling small volumes of 3 µL which limits its application in case multiple assays are needed, or for assays that require larger sample volumes. Altogether, current microfluidic techniques are based on the capillary interaction of the sample itself and do not allow parallel loading of different DBS from a single blood drop or further downstream processing of the sample.

In this work, a passive, low-cost and user-friendly microfluidic DBS sampling device (SIMPLE-DBS) is presented, utilizing coordinated burst actions of hydrophobic burst valves (HBVs) with configurable burst pressures. Hereto, the influence of two fluorinated solutions coated on specific channel regions on the contact angle and burst pressure is assessed. The HBVs enable parallel metering of predefined blood volumes starting from an unknown sample volume, ideal for multiplexed analyses on the same sample. To bring this concept at the point-of-care (POC) in a portable and autonomous device, the HBV-based metering system is integrated with our established SIMPLE platform with integrated pre-cut DBS papers[29–31]. To prove not only the technical advantages but also the analytical performance, our system is validated in the context of TDM of biologicals comparing it with the current traditional DBS method (e.g. Whatman 903 card) using citrated blood samples spiked with adalimumab (ADM).

3.2. Materials and methods

3.2.1 Reagents and materials

Whatman quantitative filter paper grades 43 and 598 (with respective thicknesses of 220 and 320 µm), Whatman 903 protein saver cards, sulphuric acid (H_2SO_4) and horseradish peroxidase (HRP) were obtained from Sigma-Aldrich (Belgium). Whatman qualitative filter paper grade CF12 was purchased from GE Healthcare (Belgium). Merck (Germany) delivered the peroxide (H_2O_2) and the o-phenylenediamine was obtained from Acros Organics (Belgium). PVC plastic films of 180 µm thickness were bought from Delbo (Belgium). Double-sided pressure-sensitive adhesive (PSA) tape (200MP 7956MP) and transfer tape (467MP) were acquired from 3M (USA). Aquapel® and Fluoropel™ 800M hydrophobic agents were purchased from Aquapel (USA) and Cytonix (USA), respectively. Adalimumab (clone DE27) was acquired from Bio-rad laboratories (Belgium). Superblock™ T20 (PBS) blocking buffer was bought at Thermofisher Scientific (Germany). Monoclonal anti-ADM capture antibodies (MA-ADM28B8) and HRP-conjugated anti-ADM detection antibodies (MA-ADM40D8) were generated in-house at the Laboratory for Therapeutic and Diagnostic Antibodies (KU Leuven, Belgium)[32].

3.2.2 Microfluidic device fabrication

All microfluidic devices were fabricated using the low-cost and rapid lamination method proposed by Yuen et al[33]. A microfluidic channel network was cut in a PSA layer using a digital craft cutter (Maxx Air 24 in., KNK, USA), and sealed with PVC films from the bottom and topside. The latter included the precut inlet, vent and prefilling holes. Single- and double-coated (sc/dc) HBVs were integrated by locally coating the bottom and/or top PVC film with hydrophobic fluorinated solutions (see Section 3.2.3). The Aquapel® solution was also used to create the gas-permeable hydrophobic stop valves (HSV), as previously described[30]. In short, small rectangular patches (1.5 x 3 mm²) were cut in Whatman grade 43 or 598 filter paper, with a second craft cutter (Silhouette Cameo, Netherlands) and afterwards impregnated with Aquapel®. The microfluidic devices used in Sections 3.3.3

and 3.3.4 were integrated with the self-powered SIMPLE pumping technology as driving source. In this technology, the wicking action of a working liquid in a paper substrate is exploited to generate pressure differences within the connected microfluidic network and, hence, to manipulate the liquid through it. For a more detailed explanation the reader is referred to our previous work[29,30,34,35]. The paper substrate (Whatman grade 598) of the SIMPLE pump module was cut with the Silhouette Cameo craft cutter and then inserted in its respective PSA chamber followed by sealing with the PVC films. The same craft cutter was used to cut the DBS paper (Whatman CF12) inserted in the integrated SIMPLE-based microfluidic DBS sampling device (SIMPLE-DBS, Section 3.3.4). After device assembly, the working liquid (1:20 diluted blue food dye in distilled water), acting as fuel of the pump module, was prefilled into the microfluidic device via the prefilling hole. The latter was finally sealed from the environment with a small PSA patch.

3.2.3 HBV fabrication

The surface properties of the microfluidic channels were locally altered by applying a hydrophobic fluorinated agent on the PVC surface via a mask-based coating strategy (**Figure 3.1A**). Hereto, a PSA mask with a rectangular cut-out (4 x 5 mm²) was applied to a PVC substrate (first rinsed with distilled water, then dried at room temperature) to retain the hydrophobic solution (Aquapel® or Fluoropel™). To ensure proper mask positioning, alignment markers were patterned on the PVC films during the cutting process. For the Aquapel® treatment, 2 µL (0.1 µL/mm²) was applied, followed by a 1-hour incubation at 50 °C. For Fluoropel™, 4 µL (0.2 µL/mm²) was used, followed by a 10 minute incubation step at 50 °C and kept for at least 2 hours at room temperature before use. After drying, the PSA mask was removed from the PVC substrate. The Aquapel® and Fluoropel™ coated substrates were integrated in a microfluidic channel as bottom to create a sc HBV or as bottom and top for the dc HBV (**Figure 3.1B**). **Figure 3.1C** shows the 5 different types of HBVs created by combining Aquapel® and Fluoropel™ coatings.

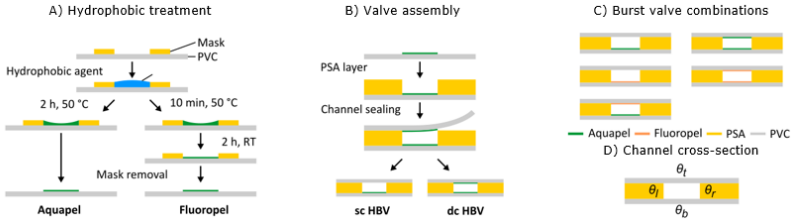

***Figure 3.1**: Schematic overviews of (A) mask-based hydrophobic treatment strategy of PVC with Aquapel® and Fluoropel™ agent, (B) assembly of microfluidic channel to form sc and dc HBVs, (C) different types of HBVs using varying Aquapel-Fluoropel combinations at top and/or bottom of the channel, and (D) cross-section of microfluidic channel with different channel wall materials and contact angles.*

3.2.4 HBV characterization

Water contact angle measurements were performed to assess the hydrophobic properties and uniformity of the coated PVC substrates. To evaluate the homogeneity of the coating, a larger mask of 5 x 15 mm² was applied to the PVC substrate which was then coated with the respective Aquapel® and Fluoropel™ hydrophobic agents. For each coating, 3 samples were prepared from which water contact angles were determined from at least 4 randomly positioned water droplets (5-10 µL) on the coated region using a CAM200 goniometer (KSV Instruments, Finland) and associated fitting software.

By combining the Fluoropel™ and Aquapel® coatings, 5 different types of HBVs were formed as illustrated in **Figure 3.1C**. To evaluate the strength of each burst valve, the burst pressure of all coating combinations was experimentally determined and compared with theoretical values. The walls of the microfluidic channels have different water contact angles due to the layer-by-layer fabrication of different materials (**Figure 3.1D**). As a consequence, the extended Young-Laplace equation (Eq. (3.1)) was used to calculate the pressure difference within the channels[35]:

$$P_c = -\gamma\left(\left(\frac{\cos\theta_t+\cos\theta_b}{h}\right)+\left(\frac{\cos\theta_l+\cos\theta_r}{w}\right)\right) \qquad \text{Eq. (3.1)}$$

Here *Pc* [Pa] reflects the pressure difference (capillary pressure) over the liquid-air interface of the meniscus, *γ* [N/m] is the water

surface tension and θ [°] with subscripts t, b, l and r is the contact angle of the top, bottom, left and right channel wall, respectively. W [m] and h [m] indicate the width and height of the channel.

Using Eq. (3.1), the burst pressure (ΔP_b [Pa]) of the HBVs was calculated as the difference of the capillary pressure from the untreated ($P_{c,1}$) and the hydrophobically treated channel part ($P_{c,2}$) with respective water contact angles of $\theta_{c,1}$ and $\theta_{c,2}$. As only the top and/or bottom of the channel were treated, the equation of the burst pressure (Eq. (3.2)) is given by:

$$\Delta P_b = -\gamma \left(\left(\frac{\cos \theta_{t,2} + \cos \theta_{b,2}}{h} \right) - \left(\frac{\cos \theta_{t,1} + \cos \theta_{b,1}}{h} \right) \right) \qquad \text{Eq. (3.2)}$$

where subscripts 1 and 2 indicate the untreated and treated channel part, respectively. By inserting the contact angles for θ_t and θ_b, in Eq.(3.2) the theoretical burst pressure for each type of HBV was calculated. From Eq. (3.2) follows that the burst pressure of the HBV is only influenced by the height and the hydrophobic properties of the bottom or/and top of the microchannel, while the channel width does not play a role (see Section 3.5.4 Supporting Information for more details).

To experimentally determine the burst pressure of each HBV type, a pressure pump (LINEUP FLOW EZ™ SERIES 1000 mBar, Fluigent, France) was connected to a microfluidic channel having a width of 1.0 mm with incorporated HBV (fabricated as described in Section 3.2.2 and 3.2.3) and used to inject distilled water. The flow was maintained at a constant rate of 2 µL/min via an attached flow rate sensor (Flow unit M, Fluigent, France), while the applied pressure was recorded in real-time at 10 Hz.

The burst pressure was obtained by taking the average pressure increase in the time interval in which the liquid meniscus is moving through the HBV after normalizing the absolute pressure to the baseline pressure. The latter refers to the required pressure to push the liquid through the channel without HBV (for more details, see Section 3.5.1 of the Supporting Information). Tukey multiple comparison tests were performed

to determine significant differences between the different mean burst pressures.

3.2.5 Sample metering system characterization

Citrated human whole blood was collected from healthy volunteers via venous puncture, after signing an informed consent form, and was processed within 24 hours of withdrawal. All experiments were approved by the UZ/KU Leuven Ethics Committee, Belgium (S62134). The blood was aliquoted in 2 mL samples and centrifuged at 2400 g for 15 minutes to separate the RBCs from the plasma. The plasma fraction in the samples was removed and volumetrically quantified from the aliquots to determine the initial Hct level. The remaining RBCs were reconstituted with a defined volume of the extracted blood plasma to prepare blood samples with specific Hct levels of 25, 40, 55 and 70%.

The volumetric performance of the microfluidic metering system was assessed by a gravimetric method (see Section 3.5.2, Supporting Information for setup and accuracy of the methodology). Microfluidic devices incorporating the metering system were fabricated and 20 µL of the blood sample was prefilled in a collection channel. A syringe pump (PHD 2000, Harvard Apparatus, USA) was used to drive the sample through the microfluidic network (Figure 3.10, Supporting Information) in which a metered volume was split from the sample and subsequently loaded on top of a circular Whatman grade CF12 paper substrate. The weight difference of the paper was quantified using a high precision weighing balance (CPA124S, Sartorius, Germany) before and immediately after sample loading, assuming negligible weight loss due to evaporation. The relative mass difference was converted to volume units using the respective density of the measured sample, which were calculated based on the relative density of the plasma (1.025 g/µL) and RBC (1.125 g/µL) fractions, resulting in 1.050, 1.065, 1.080, and 1.095 g/µL for Hct levels of 25, 40, 55 and 70%, respectively. The accuracy and reproducibility of the metering system were determined in two ways: i) for 3 volumes, 5, 10 and

15 µL, using 40% Hct blood samples, and ii) for 4 Hct levels of 25, 40, 55 and 70% using a fixed target volume of 10 µL.

3.2.6 Validation of the SIMPLE-DBS sampling device

To assess both the technical and the analytical system performance, a comparative study between the developed microfluidic SIMPLE-DBS sampling device, with integrated self-powered SIMPLE pumping unit (see Section 3.2.2), and traditional Whatman protein saver cards was executed. In particular, 16 SIMPLE-DBS devices were run with human citrated blood (40% Hct) spiked with different ADM concentrations of 0, 1, 4 and 16 µg/mL to prepare 10 µL metered DBS samples. Standard DBS samples were prepared by spotting (using a micropipette) 40 and 10 µL of the same citrated blood samples on traditional Whatman protein saver cards. All DBS samples were left open to the air at room temperature for 24 hours to ensure complete drying. For extracting the 40 µL spotted DBS samples, a 6 mm diameter disc was punched out the center of the spot and transferred to a 1.5 mL Falcon tube holding 240 µL Superblock™ T20 (PBS) buffer. The samples were incubated under continuous shaking for 1 hour at 21 °C and 300 rpm, followed by a 5 minute centrifugation step at 14 000 RCF. Finally, 180 µL of the supernatant was transferred to an Eppendorf tube and stored at -20 °C. Both the Whatman protein saver cards spotted with 10 µL and the SIMPLE-DBS samples were extracted as a whole, i.e. without taking a sub-punch from the blood spot, using the same protocol.

To quantify the ADM concentrations in the DBS samples, an in-house developed sandwich ELISA was used[31]. Briefly, 96-well plates were coated with the capturing antibody MA-ADM28B8 for 72 h at 4 °C and blocked with 1% bovine serum albumin (BSA) in PBS, after which the diluted DBS extract samples were incubated overnight at 4 °C. Detection was performed using the HRP conjugated detecting antibody MA-ADM40D8 at room temperature. The plate was then washed and developed with o-phenylenediamine and H_2O_2 in citrate buffer for signal generation. The enzymatic reaction was stopped with H_2SO_4 (4 M), followed by measuring the absorbance at 492 nm with an

ELx808 Absorbance Microplate Reader (BioTek Instruments Inc., USA). Optical density values were interpolated from the standard curve to calculate the ADM concentrations in the DBS samples. Next, the bias was calculated as the difference of the measured and spiked ADM concentration divided by the spiked one and evaluated for the 3 different configurations (SIMPLE-DBS system, traditional 40 µL spotted Whatman protein saver cards and the 10 µL spotted cards).

3.3. Results and discussion

3.3.1 HBV characterization

The hydrophobic surface properties of the treated PVC substrates were analyzed for both Aquapel® and Fluoropel™ agents and compared with the properties of the untreated PVC surface. As depicted in **Figure 3.2**, the water contact angle of untreated PVC (91.6 ± 3.4°) was increased to 119.0 ± 2.8° and 161.1 ± 5.0° for Aquapel® and Fluoropel™, respectively. The small standard deviations illustrate that both Fluoropel™ and Aquapel® coatings led to homogenous properties over the entire treated region which were reproducible over multiple samples.

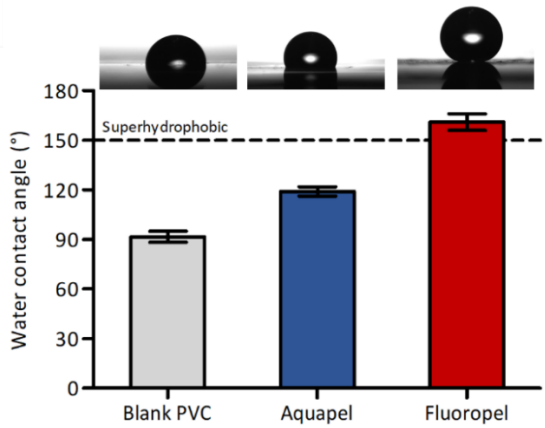

***Figure 3.2**: Bar chart indicating average water contact angles of the untreated and Aquapel®, Fluoropel™ treated PVC substrates. For each condition 3 samples were prepared and the contact angles for at least 4 droplets were measured per sample. Error bars represent one standard deviation. The dotted line indicates the superhydrophobic region (> 150°). Above each bar, a picture of a measurement is shown for the respective coating.*

To characterize the burst pressures, 5 different types of HBVs were fabricated by combining the Aquapel® and Fluoropel™ coatings as described in Section 3.2.3. In **Figure 3.3A**, the normalized average pressure profiles for sc Aquapel® and dc Fluoropel-Aquapel HBVs are illustrated as an example. These profiles are in agreement with the expected pressure profile (Figure 3.9B, Supporting Information), showing that the required pressure to maintain a constant flow rate, increases from the moment the meniscus of the liquid front reaches the HBV. Once the meniscus passes the full length of the HBV, the pressure drops again to its baseline pressure. As shown in **Figure 3.3A**, the required pressure to push a liquid over the dc Fluoropel-Aquapel HBV is significantly higher than the sc Aquapel® HBV. The average burst pressure for each valve combination is summarized in **Figure 3.3B** (complete values are compiled in Table 3.1, Supporting Information). The developed HBVs are configurable within a burst pressure range between ~175 and 600 Pa using a simple but robust approach without complex geometric features in the channel as mostly reported in literature[36]. Additionally, 4 out of the 5 valve types show a significant difference ($p < 0.05$) in burst pressure which is particularly interesting for enabling passive sequential liquid handlings.

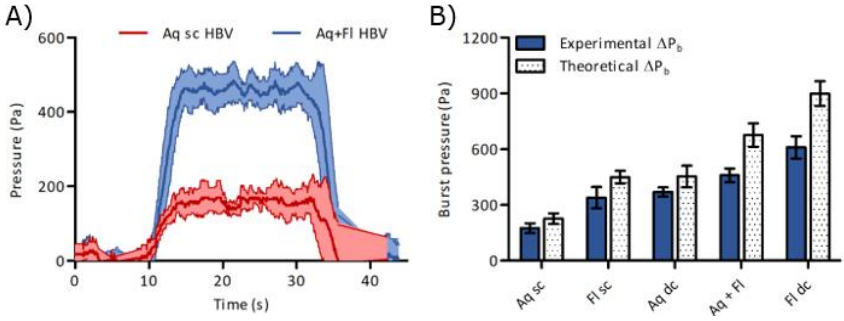

Figure 3.3*: A) Normalized average pressure profiles (solid lines) of sc Aquapel® and dc Fluoropel-Aquapel HBVs. Shaded zones represent one standard deviation (n = 6). B) Theoretical vs. experimental burst pressures of the different HBVs in 1.0 mm wide microfluidic channels. Error bars represent one standard deviation (n ≥ 6). Different letters above bars indicate significant differences between the means (α = 0.05).*

Figure 3.3B only illustrates the effect of the valve configuration (e.g. different combinations of hydrophobic coatings) on the burst pressure, while the relation between the microchannel dimensions (width and height) and burst pressure was evaluated in depth as well (Section 3.5.4, Supporting Information). The obtained results are in agreement with Eq. (3.2) and confirm that only the channel height influences the burst pressure while the effect of the channel width was found to be negligible.

The experimentally determined burst pressures were also compared with their respective theoretical values (**Figure 3.3B**). These were calculated by inserting the obtained water contact angles (Section 3.3.1) of the untreated PVC and Aquapel®/Fluoropel™ treated substrates in Eq. (3.2). As expected, a similar trend for the theoretical and experimental burst pressures for the five valve types was observed (**Figure 3.3B**), although, measured burst pressures are significantly lower. This discrepancy might be explained by the current manual coating and assembly process or the use of the static instead of dynamic contact angles in the theoretical calculations (see Supporting Information Section 3.5.3)[37,38].

3.3.2 Sample metering system

Two of the four valve types (sc Aquapel® and dc Aquapel-Fluoropel) presented in the previous section were combined and integrated into a microfluidic system to enable the isolation and further manipulation of a precisely metered liquid volume from an unknown source volume. In **Figure 3.4**, the different steps of the metering workflow are shown.

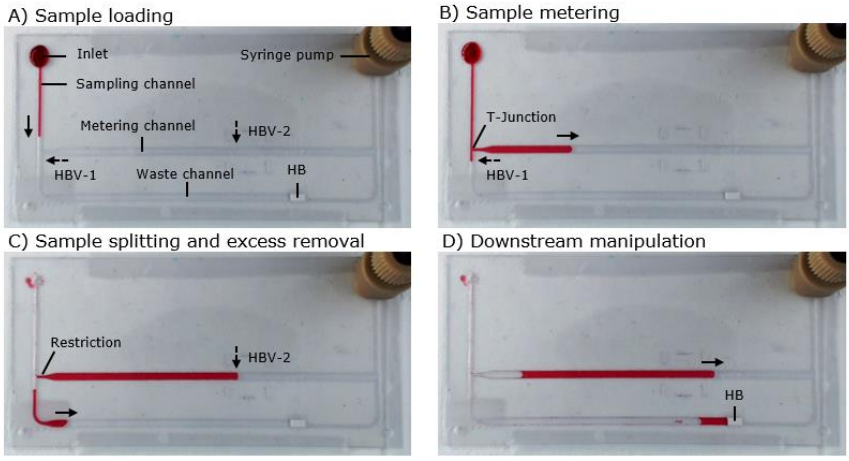

***Figure 3.4**: Working principle of sample metering system. A) The sample is first loaded into the sampling channel until B) its front meniscus reaches the T-junction where the sc HBV (HBV-1) directs the liquid into the metering channel. C) Upon complete filling of the metering channel, the sample is blocked by dc HBV (HBV-2) leading to HBV-1 to burst and flowing of sample excess into the waste channel. As a result, the liquid in the metering channel becomes an isolated plug. D) Finally, the HSV forces the metered sample liquid to burst through the HBV-2 and becomes available for downstream processes.*

First, a droplet of red colored aqueous liquid is deposited on the inlet of the microfluidic network. Next, the sample is drawn in the sampling channel by a syringe pump (**Figure 3.4A**). A T-junction is located downstream the sampling channel, splitting the system into a metering and a waste channel. As the meniscus of the incoming sample liquid reaches this junction, a sc Aquapel® HBV (HBV-1) directs the flow into the metering channel (**Figure 3.4B**). Upon complete filling of the metering channel, the sample is stopped by a dc Fluoropel-Aquapel HBV (HBV-2), which forces HBV-1 to burst according to the respective burst pressures. This way, the sample excess is directed into the waste channel until the receding liquid front reaches the T-junction and the excess volume splits from the metered plug (**Figure 3.4C**). Next, the sample excess is pulled to the end of the waste channel where a HSV blocks the flow. As a result, the isolated sample plug in the metering channel bursts through HBV-2 (**Figure 3.4D**) and the metered sample volume can then be further manipulated downstream.

Gravimetric measurements were performed to determine the volumetric performance of the metering system as exact blood volume metering and loading are key in DBS sampling to convert the measured analyte values to correct concentrations. The results of the gravimetric measurements (10 repetitions each), shown in **Figure 3.5A**, illustrate a good reproducibility (CV < 3%) of the metering system for each target volume (5, 10 and 15 µL). The high accuracy of the system was confirmed as well as the bias of the average metered volumes were found to deviate maximally 3% below the target volumes. This drop was expected to some extent because a small fraction of the sample liquid remains trapped in the channel walls imperfections. The bias between the measured and target volume slightly increases with larger target volumes (close ups in **Figure 3.5A**) confirming that the loss is proportional to the length of the channels, and, hence, this loss can be compensated for when designing the channel network. The overall good performance over the range of target volumes is confirmed by the good linear fit (R^2 = 0.99) to all gravimetric data points with a slope close to 1 as is illustrated in **Figure 3.5A** (see Table 3.4 in Supporting Information for the exact values).

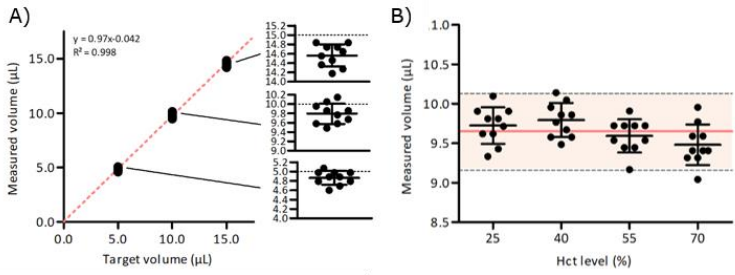

***Figure 3.5**: Gravimetric characterization of sample metering system. A) Measured vs. target volumes (5, 10 and 15 µL) of metered blood samples (Hct level of 40%) with close-ups of individual volume measurements (n=10) with mean and standard deviation for each target volume. B) Measurements of metered blood samples with different Hct levels of 25, 40, 55 and 70%. Solid red and dashed grey lines illustrate the global volume average (9.65 µL) over all Hct levels and 5% error zone around this average, respectively. For each Hct level, also separate averages (black lines) are given with error bars reflecting one standard deviation (n=10).*

To even further improve the accuracy and reproducibility, the system would benefit from automated fabrication methods such as roll-to-roll manufacturing and micropatterning techniques. Consequently, channels with higher resolution and better alignment of the hydrophobic patches and different plastic layers can be achieved.

Similar gravimetric measurements were performed to evaluate the Hct-dependency of the microfluidic metering system. As the Hct levels between different patients can show large variability, the analyzed results from traditional DBS sampling methods often show bias and cannot be trusted[15,39]. To account for these variations, the Hct levels were varied between 25 and 70%, covering more than the typical physiological range for humans. The results (again 10 repetitions each) are depicted in **Figure 3.5B** (and Table 3.4, Supporting Information) showing no significant difference in measured volumes (target volume 10 µL) for 25, 40, 55 and 70% Hct levels. Remarkably, CV values below 3% were observed for all measurements indicating that a varying level of RBCs does not influence the reproducibility of the metering system. When all individual gravimetric measurements are compared to the global average (9.65 µL, represented by the full red line in **Figure 3.5B**), 95% (38 out of 40) of the data points are located within the 5% error zone around the mean (dashed grey lines in **Figure 3.5B**).

The data show a significant improvement to traditional methods, where a volume variability up to 29% was observed across a similar Hct range[10]. VAMS were shown to have a variability of 3.6% (CV%)[21], however, an inter-laboratory experiment showed a variability up to 8.7% (CV%)[22], illustrating the need for user-independent metering systems. Channel-based systems like the ones from Neto et al. and Lenk et al. show overall CVs of ≤ 3.0%, a threshold that is matched by our metering system[26,27].

3.3.3 Parallel sample metering on SIMPLE

To show the potential of the metering system in splitting a single sample drop in multiple liquid plugs of exact volume sizes, a microfluidic chip (**Figure 3.6A**) with 3 metering channels of different volumes (5, 10 and 15 µL) was designed. Here, the syringe pump was replaced by a SIMPLE unit acting as a passive driving source to manipulate the liquid through the system, showing the applicability of this concept at the POC. The working principle of the SIMPLE has been presented previously[29,30,33,34], but briefly, a triangular-shaped nitrocellulose porous substrate (Whatman grade 598) creates a negative pressure upon wicking in the prefilled working liquid (blue water in **Figure 3.6**). Hence, the sample is drawn into the inlet and through the metering system. Similar to the metering concept discussed in Section 3.3.2 above, a sc HBV first forces the incoming sample liquid to fill the metering channels, after which the sample excess is discarded to the waste channel. After removal of the sample excess, each individually isolated sample volume bursts through the dc HBV and is manipulated downstream until they reach the HSVs (see **Figure 3.6B**). An additional HSV (HSV-5) was inserted at the receding backside of the prefilled working liquid to direct the working liquid towards the porous paper upon finger-press activation.

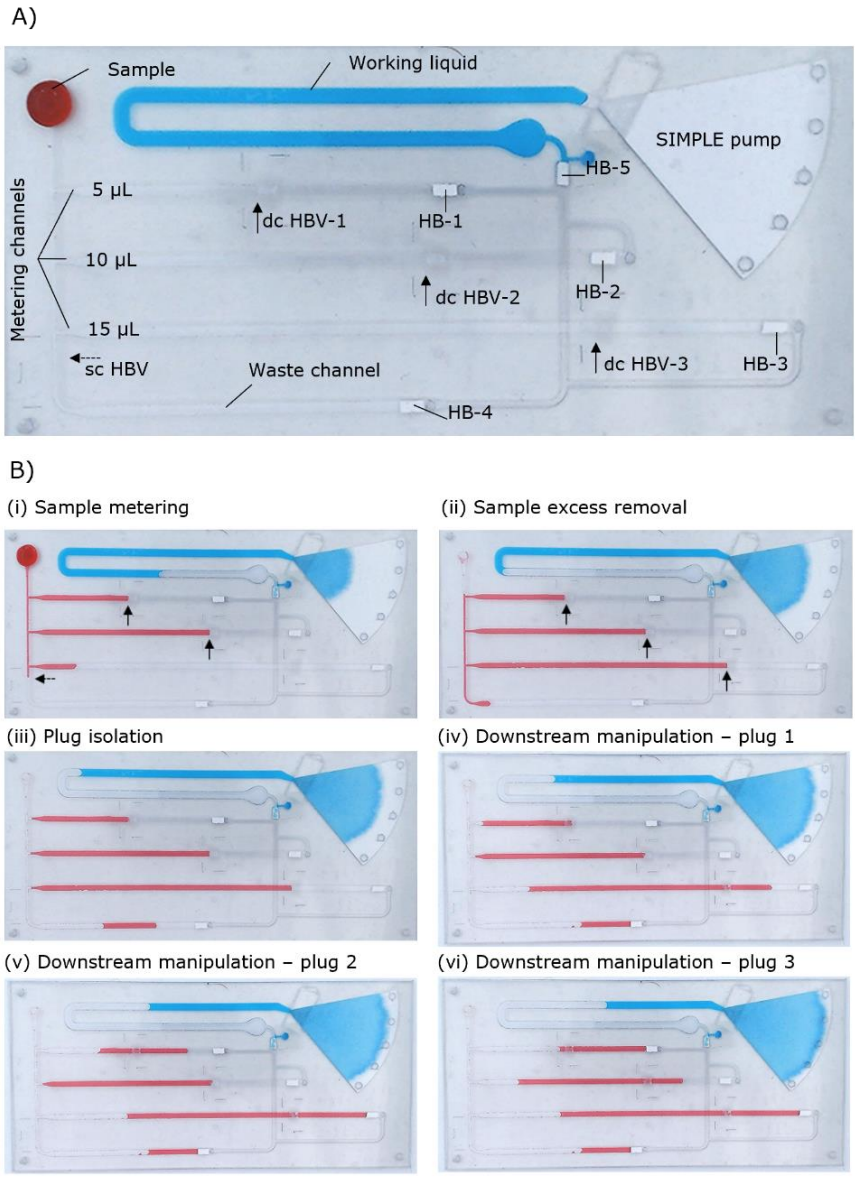

***Figure 3.6**: A) Microfluidic chip design for parallel sample metering with integrated SIMPLE unit. B) Snapshots of different liquid manipulation steps through the microfluidic system: (i) filling the metering channels by the sample, (ii) removal of the sample excess to the waste channel, (iii) isolation of the metered volume plugs and (iv-vi) subsequent bursting of each volume plug through the dc HBVs.*

The ability to split and further manipulate multiple precisely metered volumes in an autonomous way using SIMPLE technology opens the door to on-chip parallelization and much more advanced liquid manipulation compared to current solutions. The use of the SIMPLE unit as passive driving source, which operates as an external pressure source on the incoming sample, is the core benefit of the currently presented strategy. This makes the propulsion of the liquid independent of the sample-channel interaction as is the case for traditional capillary microfluidics[37,40].

3.3.4 Integrated volumetric SIMPLE-DBS sampling device

To translate the sample metering principle towards an integrated Hct-independent DBS sampling device that can be used at the POC, again a SIMPLE unit was integrated for liquid propulsion. This way, the SIMPLE-DBS sampling device (**Figure 3.7**) becomes completely autonomous and ideal for self-sampling in decentralized POC settings (e.g. patient's home). As consistent 'parallel loading' of multiple isolated volume plugs (possibility of parallel plug isolation itself was shown Section 3.3.3) on separate DBS papers requires novel technical innovations, which fall out of the scope of this work, the working principle of an integrated device with single DBS paper is shown. Furthermore, it is not expected that the analytical performance of the system will be influenced by moving towards multiple DBS samples. Hereto, a circular DBS paper (7 mm diameter, Whatman grade CF12) was incorporated in a second microfluidic layer underneath the metering system (Figure 3.13, Supporting Information). Immediately downstream the DBS paper, an HSV (HSV-2) was placed to avoid the blood sample to be pulled out from the DBS paper. Also here, the working liquid is flanked by a HSV (HSV-3) to avoid the occurrence of backflow of the working liquid upon activation. After sample loading and drying, the DBS paper can be removed via a removable back-film (see Section 3.5.6 of Supporting Information), ready to be analyzed in clinical laboratories without the need of taking a sub-punch. The different phases of the integrated SIMPLE-DBS microfluidic device working principle are illustrated in **Figure 3.7A-E**. It is important to

mention that all phases described are performed within 5 minutes and that this turnover time can be further reduced by increasing the pump flow rate (function of the angle and porosity of the paper)[34].

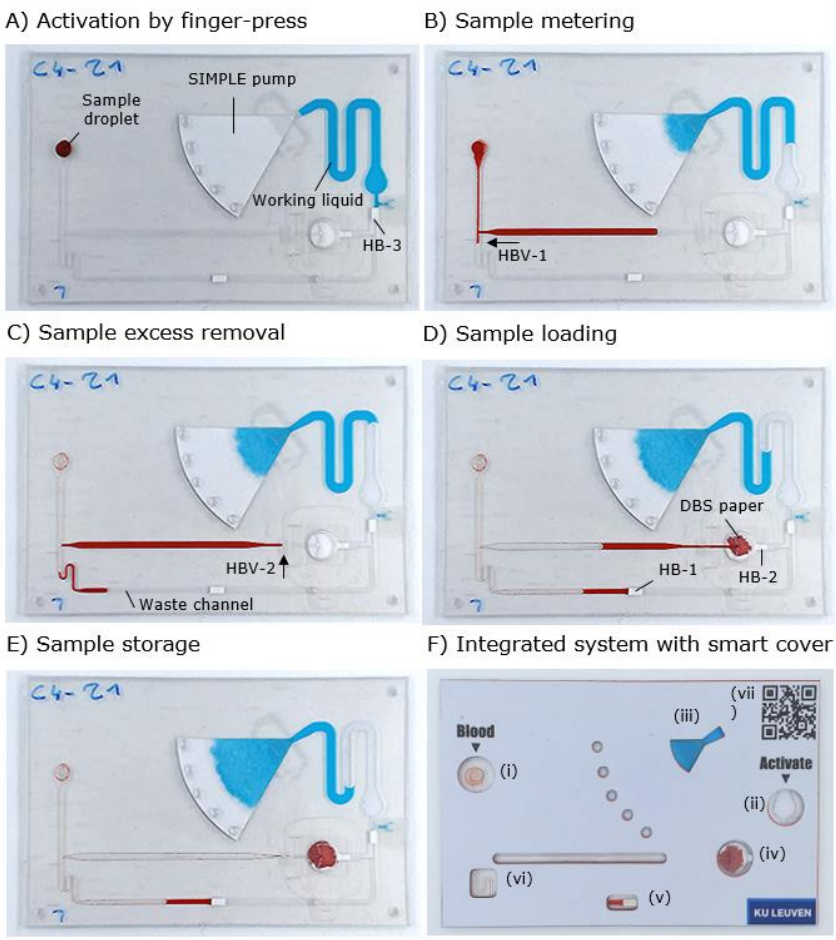

Figure 3.7*: Snapshots of the working principle of the integrated microfluidic DBS sampling device. A) A drop of citrated-blood is applied at the inlet of the sampling channel and the system is activated by a single finger-press. B) The activated SIMPLE unit draws the blood sample in the microfluidic network. C) Upon complete filling of the metering channels, the sample excess is directed to the waste channel followed by (D) loading of both metered sample plugs on the DBS papers. E) Once loaded, the samples are stored on the chip for drying and transported to the laboratory for analysis. F) Cartridge of integrated DBS system with cover sticker, illustrating the different control zones for assessing successful chip performance.*

Figure 3.7F shows the final integrated SIMPLE-DBS system with an attached cover sticker making the device more intuitive and user-friendly for people without special training. The cover features indicate (i) where to apply the finger-prick blood drop, (ii) an activation spot for the SIMPLE pump, (iii) indicator of successful SIMPLE activation, (iv) windows to confirm successful loading of the metered sample volumes on the DBS papers, (v) a control zone to assess if sufficient sample volume was applied at the inlet to fill the metering channel (true if blood is visible), (vi) a second control zone to check successful splitting of the sample excess from the metered sample (true if no blood is visible), and (vii) a QR-code used for tracking each sampling device and possibly access to the patient's information. This QR-code can also be replaced by a zone available for written text.

3.3.5 Device validation with adalimumab-spiked blood samples

TDM of biologicals is an expanding field which would benefit from a reliable remote self-sampling DBS device. In fact, for ADM, world's bestselling drug and biological used to treat patients suffering from chronic autoimmune diseases (e.g. inflammatory bowel disease, rheumatoid arthritis), dosing is in practice not straightforward because of intra- and interpatient pharmacokinetic variability, leading to i) underexposure in case of sub-therapeutic serum drug concentrations or due to the production of neutralizing anti-drug antibodies[41–44], and ii) possible drug overexposure resulting in unnecessarily high therapy costs[45]. The DBS sampling method facilitates patients to routinely collect blood samples at home and send them via regular mail to a clinical laboratory for analysis, reaching a personalized treatment plan in a much more effective way.

In this context, the SIMPLE-DBS sampling device was compared to traditional Whatman protein saver cards to evaluate whether or not the obtained ADM concentrations measured from the DBS extracts are similar. To do so, ADM-spiked citrated blood samples corresponding to a clinically relevant concentration range (0, 1, 4 and 16 µg/mL) were used to prepare DBS samples with the SIMPLE-DBS device. For comparison, Whatman protein

saver cards were loaded with a volume of 40 µL in combination with sub-punches as the standard method, while different cards were loaded with precisely 10 µL of blood as the whole-spot analysis reference.

All the extracted samples were analyzed with the ELISA reference technology as described in Section 3.2.6 from which the results are summarized in **Figure 3.8** (exact values are given in Table 3.5 of the Supporting Information).

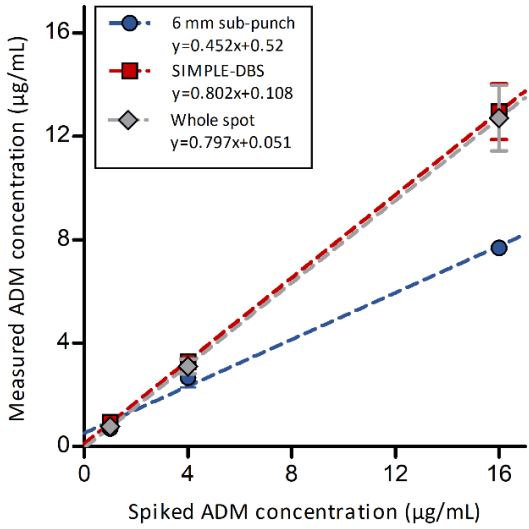

***Figure 3.8**: Calibration curves of the measured ADM concentrations for the different DBS sample preparation methodologies (6 mm sub-punch (n = 9), SIMPLE-DBS (n = 12) or whole spot (n = 9)). Error bars represent one standard deviation around the mean ADM concentration. Linear fitted curves (R^2 > 0.96) are plotted as dashed lines through the data points of each DBS method.*

The graph shows that the fitted regression curves of the SIMPLE-DBS device and whole spot overlap (slope ~ 0.80), while the one of the 6 mm sub-punch methodology has a much lower slope of 0.452. This difference in slopes was determined to be strongly significant ($p < 0.0001$, F-test on the interaction effect between sampling method and spiked concentration, via general linear regression model (GLM)). When the measured ADM concentrations of each methodology are evaluated, a lower bias (%) with the spiked concentrations is observed for the SIMPLE-DBS and whole-spot analysis methodology (14% and 22%,

respectively) compared to the 6 mm sub-punch (38%). However, these are the average values taken over all concentrations and should be interpreted carefully. The GLM showed that the differences in bias are proportional (cf. different slopes of the regression curves) and might be explained by an unknown but significant difference in volume obtained by taking a 6 mm sub-punch, while the volumes for the whole-spot methods (SIMPLE-DBS and reference) are exactly known. The observed characteristics of the SIMPLE-DBS regression curve, including a greater slope and reduced proportional bias, indicate a potential enhancement in sensitivity.

3.4. Conclusions

In this chapter, a user-independent system for producing precisely metered dried blood spots was developed, characterized and integrated with a self-powered microfluidic pump (SIMPLE). First, hydrophobic burst valves were developed to temporarily retain a liquid flow by locally coating the channels with Aquapel® and Fluoropel™. Applying these fluorinated compounds to obtain single and/or double coated channel sections, 4 significantly different burst pressures between 175 and 600 Pa were accomplished. The sequential burst actions of 2 hydrophobic burst valves with different burst pressures was then used to create a passive metering system. The accuracy and reproducibility of the system was evaluated for different metered blood volumes (5, 10 and 15 µL), as well as for a broad blood Hct range (25-70%). For both, gravimetric characterization showed CV values below 3%. The system's capability and flexibility to meter multiple different volumes starting from an unknown sample volume in an autonomous way was also shown by integration with the SIMPLE technology.

Next, the metering system was further implemented towards an autonomous and portable DBS sampling system, i.e. SIMPLE-DBS. In this approach, the blood sample was passively manipulated by SIMPLE through the metering system and subsequently loaded on a pre-cut DBS paper, embedded and sealed in the device to avoid any risk of contamination.

Importantly, the system is adjustable to split-off multiple metered volumes in parallel within a range of 1-10's of microliters each from a single blood drop in parallel.

The performance of the integrated SIMPLE-DBS system was finally validated in the context of TDM for biologicals. Here, citrated blood samples spiked with clinically relevant adalimumab concentrations (0-16 µg/mL) were used to compare the SIMPLE-DBS system with the traditional Whatman protein saver card approach. Based on GLM analysis, the SIMPLE-DBS system showed an overall lower bias between the measured and spiked ADM concentrations and equal reproducibility compared to the traditional 6 mm sub-punched DBS samples on Whatman protein saver cards. The results were in good agreement with the whole-spot 10 µL reference DBS samples.

The obtained results show the value of metered SIMPLE-DBS in combination with whole-spot analysis. Furthermore, the potential of the presented device to integrate this sample metering strategy in the current workflow for TDM was clearly demonstrated. Moreover, our system challenges the current state of the art by manipulating the sample with an external, passive driving source instead of relying solely on the capillary action of the sample in the microfluidic system. As a consequence, multiple metered volumes can be isolated in parallel from a single sample drop. This paper presents the first steps towards a novel method for preparing accurate DBS samples. Future work will focus on enabling parallel DBS loading and evaluating the influence of the Hct effect on the recovery efficiency. Furthermore, to make the device applicable for clinical field testing, a user-friendly chip-to-world interface has to be integrated which allows proper application of finger-prick capillary blood. Even more, we believe that our system is not restricted to sample collection but also allows for downstream manipulation of the metered sample, making it employable in a myriad of on-chip diagnostic POC applications.

3.5. Supporting information

3.5.1 Burst pressure calculation and experimental setup

In **Figure 3.9A-B**, a schematic overview of the theoretical pressure profile with changing meniscus position in the HBV incorporated microfluidic channel is illustrated.

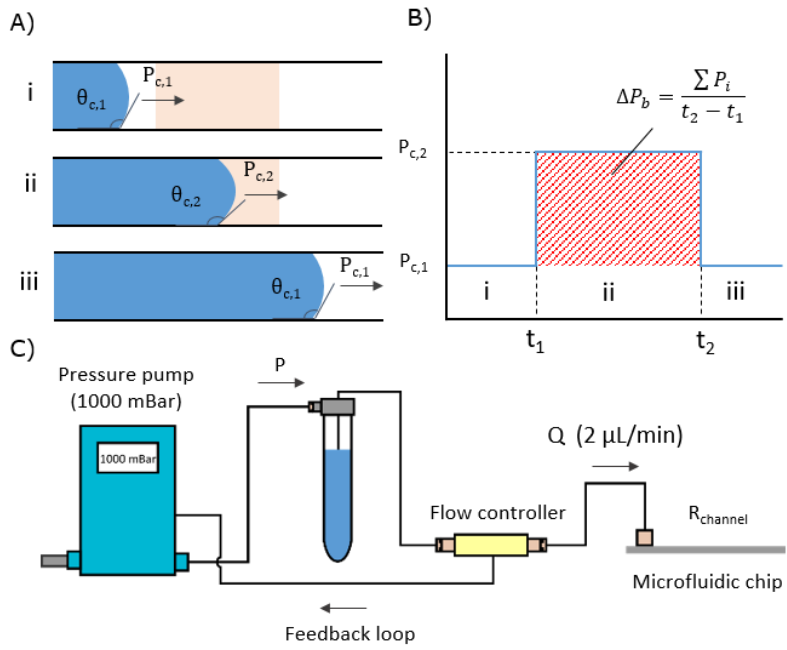

***Figure 3.9**: (a) Overview of the fluid meniscus position ([i] before, [ii] over, and [iii] after the HBV) within the channel. (b) Theoretical pressure profile to push a fluid front over the HBV. Average burst pressure is calculated as the average normalized pressure difference over the time interval t2-t1. (c) Schematic representation of the experimental measurement setup.*

A certain baseline pressure ($P_{c,1}$) is required to push the liquid at a constant flow rate through the non-treated channel with a contact angle $\theta_{c,1}$. Once liquid-air interface reaches the HBV it stops moving and an additional pressure is required to increase the surface area of the meniscus in order to meet the contact angle properties ($\theta_{c,2}$) of the local hydrophobic region. From the moment the applied pressure ($P_{c,2}$) is high enough so the contact angle of the meniscus meets the one of the hydrophobic coating, the liquid will be pushed through the HBV.

Finally, when the meniscus reaches again the non-treated channel surface, the required pressure to maintain the flow rate drops again to its initial value ($P_{c,1}$) .

To calculate the burst pressure (ΔP_b) of the HBV, the measured pressure profile was first normalized by the average baseline pressure ($P_{c,1}$). This one was calculated as the average pressure value of the 10 second pressure profile before reaching the HBV. The burst pressure of the HBV was then calculated by taking the average pressure value over the time interval ($\Delta t = t_2$-t_1) in which the liquid meniscus is moving over the HBV as is indicated in **Figure 3.9B**.

Liquid was injected in the microfluidic chips using pressure pumps (LINEUP FLOW EZ™ SERIES 1000 mBar, Fluigent, France). The experimental setup is illustrated in **Figure 3.9C** where a flow controller (Flow unit M, Fluigent, France) is used the control the injection flow rate precisely at 2 µL/min by controlling the applied pressure via a feedback loop system. The change in applied pressure and effective flow rate are recorded in real-time at a frequency of 0.1 Hz.

3.5.2 Gravimetric methodology for the volumetric performance characterizations

A schematic of the experimental setup and the microfluidic design are illustrated in **Figure 3.10A-B**. Snapshots of different steps in the gravimetric volume characterization strategy are shown in **Figure 3.10C**. (i) An initial volume (20 µL) of citrated blood was preloaded via a prefilling hole in the microfluidic chip. Hereto, an extra HSV was implemented to direct the blood into the desired direction, avoiding it to flow toward the syringe pump connection. (ii) The sample plug was then pushed (15 µL/min) through the microfluidic network via a connected syringe pump. (iii) After volume metering the sample excess was discarded in the waste channel and (iv) finally the isolated metered sample volume was loaded on the circular filter paper. For this experiment, the device worked essentially as a non-integrated DBS system. This way, the filter paper, together with a supporting piece of PVC, can

easily be removed from the chip in order to weigh the metered volume before and after sample loading.

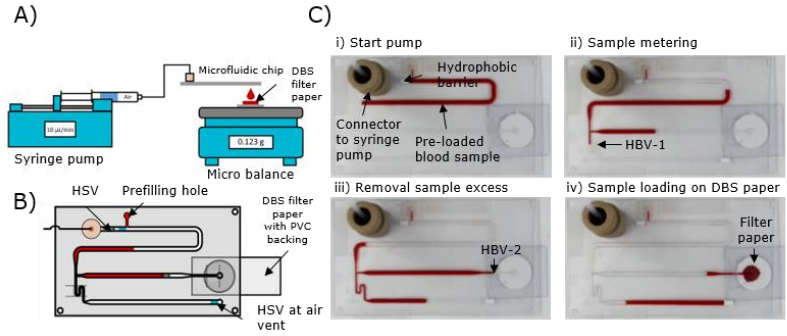

***Figure 3.10**: (a) Overview of the gravimetric measurement method. (b) Top view of the microfluidic device designed for these measurements. Below the metering outlet, a DBS filter paper is placed on top of a PVC backing for easy handling during weight measurements with the micro balance. c) Snapshots depicting the working principle of the gravimetric method to assess the accuracy, repeatability and Hct-independency of the metering system.*

The accuracy and reproducibility of the gravimetric measurement method was evaluated by measuring the weight difference of paper substrates before and after application of a fixed volume of distilled water using a micropipette. Six repetitions were performed for the volumes of 5, 10 and 15 µL, for which the results are summarized in **Figure 3.11**.

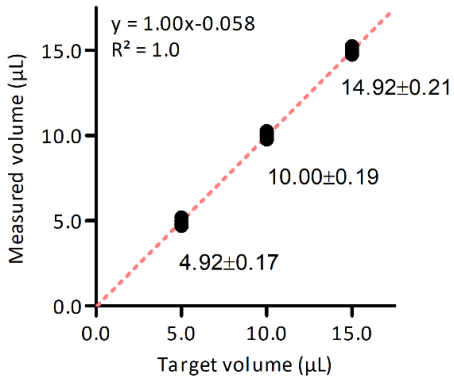

***Figure 3.11**: Reference gravimetric measurements with distilled water.*

The measurements show a good reproducibility for each evaluated target volume (CV < 4%). Also, a strong agreement between the measured and target volumes (slope = 1) is observed, which confirms the good accuracy of the measurement method.

3.5.3 Characterization of the burst pressures for different HBV types

Although the performed water contact angle measurements illustrated a good homogeneity of the coated surfaces, these measurements only give an indication of the surface properties on a relatively large scale. The required pressure to push the liquid over the hydrophobically treated zones in the channel is, however, only determined by the local surface properties of the coating at the meniscus interface of liquid. As a consequence, small artefacts in the coating might have a rather large influence on the burst pressure. It is expected that the local surface homogeneity of the Fluoropel™ coating is lower compared to the Aquapel® solution as the solution contains silica nanoparticles which might cluster together upon evaporation of the solvent and this way introduce local artefacts. This hypotheses is reflected in the calculated differences between the measured and theoretical burst pressures. In particular, higher discrepancies can be observed for Fluoropel™-based HBVs compared to Aquapel® based ones.

***Table 3.1**: Theoretical and experimental obtained burst pressures for the different HBV types.*

	Aq sc	Fl sc	Aq dc	Fl + Aq	Fl dc
$\Delta P_{b,\,theo}$ (Pa)	226	449	453	676	898
SD	29	33	58	62	67
$\Delta P_{b,\,exp}$ (Pa)	175	338	369	459	609
SD	26	57	25	37	60
$\Delta P_{b,\,theo}$- $\Delta P_{b,\,exp}$ (Pa)	52	111	83	217	289

Moreover, the performed contact angle measurements do not give any information on the patterning resolution and homogeneity of the coating at the edge of the hydrophobic region. The surface properties at the edge of the coating are, however, crucial in determining the burst pressure of the valve as at this interface the local change in contact angle occurs. In addition to this, due to the manual fabrication of the HBVs it can be expected that for dc HBV valves, the top and bottom coating are not perfectly aligned, what again can have an influence on the overall burst pressure. In general it is believed that by using an automated manufacturing process with a spray coating strategy, a clear reduction in the discrepancy can be achieved.

Another potential explanation for the observed discrepancy is the use of static instead of dynamic contact angles in the calculations of the burst pressure (Eq. (3.2) main manuscript). The bursting event of the HBV can be seen as a dynamic process in which the meniscus of the liquid has to change its interface to modify its contact angle from the non-treated PVC to meet the properties of the hydrophobically coated region. In general, the dynamic contact angle is smaller compared to the static one, what would result in overall lower burst pressures. The dynamic contact angle might also explain why a larger discrepancy between the theoretical and experimentally measured values was observed for HBVs in which the Fluoropel™ coatings are used. These coatings have superhydrophobic properties for which the difference between static and dynamic contact angles is almost negligible. As a consequence, the insertion of the dynamic contact angle in Eq. (3.2) of the main manuscript, only has an effect on the second term in brackets on the right hand side and not the first one, leading to a bigger difference in the burst pressure compared to when both terms are affected.

3.5.4 Influence of microchannel dimensions on HBV burst pressure

According to Eq. (3.2) in the main text, the burst pressure of the HBV only depends on the height and not the width of the microchannel. This is because the mask-based coating strategy only alters the contact angle properties of the bottom or/and top

of the microchannel while the contact angles of the side walls remain unchanged. To confirm this relation, the burst pressures of all five HBV configurations were also measured in 0.5 and 2.0 mm wide microchannels using the same methodology as described in the Section 3.2.4 of the Materials and methods. These burst pressures were then compared with the one of the 1.0 mm wide microchannels. A summary of these results is given in **Figure 3.12A**. Overall, the measured results confirm Eq. (3.2) as the burst pressures of each HBV configuration are within the same range for the different channel widths (see Tukey multiple comparison statistics). However, in case of the dc HBVs a significant increase in burst pressure was observed for the 2.0 mm wide channels compared to the ones with a width of 0.5 and 1.0 mm.

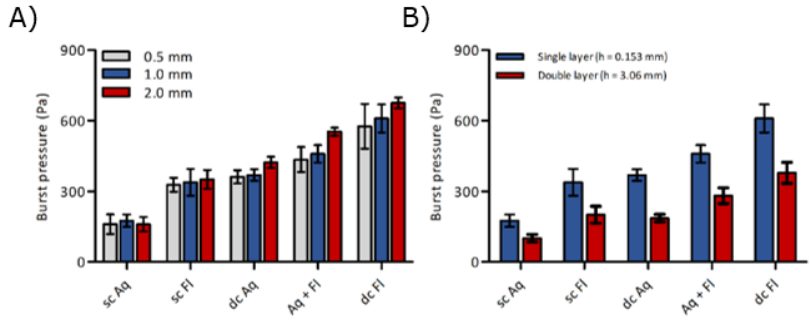

***Figure 3.12**: Average measured burst pressures of all HBV configurations for A) different channel widths of 0.5, 1.0 and 2.0 mm, and B) different channel heights of 0.153 and 0.306 mm. Error bars represent one standard deviation (n ≥ 5).*

This increase is not problematic in the context of this work as the dimensions of the microchannels, in which the HBVs are located, never exceed a width of 1.0 mm within our system. Moreover, when the trend in burst pressures for all HBV configuration is evaluated, the same 4 HBV configurations (even 5 for the 2.0 mm wide microchannels) show a significantly different burst pressure for each channel width. As a consequence, we implemented a rule of thumb to use HBVs of the same width within the same microfluidic network.

Apart from the influence of the channel width, also the dependency of the channel height on the burst pressure was

studied. Hereto, HBVs were made in microchannels consisting of a double PSA layer (0.306 mm thickness). As illustrated in **Figure 3.12B**, a clear drop in the measured burst pressure was observed what is in agreement with Eq. (3.2) of the main manuscript.

***Table 3.2**: Summary of Tukey multiple comparison statistics: overview of significantly different burst pressures between the evaluated channel widths (0.5, 1.0 and 2.0 mm) for each HBV configuration.*

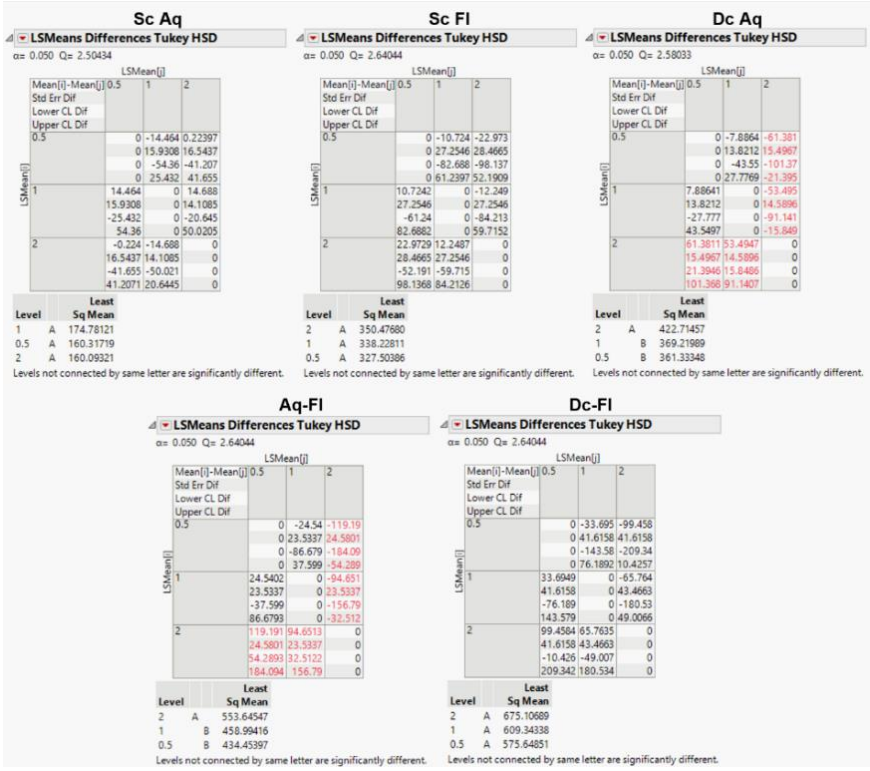

***Table 3.3**: Summary of Tukey multiple comparison statistics: overview of significantly different burst pressures between the 5 HBV configurations for each microchannel width.*



3.5.5 Volumetric characterization of the metering system by a gravimetric method

The results of the gravimetric characterization of the volumetric performance are listed in **Table 3.4**. This is the summary of the results as depicted in **Figure 3.5** and **Figure 3.6** of the main manuscript.

***Table 3.4**: Gravimetric measurements of the metering system its volumetric performance for different target volumes and varying Hct levels of blood samples.*

Hct level (%)	Target volume (µL)	Average volume (µL)	SD	CV (%)
25	10	9.72	0.23	2.37
40	5	4.86	0.15	2.99
	10	9.79	0.22	2.22
	15	14.56	0.24	1.62
55	10	9.59	0.21	2.19
70	10	9.48	0.24	2.58

Concerning the system accuracy, a slightly increased offset with the 10 µL target volume is observed for higher Hct levels (5.2% for 70% Hct level). However, when the average measured volumes for each Hct level are compared to the global average over all Hct levels (9.65 µL, which was plotted as the full red line in **Figure 3.6**), these differences reduce below 2%.

Although these results are highly promising, the volumetric performance could be further improved by i) replacing manual chip assembly and coating steps with an automated manufacturing process (i.e. roll-to-roll assembly and spray coating), ii) reducing the roughness of the channel walls by shifting to CO2 laser cutting and iii) accounting for the volume loss and correcting by adjusting the location of the HBV within the metering channel.

3.5.6 Multilayer configuration of SIMPLE-DBS sampling device, DBS loading, drying and removal

The configuration of the integrated SIMPLE-DBS device is illustrated in **Figure 3.13**.

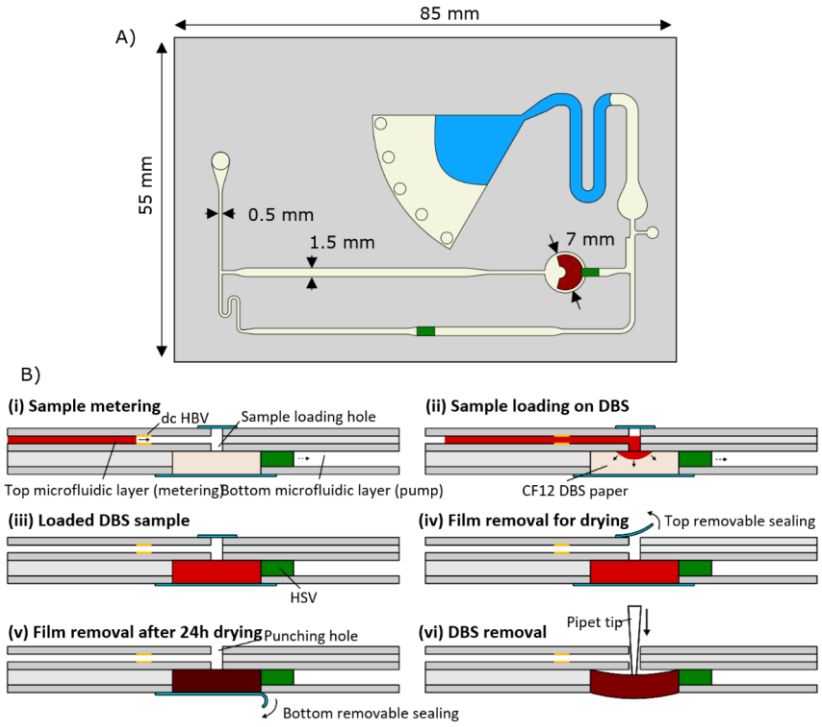

***Figure 3.13**: A) Top view of the SIMPLE-DBS device, (B) cross-sections of the SIMPLE-DBS device illustrating the (i-iii) loading of the metered blood sample on the CF12 DBS paper, (iv) removal of the top sealing for a 24 h drying step and (v,vi) finally after peeling off the bottom sealing tape the DBS paper is pushed out of the chip by means of a regular pipet tip.*

A CF12 DBS paper is positioned underneath the distant part (after the dc HBV) of the metering channel which are in connection with each other via a sample loading hole. The top side of the metering channel is also foreseen with a hole at the same position of the sample loading hole. This punching hole is used for removing the dried DBS paper out of the chip before analysis by means of a pipet tip. During the sampling process, this hole is sealed with a removable film to prevent the intake of air. Likewise, a second removable film is attached to the bottom

of the DBS paper. The metering system is in connection, via the DBS paper, with the bottom microfluidic layer in which the SIMPLE pumping mechanism is present which acts as the passive negative pressure source. In order to prevent the pulling of loaded blood sample out of the DBS paper in the connected microfluidic channel, a HSV is situated right next to the DBS paper.

3.5.7 ELISA measurements on extracted DBS samples

***Table 3.5**: Overview table of ELISA measurements on extracted DBS samples*

DBS sample type	ADM conc. [µg/mL]	Loaded sample volume [µL]	ADM [µg/mL]	Stdev [µg/mL]	%CV	$ADM_{Measured}$ /ADM_{theor} conc. [%]
Whatman protein saver card - 6 mm sub-punch (gold standard)	0	40	**0.26**	0.02		
	1	40	**0.70**	0.11	15%	70%
	4	40	**2.67**	0.67	25%	67%
	16	40	**7.69**	0.23	3%	48%
			AVERAGE:		**15%**	**62%**
SIMPLE-DBS	0	9.65	**<0.03**	<0.03		
	1	9.65	**0.94**	0.08	8%	94%
	4	9.65	**3.28**	0.27	8%	82%
	16	9.65	**12.95**	2.15	17%	81%
			AVERAGE:		**11%**	**86%**
Whatman protein saver card – no sub-punch (whole spot analysis reference)	0	10	**<0.03**	<0.03		
	1	10	**0.77**	0.05	7%	77%
	4	10	**3.10**	0.50	16%	78%
	16	10	**12.71**	2.19	17%	79%
			AVERAGE:		**13%**	**78%**

3.6. References

1. Lei, B. U. W. & Prow, T. W. A review of microsampling techniques and their social impact. *Biomed. Microdevices* 21, (2019).
2. Bang, I. Ein verfahren zur mikrobestimmung von blut-bestandteilen. *Biochem. Ztschr.* 49, 19–39 (1913).
3. Guthrie, R. & Susi, A. A simple phenylalanine method for detecting phenylketonuria in large populations of newborn infants. *Pediatrics* 32 (3), 338–343 (1963).
4. Wilhelm, A. J., den Burger, J. C. G., Vos, R. M., Chahbouni, A. & Sinjewel, A. Analysis of cyclosporin A in dried blood spots using liquid chromatography tandem mass spectrometry. *J. Chromatogr. B Anal. Technol. Biomed. Life Sci.* 877, 1595–1598 (2009).
5. Velghe, S., Delahaye, L. & Stove, C. P. Is the hematocrit still an issue in quantitative dried blood spot analysis? *J. Pharm. Biomed. Anal.* 163, 188–196 (2019).
6. Rowland, M. & Emmons, G. T. Use of dried blood spots in drug development: Pharmacokinetic considerations. *AAPS J.* 12, 290–293 (2010).

7. Sikombe, K. *et al.* Accurate dried blood spots collection in the community using non-medically trained personnel could support scaling up routine viral load testing in resource limited settings. *PLoS One* 14, 1–14 (2019).
8. Amsterdam, P. Van & Waldrop, C. The application of dried blood spot sampling in global clinical trials. *Bioanalysis* 2, 1783–1786 (2010).
9. Martial, L. C. *et al.* Cost evaluation of dried blood spot home sampling as compared to conventional sampling for therapeutic drug monitoring in children. *PLoS One* 11, (2016).
10. Timmerman, P. *et al.* EBF recommendation on the validation of bioanalytical methods for dried blood spots. *Bioanalysis* 3, 1567–1575 (2011).
11. Denniff, P. & Spooner, N. The effect of hematocrit on assay bias when using DBS samples for the quantitative bioanalysis of drugs. *Bioanalysis* 2, 1385–1395 (2010).
12. De Kesel, P. M. M., Sadones, N., Capiau, S., Lambert, W. E. & Stove, C. P. Hemato-critical issues in quantitative analysis of dried blood spots: Challenges and solutions. *Bioanalysis* 5, 2023–2041 (2013).
13. Abu-Rabie, P., Denniff, P., Spooner, N., Chowdhry, B. Z. & Pullen, F. S. Investigation of different approaches to incorporating internal standard in DBS quantitative bioanalytical workflows and their effect on nullifying hematocrit-based assay bias. *Anal. Chem* 87, 4 (2015).
14. Carter, G. F. The paper punched disc technique for lead in blood samples with abnormal haemoglobin values. *Br. J. Ind. Med.* 35, 235–240 (1978).
15. Chao, T. C., Trybala, A., Starov, V. & Das, D. B. Influence of haematocrit level on the kinetics of blood spreading on thin porous medium during dried blood spot sampling. *Colloids Surfaces A Physicochem. Eng. Asp.* 451, 38–47 (2014).
16. Stickle, D. F., Rawlinson, N. J. & Landmark, J. D. Increased perimeter red cell concentration in filter paper bloodspot samples is consistent with constant-load size exclusion chromatography occurring during application. *Clin. Chim. Acta* 401, 42–45 (2009).
17. Moat, S. J. *et al.* Effect of blood volume on analytical bias in dried blood spots prepared for newborn screening external quality assurance. *Bioanalysis* 12, 99–109 (2020).
18. O'Mara, M. *et al.* The effect of hematocrit and punch location on assay bias during quantitative bioanalysis of dried blood spot samples. *Bioanalysis* 3, 2335–23347 (2011).
19. Resano, M., Belarra, M. A., García-Ruiz, E., Aramendía, M. & Rello, L. Dried matrix spots and clinical elemental analysis. Current status, difficulties, and opportunities. *TrAC - Trends Anal. Chem.* 99, 75–87 (2018).
20. Youhnovski, N., Bergeron, A., Furtado, M. & Garofolo, F. Pre-cut Dried Blood Spot (PCDBS): An alternative to Dried Blood Spot (DBS) technique to overcome hematocrit impact. *Rapid Commun. Mass Spectrom.* 25, 2951–2958 (2011).
21. Li, F., Ploch, S., Fast, D. & Michael, S. Perforated dried blood spot accurate microsampling: the concept and its applications in toxicokinetic sample collection. *J. Mass Spectrom.* 47, 655–667 (2012).
22. Spooner, N. *et al.* A device for dried blood microsampling in quantitative bioanalysis: Overcoming the issues associated blood hematocrit. *Bioanalysis* 7, 653–659 (2015).
23. Denniff, P. & Spooner, N. Volumetric Absorptive Microsampling: A dried sample collection technique for quantitative bioanalysis. *Anal. Chem* 86, 8489–8495 (2014).
24. Fuller, G. *et al.* Feasibility of patient-centric remote dried blood sampling:

the prediction, risk, and evaluation of major adverse cardiac events (PREMACE) study. *Biodemography Soc. Biol.* 65, 313–322 (2019).
25. Nakahara, T., Otani, N., Ueno, T. & Hashimoto, K. Development of a hematocrit-insensitive device to collect accurate volumes of dried blood spots without specialized skills for measuring clozapine and its metabolites as model analytes. *J. Chromatogr. B Anal. Technol. Biomed. Life Sci.* 70–79 (2018).
26. Leuthold, L. A. *et al.* New microfluidic-based sampling procedure for overcoming the hematocrit problem associated with dried blood spot analysis. *Anal. Chem.* 87, 2068–2071 (2015).
27. Lenk, G. *et al.* A disposable sampling device to collect volume-measured DBS directly from a fingerprick onto DBS paper. *Bioanalysis* 7, 2085–2094 (2015).
28. Neto, R., Gooley, A., Breadmore, M. C., Hilder, E. F. & Lapierre, F. Precise, accurate and user-independent blood collection system for dried blood spot sample preparation. *Anal. Bioanal. Chem.* 410, 3315–3323 (2018).
29. Kokalj, T., Park, Y., Vencelj, M., Jenko, M. & Lee, L. P. Self-powered imbibing microfluidic pump by liquid encapsulation: SIMPLE. *Lab Chip* 14, 4329–4333 (2014).
30. Dal Dosso, F., Tripodi, L., Spasic, D., Kokalj, T. & Lammertyn, J. Innovative hydrophobic valve allows complex liquid manipulations in a self-powered channel-based microfluidic device. *ACS Sensors* 4, 694–703 (2019).
31. Dal Dosso, F. *et al.* Creasensor: SIMPLE technology for creatinine detection in plasma. *Anal. Chim. Acta* 1000, 191–198 (2018).
32. Bian, S. *et al.* Generation and characterization of a unique panel of anti-adalimumab specific antibodies and their application in therapeutic drug monitoring assays. *J. Pharm. Biomed. Anal.* 125, 62–67 (2016).
33. Yuen, P. K. & Goral, V. N. Low-cost rapid prototyping of flexible microfluidic devices using a desktop digital craft cutter. *Lab Chip* 10, 384–387 (2010).
34. Dal Dosso, F., Bondarenko, Y., Kokalj, T. & Lammertyn, J. SIMPLE analytical model for smart microfluidic chip design. *Sensors Actuators, A Phys.* 287, 131–137 (2019).
35. Dal Dosso, F., Kokalj, T., Belotserkovsky, J., Spasic, D. & Lammertyn, J. Self-powered infusion microfluidic pump for ex vivo drug delivery. *Biomed. Microdevices* 20, 1–11 (2018).
36. Hagmeyer, B., Zechnall, F. & Stelzle, M. Towards plug and play filling of microfluidic devices by utilizing networks of capillary stop valves. *Biomicrofluidics* 8, (2014).
37. Olanrewaju, A., Beaugrand, M., Yafia, M. & Juncker, D. Capillary microfluidics in microchannels: From microfluidic networks to capillaric circuits. *Lab Chip* 18, 2323–2347 (2018).
38. Hagmeyer, B., Zechnall, F. & Stelzle, M. Towards plug and play filling of microfluidic devices by utilizing networks of capillary stop valves. *Biomi* 8, 1–9 (2014).
39. Lenk, G., Ullah, S., Stemme, G., Beck, O. & Roxhed, N. Evaluation of a volumetric dried blood spot card using a gravimetric method and a bioanalytical method with capillary blood from 44 volunteers. *Anal. Chem.* 91, 5558–5565 (2019).
40. Kim, J. H., Kavehpour, P. & Rothstein, J. P. Dynamic contact angle measurements on superhydrophobic surfaces. *Phys. Fluids* 27, (2015).
41. Bastida, C. *et al.* Is there potential for therapeutic drug monitoring of biologic agents in rheumatoid arthritis? *Br. J. Clin. Pharmacol.* 83, 962–975 (2017).

42. Baert, F. *et al.* Influence of immunogenicity on the long-term efficacy of infliximab in Crohn's disease. *N. Engl. J. Med.* 348, 601–608 (2003).
43. Fasanmade, A. A. *et al.* Population pharmacokinetic analysis of infliximab in patients with ulcerative colitis. *Eur. J. Clin. Pharmacol.* 65, 1211–28 (2009).
44. Fasanmade, A. A., Adedokun, O. J., Blank, M., Zhou, H. & Davis, H. M. Pharmacokinetic properties of infliximab in children and adults with crohn's disease: a retrospective analysis of data from 2 phase III clinical trials. *Clin. Ther.* 33, 946–964 (2011).
45. Undevia, S. D., Gomez-Abuin, G. & Ratain, M. J. Pharmacokinetic variability of anticancer agents. *Nat. Rev. Cancer* 5, 447–458 (2005).

Chapter 4

Multiple dried blood spot sampling device for therapeutic drug monitoring of biologicals

*Equal contribution with Dr. Vloemans D.

Van Hileghem L. contributed to this work in terms of conceptualization, experimental design, planning and execution of the experiments, next to writing and editing of the manuscript.

4.1. Introduction

Today, the increasing demand for *in vitro* diagnostic testing is contradicting the resource-intensive centralized healthcare system. Furthermore, the traditional blood sampling procedure by venipuncture is cumbersome and the availability of skilled healthcare workers for routinely collecting samples the is decreasing detrimentally[1]. As a solution, dried blood spot (DBS) collection has gained interest as the reduced invasiveness and improved user-friendliness allow for self-sampling, for instance at the patient's home[2–4]. Moreover, DBS sampling permits the collection of multiple samples in parallel, which is beneficial for performing confirmatory tests, e.g. after a positive infectious disease screening result or doping test, biobanking or therapeutic drug monitoring (TDM) of biologicals[3,5,6]. In the standard protocol of DBS sampling, capillary blood is mostly obtained by finger-pricking. The generated drops can then be loaded and dried on a filter paper. Once arrived in the lab, multiple sub-punches can be reconstituted from a single DBS to obtain multiple test samples in parallel. Despite their advantages, chromatographic and coffee stain effects give rise to unequal analyte concentrations at different locations on the DBS[7–9]. Alternatively, multiple spots can be prepared, although, this often requires multiple finger-pricks to be performed compromising on invasiveness and increasing the drop-to-drop variability[10]. The main constraint of DBS sampling today, however, is the blood hematocrit (Hct) level, which shows high inter- and intra-patient variability[2,11–13]. This causes differences in (i) distribution through filter paper, (ii) analyte recovery, and (iii) background matrices during measurement, eventually leading to area, recovery and matrix biases[14].

Multiple solutions based on microfluidic sample manipulation have shown the potential of preparing multiple volumetric DBS samples to solve above-mentioned drawbacks. First, HemaPEN® (Trajan Scientific and Medical, UK) is a pen-like sampler that loads multiple pre-cut DBS in parallel[15]. However, the volume capacity is only 3 µL per DBS, compromising on accuracy and

sensitivity for low analyte concentrations. Alternatively, HemaXis™ DB (DBS System SA, Switzerland) cartridges combine this concept with a traditional protein saver card to load 10 µL samples[16]. Though, the cartridge lacks a user-friendly inlet making sample loading difficult, for instance for people with impaired vision or tremors. Capitainer®B (Capitainer AB, Sweden), on the other hand, has an integrated inlet chamber that, upon sample loading of minimally 18 µL as a single droplet, automatically removes sample excess and loads a 13.5 µL DBS[17]. Both HemaXis™ DB and Capitainer®B still require the deposition of multiple drops in different inlets for parallel DBS which increases the risk of error and requiring a higher blood volume. Finally, Tasso M-20 (Tasso, US) collects multiple DBS from the upper arm by an integrated lancing and collection device. Upon activation, the blood is collected in the sampling pod and converted into four 20 µL DBS samples. However, besides the high withdrawn total volume, the need for mechanical elements makes the disposable device significantly more expensive which is problematic for applications requiring frequent blood analyses for a prolonged time. Despite the solutions for remote microsampling, no device yet ensures the self-collection of multiple, high-quality volumetric DBS samples in parallel while integrating a user-friendly interface without compromising on cost or robustness. Furthermore, the evaluation and use of the existing microfluidic technologies have mostly been focused on small molecules[18–22], and limited focus went yet to applications including complex biological analytes with molecular weight (MW) > 100 kDa[23–25].

The aim of this work is to enable the autonomous collection of multiple high-quality DBS samples from a single finger-prick drop of blood in a field-ready device with a user-friendly interface. To this end, we report on the further developments of our previous work on a self-powered parallel metering system[26]. First, the microfluidic solution to enable parallel DBS loading is introduced as a split-pump system compatible with the self-powered microfluidic pumping technology referred to as SIMPLE[27]. Subsequently, a user-friendly

interface is established by the implementation of a hydrophobically treated conical inlet and the development of a volumetric sample inlet to prevent over- or underloading the DBS cartridge by, respectively, removing sample excess or indicating insufficient sample deposition. Finally, the analytical performance of the device is studied in the context of TDM of biologicals and compared to the traditional sub-punching method. Hereto, the TNF-inhibiting monoclonal antibody, adalimumab (ADM), is spiked in venous blood to validate the functionality for both a wide range of concentrations and a wide range of blood hematocrit values.

4.2. Materials and methods

4.2.1. Reagents and materials

Double-sided pressure sensitive adhesive (PSA) tape (200 MP 7956 MP) and transfer tape (467 MP) were acquired from 3M (USA). Polyvinyl chloride (PVC) lamination films (0.18 mm thick) were purchased from Delbo (Belgium). Polymethyl methacrylate (PMMA) sheets of 1 mm thickness were obtained from PyraSied (Netherlands). Sulfuric acid, horse radish peroxidase (HRP), bovine serum albumin (BSA), citric acid, Whatman® 903 protein saver cards, Whatman® qualitative (grade 113) and quantitative (grades 43 and 598) filter papers were purchased from the Merck group – Sigma Aldrich (Belgium). Cytiva (Belgium) provided the Whatman® CF12 qualitative filter paper. Hydrophilic coatings P100 and X100 were obtained from Joninn (Denmark) while the hydrophobic coatings Aquapel®, Fluoropel™ (800 and 800M) were acquired from Aquapel (USA) and Cytonix (USA), respectively. Superblock™ T20 (PBS) blocking buffer and tape (96-well sealing tape, Pierce™) for DBS sealing were purchased from Thermofisher Scientific (Germany). Peroxide (H_2O_2) and o-phenylenediamine were bought at Acros Organics (Belgium). The therapeutic antibody ADM (clone DE27) was acquired from Biorad Laboratories (Belgium) while the monoclonal anti-ADM capture antibodies (MA-ADM28B8) and HRP-conjugated anti-ADM detection antibodies (MA-ADM40D8) were produced in-house at the Laboratory for Therapeutic and Diagnostic Antibodies (KU

Leuven, Belgium)[28]. Accu-Chek® finger-prick lancets were obtained from Novolab (Belgium).

4.2.2. Hydrophilic PVC treatment

PVC substrates were coated hydrophilic by a mask-based approach. Herein, a PSA mask with a 20 x 15 mm² opening was attached to the PVC film in which 15 (0.05 µL/mm²), 30 (0.1 µL/mm²), 60 (0.2 µL/mm²) or 120 µL (0.4 µL/mm²) of the P100 or X100 hydrophilic coating agent was pipetted. Next, it was allowed to dry for 5 minutes at room temperature, followed by mask detachment. Contact angle (CA) measurements were performed to determine the hydrophilic properties of the coatings. A CAM200 goniometer (KSV instruments, Finland) with associated fitting software was used to measure the CAs from at least 4 randomly deposited water droplets (5-10 µL) per applied coating. For each coating condition, 3 independent samples were prepared and measured for both the P100 and X100 coating agents.

4.2.3. Fabrication and testing of the sample inlet system

The three-dimensional conical shape of the inlet piece was prepared from a 1 mm PMMA sheet using a 80 watt Trotec Speedy 300 laser cutter (Trotec, The Netherlands). A radial relief was engraved with increasing power from 0 to 80 watt between 12-5 mm as from the center of the inlet. After engraving, the 5 mm inlet hole, as well as the vent holes were cut from the PMMA. Next, the laser cut PMMA pieces were cleaned with isopropanol using an anti-static cleanroom wipe to remove debris before treating hydrophobically by immersing the piece in Fluoropel™ 800 solution for 1 minute. Subsequently, the piece was incubated for 10 minutes at 50 °C. The volumetric part of the inlet system consists of three PVC and two PSA layers (**Figure 4.1**). First, the bottom and top PVC-PSA layers were laminated and all inlet and vent holes were temporarily sealed with scotch tape. Next, 0.2 µL/mm² of P100 solution was pipetted in the top and bottom PSA cut-outs, followed by a five minute incubation at 50 °C. The same coating strategy was used to coat the side walls of the sample chamber in the middle PVC layer. Finally, the waste paper

(Whatman grade 113) and droplet-shaped air vent (Whatman grade 43) were inserted in their respective positions before laminating all parts together.

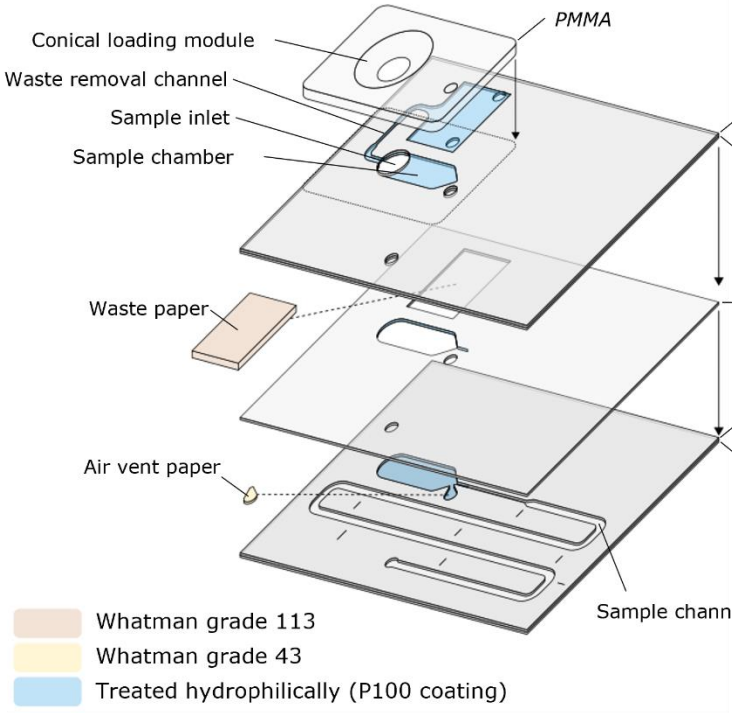

Figure 4.1: *Exploded view of the sample inlet system, giving a detailed insight of the layer-by-layer assembly method and positioning of all paper elements as well as hydrophilic treated regions.*

4.2.4. Finger-prick blood sample acquisition

For technical performance validation of the SIMPLE-DBS cartridge and the sample inlet system, capillary blood samples were obtained from healthy volunteers by finger-pricking. The standard finger-pricking procedure was approved by the UZ/KU Leuven Ethics Committee, Belgium (S65868). First, hands were washed for 30 seconds with warm water, improving the blood flow, and dried thoroughly. Next, a Velcro strap was firmly applied around the tip of the middle or ring finger of the volunteer's non-dominant hand, acting as a finger-tourniquet, after which the finger-tip was disinfected with an alcohol wipe.

For more information on this finger-pricking protocol, the reader is referred to Chapter 5. To pierce the finger, an Accu-Check® disposable lancing device was used at its longest stand (2.2 mm length). After pricking, no squeezing of the finger-tip was allowed.

4.2.5. Fabrication and testing of SIMPLE-DBS cartridges

Microfluidic chips were fabricated by a rapid layer-by-layer lamination method like previously presented[26]. Designs of the different layers were prepared in Inkscape (Inkscape, USA), after which a KNK Maxx air blade cutter (Klic-N-Kut, USA) was used to cut out the designed shapes from the PVC and PSA layers. The SIMPLE-DBS cartridge is comprised of three parts: the volumetric inlet layer (see Section 4.2.3), a metering layer and a pump layer (**Figure 4.2A**). A more detailed description on the fabrication of the latter two is presented in previous work presented in Chapter 3[26]. Here, the preparation of the different microfluidic elements are briefly described. First, hydrophobic burst valves (HBV) for the metering layer were introduced by locally treating the PVC with 0.1 µL/mm² hydrophobic (Aquapel®) and 0.2 µL/mm² superhydrophobic (Fluoropel™ 800M) solution by a mask-based coating strategy to form single-coated (sc) Aquapel® or double-coated (dc) Aquapel-Fluoropel HBVs (**Figure 4.2B**). After coating, an incubation step of 60 and 10 minutes, respectively, was performed at 50 °C. Second, hydrophobic barriers (HB) for the metering and pump layers were created by cutting 1.5 x 3 mm² rectangular filter papers from Whatman grades 43 and 598 with the Cameo blade cutter, afterwards impregnating with, respectively, 1 and 2 µL of Aquapel® hydrophobic solution and subsequently drying them overnight in the oven at 50 °C[29].

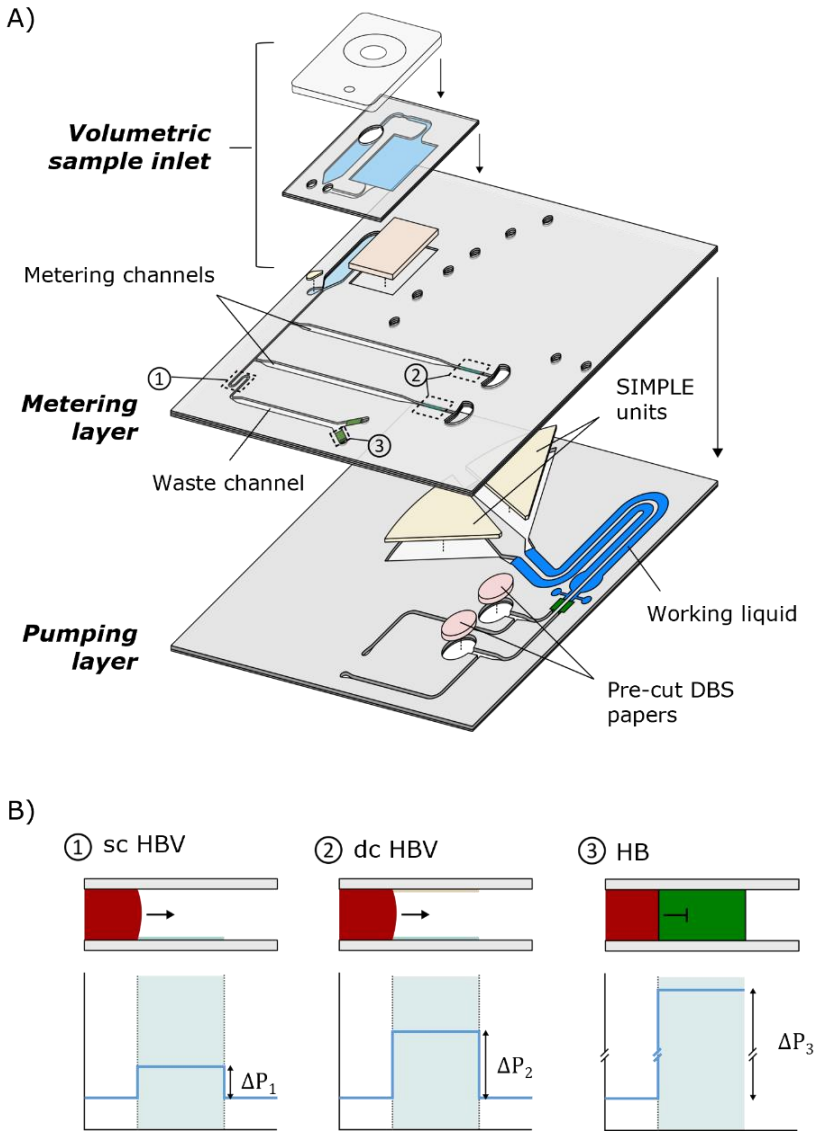

Figure 4.2: *A) Exploded view of the SIMPLE-DBS cartridge, consisting of three stacked microfluidic layers: the sample inlet system for user-friendly sample application, the metering layer for isolating two precisely metered sample volumes, the pumping layer holding the SIMPLE pumping units and DBS papers. The different valving principles: sc HBVs, dc HBVs and HBs are identified with numbers 1-3, respectively, from which the configuration and their respective burst pressure profiles are schematized in B). It is important to notice that* $\Delta P_1 < \Delta P_2 < \Delta P_3$.

Next, the fan-shaped SIMPLE pumping elements were cut from Whatman grade 598 filter paper, whereas circular DBS papers of 7mm in diameter were cut from Whatman CF12 filter paper, both using the Cameo blade cutter. After assembly of all microfluidic elements per layer, the three parts of the SIMPLE-DBS cartridge were laminated together and the DBS chamber was sealed by a removable film both on top and bottom. Finally, the working liquid (1/20 dilution of blue aqueous dye with distilled water) was pre-loaded on the cartridge by pipetting, after which the pre-filling holes were sealed.

4.2.6. Preparation of spiked blood samples

Citrated venous blood for all validation experiments on spiked samples was obtained from healthy volunteers, as approved by the UZ/KU Leuven Ethics Committee (S62134), and used within one week after collection. For the experiments of Section 4.3.3, unprocessed blood was spiked with ADM to obtain the concentrations of 0, 1, 4, 8 and 16 µg/mL. Blood samples with different Hct-levels were first prepared before spiking with 8 µg/mL ADM. The initial Hct-level of the unprocessed blood was determined in microcentrifuge tubes after centrifugation at 2400 g for 10 minutes. Next, plasma obtained from the same (pooled) blood samples was either added or removed to obtain 25, 40 and 55% Hct-levels.

4.2.7. Loading, extraction and analysis of DBS samples

Throughout this work, three different DBS preparations were compared (see also Figure 4.7 in Section 4.5.1 of the Supporting Information): (1) the traditional method – sub-punched samples of 40 µL spotted on Whatman® protein saver cards by pipetting; (2) the pre-cut reference method – pre-cut Whatman CF12 filter papers of 7 mm in diameter loaded with 10 µL of blood; (3) the SIMPLE-DBS method – pre-cut Whatman CF12 filter papers loaded by the SIMPLE-DBS cartridges. The latter were prepared by pipetting a volume of 40 µL on the conical inlet and, immediately after the cartridge finished loading both DBS, removing the sealings from both sides. All prepared DBS samples were allowed to dry for at least 16 hours at room temperature

before extraction (see Section 4.5.2 of the Supporting Information). The latter was performed by immersing each DBS sample in 240 µL of Superblock™ T20 buffer (0.05% Tween® 20) inside Eppendorf tubes. Hereto, for the traditional method, 6 mm sub-punches were taken from the center of the prepared DBS while all other DBS types were extracted as a whole. Subsequently, the samples were continuously shaken at 21 °C for 1 hour at 300 rpm, after which they were centrifuged for 5 minutes at 14000 g at the same temperature. After centrifugation, 180 µL of eluent was stored at -20 °C until analysis.

The ADM concentrations within the extracted eluents were analyzed using an in-house developed sandwich ELISA protocol[28]. Briefly, 96-well plates were incubated with the capturing monoclonal antibodies (MA-ADM28B8) for 72 hours at 4 °C, followed by a blocking step with 1% BSA in PBS. Next, the supernatant was incubated overnight at 4 °C to allow ADM binding. The sandwich assay was completed by an incubation with HRP-conjugated detection antibodies (MA-ADM40D8). After plate washing, signal was generated by adding o-phenylenediamine and H_2O_2 in citrate buffer to the wells. The enzymatic HRP reaction was stopped with H_2SO_4 and the absorbance was measured at 492 nm with an EL808 Absorbance Microplate Reader (BioTek Instruments Inc., USA). The obtained measurements were calibrated and interpolated from a reference standard curve of known ADM concentrations in the range of 0-5 ng/mL in serum given the 2000-fold dilution after DBS extraction. To determine the recovery rate, the measured ADM concentration in the supernatant was divided by the spiked ADM concentration in the citrated blood samples.

4.3. Results and discussion

4.3.1. User-friendly sample inlet system

Previous work showed the potential of a parallel metering concept, based on the coordinated burst actions of sc and dc HBVs[26]. However, when the loaded volume was too high, the metering system would not split-off metered plugs due to overfilling of the waste channel, while an insufficient volume would not be loaded onto the DBS papers (see also Supporting Information Section 4.5.3). To verify that the loaded sample volume is within a certain volume range, a user-friendly sample inlet system was developed to load the finger-prick blood drops. The system consists of two parts: the conical sample loading module (**Figure 4.3A-B** and the actual volumetric inlet (**Figure 4.3C-F**). The first serves as a chip-to-world interface to guide the applied blood into the small (5 mm) opening. It consists of a PMMA piece with an engraved conical-shaped inlet structure with an opening of 12 mm in diameter. The cone was hydrophobic treated to facilitate the blood application while avoiding the blood to spread over the inherently hydrophilic PMMA surface, which would lead to significant spillage. This was successfully confirmed by applying finger-prick blood drops to both an untreated (**Figure 4.3A**) and hydrophobically treated (**Figure 4.3B**) inlet. The second part of the sample inlet system, the volumetric inlet, prevents the chip from being activated in case the applied volume is too low, while removing the sample excess in case the applied volume is too high (**Figure 4.3C-F**). Passive uptake of the sample into the different parts of the sample inlet system by capillary forces requires a hydrophilic treatment of the PVC substrate to alter the inherently hydrophobic properties ($90° \leq CA \leq 95°$). This was done by applying a coating of hydrophilic agent P100 using a mask-based coating strategy with a surface coverage of 0.2 µL/mm² which resulted in a water contact angle of 11.9 ± 1.7°. For the complete data of the hydrophilic coating optimization the reader is referred to Section 4.5.4 of the Supporting Information.

To validate the working of the volumetric inlet system, 40 µL of citrated blood was applied per 10 µL drops and as a single drop. When the volume required to fill the sample chamber was not met, the droplet-shaped air vent remained unsaturated, thus open, so that the sample could not be drawn into the downstream sampling channel and air was pulled by the connected pump (**Figure 4.3C**). When the sample chamber was completely filled, the air vent was saturated with blood and sealed the connection with the downstream channel (**Figure 4.3D**). Meanwhile, the excess blood was removed by the waste paper through the waste removal channel (**Figure 4.3D-F**). Sealing of the air vent allowed the isolated blood sample to be withdrawn from the sample chamber (**Figure 4.3E**) and further manipulated in the downstream channel (**Figure 4.3F**).

The collected volume was determined to be slightly lower (22.9 ± 0.7 µL) than designed (25 µL) as a result of a small but unknown bias caused by blade cutting. The compatibility of the system to handle a wide sample volume range, while enabling multiple sample drop depositions, is a valuable asset as it makes the system more user-friendly and robust to variable bleeding intensities of different users. Additionally, the inlet system serves as a smart system with visual controls. The first visual control is the droplet-shaped air vent which has to turn red before activating the SIMPLE-DBS cartridge. In case this is not followed-up, the sample cannot be drawn into the downstream system and no DBS will be loaded. This prevents the generation of DBS with uncontrolled volume. The second visual control is the opening of the inlet, which has to be empty after the air vent has turned red. This ensures that the sample excess is removed, isolating a controlled volume of blood in the sample chamber. The time between sample loading and satisfaction of the visual controls in the sample inlet system mostly remained < 2 minutes (Supporting Information Section 4.5.5). Furthermore, the performance was found to be independent from the Hct-level within the range of 25-55%, as confirmed by a t-test ($p < 0.05$).

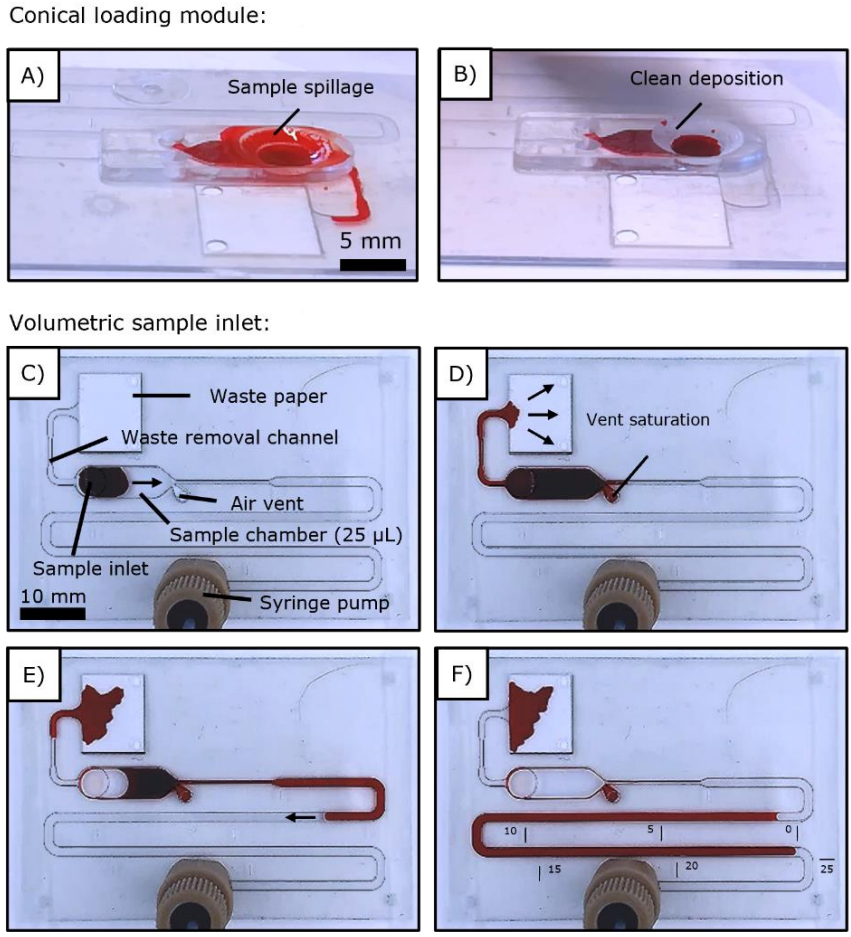

Figure 4.3: *A-B) volumetric sample inlet with attached conical loading module. Pictures of the loading module after application of a finger-pricked capillary blood sample on an untreated (A) and hydrophobically treated (B) PMMA conical loading module. C) Capillary filling of the sample chamber after deposition of the first citrated blood sample drop. D) Removal of sample excess by the waste paper through the waste removal channel after deposition of another citrated blood sample drop. E) Successful withdrawal of the isolated blood sample from the sample chamber by the downstream connected syringe pump. F) Further manipulation of the isolated sample volume in the channel.*

4.3.2. SIMPLE-DBS cartridge working principle

The proof-of-concept SIMPLE-DBS cartridge reported in Chapter 3 was only demonstrated for a single DBS sample. Here, this is expanded to two DBS samples by a novel microfluidic pumping concept in a cartridge which also includes the previously explained sample inlet system. These innovations ensure robust working of the SIMPLE-DBS cartridge by enabling double DBS loading and by avoiding sample under-/overloading, respectively. **Figure 4.4** summarizes the working principle of the SIMPLE-DBS cartridge. An overview of the main elements is given in **Figure 4.4A**. When the sample is applied on the inlet, it gets automatically drawn into the hydrophilic sample chamber through capillary forces (**Figure 4.4B**). When the sample chamber is completely filled, as visually indicated by the air vent being saturated with blood (visual control 1, **Figure 4.4C**), the waste removal system starts withdrawing the sample excess. As soon as the sample inlet is empty (visual control 2, **Figure 4.4D**), the sample chamber contains a controlled sample volume and the SIMPLE-DBS cartridge can be activated. This is done by simultaneously activating the two pumping units by a single finger-push (**Figure 4.4E**). As a result, the working liquid is absorbed into the porous medium, which generates a negative pressure gradient in the connected microfluidic network. This pulls the blood into the microfluidic channels of the metering system (**Figure 4.4F**). During the parallel metering of the sample (**Figures 4.4F-G**), both SIMPLE pumping units act as a single driving source because of their fluidic connection at the waste channel. Once the separated sample excess plug reaches the branched end of the waste channel, its flow is blocked by hydrophobic barriers (**Figure 4.4H**), fluidically disconnecting the two SIMPLE pumping units. Consequently, each pumping unit becomes a separate driver for independently loading the metered sample plugs on their respective DBS paper (**Figures 4.4H-I**). This system, called pump splitting, avoids loading only a single DBS due to air leaking into the microfluidic channels once the first metering channel is empty. For more detailed information about

the device engineering and design choices, the reader is referred to the Supporting Information Section 4.5.6.

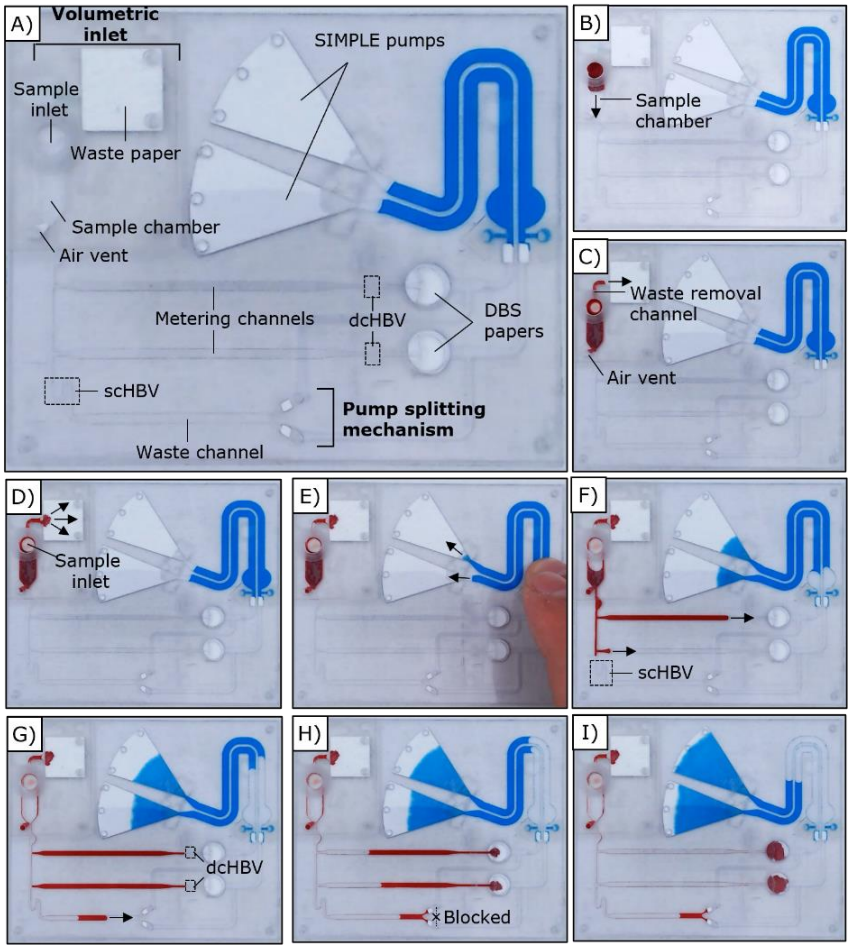

Figure 4.4: *A) Top view of the integrated SIMPLE-DBS device giving an overview of all microfluidic and paper elements. B-D) Capillary filling of the sample chamber after application of a finger-prick blood drop and sample excess removal to the waste paper. E) Finger-push activation of the SIMPLE pumping units. F-G) Parallel isolation of 2 metered sample volumes and discarding of the excess to the waste channel. H) Splitting of the coupled SIMPLE pumping units. I) Loading of both metered sample volumes on the DBS papers.*

4.3.3. Analytical performance of the SIMPLE-DBS sampling device

The SIMPLE-DBS cartridge was validated in the context of TDM. This application would benefit significantly from a DBS self-sampling solution to systematically monitor blood concentrations to keep them within the narrow therapeutic window. We focused specifically on the highly relevant case of TDM of biological drugs with MW > 100 kDa as, until today, microfluidic DBS micro-sampling devices have mainly been validated for several small molecules[21,22,30]. It can be expected that the analyte characteristics (e.g. size, shape, polarity, denaturation, etc.) have a significant influence on the analyte recovery[32]. To challenge the SIMPLE-DBS cartridges, a recombinant IgG1 monoclonal antibody ADM biosimilar was spiked in whole blood to validate the accuracy (< 15% from spiked concentration), precision (CV < 15%), Hct independency (< 15% from medium Hct level) and the within-cartridge equality of the DBS (regression coefficient between 0.85 and 1.15). Thresholds were set according to often used acceptance criteria in literature[33,34].

4.3.3.1. Validation for different ADM concentrations

First, the SIMPLE-DBS cartridges were compared to traditional Whatman® protein saver cards for a clinically relevant ADM concentration range of 0-16 µg/mL, spiked in citrated blood (45% Hct). After extracting the DBS samples, the ELISA reference technology described in Section 4.2.7 was used to analyze the extracted concentrations. **Figure 4.5A** shows the measured concentrations for SIMPLE-DBS (blue) and protein saver cards (orange) as compared to the spiked concentrations (grey). The data show that it was possible to significantly ($p < 0.05$) distinguish each spiked concentration using the SIMPLE-DBS cartridges. This confirms the ability to discriminate between the different ADM concentrations upon clinical treatment, being too low (< 4 µg/mL), optimal (4-12 µg/mL) and too high (> 12 µg/L). Furthermore, all the measured averages for the SIMPLE-DBS extracts show acceptable accuracy as they deviate < 15% from the spiked ADM concentrations. However, the variability is still

relatively high (average $CV_{SIMPLE\text{-}DBS}$ = 0.16 ± 0.03) and not significantly ($p > 0.05$) better than the protein saver cards (average CV_{PSC} = 0.12 ± 0.04). In addition, it was shown that the integrated sample inlet system did not influence the measured analyte concentrations (data presented in Section 4.5.7 of the Supporting Information).

Secondly, the agreement between the DBS spots on the same cartridge was evaluated by comparing the relationship between the measured concentrations of spot 1 and 2 per cartridge. These data are plotted in **Figure 4.5B** and the regression line for these data confirms both the absence of a proportional and systematic bias as the slope (0.97 ± 0.04) is close to 1 and the intercept (0.40 ± 0.31) is not significantly different from 0.

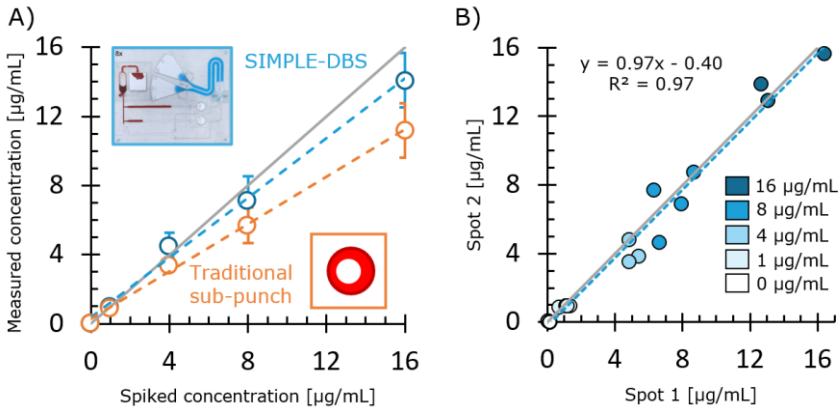

Figure 4.5: *A) Measured ADM concentrations using SIMPLE-DBS (blue) and traditional Whatman® protein saver cards (orange) compared to the theoretically spiked concentrations (grey) for a clinically relevant range (0, 1, 4, 8 and 16 µg/mL). Dashed lines represent the regression lines and error bars one standard deviation (n ≥ 3). B) Comparison of the measured concentrations of spot 1 and 2 for each tested cartridge with the blue dashed line the regression curve. Different shades of blue distinguish the different spiked ADM concentrations between 0 – 16 µg/mL. The solid grey line represents the reference curve y = 1.*

In accordance with the validation experiments of Chapter 3, the different slopes in the regression lines of **Figure 4.5A** for SIMPLE-DBS (slope = 0.87 ± 0.04) and protein saver cards (slope = 0.69 ± 0.02) indicate a proportional bias compared to the

reference line, which may be explained by a different effective volume residing in the sub-punches compared to the SIMPLE-DBS. The latter volume was characterized to be precisely 9.65 µL (cf. Chapter 3). The difference in slopes also suggests that the SIMPLE-DBS method may improve the sensitivity, but only if the analytical precision would further improve.

4.3.3.2. Validation for different Hematocrit levels

Next, the effect of a varying Hct-level on the measured ADM concentrations from DBS extracts was characterized for a range of 25-55%, which is beyond the clinical range (36-54%) typically seen in patients with Crohn's disease. During this experiment, the spiked concentration was kept constant, i.e. 8 µg/mL. The orange dashed line in **Figure 4.6A** shows a clearly increasing trend for the measured extracts for the traditional sub-punches, demonstrating the DBS area bias caused by the varying Hct levels. In fact, higher Hct leads to higher viscosity, which implies less spreading through the filter paper. Due to this, sub-punching leads to a higher measured concentration compared to samples with lower Hct level. On the other hand, the blue dashed line shows a decreasing trend in the measured ADM-levels from the SIMPLE-DBS extracts. This was additionally confirmed by the volumetric reference, obtained by pipetting 10 µL on pre-cut filter paper. These data indicate that, by solving the DBS area bias by volumetric DBS sampling, another source of Hct dependency is exposed (see further). Nevertheless, the analytical precision for each Hct level for the SIMPLE-DBS was very high ($CV_{Hct\text{-}25\%}$ = 0.03, $CV_{Hct\text{-}40\%}$ = 0.03, $CV_{Hct\text{-}55\%}$ = 0.04).

By comparing again the measured concentrations for spot 1 and 2, in **Figure 4.6B**, the Hct dependency is also reflected by the existence of a linear relationship. Nevertheless, the regression line shows also for this experiment that the DBS on the same cartridges led to equal results without significant proportional (slope = 1.02 ± 0.12) and systematic biases (intercept = -0.26 ± 0.84).

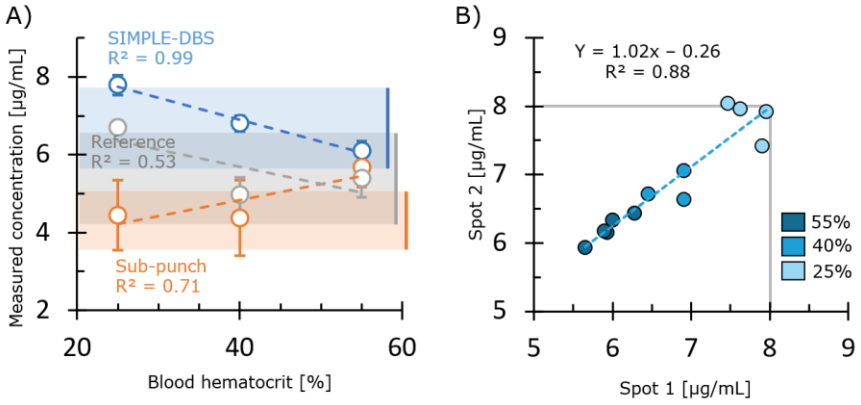

Figure 4.6: *A) Measured ADM concentrations comparing SIMPLE-DBS (blue), traditional Whatman® protein saver cards (orange) and pipetted pre-cut DBS reference (grey) for different Hct levels (25, 40 and 55%). Dashed lines represent the regression lines, shaded areas the 15% acceptance ranges around the medium Hct level and error bars one standard deviation (n ≥ 4). B) Comparison of the measured concentrations of spot 1 and 2 for each tested cartridge with the blue dashed line the regression curve. Different shades of blue distinguish the three different Hct levels while the grey lines represent the spiked concentration (8 µg/mL).*

This experiment shows a good analytical performance of our sampling device. The fact that more of the SIMPLE-DBS data points (77%) deviate less than 15%[33,34] from the medium Hct level measurements, suggests a lower Hct dependency compared to the traditional sub-punches, for which only 25% falls within this acceptance range. Nevertheless, the volumetric methods (blue and grey) expose the clearly hampered recovery for higher Hct levels. These sub-optimal extractions are also reflected by the very low R^2 value for the volumetric reference, indicating that only 53% of the concentrations can be explained by the fitted regression model. Although the optimization of the downstream analytical procedure was outside the scope of this work, it is important to mention that the aqueous extraction protocol should be further optimized (e.g. by increased agitation and duration[31]) until the volumetric reference shows no longer this Hct dependency.

4.4. Conclusion

Building further on the formerly reported single DBS sampling, in this chapter, a user-friendly cartridge for the collection of two parallel DBS samples from an unknown finger-prick blood volume was presented. Two novel microfluidic concepts were hereto introduced: a self-filling volumetric sample inlet system and a pump-splitting mechanism to robustly load both DBS samples. The SIMPLE-DBS sampling cartridges were validated *in vitro* in the context of TDM for ADM for a varying spiked concentration, as well as for varying Hct levels beyond the physiological range. In the comparison with traditionally sub-punched protein saver cards, the SIMPLE-DBS showed a significantly improved reproducibility. However, to be able to correctly compare the new technology with the current state of the art, the extraction protocol needs further optimization to eliminate the still existing Hct dependency.

Overall, these results show the capacity of the developed SIMPLE-DBS cartridge to collect multiple DBS in parallel starting from a single finger-pricked drop of blood with reduced potential for user errors. The newly developed microfluidic concepts offer a clear added value over the state-of-the art in terms of parallelization and user-friendliness. Although the cartridge was presented for dual DBS loading, the number can be increased with minimal design adjustments. Furthermore, the validation of such a cartridge was shown for a complex biological analyte with MW > 100 kDa. The next step is to perform a clinical performance study with Crohn disease patients to evaluate the field-readiness and user acceptance.

4.5. Supporting information

4.5.1. Overview of the DBS sample types for *in vitro* validations

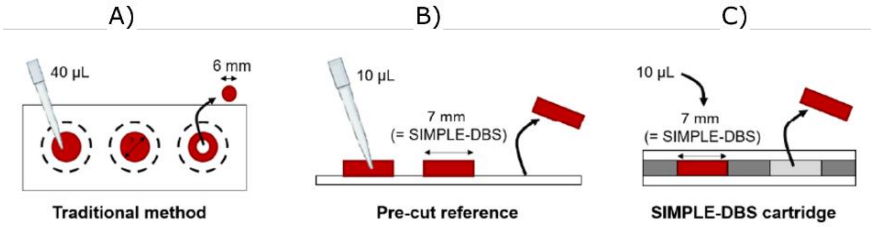

Figure 4.7: *Overview of the 3 different DBS preparation types used throughout the in vitro validations. A) The traditional method by spotting a large drop (40 µL) on a Whatman® protein saver card and sub-punching a 6 mm disc for extraction, also referred to as the traditional method. B) Pre-cut reference by pipetting a 10 µL sample on pre-cut filter papers. C) The SIMPLE-DBS cartridge used for DBS sample preparation.*

4.5.2. Influence of DBS drying time

To investigate DBS drying times, first, the absorbance spectrum was measured for whole blood, plasma and DBS extracts, all 1/208 diluted in Superblock™ T20 buffer. This allowed to measure the presence of free haemoglobin (Hb) and non-free Hb as they absorb light at 414 nm and 541 nm, respectively. **Figure 4.7A** shows a clearly increased optical density (OD) at a wavelength of 414 nm for the DBS extracts, which confirms the presence of free Haemoglobin (Hb) in the sample due to red blood cell lysis. The whole blood sample shows a small increase at 541 nm, which confirms the presence of non-lysed red blood cells. Plasma, for comparison, shows no increase since no Hb is present at all. Next, free Hb at 414 nm was measured for DBS extracts after drying times between 30 minutes and 16 hours (**Figure 4.8B**). It can be deducted that after 30 minutes, the amount of free Hb is rather low, indicating that almost no red blood cells were lysed. When the DBS were dried for about 1 hour, the highest amount of free Hb was measured. For longer drying times, this free Hb reduced again as a result of oxidation of Hb into Met-Hb, which is a process going along with drying of blood.

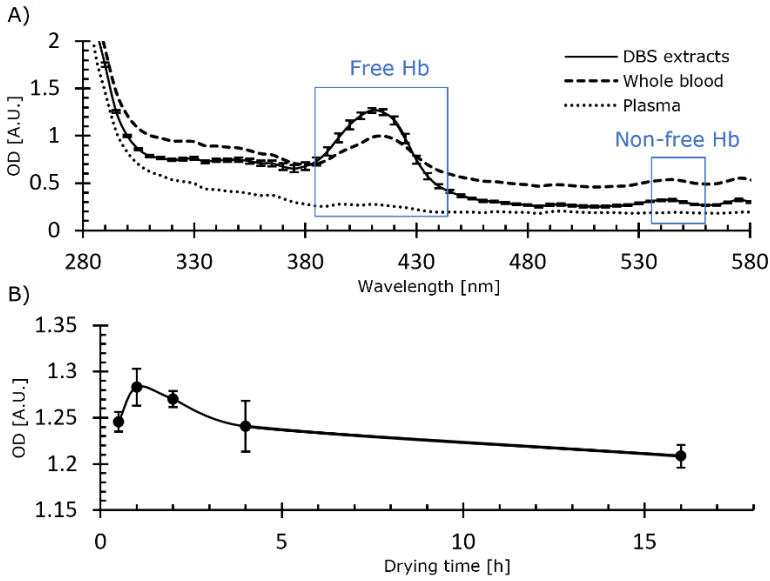

Figure 4.8: *A) Optical density spectrum of whole blood, plasma and DBS diluted 208 times in Superblock™ T20 PBS blocking buffer. Free haemoglobin (Hb) shows a peak at 414 nm, while non-free Hb at 541 nm. The shaded area shows one standard deviation around the averages measured for DBS extracts (n = 3). B) Average optical densities in function of DBS drying time, measured at 414 nm (free Hb). The error bars represent one standard deviation (n = 3). The microscopy picture inset shows the non-lysed red blood cells in the extract of a DBS which was dried for only 30 minutes.*

Based on these data, we can assume that lab experiments with drying times shorter than 16 hours are subjected to measurement bias. Furthermore, processing samples in the analytical laboratory immediately after DBS self-sampling is unrealistic in real-life situations. It was, therefore, chosen to dry the DBS at room temperature for at least 16 hours before extraction so that the DBS were completely dried and, most importantly, stable.

4.5.3. Device failure upon addition of insufficient or excess sample volume

As it is impossible for the patients to control at the point-of-care how much blood is added to the inlet of a sampling device in a user-friendly way, this work shows a concept whereby the added blood sample is roughly metered upon deposition on the inlet.

Figure 4.9 illustrates the importance of a rough metering system on the SIMPLE-DBS cartridge.

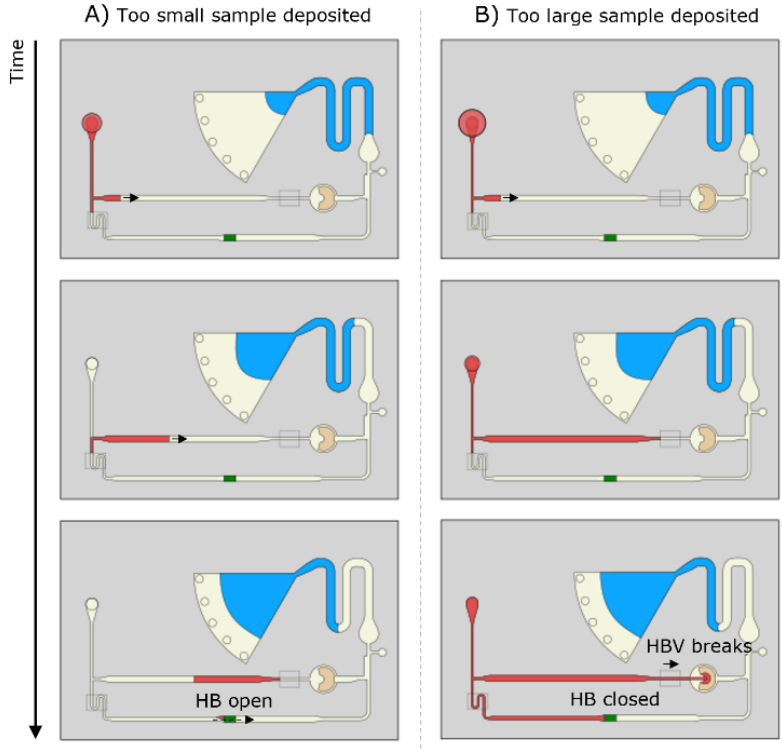

Figure 4.9: *Schematic illustration of the SIMPLE-DBS cartridge (shown for a single DBS) failure due too insufficient (left) or excess (right) blood sample volume.*

The schematic representation shows a situation where an insufficient amount of blood (left) is added on the inlet. If the system is activated, the metering channel will not be completely filled. This leads not only to a too small volume, but also no DBS will be formed as the HB at the end of the waste channel remains open. In case an excess sample volume is added on the inlet (right), no metered volume will split-off before DBS loading, leading to an overfilled pre-cut DBS paper and thus an overestimation of the analyte concentration.

4.5.4. Characterization of hydrophilic coating strategies

The protocol to treat the PVC substrate with P100 and X100 coating agents was first optimized in terms of hydrophilicity (water contact angle - CA) and reproducibility/uniformity of the coating. Besides the mask-based coating presented in the main manuscript, also a dip-based coating strategy was explored (**Figure 4.10**). In this strategy, the PVC substrate was immersed for 30 seconds in the hydrophilic coating solution (P100 or X100) and afterwards dried at room temperature for 5 minutes. Also here, CA measurements were performed to determine hydrophilic properties. Dip-based coating showed reproducible results for the X100 hydrophilic agent, however, it was not well-suited for the P100 hydrophilic agent. The inconsistent and high contact angles of the latter are assumed to be a result of a too low surface coverage due to the dip coat process, similar to what was observed in the mask-based strategy. Additionally, the dip-based coating strategy does not allow for localized application of the coating what is required in this application. Therefore, only the results of the mask-based coating strategy were shown in the main manuscript.

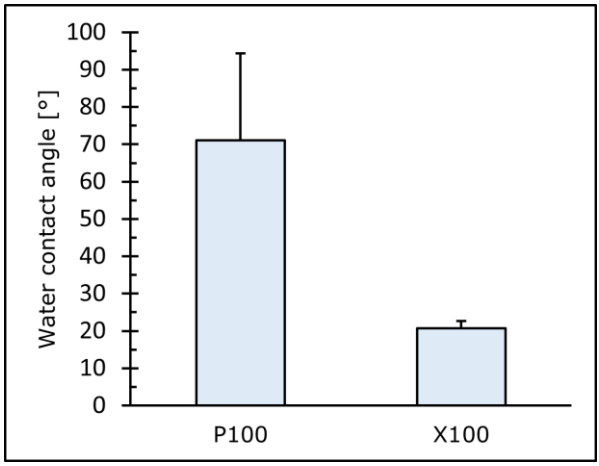

Figure 4.10: *Average of measured water CAs for the dip-coating strategy for the hydrophilic agents P100 and X100 on PVC. Error bars represent one standard deviation (n ≥ 8).*

The effect of different coating volumes per surface area on the uniformity and consistency was evaluated by CA measurements (see **Figure 4.11**). As can be deducted from Figure 4a, the P100 agent (orange) requires at least a surface coverage of 0.2 µL/mm² as for lower volumes very inconsistent CAs with insufficient hydrophilic properties (CA > 40°) were obtained. When using a surface coverage between 0.2 and 0.4 µL/mm², however, very reproducible CAs were measured (11.9 ± 1.7° and 16.6 ± 4.6°, respectively). For the X100 treatment (blue), on the other hand, the variability was independent from the applied coating volume as reproducible results were obtained over the whole range of tested volumes. Although, a slight increase in absolute CA (18.4 ± 2.4° to 27.5 ± 6.6° for 0.05 and 0.4 µL/mm², respectively) was observed upon increasing coating agent volume. This change can be explained by the increased thickness of the coated film which introduces surface inhomogeneities, resulting in increased hydrophobic properties. To maximize the capillary forces in the volumetric sample inlet, the P100 hydrophilic agent with a surface coverage of 0.2 µL/mm² was selected for treating the PVC substrate.

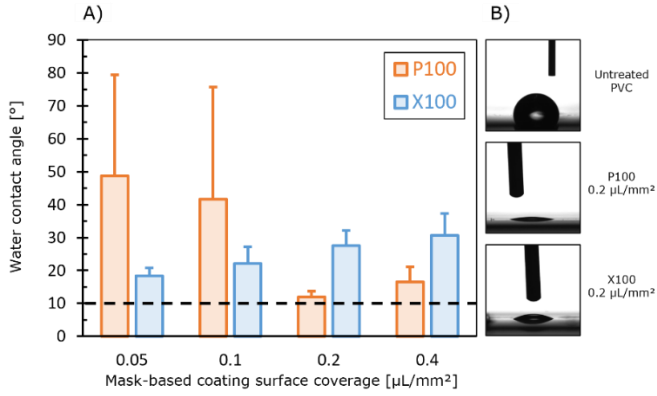

Figure 4.11: *A) Averages of measured water CA for the mask-based coating strategy with surface coverages of 0.05, 0.1, 0.2 and 0.4 µL/mm². Black dashed line indicates the threshold of super hydrophilic surface properties (water CA ≤ 10°). Error bars represent a single standard deviation (n ≥ 8). B) Images of CA measurements of an untreated PVC substrate and a P100/X100 treated PVC surface with a surface coverage of 0.2 µL/mm².*

4.5.5. Volumetric inlet independency from Hct level

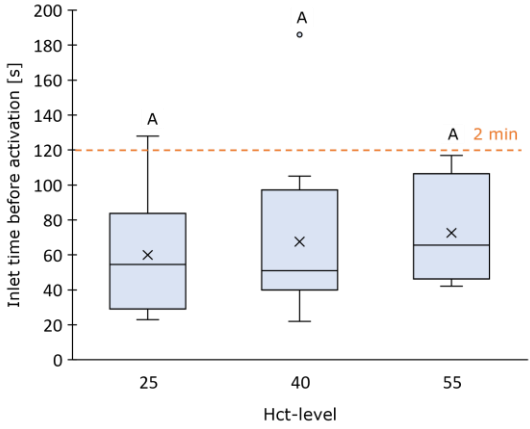

Figure 4.12: *Box plots depicting the measured time between sample deposition into the volumetric sample inlet and the satisfaction of the two visual controls for a varying Hct level between 25% and 55%. The line within the boxes represent the medians, the crosses the averages and the error bars the 95% confidence intervals (n = 26). The connected letters report indicates that, as a result of a t-test, no differences in required time between the Hct levels could be shown ($p < 0.05$).*

4.5.6. Device engineering and design choices

The final design of the SIMPLE-DBS cartridges is the result of many iterations and adjustments. The most important inventive step to ensure a robust double-loading, i.e. the pump splitting mechanism, is further clarified in **Figure 4.13**.

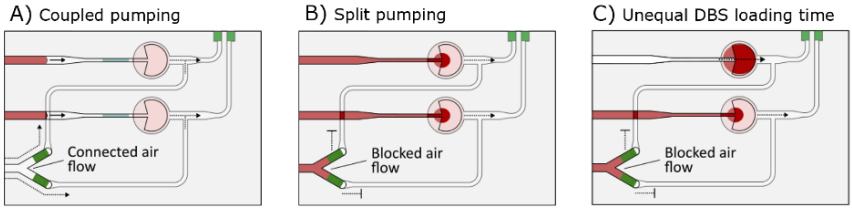

Figure 4.13: *Schematic explanation of the pump splitting mechanism. A) When the waste channel is empty, the channel network in the pumping layer is fully connected. B) When the waste channel is completely filled and the proceeding front has reached the barriers, the air flow at the t-junction is blocked. This decouples the loading of both DBS. C) This image shows the situation of unequal DBS loading times. After DBS loading, air can pass via the inlet to the pumping layer. Thanks to the pump splitting mechanism, the second DBS can still be loaded since the air flow is blocked.*

The system made it possible to move from single DBS loading (as shown in Chapter 3) to multiple DBS loading by coupling an individual 30° SIMPLE unit (allowing an individual flow rate of about 9.5 ± 1.5 µL/min per unit) to each metering channel by blocking the bifurcation at the end of the waste channel. Before this event, both 30° SIMPLE units act together as a single 60° SIMPLE unit allowing a flow rate of about 18.2 ± 4.8 µL/min. The latter has been used in Chapter 3 to allow single DBS loading within 5 minutes after activation. The current split pump mechanism allows double-loading without substantially longer operation times, however, the pumping speed could be further increased by, among other methods, increasing the angle of the sector-shaped paper.

To further elaborate on the other parts of the SIMPLE-DBS cartridge, **Table 4.1** describes with more detail some of the specific design choices and pass/fail criteria followed during the iterative development process.

Table 4.1: *Schematic overview of the measures and essential design choices for the final version of the SIMPLE-DBS cartridge*

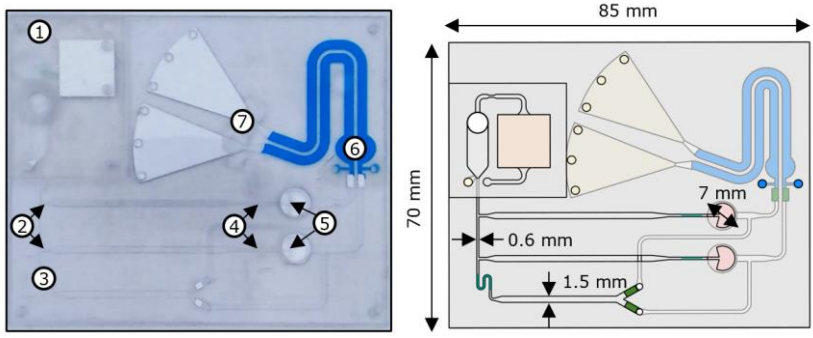

	Schematic	Rationale behind design choice	Pass/fail criterium
1		Constriction in the waste removal channel: to temporarily slow down the waste removal	Sample chamber completely filled before the excess reaches the waste paper
2		Constriction at the bifurcation toward the metering channels: to ensure precise splitting of the blood	Precise sample metering (see characterization in Chapter 3, CV < 3%)
3		Serpentine channel at HBV-1: To improve the HBV robustness (cf. non-Newtonian shear thinning effect for higher Hct levels reduces burst pressure)	Metering success for large range of Hct levels (see Chapter 3, Hct tested in range 25-70 Hct%)
4	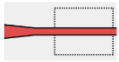	Reduced channel width at HBV-1: To equalize the channel width for different burst pressures (cf. Chapter 3, Section 3.5.4)	Metering success (see Section 3.5.4 of Chapter 3)
5	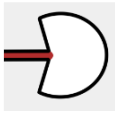	Wide angle at the end of the metering channel: To ensure proper DBS loading and increase the area open to air for faster drying. The blood drops onto the center of the pre-cut filter paper	Successful DBS loading + complete emptying of metering channel
6		Activation spots as two half-circles: To allow the simultaneous activation of both (independent) SIMPLE pumping units	Successful dual SIMPLE unit activation upon single finger-press
7		Width of the tip of the SIMPLE filter paper: The width has been normalized to ensure similar pumping flow rates between different cartridges.	Similar average flow rate in the range of 10-15 µL/min (i.e. total duration between 5-7 min per cartridge)

4.5.7. Influence of the hydrophilic coating of the inlet

The application of hydrophobic and hydrophilic chemical coatings might lead to increased non-specific binding of the analyte molecules or an affected stability. Therefore, the potential influence of the sample inlet system on the adalimumab (ADM) measured recoveries was investigated for SIMPLE-DBS cartridges with and without inlet system. This was also compared to the traditional sub-punching method on Whatman® protein saver cards. Citrated blood was spiked with 8 µg/mL ADM as sample source for this experiment. Results can be found in **Figure 4.14**. The difference between the recovered concentrations for SIMPLE-DBS with and without integrated sample inlet system was not found to be significant ($p < 0.05$). Moreover, both cartridge types showed a similar variability (CV ≈ 12%). This confirms that the

integration of the volumetric sample inlet system, and in particular its chemical coatings, do not influence the DBS samples. Additionally, the much lower back-calculated concentrations for the sub-punched DBS were again confirmed in this experiment.

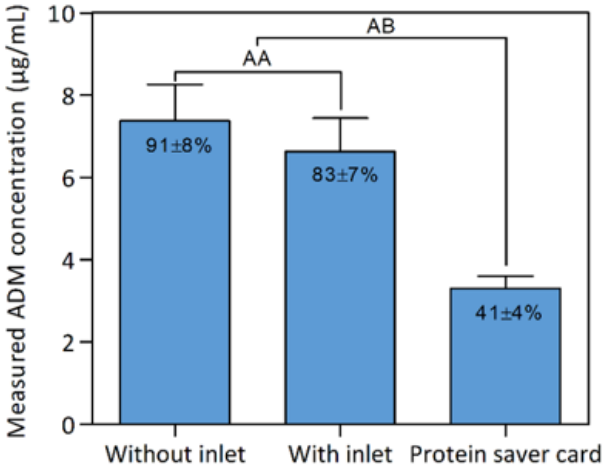

Figure 4.14: *Average measured ADM recoveries for SIMPLE-DBS cartridges with (n=4, 2 spots per cartridge) and without (n = 5, 2 spots per cartridge) volumetric sample inlet system, compared to the golden standard sub-punched DBS from Whatman® protein saver cards (n = 5), for a blood sample source spiked with 8 µg/mL ADM. Error bars represent 1 standard deviation. Significant differences are indicated using connected letters reporting.*

4.6. References

1. Drennan, V. M. & Ross, F. Global nurse shortages - The facts, the impact and action for change. *British Medical Bulletin* 130, 25–37 (2019).
2. Zakaria, R., Allen, K. J., Koplin, J. J., Roche, P. & Greaves, R. F. Advantages and challenges of dried blood spot analysis by mass spectrometry across the total testing process. *Ejifcc* 27, 288–317 (2016).
3. Freeman, J. D. *et al.* State of the science in dried blood spots. *Clinical Chemistry* 64, 656–679 (2018).
4. Prinsenberg, T. *et al.* Dried blood spot self-sampling at home is a feasible technique for hepatitis C RNA detection. *PLoS ONE* 15, 1–13 (2020).
5. Ogrič, M. *et al.* Detection of adalimumab and anti-adalimumab antibodies in patients with rheumatoid arthritis: a comprehensive overview of methodology pitfalls and benefits. *Immunologic Research* 65, 172–185 (2017).
6. Thevis, M., Kuuranne, T., Dib, J., Thomas, A. & Geyer, H. Do dried blood spots (DBS) have the potential to support result management processes in routine sports drug testing? *Drug Testing and Analysis* 12, 704–710 (2020).

7. O'Mara, M. *et al.* The effect of hematocrit and punch location on assay bias during quantitative bioanalysis of dried blood spot samples. *Bioanalysis* 3, 2335–2347 (2011).
8. Lenk, G., Hansson, J., Beck, O. & Roxhed, N. The effect of drying on the homogeneity of DBS. *Bioanalysis* 7, (2015).
9. Moat, S. J. *et al.* Effect of blood volume on analytical bias in dried blood spots prepared for newborn screening external quality assurance. *Bioanalysis* 12, 99–109 (2020).
10. Bond, M. M. & Richards-Kortum, R. R. Drop-to-drop variation in the cellular components of fingerprick blood: Implications for point-of-care diagnostic development. *American Journal of Clinical Pathology* 144, 885–894 (2015).
11. De Kesel, P. M. M., Sadones, N., Capiau, S., Lambert, W. E. & Stove, C. P. Hemato-critical issues in quantitative analysis of dried blood spots: Challenges and solutions. *Bioanalysis* 5, 2023–2041 (2013).
12. Chao, T. C., Trybala, A., Starov, V. & Das, D. B. Influence of haematocrit level on the kinetics of blood spreading on thin porous medium during dried blood spot sampling. *Colloids and Surfaces A: Physicochemical and Engineering Aspects* 451, 38–47 (2014).
13. Daousani, C., Karalis, V., Malenović, A. & Dotsikas, Y. Hematocrit effect on dried blood spots in adults: a computational study and theoretical considerations. *Scandinavian Journal of Clinical and Laboratory Investigation* 79, 325–333 (2019).
14. Velghe, S., Delahaye, L. & Stove, C. P. Is the hematocrit still an issue in quantitative dried blood spot analysis? *Journal of Pharmaceutical and Biomedical Analysis* 163, 188–196 (2019).
15. Neto, R., Gooley, A., Breadmore, M. C., Hilder, E. F. & Lapierre, F. Precise, accurate and user-independent blood collection system for dried blood spot sample preparation. *Analytical and Bioanalytical Chemistry* 410, 3315–3323 (2018).
16. Leuthold, L. A. *et al.* New microfluidic-based sampling procedure for overcoming the hematocrit problem associated with dried blood spot analysis. *Analytical Chemistry* 87, 2068–2071 (2015).
17. Lenk, G. *et al.* A disposable sampling device to collect volume-measured DBS directly from a fingerprick onto DBS paper. *Bioanalysis* 7, 2085–2094 (2015).
18. Velghe, S., De Troyer, R. & Stove, C. Dried blood spots in therapeutic drug monitoring and toxicology. *Expert Opinion on Drug Metabolism and Toxicology* 14, 1–3 (2018).
19. Lenk, G., Ullah, S., Stemme, G., Beck, O. & Roxhed, N. Evaluation of a volumetric dried blood spot card using a gravimetric method and a bioanalytical method with capillary blood from 44 volunteers. *Analytical Chemistry* 91, 5558–5565 (2019).
20. Velghe, S., Deprez, S. & Stove, C. P. Fully automated therapeutic drug monitoring of anti-epileptic drugs making use of dried blood spots. *Journal of Chromatography A* 1601, 95–103 (2019).
21. Protti, M. *et al.* Assessment of capillary volumetric blood microsampling for the analysis of central nervous system drugs and metabolites. *Analyst* 145, 5744–5753 (2020).
22. Salamin, O. *et al.* Is pain temporary and glory forever? Detection of tramadol using dried blood spot in cycling competitions. *Drug Testing and Analysis* 12, 1649–1657 (2020).
23. Marchand, A., Roulland, I., Semence, F. & Ericsson, M. Adaptation of Elecsys®anti-severe acute respiratory syndrome coronavirus-2

immunoassay to dried blood spots: Proof of concept. *Bioanalysis* 13, 165–171 (2021).
24. Li, H., Myzithras, M., Bolella, E., Leonard, A. & Ahlberg, J. Whole blood stability evaluation of monoclonal antibody therapeutics using volumetric absorptive microsampling. *Bioanalysis,* 13 (2021).
25. Michielin, G. *et al.* Clinical sensitivity and specificity of a high-throughput microfluidic nano-immunoassay combined with capillary blood microsampling for the identification of anti-SARS-CoV-2 Spike IgG serostatus. *medRxiv* (2022).
26. Vloemans, D. *et al.* Precise sample metering method by coordinated burst action of hydrophobic burst valves applied to dried blood spot collection. *Lab on a Chip* 21, 4445–4454 (2021).
27. Dal Dosso, F. *et al.* Creasensor: SIMPLE technology for creatinine detection in plasma. *Analytica Chimica Acta* 1000, 191–198 (2018).
28. Bian, S. *et al.* Generation and characterization of a unique panel of anti-adalimumab specific antibodies and their application in therapeutic drug monitoring assays. *Journal of Pharmaceutical and Biomedical Analysis* 125, 62–67 (2016).
29. Dal Dosso, F., Tripodi, L., Spasic, D., Kokalj, T. & Lammertyn, J. Innovative Hydrophobic Valve Allows Complex Liquid Manipulations in a Self-Powered Channel-Based Microfluidic Device. *ACS Sensors* 4, 694–703 (2019).
30. Deprez, S., Paniagua-González, L., Velghe, S. & Stove, C. P. Evaluation of the performance and hematocrit independence of the HemaPEN as a volumetric dried blood spot collection device. *Analytical Chemistry* 91, 14467–14475 (2019).
31. Bloem, K. *et al.* Capillary blood microsampling to determine serum biopharmaceutical concentration: Mitra® microsampler vs dried blood spot. *Bioanalysis* 10, 815–823 (2018).
32. Koster, R. A. *et al.* What is the right blood hematocrit preparation procedure for standards and quality control samples for dried blood spot analysis? *Bioanalysis* 7, 345–351 (2015).
33. Capiau, S. et al. Official international association for therapeutic drug monitoring and clinical toxicology guideline: Development and validation of dried blood spot-based methods for therapeutic drug monitoring. *Therapeutic Drug Monitoring* 41(4), 409-430 (2019)
34. Mingas, P. D., Zdovc, J., Grabnar, I. & Vovk, T. The evolving role of microsampling in therapeutic drug monitoring of monoclonal antibodies in inflammatory diseases. *Molecules* 26, (2021).
35. Lehmann, S., Delaby, C., Vialaret, J., Ducos, J. & Hirtz, C. Current and future use of 'dried blood spot' analyses in clinical chemistry. *Clinical Chemistry and Laboratory Medicine* 51, 1897–1909

Chapter 5

An improved finger-prick procedure for capillary blood self-sampling

5.1. Introduction

Capillary blood sampling by skin puncture is becoming widely known as an important alternative to venous puncture. Nevertheless, obtaining a sufficient amount of capillary blood by a single finger-prick is often unfeasible which leads to, among others, false negative analysis results[1–5]. For example, to obtain high-quality samples on a traditional dried blood spots (DBS) card, 35-75 µL of blood is required for each spot, deposited as a single drop without touching the paper[6–8]. To increase the available volume, capillary tubes or other blood transferring methods can help, however, they are not preferred since they require an extra manual intervention and result in an extra source of variability[9,10]. Most standardized finger-prick protocols also require wiping off the first drop of blood to avoid contamination with, e.g., skin surface debris due to skin sloughing[11]. Additionally, if plasma/serum separation is required for the analysis, it has to be taken into account that the maximally achievable volumetric yield is 65%[12]. Overall, the volume losses on top of the often already insufficient capillary blood availability by skin puncture do not comply with the required volumes up to 250 µL[3,13]. This is especially cumbersome for applications where multiple repetitions or multiple analyses are needed, e.g. to measure both therapeutic biologicals and their anti-drug antibody concentrations for therapeutic drug monitoring (TDM)[14].

To maximize the collected blood sample volume, non-physiological factors influencing the size of the injury (i.e. the pricking technique) can be controlled. It has been shown that thinner needles require deeper and more painful penetration into the skin, whereas thicker lancets can increase the size of the injury without significantly increasing the number of affected nerve endings[3,15]. Warming up hands and fingers before lancing improves blood perfusion of the fingers, helping to collect higher volumes[16]. Another non-physiological factor that can improve the obtained blood volume is the protocol to extract the blood. Often, fingers are milked by squeezing the finger-tips, yielding volumes up to hundreds of microliters[1,13]. However, applying these

uncontrolled forces increases the risk of haemolysis, which in turn promotes coagulation of the blood[18–20]. In fact, the most common reason for the rejection of both venous and capillary blood samples in the clinical laboratory is haemolysis[4,17]. The induced coagulation is especially problematic for sample manipulations (e.g. metering, reagent mixing, sample dilution, etc.) in channel- or paper-based microfluidic devices. Furthermore, squeezing the finger-tip might lead to sample dilution with intra- and intercellular fluid, causing biased analysis results[10,19]. Alternatively, multiple finger-pricks on different fingers can be performed to increase the overall obtained sample size, however, this compromises on user-friendliness and invasiveness. Next to these non-physiological parameters, finger-pricking also suffers from a substantial variability due to physiological patient dependent factors, such as poor peripheral perfusion or vascular diseases[4,17].

To overcome the limitations of the traditional finger-pricking procedure, this work proposes an improved procedure by applying a finger-tourniquet to locally increase the blood pressure before activating the lancet. The proposed finger-tourniquet procedure is compared to the traditional procedure in a validation study with healthy volunteers by executing paired measurements of the bleeding intensity. The blood volumes are measured using a custom built accurate self-filling microfluidic metering tool.

5.2. Materials and methods

5.2.1. Reagents and materials

Double-sided pressure-sensitive adhesive (PSA) with thickness 153 µm (200MP 7956MP) was acquired from 3M (USA). PVC 180 µm plastic films were bought from Delbo (Belgium) whereas PMMA 1 mm cast acrylic sheets were obtained from Pyrasied (Netherlands). The hydrophobic agent Fluoropel™ 800 and the surfactant Tween 20 were obtained from Cytonix (USA) and Sigma-Aldrich (Belgium), respectively. Blood flow equivalent TL4 (60% hematocrit) was ordered from Joninn (Denmark). Romed

alcohol pads and Accu-Check® finger-prick lancets were bought from Novolab (Belgium).

5.2.2. Metering tool fabrication and characterization

Metering tools with a long, self-filling channel were fabricated by the low-cost lamination method exploited in this dissertation (see also **Figure 5.1**)[21–23]. A Trotec Speedy 300 CO_2 laser cutter (Trotec, Austria) was used to cut and engrave the PSA and PMMA layers. First, a single channel was cut in a double-layer PSA sheet to obtain channels with 306 µm (2 × 153 µm) in height. Next, the conically-shaped inlets and volume indications were obtained by laser engraving before cutting out the air-vent holes. The bottom plastic layer was cut from the PVC sheets using a Maxx Air blade-cutter (KNK, USA). The conical inlet and its surroundings were hydrophobically coated by pipetting 10 µL of Fluoropel™ 800 hydrophobic agent and, subsequently, drying in the oven for 5 minutes at 50 °C.

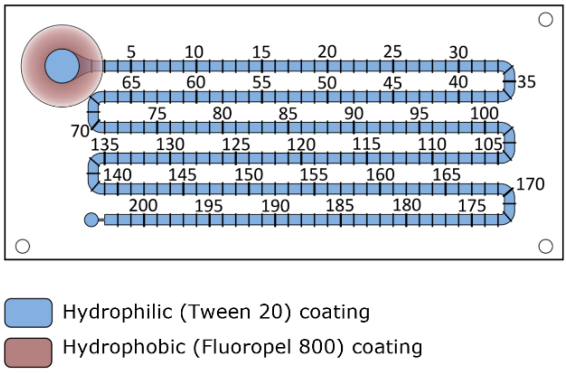

Figure 5.1: *Top view of the metering tool giving insight into the layer-by-layer assembly and coating.*

To obtain a sufficiently high flow rate, all sides of the channel were coated by filling it with a 0.01% (v/v) Tween 20 solution in Milli-Q water. This way, both the contact angle (CA) and interfacial tension were reduced, which induced capillary filling (cf. Eq. (3.1) of Chapter 3). After the metering channel was completely filled with Tween 20 solution, it was incubated at room temperature for 30 minutes, after which the channel was emptied

again by blowing air through it. Finally, the metering tools were dried overnight (> 16 hours) in the oven at 50 °C.

To characterize the obtained water contact angle (CA) after Tween 20 coating, the coating strategy described in previous paragraph was mimicked on larger open surfaces. First, an excess of 0.01% (v/v) Tween 20 was pipetted into a PSA mask, attached to either PMMA or PVC substrates, to cover an area of 1.5 cm^2, and incubated for 30 minutes at room temperature. Next, the Tween 20 solution was completely removed and air was gently blown over the surface as would be the case while emptying the metering tool channel. Then, the PMMA and PVC sheets were incubated at 50 °C overnight. The CAs from 5 µL droplets deposited on the coated PMMA and PVC surfaces were measured in 5-fold using a CAM200 goniometer (KSV Instruments, Finland). The statistical software JMP Pro 15 (JMP Statistical Discovery, USA) was used to perform t-tests for comparing the CAs of hydrophilically treated PVC and PMMA.

The filling of the metering tools was video recorded using a Logitech C920 digital webcam (Logitech, Switzerland) and the measured volumes over time were assessed using the laser-engraved indication marks. The accuracy and reproducibility were validated by a gravimetric method. Hereto, TL4 blood equivalent (60% hematocrit) was pipetted onto the hydrophobic inlet per 50 µL drops. Once the flow stopped after each addition, and besides reading the volume indication on the tool, the accumulated weight was assessed using a CPA124S high precision balance (Sartorius, Belgium) to obtain a calibration curve. Weight to volume conversion was done using the specific gravity of 1.0 g/mL as specified by the blood equivalent supplier.

5.2.3. Finger-prick procedure

The study protocol described below was approved by the Ethical Committee UZ/KU Leuven (S65868). Participants were asked to follow the instructions with the guidance from a trained professional, a short instruction video and an instruction leaflet. Before every prick, all materials (lancet, tourniquet, alcohol wipe, band-aid and metering tool) were collected and made ready. The

finger-prick lancet (AccuChek Safe-T-Pro Plus, Roche Diabetes Care, Belgium) was turned to its longest length setting (2.3 mm) and the safety cap was removed. Then, hands were washed with warm water (as warm as tolerable) for at least 30 seconds and dried afterwards. Next, in case of the finger-tourniquet method, the Velcro strap (i.e. tourniquet) was applied around the distal phalanx of the finger (**Figure 5.2**). In case of the traditional method, the rest of the protocol was carried out without applying the Velcro strap.

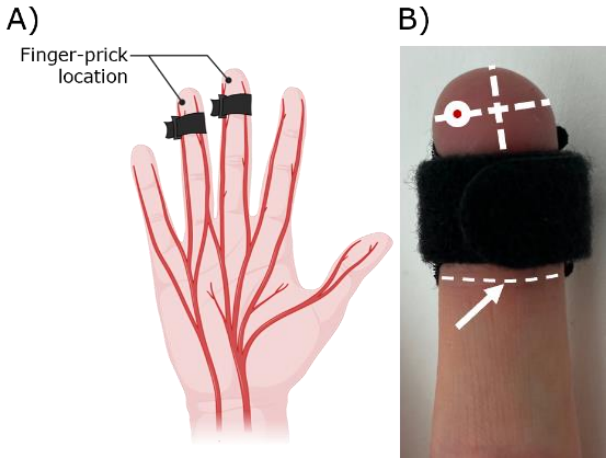

Figure 5.2: *A) Finger-tourniquet application and finger-prick locations on the distal phalanges of ring- and middle-finger [created with BioRender.com]. B) close-up view of a finger with finger-tourniquet applied. The arrow indicates the joint of the distal phalanx, which should not be ligated by the strap. The dashed lines and red dot indicate the best finger-pricking location.*

In the next step, the finger-tip was thoroughly disinfected with the provided alcohol wipe and after it had dried up, the side of the finger pad was punctured by the finger-prick lancet. At this moment, the timer was started for 40 seconds and during this time participants were asked to deposit as much blood drops as possible into the inlet of the metering tool without touching it. As soon as the time ran out, the added blood volume was assessed using the indicators on the metering tool. It must be remarked that for blood volumes below the detection limit of the metering tool (i.e. 2 µL), the measured volume was set to 0 µL.

A summary of the finger-pricking workflow is given by **Figure 5.3**. To comply with the standard medical practice, finger-pricks were carried out on both ring- or middle finger of the non-dominant hand.

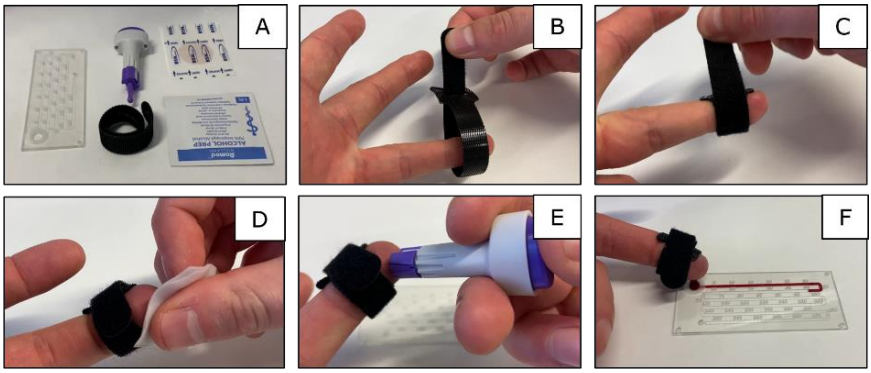

Figure 5.3: *Overview of the workflow (except for hand washing) for the finger-tourniquet method. A) All materials required for the finger-tourniquet procedure: lancet, Velcro strap, alcohol wipe, band-aid and metering tool. B) Application of the Velcro strap around (in this case) the ring finger beyond the top phalanx, and C) tightening of the strap. D) disinfection of the finger-tip by cleaning using the alcohol wipe. E) puncturing of the side of the finger-tip pad. F) Deposition of blood drops on the inlet and automatic propulsion of the blood into the channel of the metering tool.*

5.2.4. Study design with participants

In total, 18 participants were included in this study, all of whom gave voluntarily written informed consent before inclusion in the study. All participants had to be adults (> 18 years) in a good health condition. Participants could not meet one or more of the following exclusion criteria: (1) any form of immune suppression, (2) bleeding disorders, (3) concomitant use of anticoagulant medication, (4) concomitant use of finger-prick lancets in daily life (e.g. diabetics for daily blood sugar monitoring), and (5) any disorder or concomitant treatment which in the investigators' opinions could jeopardize the participant's safety or compliance with the protocol.

Participants were asked to take two finger-pricks on three sampling moments: one according to the traditional procedure[11] and one by applying the finger-tourniquet to increase locally the blood pressure before lancing. This way, both the ring- and

middle finger were pricked during each sampling moment. Although no differences between the volumes resulting from either the ring- or middle finger were expected, any potential systematic bias was avoided by varying the order of the applied protocols (finger-tourniquet or traditional) and the used finger (ring- or middle finger) for the three sampling moments. An example of such a finger-pricking scheme is shown in **Table 5.1**. Furthermore, to allow complete healing of the finger-tips, it was chosen to separate two consecutive sampling moments by at least three full days. In total, each participant collected 6 finger-pricks over the course of minimally two and maximally four weeks.

Table 5.1: *Example of a finger-pricking scheme of a single study participant, showing how the two finger-pricking protocols (tourniquet and traditional) and pricked finger of the non-dominant hand were changed for each sampling moment to avoid potential systematic biases.*

Sampling moment	Finger-prick 1	Finger-prick 2
1	- *Tourniquet method* - *Ring finger*	- *Traditional method* - *Middle finger*
2 *(>3 days later)*	- *Traditional method* - *Middle finger*	- *Tourniquet method* - *Ring finger*
3 *(>3 days later)*	- *Tourniquet method* - *Middle finger*	- *Traditional method* - *Ring finger*

One participant dropped out of the study after the first sampling moment so the sample size reduced to 17 participants or 51 paired measurements. These data were analyzed using the non-parametric Wilcoxon signed-rank test in JMP as they did not meet the normality requirement for a paired difference t-test.

5.3. Results and Discussion

5.3.1. Characterization of an accurate volume metering tool

To assess the effect of the Tween 20 coating on both the PMMA and PVC surface, the CAs were measured. As can be deducted from **Figure 5.4**, the coating of PMMA results in a significantly ($p < 0.05$) lower CA compared to PVC, as confirmed by a paired t-

test. This was expected since the PMMA used is inherently hydrophilic (± 73°) whereas PVC is relatively hydrophobic (± 84°)[24]. The obtained CAs for both polymers were very low and close to super-hydrophilicity (10°): 11.2° ± 0.5° for PMMA and 14.5° ± 0.9° for PVC. Furthermore, a good reproducibility was achieved with CV-values of 4.5% and 6.0% for PMMA and PVC, respectively.

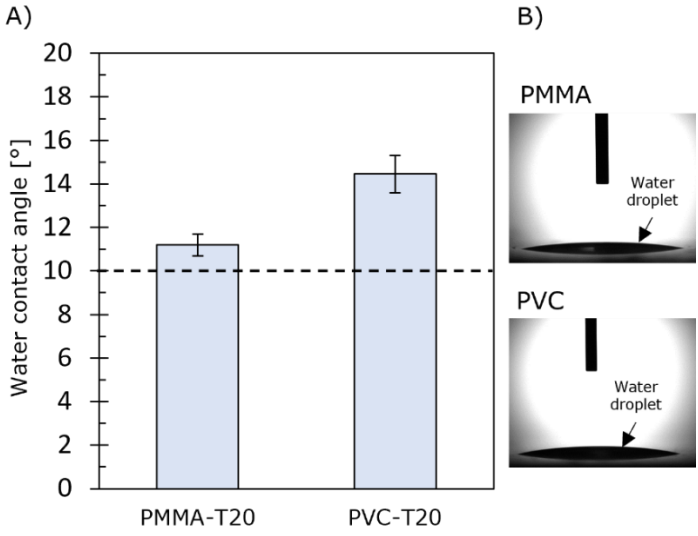

Figure 5.4: *A) Obtained water CAs for coating PMMA and PVC by mimicking the channel coating protocol. The error bars represent one standard deviation (n = 5) and the dashed line the super-hydrophilicity threshold. B) Images of CA measurements for both polymers, showing that the water droplets spread well out over the Tween 20 treated surface.*

After the characterization of the hydrophilic coating, metering tools with a capacity of maximum 200 µL were fabricated. Volume indicators were engraved per 1 µL in the PMMA top layer and a conical-shaped inlet was engraved and treated hydrophobically to obtain a user-friendly chip-to-world interface as introduced in Chapter 4. The assembled metering tools were then validated using an artificial blood equivalent to mimic the non-Newtonian flow behavior of real blood. This was, first of all, important to assess the time-to-result as the wicking flow rate for a single capillary channel decreases over the distance in the channel, according to the typical square root

relation as described by E. Washburn[25]. The filling of the metering tools over time or distance clearly corresponds to a square root curve (**Figure 5.5A)**. From these data it can be deducted that up to 140 µL of blood can be taken up by the metering channel within 2 minutes after deposition into the inlet. This is an important result for realizing a smooth workflow with study participants. Furthermore, the filling over time was highly reproducible, which could be expected from the above-mentioned repeatable Tween 20 coatings.

Next, the accuracy and variability of the metering tools were characterized by pipetting drops of artificial blood equivalent into the inlets and comparing these volumes with what was indicated on the metering tools. To correct for pipetting inaccuracies, the drop volumes were corrected for by assessing their effective weight by a gravimetrical method. This resulted in the calibration curve in **Figure 5.5B**.

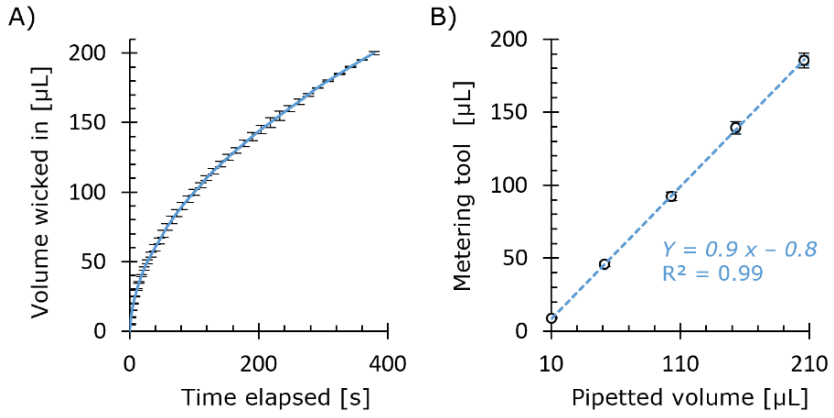

Figure 5.5: *A) Average filling profile of the metering tools with the error bars representing a single standard deviation (n = 4) when using artificial blood. B) Calibration curve of the metering tools. The data show again high repeatability, by the error bars representing a single standard deviation (n = 4), and accuracy, by the slope of 0.9.*

The regression line has an intercept at -0.8 ± 0.7 µL and a slope of 0.9 ± 0.006, indicating an underestimation of 10%. This might be attributed to the fabrication of the channels by laser cutting, for which the exact bias compared to the design settings

is not exactly known, or by the compression of the PSA layer after lamination. Nevertheless, the high repeatability with CV-values ranging from 5.7% to 2.7% (first and last drop, respectively) allows for applying a volume correction factor to the results in next section.

5.3.2. Validation of the obtained sample volume by the finger-tourniquet procedure

The calibrated metering tools were then used to quantitatively validate the new finger-pricking protocol presented in Section 5.2.3. In this validation, we explored whether the finger-tourniquet application increases bleeding after finger-pricking in comparison to the traditional protocol, without milking the finger to avoid coagulation and/or dilution with ISF. To quantitatively compare both finger-prick protocols in a standardized way, the volumes were obtained within the time window of 40 seconds after pricking. This time window was long enough to obtain adequately large volumes to allow for comparing the two finger-prick protocols while keeping the waiting time for the patient after lancet activation as short as possible. Therefore, the reported volumes should not be interpreted as the total achievable volumes. Additionally, it must be remarked that the obtained volume data did not take into consideration any differences in the time it took for the first blood drop formation after lancing. The data are represented as histograms for both finger-prick protocols in **Figure 5.6**. It can be deducted that the frequency of achieving > 20 µL of blood increased from 8% to 62% by the finger-tourniquet protocol. Reaching this volume within 40 seconds is regarded as an important threshold as it shows that the finger-tourniquet protocol can increase the applicability of the DBS cartridges presented in Chapter 3 and 4. Furthermore, the data show that the range of obtained volumes more than doubled and that the spreading on the obtained volumes increased accordingly. Both methods were also statistically compared by the non-parametric Wilcoxon test. This indeed confirmed that the tourniquet method overall results in larger bleeding intensity, with the mean difference between the two methods being equal to 33 µL.

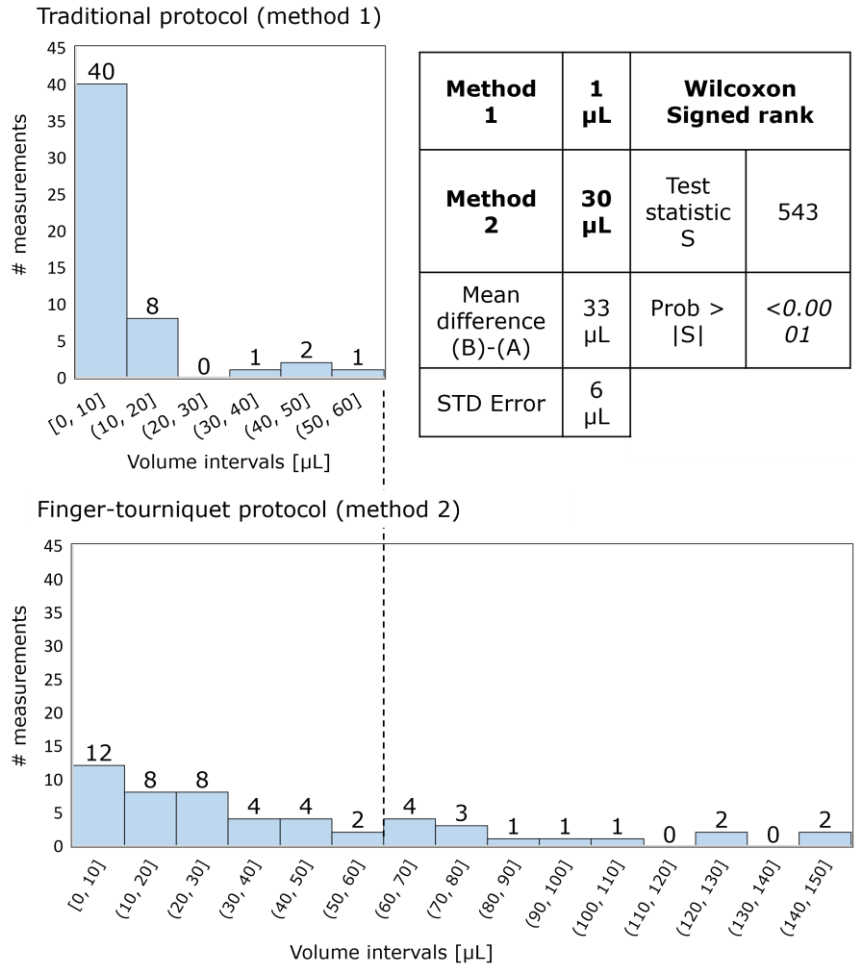

Method 1	**1 µL**	**Wilcoxon Signed rank**	
Method 2	**30 µL**	Test statistic S	543
Mean difference (B)-(A)	33 µL	Prob > |S|	*<0.0001*
STD Error	6 µL		

Figure 5.6: *Bleeding intensities, represented as the blood volumes collected within 40 seconds, after finger-pricking according to the traditional protocol (method 1) without milking the finger (A) and the finger-tourniquet protocol (method 2) (B). The summary of the non-parametric Wilcoxon test is shown in the table supporting the histograms. Median volumes for both methods are shown in bold.*

To further analyze the data, the paired differences between the obtained volumes by the traditional protocol and finger-tourniquet protocol per sampling moment were plotted (**Figure 5.7**). The data of the 3 sampling moments per participant were grouped and indicated by the white-grey zones.

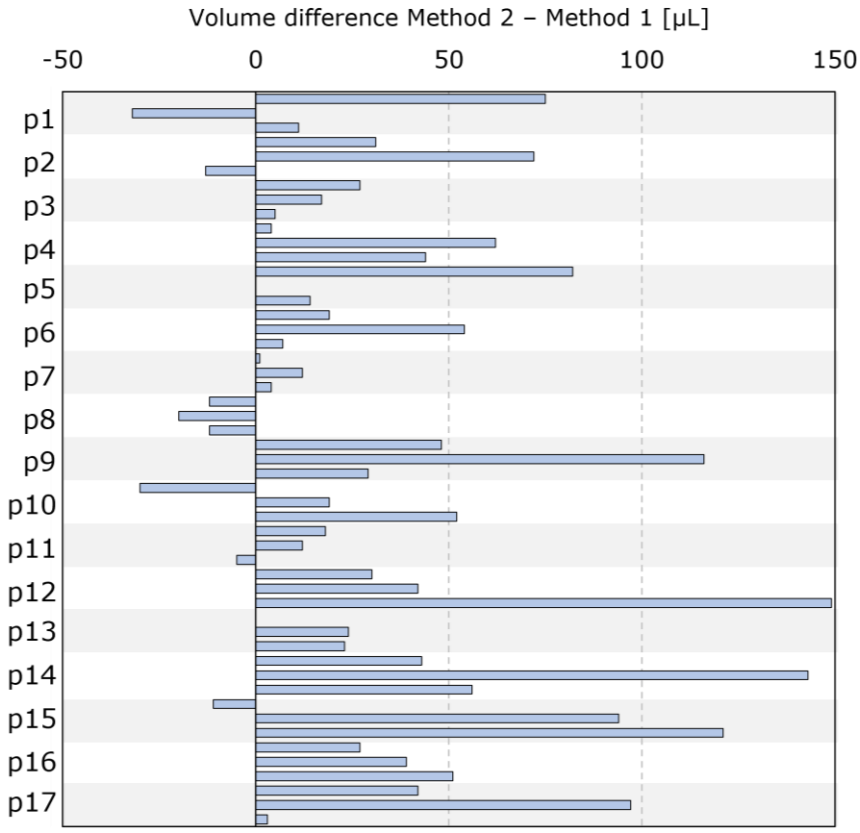

Figure 5.7: *Paired differences between the bleeding intensities for the traditional protocol (method 1) and finger-tourniquet protocol (method 2). The data for the three sampling moments are grouped per participant as indicated by the alternating white-grey shaded sections.*

In 81% of the sample collections, the paired difference was positive, meaning that a higher bleeding intensity was measured with the finger-tourniquet method. For 15% of the sample collections, the paired difference was negative, and zero in 4% of the cases. Only for one participant (p8), the obtained capillary blood volumes were even consistently smaller when applying a Velcro strap. Furthermore, a relatively large intra- and interperson variability was observed. However, as previously mentioned, the bleeding intensities should not be interpreted as absolute values and serve to make a quantitative comparison between two finger-pricking protocols possible.

A full detailed study on what causes the improved bleeding intensities by applying a finger-tourniquet was not in the scope of this validation study. Nevertheless, some observations were made. First of all, the number of finger-pricks for which the standard protocol led to a volume below the detection limit (i.e. 2 µL) of the metering tool was high (50%). It was noticed that in most of these cases, a bruise was forming below the lancing location. Therefore, it was hypothesized that locally increasing the blood pressure by applying the finger-tourniquet before pricking helps releasing the capillary blood through the skin incision made by the lancet. This is similar to milking, but more controlled and gentle while avoiding the risk of applying peak pressures. Whether the finger-tourniquet leads to dilution of the obtained capillary blood by ISF, which is a risk when excessively milking the finger, has to be investigated in follow-up work. Secondly, no coagulation was observed in the metering tools indicating the no or low haemolysis was present, but this has to be further explored. Thirdly, zero bleeding also happened for two participants when applying the finger-tourniquet protocol. In these cases, the bleeding only started from the moment the finger-tourniquet was removed. It was assumed that the Velcro band was ligating their vein perfusing the distal phalanx. This was also confirmed in one occasion where the finger-tip turned white instead of red upon tourniquet application and suggests that a more precise and user-friendly way of applying the tourniquet should be investigated in the future. Finally, the finger-tourniquet method was multiple times perceived less painful by the participants, both during lancing as right after the prick. This can possibly be linked to the fact that no bruising of the finger-tips was seen by applying this method while this clearly happened with the traditional protocol.

5.4. Conclusion

In this chapter, we studied a new finger-pricking protocol making use of a finger-tourniquet around the distal phalanx, to improve the volume of the blood sample taken. To quantitatively assess the available capillary blood upon finger-pricking, first, a self-filling metering tool with a maximum volume of 200 µL was

developed. Hereto, passive wicking of blood into a single microfluidic channel was induced by adding a highly concentrated Tween 20 coating. It was found that the coating reduced the water CA to 11.2° ± 0.5° for PMMA and 14.5° ± 0.9° for PVC. Assessing the filling profiles and calibration curves showed that the metering tools were fast, accurate and highly repeatable. The metering tools were then used to validate the tourniquet-based finger-prick protocol and compare it to the traditional protocol in terms of bleeding intensity. Seventeen healthy donors self-sampled capillary blood on three different sampling moments, each time following both protocols. This allowed direct comparison between the finger-prick methods per sampling moment. In 81% of the sample collections, the finger-tourniquet method bleeding intensity was higher compared to the traditional protocol as confirmed by the non-parametric Wilcoxon test. Although a large intra- and inter-person variability was observed, the mean volume difference was assessed to be 33 µL within 40 seconds after lancing.

The proposed finger-tourniquet method showed its potential to improve finger-prick sample collection at the POC. Still, the goal of this work was only to set-up the experiment and to carry out an initial validation. Therefore, studying this further is required before making strong conclusions. The number of participants as well as their age range should be increased. Furthermore, the effects of warming up hands and fingers before finger-pricking and the length of the lancet should also be investigated in a follow-up validation. When an optimal finger-prick protocol is available, the possible effect of this sampling protocol on the quality of the obtained capillary blood (i.e. presence of inflammation factors or the dilution with ISF) has to be investigated further before use at the POC. Nevertheless, the obtained data in this work are pointing into a positive direction.

5.5. References

1. Morgan, P. E. Microsampling devices for routine therapeutic drug monitoring-are we there yet? *Ther Drug Monit* 43, 322–334 (2021).
2. Tang, R. *et al.* Capillary blood for point-of-care testing. *Crit Rev Clin Lab Sci* 54, 294–308 (2017).

3. Katarzyna, J.-D., Gajane, Z., Karolina, B. & Justyna, M. The impact of needle diameter and penetration depth of safety lancets on blood volume and pain perception in 300 volunteers: A randomized controlled trial. *Journal of Medical Laboratory and Diagnosis* 10, 1–12 (2019).
4. Jankowski, C. A. *et al.* Preanalytical Challenges during Capillary Fingerstick Sampling Preclude Its Widespread Use in Adult Hospitalized Patients. *Am J Clin Pathol* 155, 412–417 (2021).
5. Warunek, D. & Stankovic, A. K. Evaluation of lancets for pain perception and capillary blood volume for glucose monitoring. *Clin Lab Sci* 21, 215–218 (2008).
6. George, R. S. & Moat, S. J. Effect of dried blood spot quality on newborn screening analyte concentrations and recommendations for minimum acceptance criteria for sample analysis. *Clin Chem* 62, 466–475 (2016).
7. Panchal, T., Spooner, N. & Barfield, M. Ensuring the collection of high-quality dried blood spot samples across multisite clinical studies. *Bioanalysis* 9, 209–213 (2017).
8. Moat, S. J. *et al.* Effect of blood volume on analytical bias in dried blood spots prepared for newborn screening external quality assurance. *Bioanalysis* 12, 99–109 (2020).
9. Luchavez, J., Lintag, M. E., Coll-Black, M., Baik, F. & Bell, D. An assessment of various blood collection and transfer methods used for malaria rapid diagnostic tests. *Malar J* 6, 1–5 (2007).
10. van der Heijden, C., Roosens, L., Cluckers, H., van Craenenbroeck, A. H. & Peeters, B. Analytical and clinical performance of three hand-held point-of-care creatinine analyzers for renal function measurements prior to contrast-enhanced imaging. *Clinica Chimica Acta* 497, 13–19 (2019).
11. *WHO guidelines on drawing blood : best practices in phlebotomy*. *World Health Organization* (2010).
12. Hauser, J. *et al.* High-Yield Passive Plasma Filtration from Human Finger Prick Blood. *Anal Chem* 90, 13393–13399 (2018).
13. Serafin, A., Malinowski, M. & Prażmowska-Wilanowska, A. Blood volume and pain perception during finger prick capillary blood sampling: are all safety lancets equal? *Postgrad Med* 132, 288–295 (2020).
14. Kearney, N. & McKenna, K. Real world use of biologic drug levels and anti-drug antibodies in patients with psoriasis–does therapeutic drug monitoring have a place in routine clinical practice? *Journal of Dermatological Treatment* 33, 1676–1681 (2022).
15. Fruhstorfer, H., Schmelzeisen-Redeker, G. & Weiss, T. Capillary blood sampling: Relation between lancet diameter, lancing pain and blood volume. *European Journal of Pain* 3, 283–286 (1999).
16. Jasna Lenicek Krleza. Nationwide survey of policies and practices related to capillary blood sampling in medical laboratories in Croatia. *Biochem Med (Zagreb)* 24, 350–358 (2014).
17. Lippi, G. *et al.* Preanalytical quality improvement: In quality we trust. *Clin Chem Lab Med* 51, 229–241 (2013).
18. Chan, P. C. R., Rozmanc, M., Seiden-Long, I. & Kwan, J. Evaluation of a point-of-care glucose meter for general use in complex tertiary care facilities. *Clin Biochem* 42, 1104–1112 (2009).
19. Lenicek Krleza, J., Dorotic, A., Grzunov, A. & Maradin, M. Capillary blood sampling: National recommendations on behalf of the Croatian society of medical biochemistry and laboratory medicine. *Biochem Med (Zagreb)* 25, 335–358 (2015).
20. DORMANDY, K. M. & HARDISTY, R. M. Coagulation tests on capillary blood. A screening procedure for use in small children. *J Clin Pathol* 14, 543–547 (1961).

21. Yuen, P. K. & Goral, V. N. Low-cost rapid prototyping of flexible microfluidic devices using a desktop digital craft cutter. *Lab Chip* 10, 384–387 (2010).
22. Vloemans, D. *et al.* Precise sample metering method by coordinated burst action of hydrophobic burst valves applied to dried blood spot collection. *Lab Chip* 21, 4445–4454 (2021).
23. Dal Dosso, F., Tripodi, L., Spasic, D., Kokalj, T. & Lammertyn, J. Innovative hydrophobic valve allows complex liquid manipulations in a self-powered channel-based microfluidic device. *ACS Sens* 4, 694–703 (2019).
24. Erbil, H. Y. Calculation of spreading pressure from contact angle data on polymer surfaces. *Langmuir* 10, 2006–2009 (1994).
25. Gardner, W. Note on the dynamics of capillary flow. *Physical Review* 18, 206–209 (1921).

Chapter 6

Innovative fabrication of hollow microneedle arrays enabling blood sampling with a self-powered microfluidic patch

The work reported in this chapter is adapted from:

Van Hileghem L., Kushwaha S., Piovesan A., Verboven P., Nicolaï B., Reynaerts D., Dal Dosso F., Lammertyn J. (2023). Innovative fabrication of hollow microneedle arrays enabling blood sampling with a self-powered microfluidic patch. Micromachines, 14(3), 615.

Van Hileghem L. contributed to this work in terms of conceptualization, experimental design, planning and execution of the experiments, next to writing and editing of the text.

6.1. Introduction

Blood acts as an important window to monitor our body's health status. Therefore, millions of blood samples are globally collected daily for diagnostic purposes. The invasive character of a venous puncture not only requires healthcare workers with phlebotomy expertise, but also holds the risk of needle-stick injuries, accidental infection after non-sterile usage and denial by people with aversion for needles[1]. To decentralize the collection of blood, cutaneous capillary blood is a good alternative as it can easily be self-sampled by finger pricking using an external piercing element[2]. However, besides still being relatively invasive, obtaining acceptable quantities while maintaining adequate quality is often challenging[3–5]. Furthermore, the generated blood droplet has to be de-posited manually on, for instance, the inlet of a point-of-care diagnostic test or a dried blood spot card, which often leads to volume losses or inaccurate results.

As a solution for self-sampling, the use of microneedles (MN) received a lot of attention as they are less painful and significantly easier to use[6]. MNs are miniaturized needles that can be employed both to extract biofluids or inject medicine in the skin. For sampling, four major MN types have been described in the literature: solid, porous, hydrogel-forming and hollow MNs (HMN). When aiming for an integrated blood self-collection device, HMN arrays (HMNAs) are the most interesting as they can form a direct fluidic connection between the cutaneous capillaries and the channels of a microfluidic device[7]. However, they are generally more challenging to fabricate, with many techniques and materials explored so far. Silicon, one of the most common materials used in micro-electromechanical systems, has been processed by means of isotropic etching together with anisotropic deep reactive-ion etching or back-side illumination electrochemical etching[8–11]. Despite its strength, silicon is brittle and prone to break after insertion in the skin, being problematic as crystalline silicon is not biocompatible[12]. Therefore, polymers such as SU-8, PEGDA or E-Shell have been used with UV-lithographic techniques[13–18], whereas PMMA is more suitable to be structured with X-ray lithography or micro-injection

molding[19–21]. Alternatively, metals have a better strength and ductility[22]. For instance, nickel and titanium have been electroplated or sputtered on structures previously prepared by lithography or etching processes[23], while stainless steel has been used in approaches like femtosecond-laser machining, electrical discharge machining (EDM) or simply assembling commercially available needles on a base substrate[24,25].

Unfortunately, the above-mentioned HMNA examples are not suitable for blood sampling applications as HMN lengths ≥ 1500 µm are required to reach the cutaneous capillary network[26,27]. As a creative solution, in-plane configured HMNAs have been fabricated[28]. Though, to be compatible with microfluidic platforms for downstream on-chip sample manipulation, out-of-plane configuration in the form of a patch is required. Hereto, Chaudhri et al. optimized the pre-exposure steps to allow UV-lithography on thicker SU-8 layers and fabricated 1540 µm tall HMNAs[26]. However, this technique did not allow for creating a direct fluidic connection with a base plane or beveled sharp tips. Alternatively, Le Thanh et al. presented 1515 µm tall SU-8 HMNAs with pyramidal beveled tips using isotropic etching and inclined UV-lithography[29,30]. Besides SU-8, Miller et al. focused on E-Shell 200 and 300 polymer to create tetrahedron-shaped HMNs by digital light processing 3D-printing and 2-photon lithography, respectively[31,32]. Furthermore, metallic HMNAs were achieved as well by a drawing lithography technique and subsequent nickel electro-plating[33,34]. This way, a single out-of-plane hollow MN was achieved with a length up to 1800 µm. For fabricating a 15° beveled tip, an extra laser cutting step was needed. In follow-up work, the integration of an elastic PDMS chamber with two passive valves, allowed to withdraw 30 ± 5 µL of blood for downstream processing and analysis on a paper-based sensor for glucose and cholesterol[35].

Although many fabrication procedures have been reported, the scarcity of useful HMNAs for blood sampling has hampered the progress toward integrated microsampling systems envisioning point-of-care sampling and diagnostic testing. First of all, the main focus on classic microfabrication materials and

methods did not solve critical shortcomings like (1) the challenge to directly create beveled sharp tips, (2) the lack of a direct fluidic connection with the base plane, (3) the need for cleanroom facilities, or (4) the need for intricate fabrication steps that do not allow for batch fabrication. Furthermore, the mechanical, biological and economic advantages of alloys like stainless steel barely received attention[36]. Even though disposable stainless steel HMNAs are less likely to be mass produced for use at the point of care (POC), the material perfectly serves the needs to be utilized as a valuable research tool, e.g. during the development of new microsampling technologies. The alloy can be provided in biocompatible grades for *in vivo* studies, it can be reused after sterilization and the material strength improves the design freedom without the need for full mechanical characterizations. Despite all these advantages, the state of the art stainless steel HMNAs remained limited to assembling commercially available hypodermic needles into a polymeric base structure[37,38].

This work presents the fabrication of entire stainless steel HMNAs and their integration in a self-powered sampling patch. With the goal of overcoming the challenging material properties of stainless steel, a novel two-step approach by laser drilling and micro-milling is first explored and characterized by brightfield microscopy, X-ray microcomputed tomography (µCT) and pressure drop measurements. Next, the HMNAs are integrated with a Self-powered Imbibing Microfluidic Pump by Liquid Encapsulation (SIMPLE), which is first characterized in terms of pressure generation. Finally, the sampling performance of a SIMPLE-based sampling patch is validated on an in vitro skin equivalent.

6.2. Materials and methods

6.2.1 Reagents and materials

Stainless steel grade 304 plates (2 mm thick) and grade 303 rods (50 mm diameter) were acquired from Dejond (Antwerp, Belgium). Milling and chamfer tools were obtained from DIXI Polytool (Le Locle, Switzerland), with a detailed tool list in Table

6.1 of the Supporting Information. Acetone was obtained from Acros Organics (Geel, Belgium). PVC plastic films of 180 and 300 µm thickness were bought from Delbo (Maldegem, Belgium). Double-sided pressure-sensitive adhesive (PSA) tapes 200MP types 7956MP (153 µm thick) and 7945MP (127 µm thick) and transfer tape type 467MP (58 µm thick) were acquired from 3M (Minnesota, USA). Sigma-Aldrich (Overijse, Belgium) delivered Whatman quantitative filter paper grades 40, 43 and 598. Aquapel® hydrophobic agent was obtained from Aquapel (Pennsylvania, USA). Aqueous dye was obtained from Darwin Microfluidics (Paris, France). Agarose powder and glycerol bidistilled 99.5% were obtained from, respectively, Melford (Ipswich, UK) and VWR (Leuven, Belgium).

6.2.2 Hollow microneedle fabrication process

HMNAs were fabricated in a two-step approach, which is schematically shown in **Figure 6.1**. First, stainless steel was selected for its (1) mechanical advantage to penetrate skin without buckling or breaking high-AR HMNs, (2) hardness and machinability to obtain sharp and durable tips, (3) availability in medical and haemocompatible grades and (4) resistance to corrosion keeping the material sterile. On top of these advantages, grade 303 was selected because of its machinability. Then, a batch of workpieces were prepared by cutting the stainless steel rod into 5 mm thick discs by wire-EDM (AgieCharmilles CUT E 600, GF Machining Solutions, Biel, Switzerland) and milling pockets with a resulting thickness of 2 mm (**Figure 6.1A**) with a micro-milling center (MMP, Kern Microtechnik, Eschenlohe, Germany). Next, the workpiece with a pocket was manually aligned upside down on the XY-stage of a JK 2000 laser processing system (Lumonics, Rugby, UK) with Nd:YAG medium, operated with a repetition rate of 50 Hz. Percussion laser drilling (**Figure 6.1B**), i.e. repeated laser pulses with a pulse duration τ (0.7 – 1.5 ms), was exploited to create microholes serving as HMN lumens. Combinations of (low) laser energies (1.0 and 1.3 J) and laser pulse durations (0.7 – 1.5 ms) were screened by measuring the resulting lumen equivalent diameter (ED) and circularity (C) at both the laser entry and exit

side by brightfield (BF) microscopy (see Section 6.2.3). An O_2 gas flow of 6 bar was used to improve material combustion upon laser-induced heating. Before removing the workpiece from the laser cutter, a reference feature was cut (**Figure 6.1C**) to align the workpiece based on the precise location of the lumens with a stereomicroscope (Keyence VHX-500F, Osaka, Japan). The workpiece was then clamped on the micro-milling center, where the needle bevels were cut by an engraving tool (**Figure 6.1D**). The bevels were finished first, as longer needle shafts (i.e. with larger length/diameter ratio) result in unstable machining. Afterwards, the shafts were finished to achieve final tolerances using an end mill cutter (**Figure 6.1E-F**).

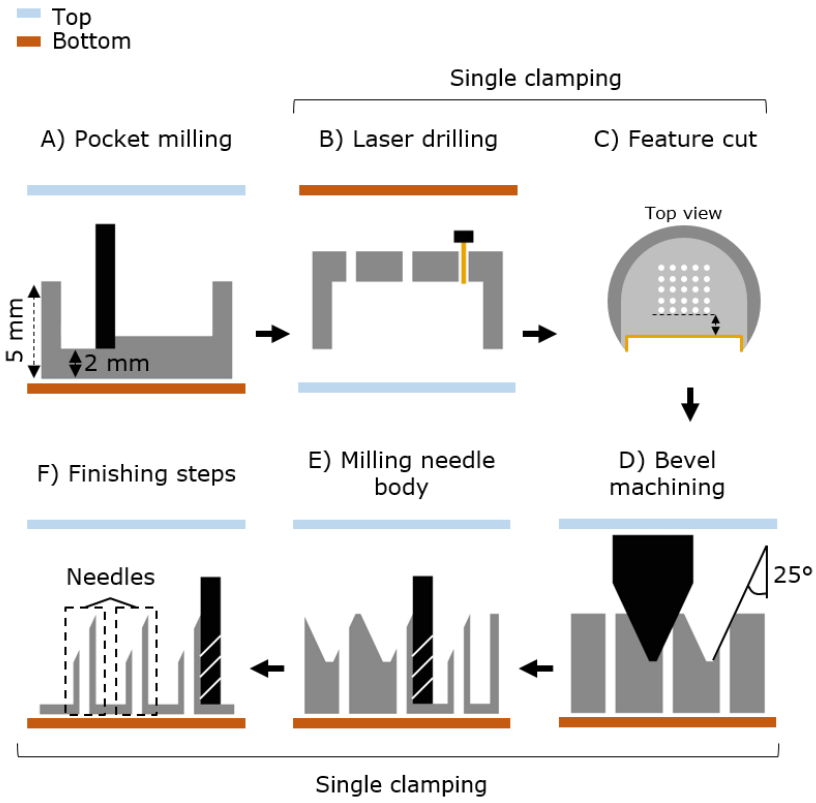

***Figure 6.1**: Overview of the HMNA fabrication process. a) A pocket with a 2 mm thick bottom is created, in which b) lumens are laser ablated, followed by c) a reference feature cut (yellow line) in a single step. Then, in a single clamping on the micro-milling center, d) the bevels were machined first followed by e) milling the needle body and f) finishing steps.*

The outer shape of the HMNAs around the laser-drilled micro-lumen was designed to yield a length of 1700 µm, an outer diameter of 450 µm and a sharp tip angle of 25°. Because of the geometric limitations of the engraving tool, an inter-needle distance of 650 µm was chosen.

6.2.3 Microscopic and tomographic inspections

BF microscopic images were obtained for both sides of the lumen, using an Eclipse Ti-e microscope (Nikon, Tokio, Japan), a pT-100-WHT LED source (CoolLED, USA) and a Nikon Plan 10x objective. Matlab (MathWorks, Massachusetts, USA) was used to analyze the binarized images to obtain the equivalent diameter (ED) $\sqrt{4A/\pi}$ and circularity (C) $4A\pi/P^2$ for each lumen at both sides, with A the area and P the perimeter.

X-ray micro computed tomography (µCT) was performed at the KU Leuven XCT Core Facility. Laser drilled blocks of stainless steel were imaged in a Phoenix Nanotom S (General Electric Research, New York, USA) with a diamond-tungsten target. The source voltage and current were 120 kV and 77 µA, respectively, and the achieved voxel size was 2.2 µm. Furthermore, an aluminum filter of 300 µm was used. This setup was used to acquire 1500 radiographic projections over a 360° angle, using 3 frames averaging. NRecon software (Bruker microCT, Kontich, Belgium) was used for reconstructing the scanned volume and subdividing it into slices. Next, the slices were imported into Matlab for binarization and de-speckling by removing all clusters below 100 pixels. Subsequently, the feature was rotated using the air-metal interface to align the lumen perpendicularly so that the ED and taper angle (to quantify the conical shape of the obtained lumen) could be characterized in function of the depth.

The entire HMNAs were imaged on a TESCAN UniTOM XL µCT-system (TESCAN XRE, Ghent, Belgium) with a reflection tungsten target. The source voltage and current were 180 kV and 88 µA, respectively, and the achieved voxel size was 4.0 µm. Again, an aluminum filter, here 1 mm thick, was used. 3500 projections were acquired over a 360° angle with an exposure time of 360 ms and two projection averaging. The sample was

scanned under a manually set inclination angle to reduce streak artifacts. Volume reconstruction was performed using the TESCAN reconstruction software Acquila (TESCAN XRE, Ghent, Belgium) and image processing, volume rendering and manual alignment with the principal axes were executed in Avizo 2020.R1 (Visual Sciences Group, Bordeaux, France). The image processing consisted of a median filter with 3 subsequent iterations to reduce the image noise and a thresholding operation to segment the solid phase. The binarized volume was then visualized in 3D using the Volume Rendering function present in Avizo.

6.2.4 Microfluidic chip fabrication

The low-cost, rapid prototyping method by Yuen et al. was adopted for the fabrication of the microfluidic devices[39]. Chips used for the HMNA flow characterization (Section 6.3.2) were prepared by cutting microfluidic channels in PSA tape using a Speedy 300 CO_2 laser cutter (Trotec, Boldon Colliery, UK) and laminated between two PVC layers (180 µm) containing the liquid in- and outlets. The latter features were previously cut out by a Maxx Air 24" digital craft cutter (KNK, Florida, USA).

Devices used for the characterization of SIMPLE[40–43] pressure generation (Section 6.3.3) were equipped with a hydrophilic stop valve (HSV), hydrophobic barriers (HB) and a filter paper pump (Whatman grade 40) before laminating with the PVC layers (300 µm thick). All paper were cut with a Silhouette Cameo craft cutter (Silhouette, Netherlands). HBs were prepared by cutting 1.5 x 3 mm^2 rectangular Whatman grade 43 filter paper pieces and by impregnating the filter paper with Aquapel®, as previously reported[44]. The HSV consisted of untreated Whatman grade 43 filter paper pieces (same size as HB).

Finally, the sampling patches with integrated HMNA (Section 6.3.4) were fabricated using transfer tape reinforcement on the paper pump tip. The connection of the finger-press activation spot to the sample liquid channel was provided through an HB so that upon activation, no air could be displaced in the direction of the inlet, and thus the skin, while working liquid displacement

toward the filter paper pump would be more effective. PVC layers of 180 µm thick were used and the bottom PVC layer was provided with a 2 mm inlet hole to connect with the HMNA. The latter was attached with a PSA 7945MP connection ring with inner dimensions of 6x6 mm.

6.2.5 Flow characterization of the HMNAs

Flow characterization of the HMNAs was performed using a LineUp push/pull pressure controller (Fluigent, Paris, France) combined with a flow sensor (Model Medium, Fluigent, Paris, France) to achieve a steady water flow rate while monitoring the required pressure in real-time at 0.1 Hz. A high flow rate of 50 µL/min was pushed through each individual needle lumen. Pushing was chosen over pulling for convenience and to avoid any air be-tween the HMN and the pressure pump system in between different repetitions. This was done by attaching the fabricated HMNAs to a chip with a single, straight fluidic channel having a width of 1.5 mm and outlet hole diameter of 2 mm and by using a PSA connector piece with a hole < 0.5 mm. For the measurement of each individual lumen, the inter-needle distance was large enough to allow easy manual alignment. Baseline pressures were obtained by repeating for each lumen the same measurement without the needle but with the connector piece attached. This way, any differences in the assembly of the experimental setup (e.g. small misalignments of the PSA connector hole with the fluidic outlet leading to different flow contraction-expansion events) were nullified. Additionally, the attached HMNA was immersed in water to avoid any effect at the water/air interface of droplet formation, and between experimental repetitions, the HMNAs were cleaned in a Branson 1510 Ultrasonic Cleaner (Branson Ultrasonics, Connecticut, USA) in acetone for 20 minutes to remove any possible debris. More details on the setup can be found in Section 6.5.2 of the Supporting Information.

6.2.6 SIMPLE pressure generation

Measurements of the pressure generated by the SIMPLE were based on Boyle's law, which describes the relation between the

pressure (*P*) and volume (*V*) of an ideal gas given a constant temperature as $PV = k$, with k a certain constant. Therefore, a pre-defined air volume enclosed in an air chamber on-chip was expanded by the SIMPLE. **Figure 6.2** depicts the chip design used. A Harvard PHD 2000 syringe pump (Harvard Apparatus, Massachusetts, USA) was operated to push the activation liquid (1/50 diluted green aqueous dye in dis-tilled water) further toward the HSV at a flow rate of 35 µL/min, leading to the activation of the pump by pushing the working liquid into the filter paper tip. As soon as the HSV was saturated, the syringe pump remained connected after stopping the flow rate. During the wicking of the working liquid (1/50 diluted blue aqueous dye in distilled water) by the porous material of the SIMPLE, which created a negative pressure in the air chamber, the activation liquid was prevented to leak from the HSV to the air plug chamber by means of the HB-2.

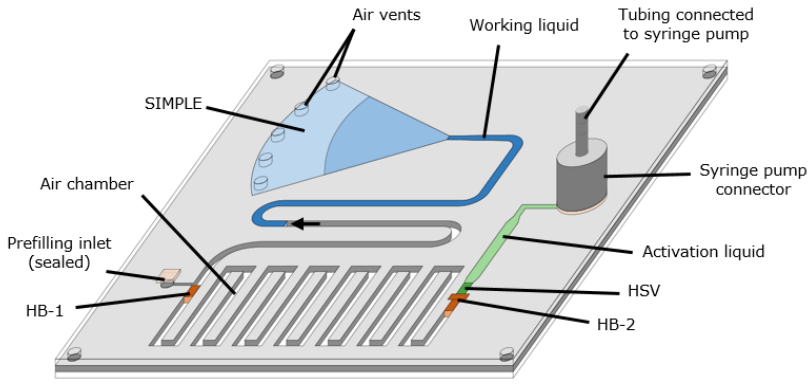

***Figure 6.2**: Chip design of a working chip as used for the SIMPLE pressure generation measurements. A syringe pump was used to push the activation liquid (green) towards the hydrophilic stop valve (HSV), which activated the SIMPLE operation by pushing the working liquid (blue) into the filter paper (indicated by the black arrow at the receding liquid front). By effect, the air in the air chamber in between the hydrophobic barriers HB-1 and HB-2 (orange) expanded as quantified by following up the working liquid volume.*

The generated pressure was indirectly obtained by measuring the decrease in volume of the working liquid in its chamber. Hereto, the chip operation was recorded by a C920 digital webcam (Logitech, Switzerland) for subsequent analysis

using an in-house developed software. The pressure P_{fin} [Pa] was calculated as:

$$P_{fin} = \frac{P_{atm} \cdot V_{in}}{V_{fin}} - P_{atm} \qquad \text{Eq. (6.1)}$$

with P_{atm} equal to 101.33 kPa (the atmospheric pressure), V_{in} [L] the initial air plug volume and V_{fin} [L] the expanded air plug volume. To avoid deflection of the chamber upon pressure reduction, which would lead to an overestimation of the generated pressures, PVC layers of 300 µm thick were used. For more details on this setup, the reader is referred to Section 6.5.3 of the Supporting Information.

6.2.7 Validation of a self-powered biofluid sampling patch with in vitro models

To assess the fluidic performance of the self-powered biofluid sampling patch, three samples were prepared: i) colored distilled water (1/10 aqueous red dye); ii) blood mimicking fluid (53.8% v/v) glycerol diluted in colored distilled water (1/10 aqueous red dye); iii) agarose gel (2.65% w/v), prepared by dissolving agarose powder in colored distilled water (1/100 aqueous red dye) on a hotplate (130 °C) under constant stirring with a magnetic stirring bar. When solidified at room temperature, the agarose gel was placed to sat-urate into a container filled with red colored distilled water (1/10 aqueous red dye). Before each experiment, its surface was dipped dry with a paper cloth and further dried to air to avoid liquid uptake from the surface. The sampling patch was then gently placed on top of the agarose gel and pushed down perpendicularly to assure insertion of the HMNA shafts without rupturing the hydrogel by horizontal movement.

6.3. Results and discussion

6.3.1 HMNA fabrication

The first aim of this work was to fabricate HMNAs with a length > 1500 µm to reach the skin's blood capillaries. Hereto, we chose top-down micromachining of stainless steel. The mechanical advantage of this alloy for skin puncture makes it, consequently,

a challenging material with respect to machinability. To create microlumens with a depth up to 2 mm and an ED between 100-200 µm to keep the final HMN design sufficiently thin while avoiding too large pressure drops, percussion laser drilling was investigated. Despite the fact that femtosecond lasers are the go-to approach for creating small features, they are not suited for creating high-AR microlumens with this depth due to the typically large taper angles caused by the plasma shielding effect[45]. Therefore, a high-power millisecond laser was exploited aiming to reach the targeted microlumen dimensions with a low amount of taper (< 1°) and high C (> 0.9).

The overview of the screening results in terms of ED and C is given in Figure 6.11 of the Supporting Information. As expected, to drill completely through the stainless steel substrate with a success rate of 100%, shorter pulses (0.9 ms) were only needed in case of a higher laser output energy (1.3 J). However, this also resulted in a larger ED, lower C and overall larger variability. This can be explained by the larger heat-affected zone by a single laser pulse removing more material at once, which can be expected to be less controllable[46]. Hence, only the results for the lowest energy at which the laser setup could be set, 1.0 J, met the requirements, as shown in **Figure 6.3**. **Figure 6.3A** shows that reducing the output energy to 1.0 J yielded lumens well within the set requirements. Furthermore, **Figure 6.3B** demonstrates that for a pulse duration of 1.3 ms, the variability of C is clearly higher compared to larger width. This can be explained by the 8% of the repetitions that failed to completely drill through the material. A pulse duration ≥ 1.4 ms yielded a 100% success rate and lower variability. However as no significantly different results were obtained between a pulse duration of 1.4 and 1.5 ms, we chose to continue the microlumen fabrication with 1.4 ms in combination with a laser output of 1.0 J.

Even though the targeted microlumens were obtained, the significantly higher ED ($p < 0.05$) for the laser entry versus exit sides suggested a significant amount of taper. To visualize this in detail, microlumens fabricated with the laser settings

combination 1.0 J and 1.4 ms was scanned by µCT. The cross-section in **Figure 6.3C** shows that, in fact, nearly straight microlumens were achieved with the diameter only considerably increasing at the laser entry side. Based on this, it was decided to laser drill the lumens from the backside of the workpiece to let the wider laser entry side coincide with the HMNA base plate instead of the tip.

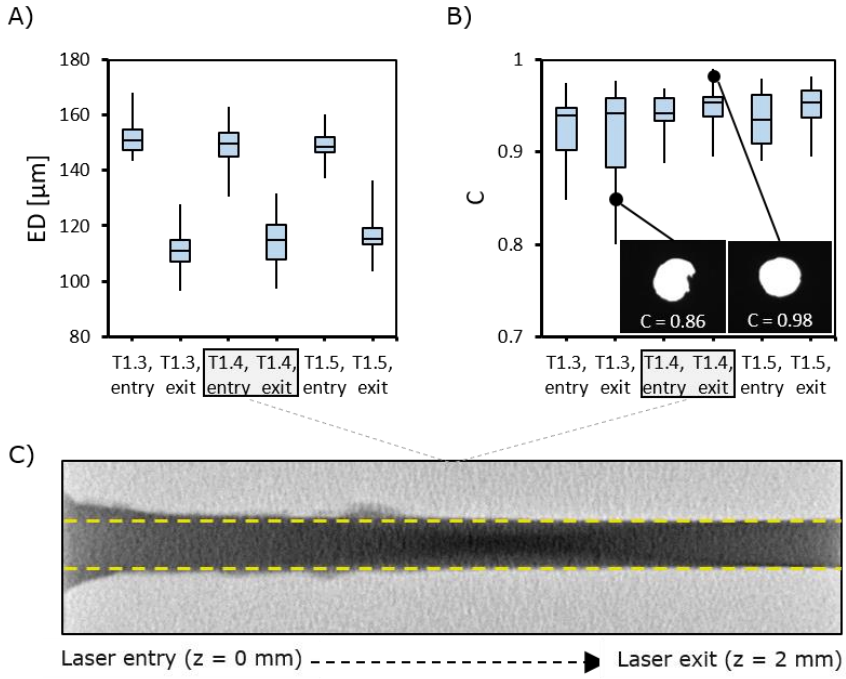

***Figure 6.3**: Boxplots for a laser output energy of 1.0 J showing a) the obtained EDs of laser drilled lumens at the laser entry and exit sides for different pulse durations (1.3, 1.4 and 1.5 ms), and b) the C values for the same laser drilled lumens. The boxes in the boxplots display (from top to bottom) the upper quartile, the median and the lower quartile. Whiskers indicate the minima and maxima (n > 22 for all conditions) and insets show examples of BF microscopy images obtained and the corresponding results. c) A cross-section by µCT scanning of a lumen percussion laser drilled with energy 1.0 J and pulse duration 1.4 ms. The yellow dashed lines indicate the width at the laser exit side, demonstrating the nearly straight microlumen and substantial widening near the laser entry side.*

For the next fabrication step, the workpiece was aligned on the micro-milling center based on the reference cut to produce 5x5 HMNAs according to the procedure described in Section 6.2.2. The needles were characterized by µCT scanning with an

achieved voxel size of 4.0 µm³ to inspect the entire HMNAs externally as well as internally. A reconstructed 3D image of a machined HMNA obtained by µCT is shown in **Figure 6.4**, demonstrating that none of the 25 HMNs have major artefacts like broken tips or irregular shapes. **Figure 6.4C** portrays the cross-section through one row of the HMNA, showing that the lumens are open after machining, although, few of the lumens show some irregularities. Their possible impact on the flow through the HMNs is discussed in the Section 6.3.2 (see also Supporting Information Section 6.5.7).

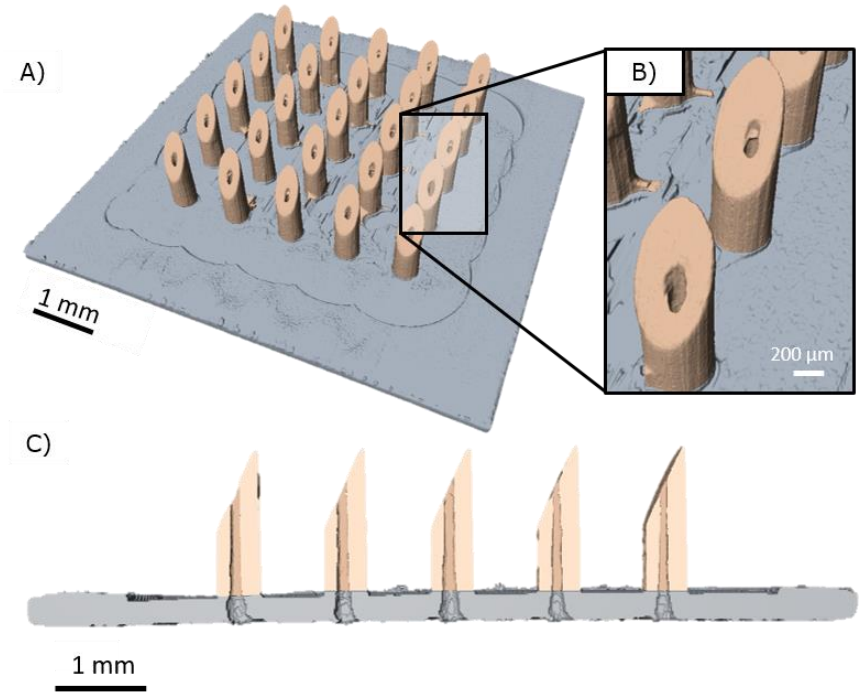

***Figure 6.4**: a) 3D reconstruction of a full 5x5 HMNA with indicative lengths of 1647 ± 12 µm and outer diameters of 451 ± 9 µm. False colors (grey and orange) were added to increase the visibility of the machined features. b) Close-up view of a 2 MN shafts. c) Cross-sectional view of the same HMNA showing 5 open lumens and sharp tips as a result of the chosen bevel angle of 25°.*

The distal tip size was found to be comparable to the image voxel size, meaning that it is below the 10-15 µm range recommended for the sharpness (see also Section 6.5.5 of the Supporting Information)[47,48]. Tip sharpness is also affected by the

bevel, for which the angle was chosen to be 25°. This is lower than the minimal bevel angle required to ensure piercing, which is reported in literature to be 30°[49]. Finally, the out-of-plane height and outer diameter were 1647 ± 12 µm and 451 ± 9 µm, respectively. Nevertheless, as a result of the limited scanning resolution, being 7 µm, it should be noted that these measurements are only giving an indication that the aimed requirements for blood sampling are met, without offering a precise characterization.

6.3.2 Flow characterization of the HMNAs

To assess the machining variability, the pressure drops over the individual needles were analyzed for 3 different arrays, with 3 technical repetitions each. A high flow rate (50 µL/min) was applied, based on the maximal flow rates found in literature for microneedle-based blood sampling[34,50]. **Figure 6.5** depicts the spatial distribution of the average pressure drops per HMN (bar charts with error bars can be found in Figure 6.13 of the Supporting Information).

Liquid was flowing through all of the HMN lumens and overall, 87% of the measured pressure drops were below 10 kPa and 36% below 1 kPa. Despite the overall satisfying results, some pressure drops were clearly deviating as highlighted in blue for pressure drops > 10 kPa. This variability can be attributed to the variability in the lumen diameter, the presence of burrs or debris and surface roughness as a result of the microfabrication process. µCT visualizes this partly (see cross-sections with some large burrs in **Figure 6.5**[51]) as it is limited to structures larger than the scanning resolution of 7 µm. In this regard, it is important to stress that there is a strong 4th order effect from the lumen diameter on the measured pressure drops, according to the Hagen-Poisseuille equation:

$$\Delta P = 128\frac{\mu L Q}{\pi D^4} \quad \text{Eq. (6.2)}$$

with ΔP [Pa] the pressure drop, μ [Pa.s] the dynamic viscosity, L [m] the length of the lumen, Q [m³/s] the flow rate and D [m] the diameter of the lumen. However, it must be noted that Eq.

(6.2) assumes smooth and straight channels and can therefore only be used as a mathematical theoretical background and a rough approximation for discussing the flow through the individual microlumens. However, given the lack of resolution, it was not possible to link all pressure drops over the individual needles to the mathematical theoretical values of Eq. (6.2).

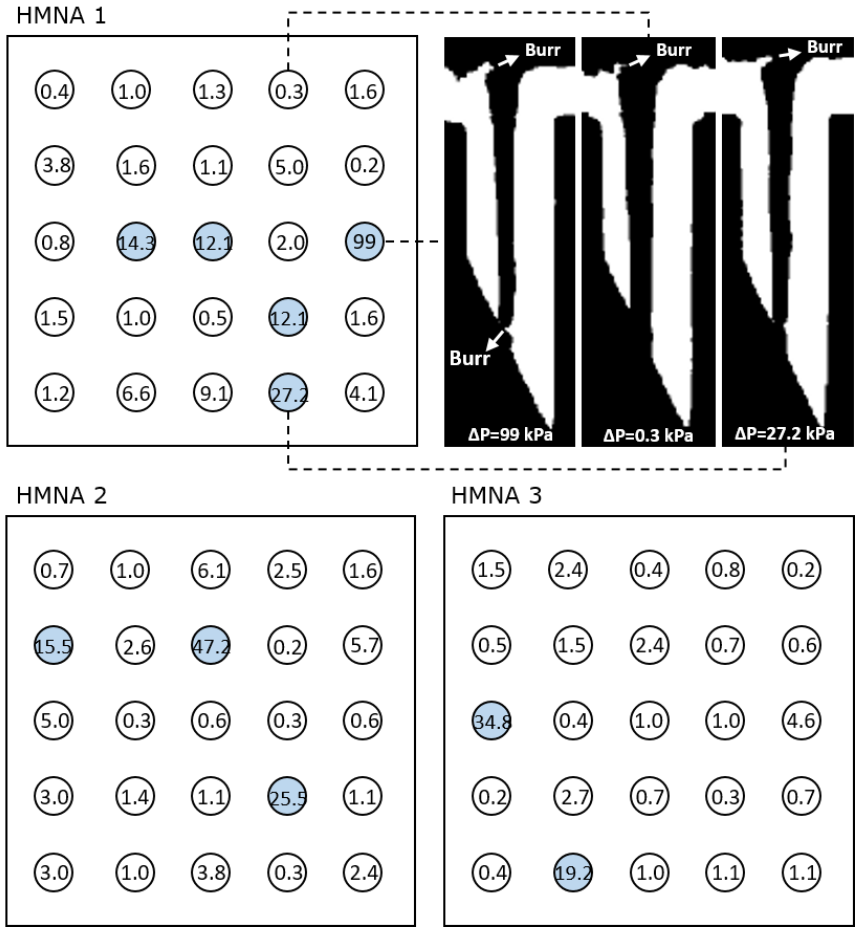

***Figure 6.5**: Spatial distribution of the measured average (n = 3) pressure drops [kPa] for 3 different arrays at the flow rate of 50 µL/min. Pressure drops > 10 kPa are indicated in blue. For information on the errors resulting from the three technical repetitions, the reader is referred to Figure 6.13 in the Supporting Information. The presence of machining artefacts like burrs can partly be visualized by µCT, as shown by the binarized cross-sections of 3 HMNs for HMNA 1.*

To statistically assess the machining variability, the pressure drops for the 3 arrays were compared by the non-parametric Kruskal-Wallis test. With a p-value of 0.093, significant differences between the 3 HMNAs could not be shown. After removing the statistical outliers, the p-value further increased to 0.145. For details on the statistics is referred to Tables 6.2 and 6.3 in the Supporting Information.

6.3.3 Characterization of SIMPLE pressure generation

The microfabricated and characterized HMNAs were then integrated with the SIMPLE microfluidic platform capable of pulling liquids in a self-powered and controlled way[52,53], as proof-of-concept of a self-powered microsampling patch. An important parameter for cutaneous biofluid extraction from skin is the pressure difference the system can overcome. The SIMPLE chip design and fabrication was optimized to achieve a maximum generated pressure difference. **Figure 6.6** depicts the pressure difference generated by 4 chips equipped with filter paper pumps (Whatman 40 quantitative filter paper) shaped as circular sectors of 60°, fabricated as described in Section 6.2.4.

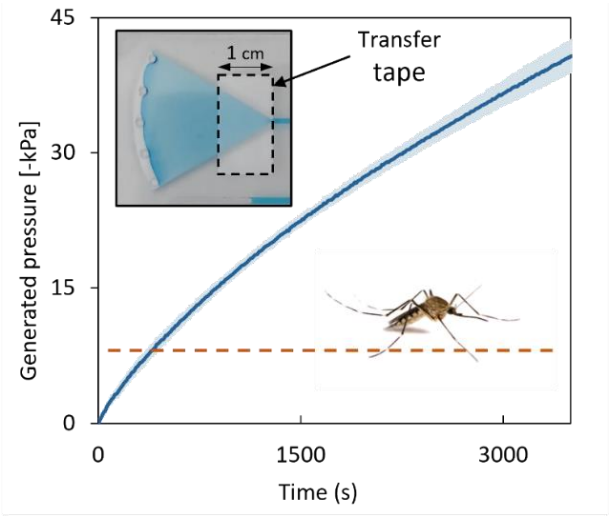

***Figure 6.6**: Average generated pressures by the SIMPLE chip reinforced by sealing the filter paper pump tip with transfer tape (see inset). The shaded area represents 1 standard deviation (n = 4). The orange dashed line depicts the reference pressure difference as generated by a mosquito when pulling blood from skin capillaries.*

It was shown that the lack of a tight sealing between the filter paper and the surrounding plastics allowed air backflow, leading to termination of the pumping (see Section 6.5.8 of the Supporting Information). This issue was solved by laminating transfer tape on both sides of the porous paper tip to seal the filter paper pump with the top and bottom PVC layers (see inset of Figure 6). As a result, after one hour, the generated pressure differences by the chips with filter paper pumps reached values of 40.9 ± 1.8 kPa, which is more than sufficient for bio-fluid extraction from the skin. For comparison, mosquitoes generate pressures up to 7 kPa for capillary blood extraction through their 20 µm diameter fascicle[54,55].

6.3.4 Validation of self-powered microsampling patch with in vitro models

Finally, a self-powered microsampling patch was assembled by integrating a HMNA with a SIMPLE chip using a PSA connection. The patch has the size of a regular credit card (86 x 54 mm, design shown in **Figure 6.7A**), an ideal feature for self-sampling applications. The chip can be easily activated by a finger-press on the activation spot (**Figure 6.7B**) to bring the working liquid (blue) into contact with the filter paper pump, which starts creating a pressure difference to withdraw the sample.

Validation of its operational performance was done for 3 different *in vitro* model systems. First, red colored distilled water was drawn from an open liquid container by immersing the HMN tips into the liquid. Next, tests were run with a glycerol-based blood mimicking fluid (**Figure 6.7C**) with a viscosity of about 4 cP[56]. Although whole blood is a non-Newtonian fluid, the relatively large lumen and microfluidic channel dimensions are not expected to cause a substantially large Fåhræus–Lindqvist effect, which describes the decreasing apparent viscosity for blood flow through microchannels[57]. However, the surface roughness after laser drilling might result in a further decreasing apparent viscosity, making a Newtonian blood mimicking fluid a worst-case scenario[58]. In a third model setup, the extraction of fluid from the human skin was mimicked by inserting the HMNAs

in a 2.65 % (w/v) agarose gel saturated with colored liquids according to Zhang et al.[59] (**Figure 6.7D**).

Volumes up to 40 µL were successfully sampled with a success rate of 100%. No significant difference in the flow rates was measured for sampling water and blood equivalent (see Supporting Information Section 6.5.9). The average flow rate reduced and the variability increased when sampling from skin equivalent. This is expected to be caused by manual HMN insertion or differences in HMNs effectively sampling due to path of least resistance, e.g. by clogging of the needle lumens with agarose. These results demonstrate that the combination of HMNA and SIMPLE delivers a small and flexible microsampling patch with large sampling volume capacity.

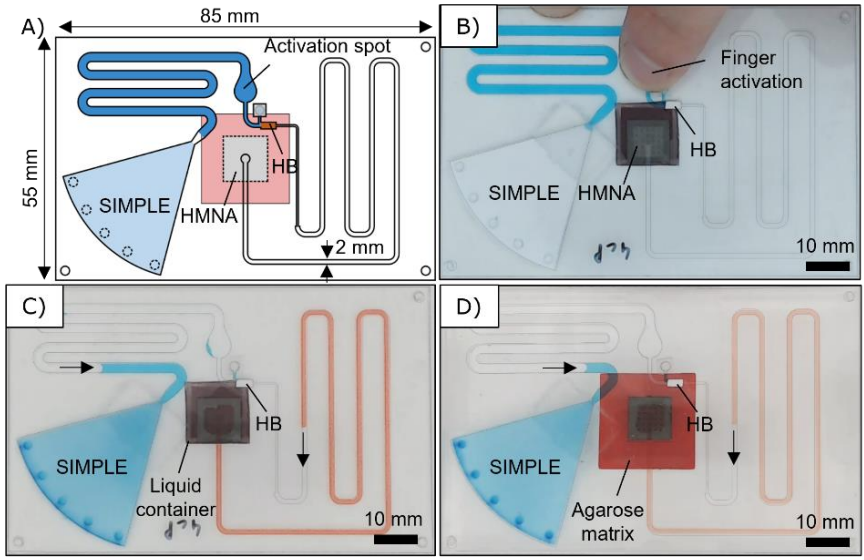

Figure 6.7*: a) Design of the sampling patch used in this experiment. b) Snapshot of a sampling patch during finger-press activation. c) Sampling blood-mimicking fluid from an open liquid container. Arrows indicate the direction of the fluid flow. d) Sampling patch while sampling from agarose skin-mimicking matrix. Arrows indicate again the direction of the fluid flow.*

6.4. Conclusions

This study demonstrated the two-step fabrication and characterization of stainless steel HMNAs and their integration in a self-powered sampling patch towards decentralized collection of capillary blood. First, percussion laser drilling by pulsed laser drilling on a single spot was explored for different laser settings. Pulses of 1.4 s in combination with a laser output energy of 1.0 J resulted in nearly straight microlumens with ED well within the required range of 100-200 µm and C higher than 0.9. Therefore, these settings were chosen for the subsequent micro-milling of 5x5 HMNAs. The µCT scans of full HMNAs showed a good agreement with the designed dimensions. The measured height (base-to-tip) and the outer diameters were on average 1647.1 ± 12.3 µm and 451.1 ± 8.5 µm, respectively. Furthermore, all tips appeared to be sharp without artefacts. Flows through each individual lumen were characterized to assess the sampling capacity of each needle in the HMNAs. In particular, for a flow rate as high as 50 µL/min, the average pressure drops were below 10 kPa in 87% of the HMNs. These results show that the proposed two-step protocol is able to produce stainless steel HMNAs with out-of-plane shafts > 1500 µm and sharp tips necessary to reach skin capillaries for blood sampling.

Next, the HMNAs were integrated with a SIMPLE microfluidic platform as proof-of-concept of a self-powered sampling patch. Hereto, it was shown that SIMPLE is able to overcome negative pressure difference up to 40.9 ± 1.8 kPa. Finally, sampling patches with an integrated HMNA were validated by sampling up to 40 µL using 3 in vitro models: water, a blood-mimicking glycerol solution and a skin-mimicking agarose gel.

This study showed by a proof-of-concept that a flexible sampling patch with large capacity can be obtained by integrating a HMNA with a SIMPLE pumping unit. A unique advantage of the SIMPLE technology is that it allows for further manipulation of the withdrawn sample in a downstream microfluidic network, like e.g. precise metering, loading of dried blood spots, or a myriad of diagnostic applications completely on-chip[43,53,60]. Furthermore,

the fabrication of tall HMNs in stainless steel has been proven to be possible and improvements to minimize the production anomalies resulting from machining this challenging material have been suggested by the authors. Finally, the possibility to make this chip flexible is interesting for interacting with highly variable curvature of different bodies and body parts in a 'wearables' format during sample acquisition.

To conclude, follow-up work will focus on the interaction with biological materials to assess the penetration efficiency, the occurrence of haemolysis and the risk of blocking the microlumens as a result of blood clot formation, protein adsorption or tissue debris.

6.5. Supporting information

6.5.1 Micro-milling tool list

Table 6.1: List of cutting tools, obtained from DIXI Polytool (Switzerland), used for machining the bevel angle and the needle bodies.

Operation	Tool type	Cutting edges	Angle (°)	Tool material	d (mm)
Milling	End mill	2		Tungsten carbide	0.40
Milling	End mill	2		Tungsten carbide	1.00
Milling	End mill	2		Tungsten carbide	4.00
Engraving	½ engraving tool		50	Tungsten carbide	0.15

6.5.2 Flow characterization of the HMNAs

For the flow characterizations, a chip (design shown in **Figure 6.8A**) with a single microfluidic channel (1.5 mm wide was prepared. A circular shaped PSA piece with a 2 mm hole in the center was used to connect the chip inlet with the pressure pump via an in-house modified connector (**Figure 6.8B-C**). At the outlet, the HMNA was attached also using a PSA piece with a hole in the center smaller than the inter-needle distance. This way, the HMNA was laminated on the plastic chip with a properly sealed connection to flow the water only through a single lumen

at the time. After attaching the HMNA, the water container was filled with distilled water (**Figure 6.8B-C**). When a steady flow and resulting pressure was reached, data logging was started. For each lumen, the same was repeated without HMNA attached to obtain a baseline per measurement. Hereto, the HMNA was removed while keeping the PSA connector piece attached to the chip outlet. This way, the obtained pressures were corrected for influences of the flow through the PSA connector, microfluidic channel and tubing or the effects at the water-air interface during droplet formation at the microneedle tip.

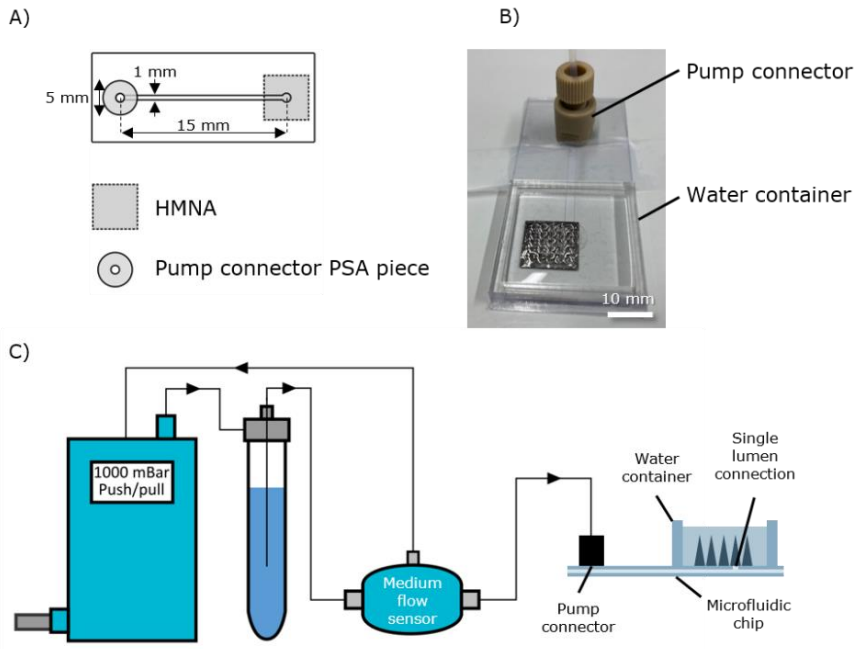

***Figure 6.8**: a) Chip design of a single microfluidic channel of 1.5 mm wide with in- and outlets of 2 mm. At the inlet, the pressure pump connector was attached by lamination with a PSA piece. At the outlet, the same concept was used for attaching the HMNA. b) Image of the microfluidic chip with attached HMNA and filled water container, ready for a measurement. c) Schematic representation of the measurement setup used for the flow characterizations of the HMNAs.*

The measurement setup (LineUp push/pull pressure controller and medium flow sensor, Fluigent, France) and how the system was connected are shown in **Figure 6.8C**. The pressure controller was connected to a falcon tube containing water, the

flow sensor and the chip with HMNA attached. By the feedback loop from the flow sensor to the pressure controller, a flow of 50 µL/min was set and kept steady while logging the pressures required to maintain this flow using the Fluigent A-I-O software.

6.5.3 SIMPLE pressure generation measurement

An exploded view showing all the elements of the chip used for this experiment is shown in **Figure 6.9A**. This setup allowed measuring the generated pressure by the SIMPLE by expanding the volume of an air plug. The top view of a chip during this process is shown in **Figure 6.9B**. For the measurement, based on Boyle's law, it was key to maintain the air pressure in the air chamber at 101.33 kPa (atmospheric air pressure). This was done by first connecting the syringe pump (Harvard PHD 2000 syringe pump, Harvard Apparatus, USA) to the chip using a connector piece and a PSA ring. Then, the activation liquid (1/50 diluted green aqueous dye in distilled water) was prefilled until an indication to keep the same distance from the HSV for all measurements. Next, the working liquid (1/50 diluted blue aqueous dye in distilled water) was prefilled via the prefilling inlet, again until an indication mark. During working liquid prefilling, the hydrophobic barrier (HB-1) directed the working liquid towards the paper pump without compressing the air plug. Last, the working liquid prefilling inlet was sealed airtight by a piece of PSA.

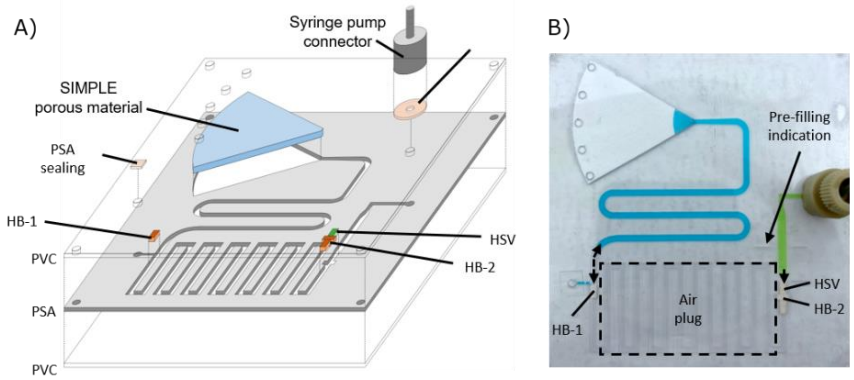

***Figure 6.9**: Chip design and top view of a chip that is being activated for SIMPLE pressure generation measurements.*

Figure 6.10 shows (1) the measured volumes of the working liquid in the working liquid chamber, (2) the wicked in working liquid into the SIMPLE paper pump and (3) the wicking in activation liquid into the HSV. It must be noted that the second and third are just indicative as it is not possible to measure the exact volumes wicked into filter paper by video analysis. Nevertheless, these measurements are valuable as the moment on which the activation liquid saturates the HSV can be exactly measured. This was done for normalizing the measured pressures by subtracting the working liquid volume change caused by the activation instead of the action of the SIMPLE paper pump itself. The moment at which the working liquid started moving during syringe pump activation is indicated with a blue dashed line.

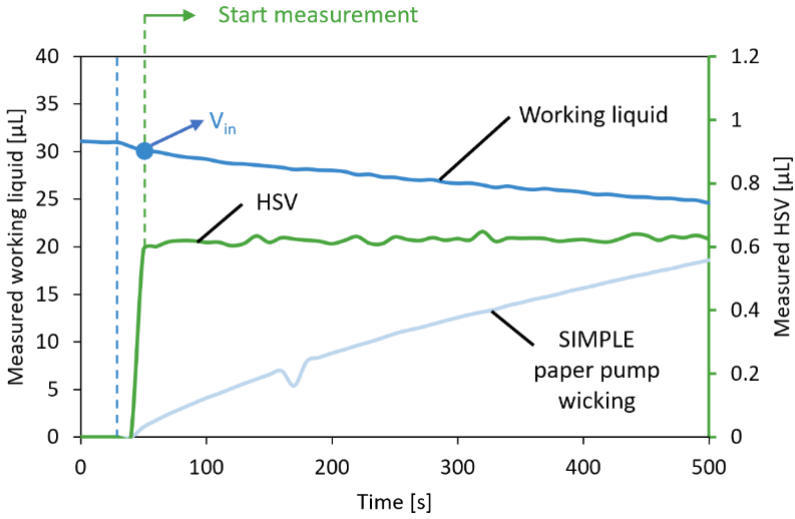

***Figure 6.10**: Measured volume of working liquid (dark blue), indicative volume of working liquid inside of the SIMPLE paper pump (light blue) and indicative volume of activation liquid into the HSV (green). The blue dashed line indicates the moment at which the working liquid starts moving toward the SIMPLE paper pump tip. The green dashed line indicates the moment at which the HSV is completely saturated, and thus from where the measurement starts. Note: the dip in the graph for the SIMPLE paper pump was caused by a video processing artefact.*

The generated pressure P_{fin} [Pa], as given in Section 6.2.6 of the main manuscript, is calculated by filling in the working liquid volume (V_{in}) at the start of the measurement (i.e. saturated HSV)

and the value of the working liquid volume during the measurement ($V(t)_{fin}$):

$$P_{fin} = \frac{P_{atm} \cdot V_{in}}{V(t)_{fin}} - P_{atm} \qquad \text{Eq. (6.3)}$$

6.5.4 Laser drilling settings characterization

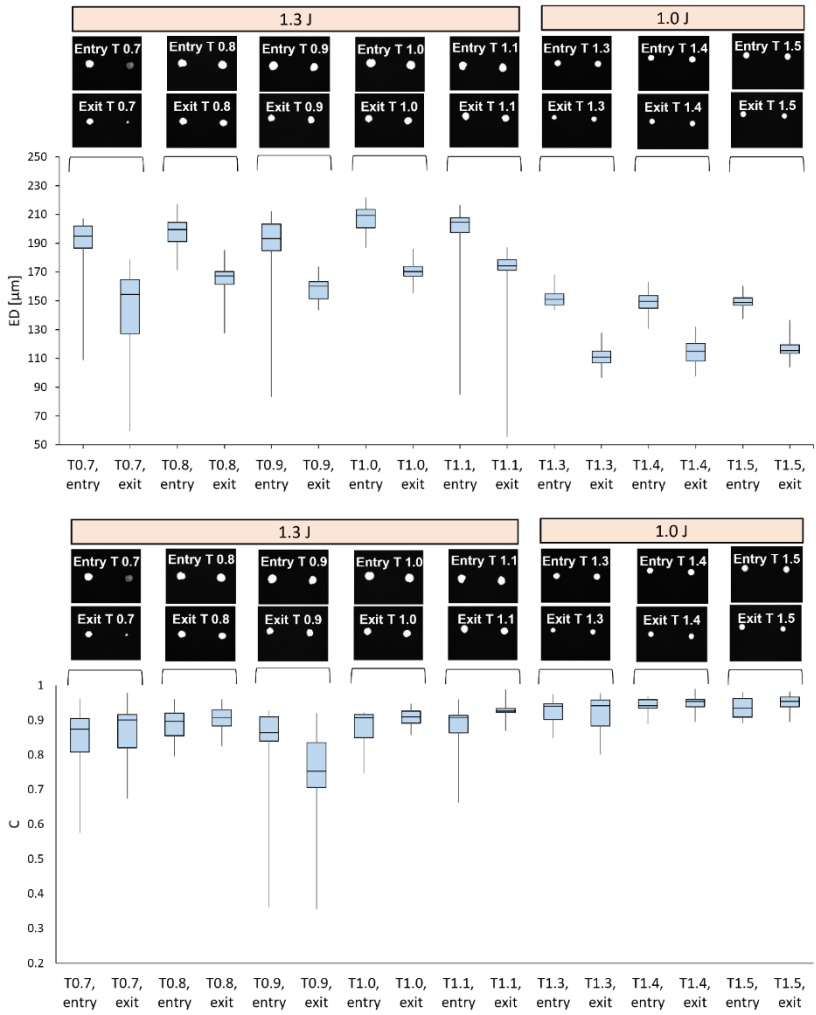

***Figure 6.11**: Complete overview of the laser drilling results on the equivalent diameter (ED) and circularity for the laser output energies 1.3 J and 1.0 J and pulse widths from 0.7 to 1.5 s. Per laser setting, an example of two obtained BF images at the laser entry and exit side are also shown. The results clearly show the improved variability when a lower laser power is used, both for the ED and the circularity results.*

6.5.5 Assessment of the HMNA sharpness

An indication on the sharpness of the MN tips was obtained by zooming in on the binarized µCT scan renderings. First, vertical and horizontal slices were obtained to inspect the MN apices in both ways. For the vertical slices, the exact center of each MN was located (**Figure 6.12A**) and the apex was measured (**Figure 6.12B**). In all cases, the distal ends were 1 to 2 pixels wide, i.e. in the range of 4-8 µm and thus below the recommended 10-15 µm range[47,48]. These sizes were also confirmed by measuring from the top (**Figure 6.12C-D**). As mentioned earlier in this chapter, the voxel size of the scans could only be reduced to 4 µm. Therefore, features smaller than this size could not be measured and the real needle sharpness might even be higher. Moreover, the measurements may also be affected by the processing steps which were carried out in the Avizo software to obtain the renderings.

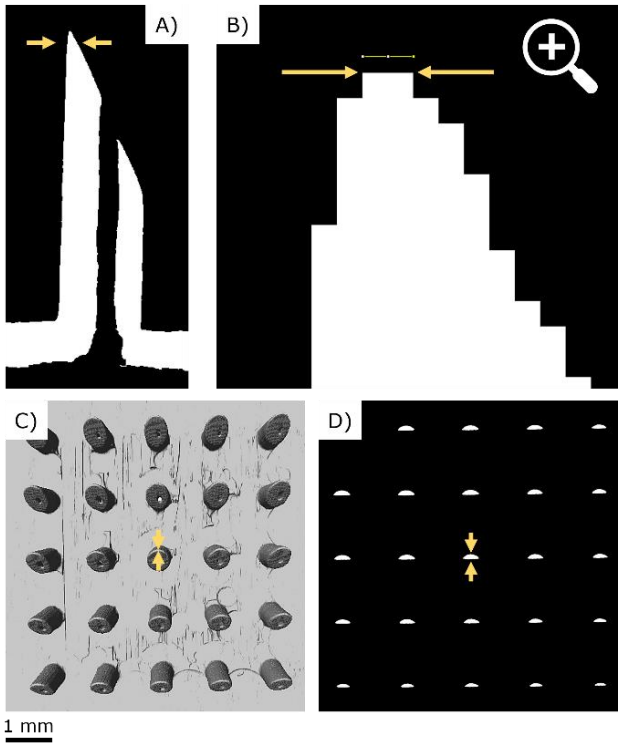

***Figure 6.12**: Analysis of the MN distal tip size based on binarized slices directed vertically (A and B) and horizontally (C and D).*

6.5.6 Flow characterization of the fabricated HMNAs

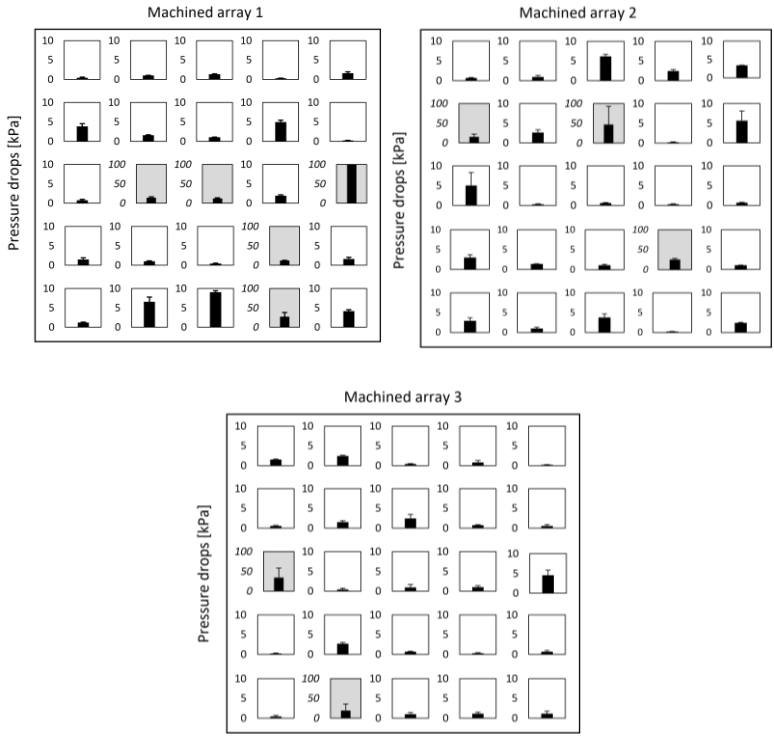

***Figure 6.13**: Bar charts of the pressure drops for distilled water flow (50 µL/min) through each individual lumen of the 3 tested HMNAs, which are represented as a heat map in the main manuscript. Bar charts with a grey background show that the y-axis (pressure drops) are shown in the range of 0-100 kPa, while the range for a white background is only 0-10 kPa. Error bars represent a single standard deviation for three repetitions.*

Table 6.2: *Results of the non-parametric Kruskal-Wallis test to show that the 3 characterized HMNAs are not significantly different from each other in terms of pressure drop. It must be noted that the results of 1 lumen on Array 1 was omitted from the data as the measured pressure exceeded the 100 kPa measurement limit for the pressure controller, resulting in a flow for which the real pressure drop could not be determined.*

Kruskal-Wallis Tests (Rank Sums)					
Level	**N**	**Score Sum**	**Expected Score**	**Score Mean**	**(Mean-Mean0)/Std0**
Array 1	24	1020.00	900.00	42.50	1.38
Array 2	25	1005.00	937.50	40.50	0.77
Array 3	25	750.00	937.50	30.00	-2.14
1-Way Test (X^2 approximation)					
X^2	**DF**	**P > X^2**			
4.73	2	0.0939			

Table 6.3: *Results of the non-parametric Kruskal-Wallis test with outliers omitted from the data (based on the quartile technique) to assure whether the conclusion is still the same.*

Kruskal-Wallis Tests (Rank Sums)					
Level	**N**	**Score Sum**	**Expected Score**	**Score Mean**	**(Mean-Mean0)/Std0**
Array 1	19	682.00	617.50	35.89	0.94
Array 2	22	791.00	715.00	35.95	1.07
Array 3	23	607.00	747.50	26.39	-1.96
1-Way Test (X^2 approximation)					
X^2	**DF**	**P > X^2**			
3.86	2	0.1448			

6.5.7 Machining artefacts

In **Figure 6.14**, extra images of the finished HMNAs are shown. Stereo-microscopy (**Figure 6.14C**) showed evidence of the creation of machining burrs (a thin material chip bending toward the inside of the lumen) that potentially restrict the microneedle lumen at the tip. However, µCT scanning did not demonstrate this and water could always pass through the lumen at high flow rates (50 µL/min).

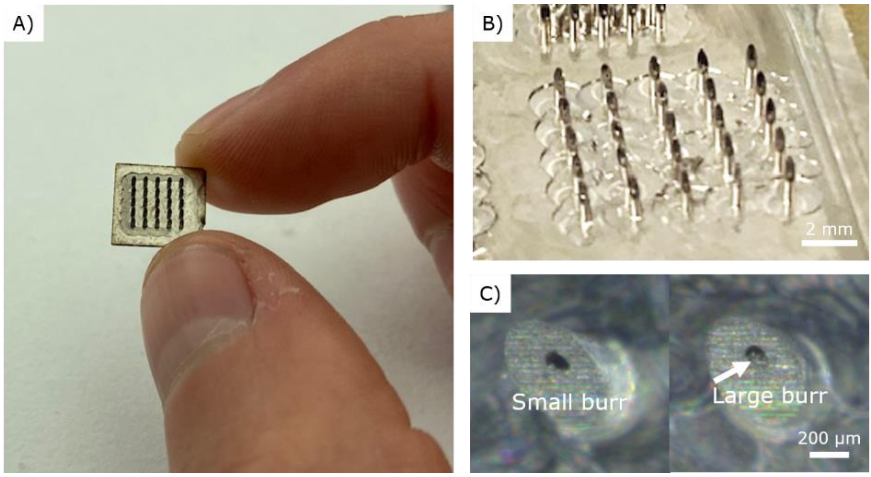

Figure 6.14: *5x5 HMNA a) after and b) before retrieval from the machining workpiece. c) Top view of a stereo-microscopy image showing that a lumen at the tip side seemed to be partially blocked, as indicated by the white arrow.*

6.5.8 Optimization of SIMPLE fabrication

The fabrication of the SIMPLE paper pump was optimized to overcome high pressure gradients. First, the standard fabrication protocol was explored, but pressure gradients of only 5.3 kPa were reached. Beyond this pressure, the connection between the working liquid and the porous paper tip broke. Such an event was captured by BF microscopy (see inset of **Figure 6.15A**), showing that, after a certain negative pressure gradient is achieved, air flows back via the interface between the porous paper and its chamber walls, breaking the working liquid-paper connection, and thus stopping the pump. It was expected that the lack of a tight sealing between the two material types allows this air backflow. Therefore, transfer tape was laminated on both sides of the porous paper tip to seal the filter paper pump (see inset of **Figure 6.15B**). This led to an almost 10-fold improvement of the achieved pressures.

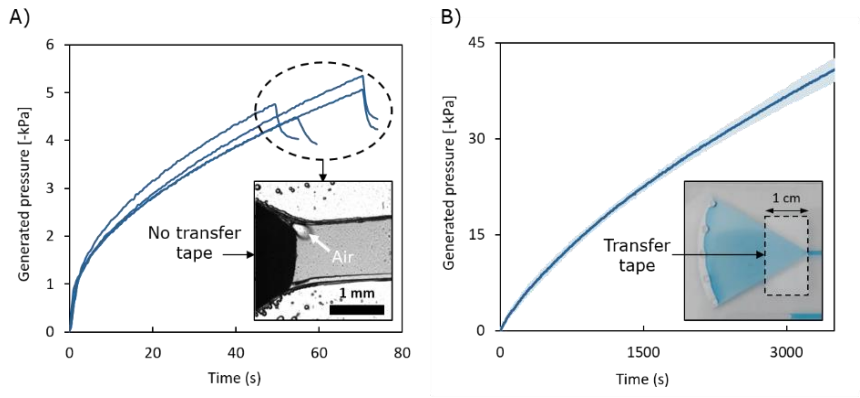

***Figure 6.15**: a) Generated pressures by the SIMPLE as fabricated without transfer tape sealing. The BF microscopy image captures the moment of pump rupture due to air leakage along the interface between the porous paper and the chamber walls (inset). b) Average generated pressures by the same chips, but reinforced by sealing the filter paper pump tip with transfer tape (inset). The shaded area represents 1 STD (n = 4).*

6.5.9 Proof-of-concept sampling patch: flow rates

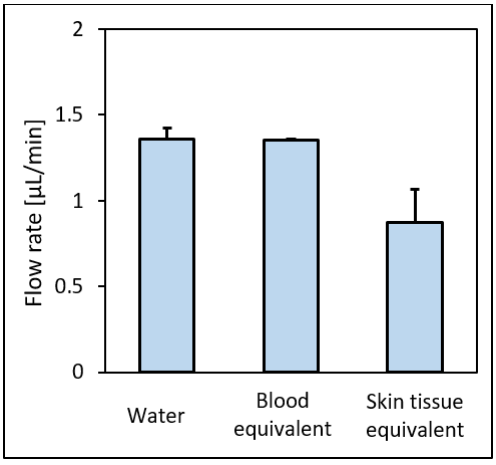

***Figure 6.16**: Bar chart depicting the average measured sampling flow rates for water, glycerol-water blood equivalent and sampling from a 2.65% (w/v) agarose gel as human skin equivalent. Error bars represent one standard deviation (n = 3).*

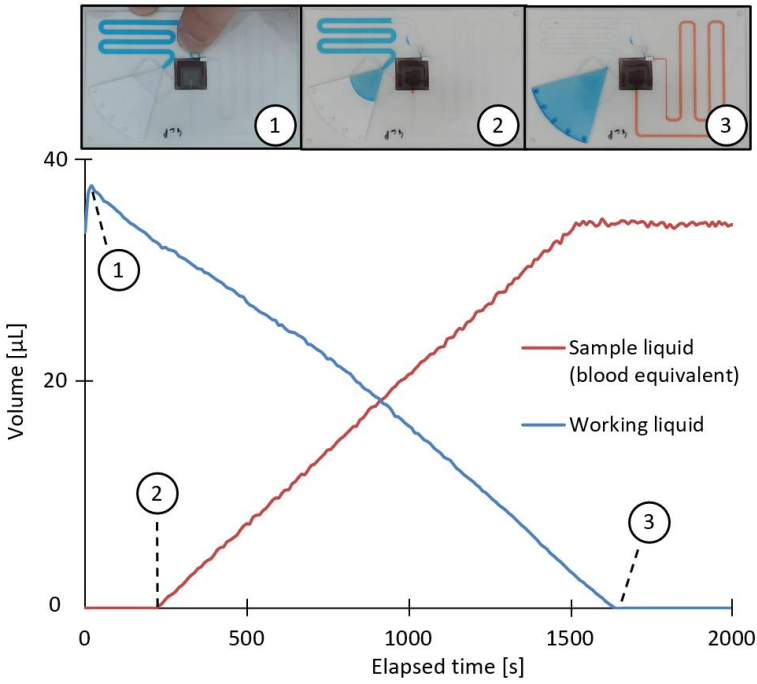

Figure 6.17: *Volume-to-time graph of working liquid (blue) and blood mimicking sample liquid (red). The insets show snapshots for three different moments during operation of the microsampling cartridge: (1) Activation of the SIMPLE unit, (2) Start measuring of the in-channel sample liquid, (3) end of the microsampling operation when all the working liquid has been consumed. The chart shows an almost linearly evolving volume change during microsampling, both for the working liquid and for the sample liquid. It must be remarked that only the sample liquid within the channel was measured as a result of the low resolution of sample liquid on top of the HMNA. The reported total sampled volumes in the manuscript have been corrected based on the designed volume of the chamber on top of the HMNA.*

6.6. References

1. Wilson, L.K.; Sullivan, S.; Goodnight, W.; Chang, E.Y.; Soper, D. The use of blunt needles does not reduce glove perforations during obstetrical laceration repair. *Am. J. Obstet. Gynecol. 199*, 639.e1–639.e4 (2008).
2. Samant, P.P.; Prausnitz, M.R. Mechanisms of sampling interstitial fluid from skin using a microneedle patch. *Proc. Natl. Acad. Sci. USA 115*, 4583–4588 (2018).
3. Shlomowitz, A.; Feher, M.D. The British journal of diabetes & vascular disease. *Br. J. Diabetes 14*, 60–63 (2014).
4. Lenicek Krleza, J.; Dorotic, A.; Grzunov, A.; Maradin, M. Capillary blood sampling: National recommendations on behalf of the Croatian society of medical biochemistry and laboratory medicine. *Biochem. Med. 25*, 335–358 (2015).
5. Morgan, P.E. Microsampling devices for routine therapeutic drug monitoring-are we there yet? *Ther. Drug Monit. 43*, 322–334 (2021).
6. Dixon, R.V.; Skaria, E.; Lau, W.M.; Manning, P.; Birch-Machin, M.A.; Moghimi, S.M.; Ng, K.W. Microneedle-based devices for point-of-care infectious disease diagnostics. *Acta Pharm. Sin. B 11*, 2344–2361 (2021).
7. Romanyuk, A.V.; Zvezdin, V.N.; Samant, P.; Grenader, M.I.; Zemlyanova, M.; Prausnitz, M.R. Collection of analytes from microneedle patches. *Anal. Chem. 86*, 10520–10523 (2014).
8. Mukerjee, E.V.; Collins, S.D.; Isseroff, R.R.; Smith, R.L. Microneedle array for transdermal biological fluid extraction and in situ analysis. *Sens. Actuators A Phys. 114*, 267–275 (2004).
9. Stoeber, B.; Liepmann, D. Arrays of hollow out-of-plane microneedles for drug delivery. *J. Microelectromech. Syst. 14*, 472–479 (2005).
10. Roxhed, N.; Gasser, T.C.; Griss, P.; Holzapfel, G.A.; Stemme, G. Penetration-enhanced ultrasharp microneedles and prediction on skin interaction for efficient transdermal drug delivery. *J. Microelectromech. Syst. 16*, 1429–1440 (2007).
11. Strambini, L.M.; Longo, A.; Diligenti, A.; Barillaro, G. A minimally invasive microchip for transdermal injection/sampling applications. *Lab Chip 12*, 3370–3379 (2012).
12. Jaganathan, H.; Godin, B. Biocompatibility Assessment of Si-Based Nano- and Microparticles. *Adv. Drug Deliv. Rev. 64*, 1800–1819 (2012).
13. Gittard, S.D.; Miller, P.R.; Boehm, R.D.; Ovsianikov, A.; Chichkov, B.N.; Heiser, J.; Gordon, J.; Monteiro-Riviere, N.A.; Narayan, R.J. Multiphoton microscopy of transdermal quantum dot delivery using two photon polymerization-fabricated polymer microneedles. *Faraday Discuss.* 149, 171–185 (2011).
14. Ceyssens, F.; Chaudhri, B.P.; Van Hoof, C.; Puers, R. Fabrication process for tall, sharp, hollow, high aspect ratio polymer microneedles on a platform. *J. Micromech. Microeng.* 23, 075023 (2013).
15. Mishra, R.; Maiti, T.K.; Bhattacharyya, T.K. Development of SU-8 hollow microneedles on a silicon substrate with microfluidic interconnects for transdermal drug delivery. *J. Micromech. Microeng. 28*, 105017 (2018).
16. Jiang, X.; Lillehoj, P.B. Microneedle-based skin patch for blood-free rapid diagnostic testing. *Microsyst. Nanoeng. 6*, 96 (2020).
17. Yadav, V.; Sharma, P.K.; Murty, U.S.; Mohan, N.H.; Thomas, R.; Dwivedy, S.K.; Banerjee, S. 3D printed hollow microneedles array using stereolithography for efficient transdermal delivery of rifampicin. *Int. J. Pharm. 605*, 120815 (2021).

18. Wu, T.; You, X.; Chen, Z. Hollow microneedles on a paper fabricated by standard photolithography for the screening test of prediabetes. *Sensors 22*, 4253 (2022).
19. Sugiyama, S.; Khumpuang, S.; Kawaguchi, G. Plain-pattern to cross-section transfer (PCT) technique for deep x-ray lithography and applications. *J. Micromech. Microeng. 14*, 1399–1404 (2004).
20. Khumpuang, S.; Kawaguchi, G.; Sugiyama, S. Quadruplets-microneedle array for blood extraction. In *Technical Proceedings of NSTI-Nanotech Conference'04*; Taylor & Francis Group: Boston, MA, USA, 2004. Available online: www.nsti.org (accessed on 18 September 2019).
21. Evens, T.; van Hileghem, L.; Dosso, F.D.; Lammertyn, J.; Malek, O.; Castagne, S.; Seveno, D.; van Bael, A. Producing hollow polymer microneedles using laser ablated molds in an injection molding process. *J. Micro Nano-Manuf. 9*, 030902 (2021).
22. Aksit, A.; Rastogi, S.; Nadal, M.L.; Parker, A.M.; Lalwani, A.K.; West, A.C.; Kysar, J.W. Drug delivery device for the inner ear: Ultra-sharp fully metallic microneedles. *Drug Deliv. Transl. Res. 11*, 214–226 (2021).
23. Davis, S.P.; Martanto, W.; Allen, M.G.; Prausnitz, M.R. Hollow metal microneedles for insulin delivery to diabetic rats. *IEEE Trans. Biomed. Eng. 52*, 909–915 (2005).
24. Vinayakumar, K.B.; Kulkarni, P.G.; Nayak, M.M.; Dinesh, N.S.; Hegde, G.M.; Ramachandra, S.G.; Rajanna, K. A hollow stainless steel microneedle array to deliver insulin to a diabetic rat. *J. Micromech. Microeng. 26*, 065013 (2016).
25. Rajabi, M.; Roxhed, N.; Shafagh, R.Z.; Haraldson, T.; Fischer, A.C.; Van Der Wijngaart, W.; Stemme, G.; Niklaus, F. Flexible and stretchable microneedle patches with integrated rigid stainless steel microneedles for transdermal biointerfacing. *PLoS ONE 11*, e0166330 (2016).
26. Chaudhri, B.P.; Ceyssens, F.; De Moor, P.; Van Hoof, C.; Puers, R. A high aspect ratio SU-8 fabrication technique for hollow microneedles for transdermal drug delivery and blood extraction. *J. Micromech. Microeng. 20*, 064006 (2010).
27. Liu, G.S.; Kong, Y.; Wang, Y.; Luo, Y.; Fan, X.; Xie, X.; Yang, B.R.; Wu, M.X. Microneedles for transdermal diagnostics: Recent advances and new horizons. *Biomaterials 232*, 119740 (2020).
28. Liu, L.; Wang, Y.; Yao, J.; Yang, C.; Ding, G. A minimally invasive micro sampler for quantitative sampling with an ultrahigh-aspect-ratio microneedle and a PDMS actuator. *Biomed. Microdevices 18*, 59 (2016).
29. Le Thanh, H.; The, H. Le; Nguyen, V.; Tran-Minh, N.; Wang, K.; Karlsen, F. Optimal design of polymer-based microneedle for improved collection of whole blood from human fingers. *Micro Nano Lett. 9*, 644–649 (2014).
30. Le Thanh, H.; Ta, B.Q.; The, H. Le; Nguyen, V.; Wang, K.; Karlsen, F. Low-cost fabrication of hollow microneedle arrays using CNC machining and UV lithography. *J. Microelectromech. Syst. 24*, 1583–1593 (2015).
31. Miller, P.R.; Gittard, S.D.; Edwards, T.L.; Lopez, D.A.M.; Xiao, X.; Wheeler, D.R.; Monteiro-Riviere, N.A.; Brozik, S.M.; Polsky, R.; Narayan, R.J. Integrated carbon fiber electrodes within hollow polymer microneedles for transdermal electrochemical sensing. *Biomicrofluidics 5*, 013415 (2011).
32. Miller, P.R.; Xiao, X.; Brener, I.; Burckel, D.B.; Narayan, R.; Polsky, R. Microneedle-based transdermal sensor for on-chip potentiometric determination of K+. *Adv. Healthc. Mater. 3*, 876–881 (2014).
33. Lee, K.; Lee, H.C.; Lee, D.S.; Jung, H. Drawing lithography: Three-dimensional fabrication of an ultrahigh-aspect-ratio microneedle. *Adv. Mater. 22*, 483–486 (2010).

34. Li, C.G.; Lee, C.Y.; Lee, K.; Jung, H. An optimized hollow microneedle for minimally invasive blood extraction. *Biomed. Microdevices 15*, 17–25 (2013).
35. Li, C.G.; Joung, H.A.; Noh, H.; Song, M.B.; Kim, M.G.; Jung, H. One-touch-activated blood multidiagnostic system using a minimally invasive hollow microneedle integrated with a paper-based sensor. *Lab Chip 15*, 3286–3292 (2015).
36. Niinomi, M. Recent research and development in metallic materials for biomedical, dental and healthcare products applications. *Mater. Sci. Forum 539–543*, 193–200 (2007).
37. Rajabi, M.; Roxhed, N.; Zandi Shafagh, R.; Haraldson, T.; Fischer, A.C.; van der Wijngaart, W.; Stemme, G.; Niklaus, F. Flexible and stretchable microneedle patches with integrated rigid stainless steel microneedles for transdermal biointerfacing. *PLoS ONE* 11(12) (2016)
38. Papich, M.G. & Narayan, R.J. Naloxone and nalmefene absorption delivered by hollow microneedles compared to intramuscular injection. *Drug Delivery and Translational Research* 12, 376-383 (2022).
39. Yuen, P. K., & Goral, V. N. Low-cost rapid prototyping of flexible microfluidic devices using a desktop digital craft cutter. Lab on a Chip, 10(3), 384–387 (2010);
40. Dal Dosso, F.; Decrop, D.; Pérez-Ruiz, E.; Daems, D.; Agten, H.; Al-Ghezi, O.; Bollen, O.; Breukers, J.; De Rop, F.; Katsafadou, M.; et al. Creasensor: SIMPLE technology for creatinine detection in plasma. *Anal. Chim. Acta 1000*, 191–198 (2018).
41. Dal Dosso, F.; Kokalj, T.; Belotserkovsky, J.; Spasic, D.; Lammertyn, J. Self-powered infusion microfluidic pump for ex vivo drug delivery. *Biomed. Microdevices 20*, 44 (2018).
42. Dal Dosso, F.; Bondarenko, Y.; Kokalj, T.; Lammertyn, J. SIMPLE analytical model for smart microfluidic chip design. *Sens. Actuators A Phys. 287*, 131–137 (2019).
43. Ordutowski, H.; Dal Dosso, F.; De Wispelaere, W.; Van Tricht, C.; Vermeire, S.; Geukens, N.; Gils, A.; Spasic, D.; Lammertyn, J. Next generation point-of-care test for therapeutic drug monitoring of adalimumab in patients diagnosed with autoimmune diseases. *Biosens. Bioelectron. 208*, 114189 (2022).
44. Dal Dosso, F.; Tripodi, L.; Spasic, D.; Kokalj, T.; Lammertyn, J. Innovative Hydrophobic Valve Allows Complex Liquid Manipulations in a Self-Powered Channel-Based Microfluidic Device. *ACS Sens. 4*, 694–703 (2019).
45. Cheng, J.; Perrie, W.; Edwardson, S.P.; Fearon, E.; Dearden, G.; Watkins, K.G. Effects of laser operating parameters on metals micromachining with ultrafast lasers. *Appl. Surf. Sci. 256*, 1514–1520 (2009).
46. Radmanesh, M.; Kiani, A. ND:YAG Laser Pulses Ablation Threshold of Stainless Steel 304. *Mater. Sci. Appl. 06*, 634–645 (2015).
47. Römgens, A. M., Bader, D. L., Bouwstra, J. A., Baaijens, F. P. T.; Oomens, C. W. J. Monitoring the penetration process of single microneedles with varying tip diameters. Journal of the Mechanical Behavior of Biomedical Materials. 397–405 (2014).
48. Park, J-H.; Yoon, Y-K.; Choi, S-O.; Prausnitz, M.R.; Allen, M.G. Tapered conical polymer microneedles fabricated using an integrated lens technique for transdermal drug delivery. IEEE Transactions on biomedical engineering. 54(5), 903-913 (2007).
49. Aoyagi, S.; Okuda, K.; Takahashi, T.; Suzuki, M. Effect of Microneedle Cross-Sectional Shape onPuncture Resistance – Investigation of Polygonal andStar-Shaped Cross Sections. Journal of Robotics and Mechatronics. 32(2), 371-381 (2020).

50. Blicharz, T.M.; Gong, P.; Bunner, B.M.; Chu, L.L.; Leonard, K.M.; Wakefield, J.A.; Williams, R.E.; Dadgar, M.; Tagliabue, C.A.; El Khaja, R.; et al. Microneedle-based device for the one-step painless collection of capillary blood samples. *Nat. Biomed. Eng. 2*, 151–157 (2018).
51. Kou, Z.; Wan, Y.; Cai, Y.; Liang, X.; Liu, Z. Burr controlling in micro milling with supporting material method. *Procedia Manuf. 1*, 501–511 (2015).
52. Kokalj, T., Park, Y., Vencelj, M., Jenko, M., & Lee, L. P. Self-powered Imbibing Microfluidic Pump by Liquid Encapsulation: SIMPLE. Lab on a Chip, 14(22), 4329–4333 (2014).
53. Vloemans, D.; Van Hileghem, L.; Verbist, W.; Thomas, D.; Dal Dosso, F.; Lammertyn, J. Precise sample metering method by coordinated burst action of hydrophobic burst valves applied to dried blood spot collection. *Lab Chip 21*, 4445–4454 (2021).
54. Tsuchiya, K.; Nakanishi, N.; Uetsuji, Y.; Nakamachi, E. Development of blood extraction system for health monitoring system. *Biomed. Microdevices 7*, 347–353 (2005).
55. Ramasubramanian, M.K.; Barham, O.M.; Swaminathan, V. Mechanics of a mosquito bite with applications to microneedle design. *Bioinspir. Biomim. 3*, 046001 (2008).
56. Boron, W.; Boulpaep, E. *Medical Physiology*; Elsevier Health Sciences: Amsterdam, The Netherlands (2016).
57. Lima, R.; Ishikawa, T.; Imai, Y.; Yamaguchi, T. Blood flow behavior in microchannels: Past, current and future trends. In *Single and Two-Phase Flows on Chemical and Biomedical Engineering*; Bentham Science Publishers: Sharjah, UAE, 513–547 (2012), ISBN 9781608053476..
58. Prentner, S.; Allen, D.M.; Larcombe, L.; Marson, S.; Jenkins, K.; Saumer, M. Effects of channel surface finish on blood flow in microfluidic devices. *Microsyst. Technol. 16*, 1091–1096 (2010).
59. Zhang, D.; Das, D.B.; Rielly, C.D. Microneedle Assisted Micro-Particle Delivery from Gene Guns: Experiments Using Skin-Mimicking Agarose Gel. *J. Pharm. Sci. 103*, 613–627 (2014).
60. Qu, J.H.; Ordutowski, H.; Van Tricht, C.; Verbruggen, R.; Barcenas Gallardo, A.; Bulcaen, M.; Ciwinska, M.; Gutierrez Cisneros, C.; Devriese, C.; Guluzade, S.; et al. Point-of-care therapeutic drug monitoring of adalimumab by integrating a FO-SPR biosensor in a self-powered microfluidic cartridge. *Biosens. Bioelectron. 206*, 114125 (2022).

Chapter 7

Producing hollow polymer microneedles using laser ablated molds in an injection molding process

The work reported in this chapter is adapted from:

Evens T., **Van Hileghem L.**, Dal Dosso F., Lammertyn J., Malek O., Castagne S., Seveno D., Van Bael A. (2021). Producing hollow polymer microneedles using laser ablated molds in an injection molding process. Journal of Micro- and Nano-Manufacturing, 9, 030902.

Van Hileghem L. contributed to this work on the microfluidics part and execution of the validation experiment with integrated single microneedles, next to writing and editing of parts of the Introduction and Results sections.

7.1. Introduction

Infectious diseases can be tackled both curatively and preventively by the administration of drugs and vaccines, respectively. Although many different administration routes exist, vaccines are most commonly administered by injection[1,2]. Drugs, on the other hand, are more frequently delivered enterally through the oral route, considering its straightforward dosing and wide acceptance[3,4]. Nonetheless, as an effect of passing through the gastrointestinal tract, the bioavailability with enteral administration can be critically reduced[5]. Therefore, like for vaccines, many drugs are still delivered parenterally by injection to avoid the gastrointestinal tract. Unfortunately, hypodermic needles used in the parenteral delivery approach are known to induce discomfort to the patient, carry the risk of infections and require well-trained medical staff[6,7]. Especially the latter two are known to be problematic in developing countries where about 50% of the needle use is regarded as unsafe[8].

A less invasive parenteral delivery approach is delivery via the skin. This can be done by topically applying formulations or transdermal patches[9]. However, only components with a specific combination of properties can be successfully administered this way, while the large majority of drugs and vaccines are unable to cross the skin's protective barrier, the stratum corneum[10]. Methods to improve absorption rates by surpassing the skin's stratum corneum have been intensively investigated and in 1976, a first concept using microneedles was described in a patent by Alza corporation[4]. Since then, a wide variety of microneedle designs have been developed with needle lengths ranging from 25 to 2500 µm. Usually these designs are developed in arrays which consist of tens or even thousands of individual microneedles[11]. A huge advantage of microneedles is the possibility of pain-free drug delivery and self-administration of drugs and vaccines. An additional advantage for vaccines is the abundance of specialized antigen presenting cells in the skin[4,12]. Moreover, due to their small volume, costs related to distribution are lower compared to traditional hypodermic needles. These benefits offer a great opportunity for delivery of medicines.

Further, it is evident that these systems would worldwide be a significant asset for solving pandemic crises, like the one caused by the COVID-19-virus[13].

In recent work[14], a novel methodology to produce solid polymer microneedles was demonstrated. This method utilizes a femtosecond laser to create cone-shaped micro-cavities in a mold insert. Contrarily to the millisecond laser used in Chapter 6, which allowed the removal of large amounts of stainless steel per pulse to achieve nearly straight microlumens, femtosecond laser pulses induce a much smaller heat-affected zone. This leads to the creation of highly precise micropatterns. The micropatterned mold insert is subsequently used in an injection molding process to create solid cone-shaped microneedles with sharp tip radii. The solid needles can be applied for drug or vaccine delivery using two approaches. In the first approach, referred to as 'poke with patch', the microneedles are used to pierce the skin, creating transient aqueous micro-pores through which a formulation can passively diffuse (**Figure 7.1A**). In the second approach, referred to as 'coat and poke', the needles are coated with a drug or vaccine formulation (**Figure 7.1B**). When inserted in the skin, the coating will be dissolved and the medicine will be deposited in the skin. Although these solid microneedles are able to offer significant advantages compared to the conventional hypodermic needles, their application area is limited because they can only deliver small amounts of medicines[15]. A third type of microneedles are dissolving microneedles. These needles consist of a soluble material, such as a biodegradable polymer, in which the drug or vaccine is encapsulated. A specific approach, referred to as 'poke and release' is used for these microneedles, in which the needles are inserted in the skin, where they dissolve and release the drug or vaccine (**Figure 7.1C**). In contrast to solid and dissolving microneedles, hollow microneedles possess a lumen, or internal bore, which enables the transportation of fluids, thus offering a huge potential (**Figure 7.1D**). This strategy, referred to as 'poke and flow', enables the injection of large amount of drugs[16,17] and vaccines[18] at higher rates.

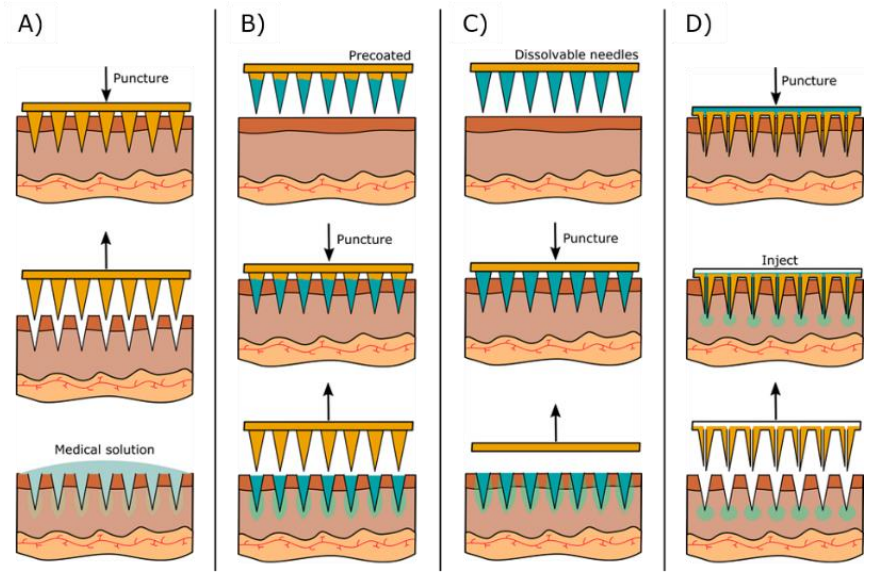

***Figure 7.1**: A schematic representation of the different types of microneedles. A) solid microneedles, B) coated microneedles, C) dissolving microneedles, and D) hollow microneedles for drug and vaccine delivery. Based on a figure from[19].*

Undoubtedly, the most challenging problem for hollow microneedles is their complex production process[19]. As mentioned in previous chapter, a production process to manufacture hollow polymer microneedle arrays in large volumes and at a low cost (i.e. scalable) is currently not available, as it brings an extra level of microfabrication complexity compared to solid microneedles. Current production methods described in literature are mostly very expensive, time consuming or unable to be used as a mass production process. Deep reactive-ion etching has been used to create off-plane hollow microneedles with a lumen of 75 to 150 µm and a length of 700 to 1000 µm[20]. However, the shapes of the microneedles are cylindrical with a blunt tip, which will be difficult to insert into skin. Wang et al. described a two-step production using photolithography and replica molding to produce hollow epoxy microneedles[21]. Inductively coupled plasma and anisotropic wet etching methods were also used to fabricate hollow microneedles on a silicon substrate. These needles were integrated with a piezoelectric pump for insulin dosage[17]. Two studies reported a method to

produce hollow glass microneedles by pulling fire-polished glass pipettes[16,22]. The needles were successfully used to deliver insulin to patients with type 1 diabetes in a less painful manner than the conventional hypodermic needles. Stereolithography 3D-printing is another technique suitable to directly create hollow microneedles[23,24] or to create molds[25] which can be used in a replication process to create hollow microneedles. Two-Photon-Polymerization is yet another additive manufacturing technique which was used in combination with a femtosecond laser to realize the production of hollow microneedles[26].

The choice of fabrication process depends on the selected material, access to manufacturing technology, and the intended application. As a result, a wide variety of needle designs is available in literature. Yet for all of these designs, the shape of the microneedle tip is important, as sharp microneedles are more effective in penetrating the skin. Furthermore, the shape of the microneedle tip is essential for the flow resistance, as a blunt-tipped microneedle will compact the skin and will bear a higher risk of clogging[27,28]. Therefore, microneedles should have a beveled shape, with the lumen off-centered or on the side of the microneedle[12].

To surpass the low scalability of the current microfabrication techniques, this work presents for the first time a method for producing hollow polymer microneedles using laser ablated molds in an injection molding process. First, two types of hollow microneedle cavities are created through laser ablation and their shape is assessed using micro-computed tomography (µ-CT). Both types of microneedles are implemented on a mold insert, which is afterwards replicated in an injection molding process using three different process conditions. The effect of these conditions on the replication process is assessed by a microscopic study of the obtained microneedles. Eventually, the hollow microneedle design with the highest replication fidelity is further validated during single-needle injections. Hereto, the needle is integrated into a microfluidic chip, which is used to inject colored water into a skin-mimicking agarose matrix.

7.2. Materials and methods

7.2.1 Reagents and materials

The thermoplastic material used in this study is polymethyl methacrylate (PMMA) due to its excellent biocompatible nature[29]. The selected grade is Plexiglas 8N from Evonik which has a melt volume flow-rate of 3.00 cm^3/10 min and a glass transition temperature of 117 °C. The selected mold material is an aluminum zinc alloy (grade 3.4365), which is regularly used for low production series and prototype molds, due to its low cost and good machinability. Agarose powder and water-based microfluidic dyes were acquired from Melford (UK) and Darwin Microfluidics (France), respectively. Pressure-sensitive adhesive (PSA) tape 200MP 7956MPL from 3M (USA) and transparent PVC sheets of 180 µm thick from Delbo (Belgium) were used for chip fabrication.

7.2.2 Representation of the process chain

A micromachining system with a laser source is employed to create hollow microneedle cavities in a mold insert with dimensions 70 mm x 60 mm x 4.6 mm (**Figure 7.2A**). The insert is then placed in the mold (**Figure 7.2B**). Injection molding is used to replicate the micro-cavities (**Figure 7.2C**), creating hollow polymer microneedles on top of a solid flat surface (**Figure 7.2D**). As we want to assess the functionality of the microneedles, a fluidic connection between the needles and the polymer plate is needed. In this study, this connection is created by drilling micro- holes though the flat surface, while in future work we aim to design a mold to directly incorporate the fluidic connections during injection molding.

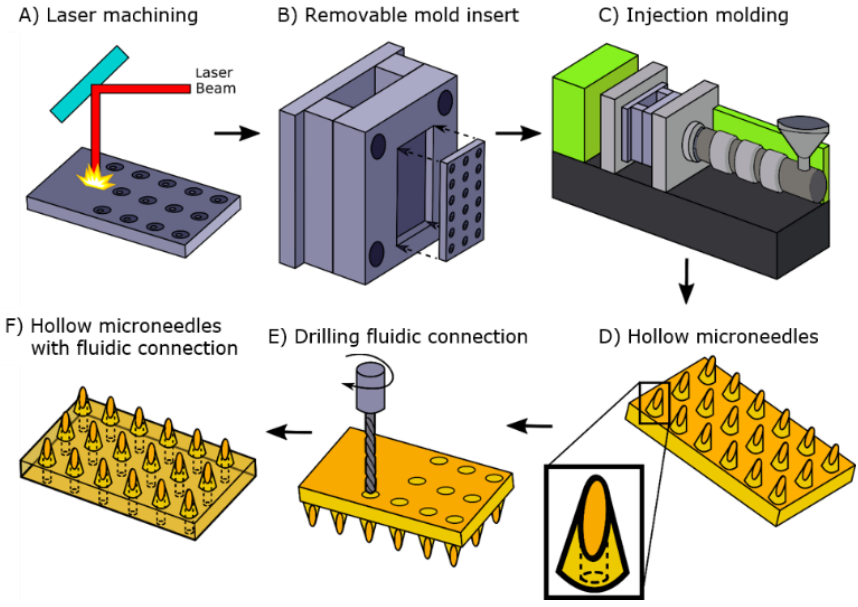

***Figure 7.2**: Illustration of the process chain to produce hollow polymer microneedles.*

7.2.3 Laser machining

A micromachining system (Lasea, Liège, Belgium) with a Satsuma HP femtosecond laser source (Amplitude, San Francisco, USA) is employed to laser ablate a mold insert with dimensions 70 mm x 60 mm x 4.4 mm. The laser source emits a beam with a pulse length of 250 fs, a wavelength of 1030 nm and a pulse repetition rate of 500 kHz. The maximum average power of the laser is 7.85 W, giving a deliverable pulse energy of 15.7 µJ. A galvanometer steers the laser beam within the focal plane, with a spot size of 15.0 µm and a pulse fluence of 8.88 J/cm². Small dust particles which are formed from ablating the metal surface are extracted by a vacuum collect unit. After the laser texturing operation, the mold insert was ultra-sonicated in an ethanol bath for 15 minutes to remove debris from the micro-holes.

The laser strategy proposed in this work is based on a previous study, in which we developed a method to create cone-shaped micro-holes for the creation of solid microneedles[30]. In

this adapted strategy, the laser spot scans a circular region and follows parallel lines in two perpendicular directions, where the distance between two consecutive lines is defined as the hatch pitch. Within the circular region, a scan-free internal area with a specific position is defined to create the lumen of the hollow microneedle. Once the laser has scanned one circular grid, the focal point is lowered with a vertical distance, defined as the layer pitch, and the laser scans again the same area. This process is repeated multiple times for a prescribed number of layers as illustrated in **Figure 7.3**. Using the proposed strategy, two arrays of 3 x 3 micro-cavities were ablated with different positions of the internal scan-free area. In the first array, the edge of the internal scan-free area is tangential to the edge of the scanned area, while in the second design there is a distance of 100 µm between both edges. In both arrays, the interspacing between the micro-cavities is 1 mm and a 475 µm base diameter was programmed with a hatch pitch of 15 µm. The diameter of the scan-free area is 100 µm and a total of 450 layers was created with an individual layer pitch of 2 µm.

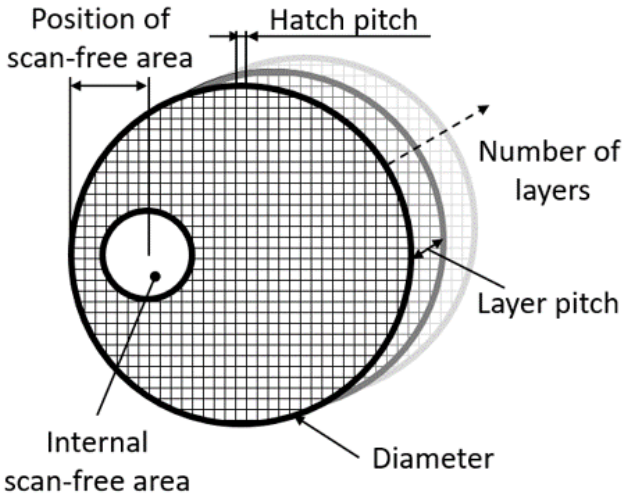

***Figure 7.3**: Illustration of the laser strategy with internal scan-free area*

7.2.4 Polymer injection molding

The injection molded part for this study is a 50 mm x 60 mm x 1.5 mm flat plate. The array of micro needles is approximately 2.5 mm x 2.5 mm in size, positioned at a distance of approximately 45 mm from the injection location.

Injection molding was done on an Engel ES 200/35 HL hydraulic injection molding machine (Engel, Schwertberg, Austria) with a maximum clamping force of 350 kN and a 25 mm screw with an L/D ratio of 24.8. The mold temperature is controlled by a WITTMANN TEMPRO Controller (Wittmann, Vienna, Austria). Three sets of injection molding parameters were defined within the recommended limits of the material supplier as given in **Table 7.1**. The first set of parameters is defined as 'low' and corresponds to the lowest recommended conditions. The second set is defined as 'middle' and corresponds to the average between the upper and lower process conditions. The third set is defined as 'high' and correspond to the highest recommended conditions. The holding pressure was kept constant in each set of parameters to completely fill the macroscopic polymer plate without sink marks. In each of the experiments, the parts produced in the first 30 cycles were discarded in order to stabilize the process, then the following parts were collected for characterization.

***Table 7.1**: Three sets of injection molding parameters: 'low', 'middle' and 'high'.*

	Low	Middle	High
Melt temperature [°C]	240	250	260
Volumetric injection rate [cm^3/s]	50	100	150
Holding pressure [Bar]	800	800	800
Mold temperature [°C]	70	90	110

7.2.5 Micro drilling

The micro drilling tests were carried out on a CNC machining center (Kern Microtechnik, Eschenlohe, Germany) at a spindle speed of 40 000 RPM. A DIXI Polytool 1131 micro drill with a diameter of 100 µm and a length of 700 µm was used. Due to the small length of the micro drill, the thickness of the polymer plate at the location of the microneedles had to be reduced to a thickness of approximately 500 µm. This operation was done using a ProtoTRAK RMX 3500 milling machine (Southwestern Industries, Rancho Dominguez, USA).

7.2.6 Topography characterization

The geometries of the ablated microneedle cavities were characterized using a Phoenix Nanotom µ-CT system (Universal Systems, Solon, USA). The device is equipped with a high-power nanofocus X-ray tube and a diamond-tungsten target was chosen for the high X-ray absorbing aluminum samples. A high-power mode was used to allow focal spot and voxel sizes in the micrometer range. The two arrays of microneedle cavities were cut into cubic samples with an edge length of approximately 3 mm, using a metallographic precision saw. The cubic samples were mounted on a sample holder and fixed on a high-accuracy computer controlled rotation stage. For each scan, 2400 X-ray 2D projection images were obtained from incremental rotation of the scanned samples over 360°. Acquisition parameters were fixed for all samples as follows: voltage = 100 kV, current = 158 A, voxel size = 3.75 µm, and a 0.1 mm copper filter was used during scanning. Reconstruction of the acquired 2D projections into 3D volumes was performed using GE Phoenix datos|x REC software. Reconstructed datasets (slices) were exported for further analysis and visualization within Fiji ImageJ. Before conducting measurements, the Nanotom instrument was calibrated using a calibration rod (Goekeler Messtechnik, VTX18CE000-022), having an uncertainty of 1.0 µm. For each set of laser parameters, one cubic sample containing nine micro-holes were measured. The average length and diameter of the nine micro-cavities, along with the standard deviation was reported in the results.

The geometry of the replicated thermoplastic microneedles were assessed using a Keyence VH-S30 digital microscope (Keyence, Osaka, Japan) with a maximum magnification of X200. The system was connected to a VHX-500F monitor with built-in measuring software. The microscope was calibrated using a stage micrometer (Olympus Tokyo, OBMM 1/100) which has an uncertainty of 0.5 µm. Ten injection molded samples were collected and on each sample one microneedle was measured. The averages of these ten measurements along with the standard deviations are reported in the results.

7.2.7 Preparation of a skin-mimicking substrate

An agarose gel with concentration of 2.65% (w/v) was prepared by dissolving the agarose powder in distilled water by heating on a hot plate under constant magnetic stirring until the solution had completely cleared out (±20 minutes). Then, the solution was poured into a petri dish to obtain a gel of about 1 cm thick. The substrates were used for injection experiments at least two hours after solidification and on the same day.

7.2.8 Validation of single-needle injections

Channels of 1 mm width were cut from the PSA using a CO_2 laser cutter (Speedy 300, Trotec Laser, Plymouth, USA). With this fabrication method, the channel height is defined by the thickness of the PSA tape, in this case being 153 µm. The PVC layers, designed to contain also the connection holes for the microneedle and pump, were cut with a digital craft cutter (Maxx Air 24 in., KNK, USA). After chip assembly (**Figure 7.4**) by exerting pressure on the well-aligned and sandwiched layers, the microneedle with its substrate was integrated using a laser cut PSA connector piece to assure a tight sealing.

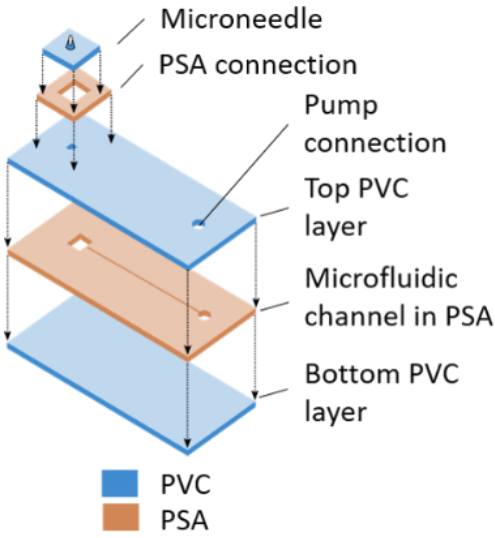

***Figure 7.4**: Exploded view of the chip containing a single, straight microfluidic channel. A single microneedle was tightly incorporated into the chip by a PSA connecting piece. At the other end of the channel, a hole serves for connecting a fluidic pump.*

To inject distilled water with a 1/100 diluted blue dye into a (biological) matrix, a fluid flow was controlled by the setup as shown in **Figure 7.5**. Using a pressure controller (LineUpTM Push/Pull, Fluigent, France) and a flow sensor (S model, Fluigent, France), injections into the agarose matrix were controlled while monitoring the obtained pressures in real-time every second (1 Hz). To guarantee a good insertion of the microneedles into the agarose slab throughout the experiment, a small weight was applied on top of the chip after manually inserting the microneedle. Injection profiles were followed-up by filming the process from the side using a smartphone camera and snapshots of the recorded dispersion profiles after 0, 2, 5, 10 and 15 minutes were collected. The injection was repeated 3 times on 3 different agarose slabs and the average pressure along with one standard deviation are reported in the results.

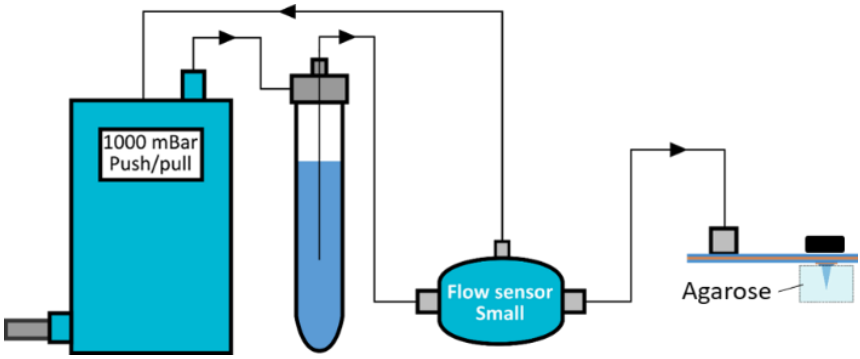

***Figure 7.5**: Setup for controlling the injection into agarose. From left to right the pressure controller, a pressurized reservoir containing the to be injected liquid, the flow sensor with feedback to the pressure controller, the microfluidic chip with integrated microneedle and the agarose slab.*

7.3. Results and discussion

7.3.1 Laser ablation

Two arrays of 3 x 3 microneedle cavities were formed during the laser ablation process, which took approximately 9.5 minutes for each array. Cross sectional views of the produced micro-cavities for both arrays are depicted in **Figure 7.6**. The XY images represent cross sections throughout the depth of the cavity, while the XZ and YZ images represent cross sections throughout the width of the cavity. The distance below each image indicates the position of the cross section. For XY, 0 µm corresponds to the mold surface, while for XZ and YZ 0 µm corresponds to the edge of the microneedle.

In both arrays, we can observe that the internal scan-free area has formed a tapered feature inside the micro-cavity, which will form the lumen of the hollow microneedle. The position of the tapered feature is different for both arrays due to the difference in position of the internal scan-free area. For array 1, the distance between the edge of the tapered feature and the edge of the micro-hole is only a few micrometers, while for array 2 this distance is approximately 100 µm. Evidently, the laser will also ablate material in the region between the tapered feature and the edge of the micro-hole, therefore inducing a trench between the

tapered feature and the edge of the micro-hole. The depth of this trench in array 2 is much deeper compared to the trench in array 1, being 508 ± 11 µm and 110 ± 9 µm, respectively. This discrepancy can be explained by the larger surface area of array 2, which will cause higher accumulated energy in this region compared to array 1.

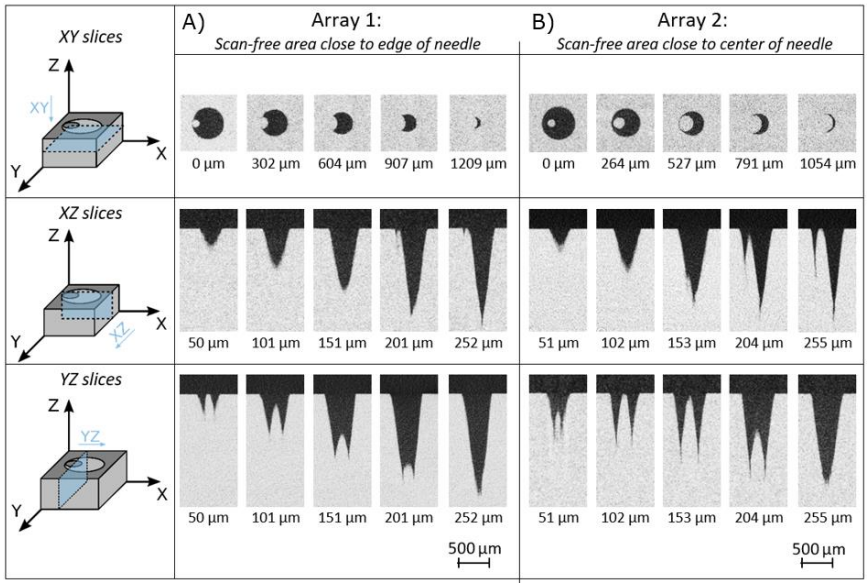

***Figure 7.6**: Cross sectional views obtained from the µ-CT measurements of the micro-hole arrays, with the scan-free area: A) close to the edge of the needle and B) close to the center of the needle. The distance below each image indicates the position of the cross section. For XY, 0 µm corresponds to the mold surface, while for XZ and YZ 0 µm corresponds to the edge of the microneedle.*

Cone-shaped micro-holes with an internal tapered feature can be observed for both arrays. The formation of this conical shape is expected to be the result of two laser phenomena, being laser reflectance on steep sidewalls and possibly a plasma shieling effect. First, steep sidewalls will cause most of the laser light to be reflected rather than absorbed. Therefore, the ablation efficiency near the edge of the cavity is drastically reduced, causing the diameter to become smaller as the micro-hole is created[31]. Moreover, the reflected laser light will partially be redirected to the bottom of the hole, contributing to a deeper and sharper cavity. A possible second phenomenon occurs for laser

ablation processes with high repetition rates[32]. Vaporized material that is unable to escape from the micro-cavity interacts with the next incoming laser pulse, forming a plasma. This plasma will defocus the laser beam, creating a protective shield referred to as "plasma shielding".

The cavity diameters at the mold surface are similar for both arrays, being 504 ± 5 µm for array 1 and 510 ± 3 µm for array 2. However, these dimensions are higher than the programmed base diameter of 475 µm. This difference can be explained as follows. During the laser ablation process, the laser focal spot is progressively moved deeper inside the mold material. Therefore, the Gaussian-shaped laser beam will start to intersect with the edge of the already created micro-hole. If in this intersecting region the power density of the Gaussian beam is higher than the ablation threshold, additional material will be removed. Thus, during the laser ablation process, the micro-cavities will progressively increase in diameter. Secondly, the depth of the micro-cavities in array 1 are deeper compared to the cavities in array 2 being 1513 ± 12 µm and 1318 ± 12 µm, respectively. As in array 2, the internal scan-free area is located more towards the center of the micro-hole, less energy can be induced in the center region of the micro-hole, resulting in shallower holes compared to array 1. We can observe low standard deviations for the cavity depth, cavity diameter at and the depth of the trench. In fact, the highest coefficient of variation for all of the measurements corresponds to approximately 3%. This indicates a very high repeatability of the laser ablation process.

7.3.2 Replication through injection molding

Figure 7.7 shows an image of the replicated polymer microneedles of array 1 created with a scan-free internal area close to the edge of the needle (**Figure 7.7A**), and array 2 created with a scan-free area close to the center of the needle (**Figure 7.7B**). These samples were created with the 'high' injection molding parameters at a cycle time of approximately 18 seconds. For both arrays, we observe hollow cone-shaped microneedles with a bevel shaped tip, which is similar to conventional hypodermic needles.

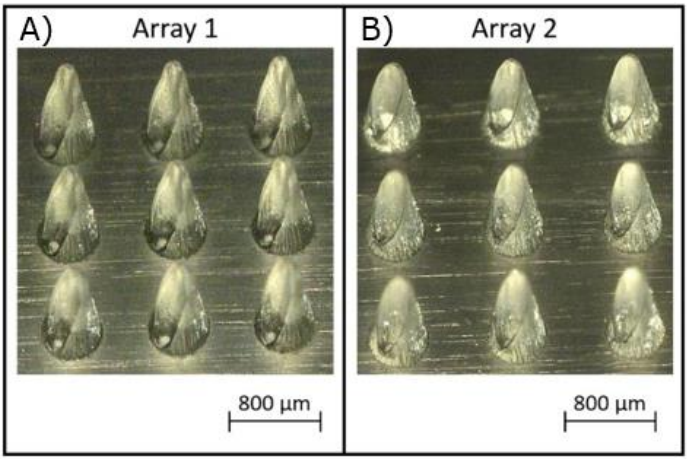

***Figure 7.7**: Microscopic image of the replicated polymer microneedle arrays created with a scan-free internal area A) close to the edge of the needle, and B) close to the center of the needle.*

The trench which was formed between the tapered feature and the edge of the micro-cavity has now been replicated to form an upstanding ridge which partially encloses the sides of the lumen. This could be beneficial, as the ridge could prevent fluids from leaking between the microneedle and the skin of the patient when the microneedle has not completely penetrated in the skin. In the further stages of this paper we continue using only array 2, as these needles have the highest potential to form functional microneedles.

The three different sets of injection molding parameters were used to replicate the microneedle cavities from array 2. **Figure 7.8** shows the microscopic images of the front and side view of the replicated microneedles and **Figure 7.9** shows the measured needle length, ridge height and tip wall thickness of the replicated microneedles in function of the three different sets of injection molding parameters.

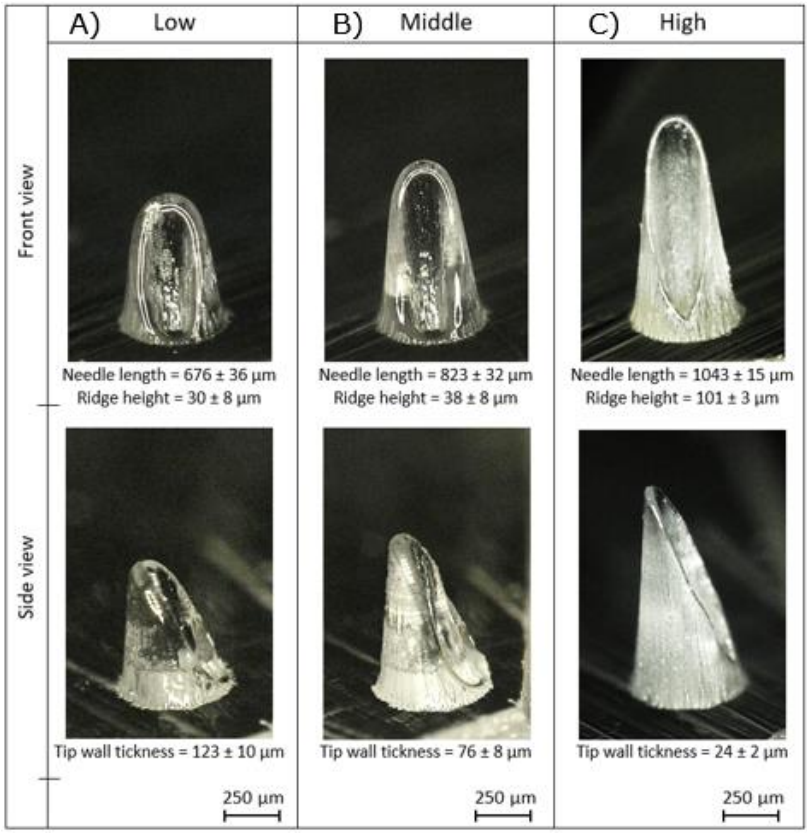

***Figure 7.8**: Microscopic image of the front and side view of the replicated polymer microneedles created with: A) 'low' injection molding parameters, B) 'middle' injection molding parameters and C) 'high' injection molding parameters. The average value of the dimensions of the needles are reported together with the standard deviation (n = 10).*

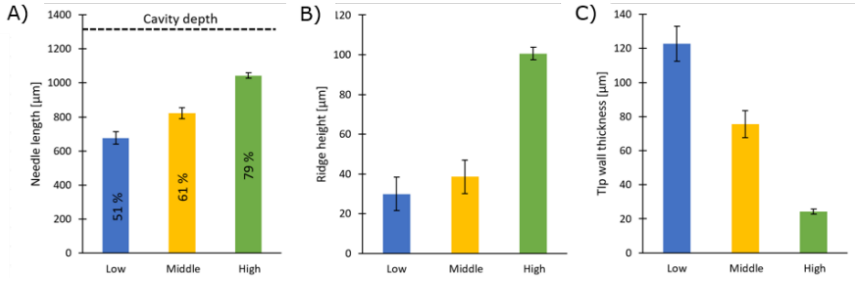

***Figure 7.9**: A) Needle length, B) ridge height and C) tip wall thickness of the replicated microneedles from array 2 in function of the three different sets of injection molding parameters, being 'low', 'middle' and 'high'. The percentages in (A) represent the replication in height.*

In addition, the replication of the microneedle in height was expressed, calculated based on the length of the needle and the depth of the corresponding micro-cavity. It is to be noted that the volumetric replication fidelity will be much higher than the expressed percentage of the replication in height. This due to the fact that the volume gradually decreases throughout the height of the cone-shaped needles.

The three parameters that were varied between the different sets of injection molding parameters are the melt temperature, the volumetric injection rate and the mold temperature. All of these parameters will, to some extent, influence the replication of the microneedles. The first parameter is the mold temperature, which is in literature known to be the most important parameter when it comes to replicating micro-features[33–35]. When a macro-scale cavity with micro-features is injection molded, the filling of the micro-features has to compete with the filling in the rest of the cavity. Since the polymer will follow the path of least resistance, most of the material will flow in the main flow direction through the macro-scale cavity, leaving the micro-features only partially filled, also known as the hesitation effect[36,37]. These micro-features will then only be filled after the rest of the cavity is filled and the pressure rises. Yet, as soon as the polymer is in contact with the mold, a layer of frozen polymer material (skin layer) will be formed. The rapid solidification of the skin layer hinders the filling of the micro-features and can lead to incomplete filling[38]. By increasing the mold temperature, the formation of the frozen layer can be delayed, leading to the polymer still being able to be deformed during the packing phase, resulting in a better replication of the micro-features[39–41]. The second parameter is the volumetric injection rate. High volumetric injection rates reduce the injection time and can prevent premature freezing of the polymer. Moreover, a high injection velocity promotes shear heating, which can locally decrease the melt viscosity and can therefore improve the replication[33]. The highest volumetric injection rate used in this study was set to the limit of the injection molding equipment. The last parameter is the melt temperature. High temperatures of melt ensure lower melt viscosity, lower cavity pressure drop, and

the ability of the melt to flow into micro-features[42]. The upper melt temperature is limited, as it should be selected consistent with the polymer properties to avoid thermal degradation.

It can clearly be observed that there is a significant difference in replication fidelity between the three different injection molding conditions. The low injection molding parameters resulted in the shortest microneedles having a very low ridge and a large wall thickness of the needle tip. The needles created with the 'middle' parameters are already better compared to the needles obtained with the low injection molding parameters. Yet, the highest replication fidelity is observed for the 'high' injection molding parameters. Here, the tallest needles are found combined with a high ridge and low tip wall thickness. Besides, these microneedles have the lowest standard deviation for all of the measurements. This indicates a more stable injection molding process, which in turn results in a high reproducibility of the produced samples. Furthermore, the microneedles created with the 'high' injection molding conditions appear to be more opaque compared to the other two sets of microneedles. This opaque appearance is caused by micro- and nano surface roughness, which are replicated using the 'high' process conditions. The replication of the microneedles will also be affected by the volumetric shrinkage of the polymer. This volumetric shrinkage can be determined using the compressibility (or PVT) behavior of the polymer and can be modelled by the double domain Tait equations[43]. An estimate of the volumetric shrinkage can be calculated by assuming the pressure at the end of the packing stage to be equal to the holding pressure and the temperature to be equal to the no-flow temperature. Consequently, a linear shrinkage of 0.28 % was calculated for the PC material, which corresponds to only a very small portion of the incomplete replication.

Not only the tip of the microneedle is subjected to incomplete replication, but also the ridge of the microneedle will be affected. In fact, the ridge of the microneedle is much more sensitive to incomplete replication as the aspect ratio of this component is much higher. With an increase in aspect ratio, the surface area

to volume ratio increases, which corresponds to a higher heat transfer between the molten polymer and the mold surface[44]. This results in a faster solidification of the polymer, causing a higher fraction of incomplete filling. For the microneedles replicated with the low injection molding conditions, the filling of in height of the ridge corresponds to only 20%.

7.3.3 Validation on skin-mimicking substrate

To proof that the microneedles are compatible with microfluidic technologies for injecting drug or vaccine substances, single microneedles were integrated into a chip connected to a pressure pump. Performing injections with a single microneedle was preferred over arrays to reduce complexity while studying release profiles and phenomena like leakage. The patch was vertically inserted into a 2.65% (w/v) agarose gel to mimic intradermal injection[45,46]. As the gel is transparent, the injection profile could be followed-up easily by the blue colored water.

The frames and graph in **Figure 7.10** show the dispersion profile through the agarose and pressure profile during the injection of 7.5 µL of colored water at a flow rate of 0.5 µL/min, respectively. Pressure data were corrected for the pressure required to maintain the flow through the setup, including the chip with microneedle, without insertion into the skin model. The results clearly depict that after a few minutes a constant pressure is reached and maintained, indicating a constant flow from the microneedle into the matrix. The injected liquid could be observed by the naked eye after approximately one minute, after which a uniform release profile consistently evolved. This proves the feasibility of the microneedles to inject liquids when integrated in a microfluidic platform.

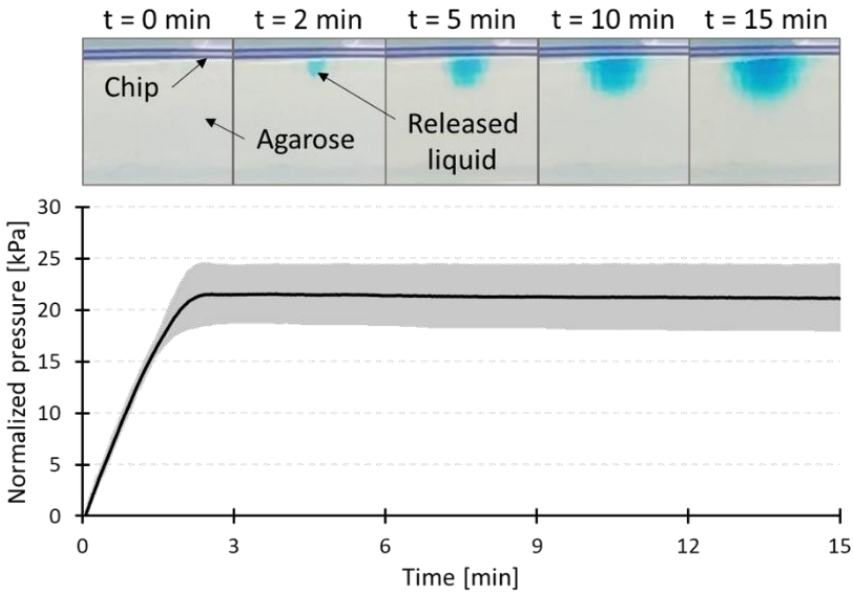

***Figure 7.10**: Injection profiles accompanied with the pressure obtained during injection through a single microneedle into skin-mimicking agarose at 0.5 µL/min. The black curve shows the average obtained pressure profile (n = 3) and the grey shaded area shows one standard deviation.*

7.4. Conclusion

In this study, a novel method to produce hollow polymer microneedles was successfully demonstrated. We were able to create hollow microneedle cavities in an aluminum mold insert by laser ablation. The position of the lumen inside the microneedle was changed by adapting the laser scanning strategy. Polymer injection molding was used to replicate the hollow microneedles using three sets of molding conditions. The replication fidelity for each of these conditions was evaluated through microscopic measurements. It was found that the combination of a high mold temperature, volumetric injection rate and melt temperature facilitated the replication. At last, the functionality of the manufactured hollow microneedles was evaluated during single-needle injections. We effectively injected colored water into an agarose matrix using a pressure pump. The developed methodology has a huge potential, as it acts as a mass production technique for low-cost, high-volume microneedle devices.

Moreover, it is possible to change the design of the microneedle by adjusting the laser scanning parameters, which allows for further improvements.

In the nearby future, we will attempt to directly incorporate the fluidic connections between the needles and the polymer plate during the injection molding process, by adapting the mold design. Besides, we will further improve the microneedle design in terms of functionality for different conditions and applications.

7.5. References

1. Hegde NR, Kaveri S V., Bayry J. Recent advances in the administration of vaccines for infectious diseases: Microneedles as painless delivery devices for mass vaccination. *Drug Discov Today* 16, 1061–8 (2011).
2. Zuckerman JN. The importance of injecting vaccines into muscle. *Br Med J* 321, 1237–8 (2000).
3. Tucak A, Sirbubalo M, Hindija L, Rahić O, Hadžiabdić J, Muhamedagić K, et al. Microneedles: Characteristics, materials, production methods and commercial development. *Micromachines* 11 (2020).
4. Donnelly RF, Singh TRR, Larrañeta E, McCrudden MTC. Microneedles for Drug and Vaccine Delivery and Patient Monitoring. Chichester (2018).
5. Guillot AJ, Cordeiro AS, Donnelly RF, Montesinos MC, Garrigues TM, Melero A. Microneedle-based delivery: An overview of current applications and trends. *Pharmaceutics* 12, 1–28 (2020).
6. Mooney K, McElnay JC, Donnelly RF. Children's views on microneedle use as an alternative to blood sampling for patient monitoring. *Int J Pharm Pract* 22, 335–44 (2014).
7. Cross S, Roberts M. Physical Enhancement of Transdermal Drug Application: Is Delivery Technology Keeping up with Pharmaceutical Development? *Curr Drug Deliv* 1, 81–92 (2005).
8. Simonsen L, Kane A, Lloyd J, Zaffran M, Kane M. Unsafe injections in the developing world and transmission of bloodborne pathogens: A review. *Bull World Health Organ* 77, 789–800 (1999).
9. Cheung K, Das DB. Microneedles for drug delivery: trends and progress. *Drug Deliv* 23, 2338–54 (2016).
10. Paudel KS, Milewski M, Swadley CL, Brogden NK, Ghosh P, Stinchcomb AL. Challenges and opportunities in dermal/transdermal delivery. *Ther Deliv* 1, 109–31 (2010).
11. Juster H, van der Aar B, de Brouwer H. A review on microfabrication of thermoplastic polymer-based microneedle arrays. *Polym Eng Sci* 59, 877–90 (2019).
12. Li X (James), Zhou Y. Microfluidic devices for biomedical applications. Woodhead Publ. Ser. Biomater., Cambridge: Woodhead Publishing Limited, 1–652 (2013).
13. Kim E, Erdos G, Huang S, Kenniston TW, Balmert SC, Carey CD, et al. Microneedle array delivered recombinant coronavirus vaccines: Immunogenicity and rapid translational development. *EBioMedicine* 55, 1–12 (2020).

14. Evens T, Malek O, Castagne S, Seveno D, Van Bael A. A novel method for producing solid polymer microneedles using laser ablated moulds in an injection moulding process. *Manuf Lett* 24, 29–32 (2020).
15. Roxhed N, Griss P, Stemme G. Membrane-sealed hollow microneedles and related administration schemes for transdermal drug delivery. *Biomed Microdevices* 10, 271–9 (2008).
16. Gupta J, Felner EI, Prausnitz MR. Erratum: Minimally invasive insulin delivery in subjects with type 1 diabetes using hollow microneedles. *Diabetes Technol Ther* 11, 471 (2009).
17. Ma B, Liu S, Gan Z, Liu G, Cai X, Zhang H, et al. A PZT insulin pump integrated with a silicon microneedle array for transdermal drug delivery. *Microfluid Nanofluidics* 2, 417–23 (2006).
18. Giri Nandagopal MS, Antony R, Rangabhashiyam S, Sreekumar N, Selvaraju N. Overview of microneedle system: A third generation transdermal drug delivery approach. *Microsyst Technol* 20, 1249–72 (2014).
19. Faraji Rad Z, Nordon RE, Anthony CJ, Bilston L, Prewett PD, Arns J-Y, et al. High-fidelity replication of thermoplastic microneedles with open microfluidic channels. *Microsystems Nanoeng* 3, 1–11 (2017).
20. Liu Y, Eng PF, Guy OJ, Roberts K, Ashraf H, Knight N. Advanced deep reactive-ion etching technology for hollow microneedles for transdermal blood sampling and drug delivery. IET Nanobiotechnology 7, 59–62 (2013).
21. Wang PC, Wester BA, Rajaraman S, Paik SJ, Kim SH, Allen MG. Hollow polymer microneedle array fabricated by photolithography process combined with micromolding technique. *Proc 31st Annu Int Conf IEEE Eng Med Biol Soc Eng Futur Biomed EMBC* 7026–9 (2009).
22. Martanto W, Moore JS, Kashlan O, Kamath R, Wang PM, O'Neal JM, et al. Microinfusion using hollow microneedles. *Pharm Res* 23, 104–13 (2006).
23. Yeung C, Chen S, King B, Lin H, King K, Akhtar F, et al. A 3D-printed microfluidic-enabled hollow microneedle architecture for transdermal drug delivery. *Biomicrofluidics* 13 (2019).
24. Ceyssens F, Chaudhri BP, Van Hoof C, Puers R. Fabrication process for tall, sharp, hollow, high aspect ratio polymer microneedles on a platform. *J Micromechanics Microengineering* 23 (2013).
25. Krieger KJ, Bertollo N, Dangol M, Sheridan JT, Lowery MM, O'Cearbhaill ED. Simple and customizable method for fabrication of high-aspect ratio microneedle molds using low-cost 3D printing. *Microsystems Nanoeng* 5 (2019).
26. Trautmann A, Roth GL, Nujiqi B, Walther T, Hellmann R. Towards a versatile point-of-care system combining femtosecond laser generated microfluidic channels and direct laser written microneedle arrays. *Microsystems Nanoeng* 5 (2019).
27. Bodhale DW, Nisar A, Afzulpurkar N. Structural and microfluidic analysis of hollow side-open polymeric microneedles for transdermal drug delivery applications. *Microfluid Nanofluidics* 8, 373–92 (2010).
28. Luttge R, Berenschot EJW, de Boer MJ, Altpeter DM, Vrouwe EX, van den Berg A, et al. Integrated lithographic molding for microneedle-based devices. *J Microelectromechanical Syst* 16, 872–84 (2007).
29. Frazer RQ, Byron RT, Osborne PB, West KP. PMMA: An essential material in medicine and dentistry. *J Long Term Eff Med Implants* 15, 629–39 (2005).
30. Evens T, Malek O, Castagne S, Seveno D, Bael A Van. Controlling the geometry of laser ablated microneedle cavities in different mould materials and assessing the replication fidelity within polymer injection moulding. *J Manuf Process* 62, 535–45 (2021).

31. Audouard E, Mottay E. Engineering model for ultrafast laser microprocessing. *Front Ultrafast Opt Biomed Sci Ind Appl XVI* 9740, 974016 (2016).
32. Cheng J, Perrie W, Edwardson SP, Fearon E, Dearden G, Watkins KG. Effects of laser operating parameters on metals micromachining with ultrafast lasers. *Appl Surf Sci* 256, 1514–20 (2009).
33. Tosello G. Micro Injection Molding. München: Carl Hanser Verlag GmbH & Co. KG (2018).
34. Attia UM, Marson S, Alcock JR. Micro-injection moulding of polymer microfluidic devices. *Microfluid Nanofluidics* 7, 1–28 (2009)
35. Baruffi F, Gülçür M, Calaon M, Romano JM, Penchev P, Dimov S, et al. Correlating nano-scale surface replication accuracy and cavity temperature in micro-injection moulding using in-line process control and high-speed thermal imaging. *J Manuf Process* 47, 367–81 (2019).
36. Yao D, Kim B. Injection molding high aspect ratio microfeatures. *J Inject Molding Technol* 6, 11–7 (2002).
37. Masato D, Sorgato M, Lucchetta G. Characterization of the micro injection-compression molding process for the replication of high aspect ratio micro-structured surfaces. *Microsyst Technol* 23, 3661–70 (2017).
38. Gornik C. Injection moulding of parts with microstructured surfaces for medical applications. *Macromol Symp* 217, 365–74 (2004).
39. Rytka C, Kristiansen PM, Neyer A. Iso- and variothermal injection compression moulding of polymer micro- and nanostructures for optical and medical applications. *J Micromechanics Microengineering* 25, 1–16 (2015).
40. Sorgato M, Lucchetta G. The evaluation of vacuum venting and variotherm process for improving the replication by injection molding of high aspect ratio micro features for biomedical application. *AIP Conf Proc* (2015).
41. Vera J, Brulez AC, Contraires E, Larochette M, Trannoy-Orban N, Pignon M, et al. Factors influencing microinjection molding replication quality. *J Micromechanics Microengineering* 28 (2018).
42. Packianather M, Griffiths C, Kadir W. Micro injection moulding process parameter tuning. *Procedia CIRP* 33, 400–5 (2015).
43. Kazmer DO. Injection Mold Design Engineering. München: Carl Hanser Verlag GmbH & Co. KG (2007).
44. Hill SDJ, Kämper KP, Dasbach U, Döpper J, Erhfeld W, Kaupert M. An investigation of computer modelling for micro-injection moulding. *Proc Microsym* 12, 275–83 (1995).
45. Zhang D, Das DB, Rielly CD. Microneedle Assisted Micro-Particle Delivery from Gene Guns: Experiments using skin-mimicking agarose gel. J Pharm Sci 103, 613–27 (2014).
46. Dal Dosso F, Kokalj T, Belotserkovsky J, Spasic D, Lammertyn J. Self-powered infusion microfluidic pump for ex vivo drug delivery. *Biomed Microdevices* 20, 1–11 (2018).

Chapter 8

Conclusions and future perspectives

8.1. Conclusions

Worldwide, millions of blood samples are daily collected for clinical testing in a centralized workflow. However, this requires highly trained personnel, an efficient logistic network and a performant healthcare system. Therefore, it is key to bridge the gap between the end-user and the centralized laboratories by shifting the healthcare system closer towards the point-of-care (POC). This can be achieved by empowering the patients to self-collect a minute sample and send it per regular post. This combines the best of both worlds by offering great accuracy and sensitivity while taking a patient-centric approach.

By bringing sample collection into the hands of inexperienced users, there is a need for reliable, safe and easy-to-use tools to collect high-quality samples. To make them minimally invasive, capillary blood collection is the go-to sample type to replace venous blood as it can be self-sampled by finger-pricking or, even better, microneedles. Furthermore, passive microfluidic technology enables the development of self-powered systems capable of performing multi-step processes without manual handling steps. In this regard, the global aim of this thesis was to exploit and further develop (i)SIMPLE-based microfluidic elements toward next-generation tools for the collection, processing and storage of capillary blood upon a single finger-activation.

The first part of the work (encompassing **Chapter 3 - 4**) focused on the development of a self-powered, low-cost and user-friendly device to split-off precisely metered volumes from a blood drop and load them on pre-cut filter paper. Hereto, in **Chapter 3**, hydrophobic burst valves (HBV) were developed to temporarily retain a fluid flow and configurable to burst at different pressures. By combining HBVs with different burst pressures, a volume metering system was developed to allow parallel metering of multiple pre-defined sample volumes. The system was shown to be accurate and consistent for blood volumes between 5-15 µL and for hematocrit levels spanning the range of 25-70%. This metering system was then implemented

in an SIMPLE-based sampling device for the collection of a 10 µL DBS sample. To validate the SIMPLE-DBS device in the context of therapeutic drug monitoring (TDM) of biologicals, citrated blood samples were spiked with adalimumab (ADM) and the SIMPLE-DBS extracts were compared to those obtained from traditional sub-punching. This experiment showed a lower bias with the different spiked concentrations for SIMPLE-DBS.

In **Chapter 4**, the functionality and field-readiness of the SIMPLE-DBS device was further enhanced. To collect multiple DBS samples in parallel starting from an unknown sample volume, two novel concepts were introduced. The first concept was a self-filling sample inlet system with automatic excess removal properties which was enhanced by a hydrophobic, conical-shaped chip-to-world interface to facilitate the correct application of finger-prick capillary blood. This integrated sample inlet system was validated to robustly release a fixed volume of blood into the downstream microfluidic channel. The second concept was a pump-splitting mechanism, developed to ensure parallel DBS loading. Both concepts were integrated into a SIMPLE-DBS cartridge for the collection of two 10 µL DBS samples, which was demonstrated to work with capillary blood. Finally, the enhanced SIMPLE-DBS devices were validated once more for the TDM of ADM on spiked citrated blood samples. These validation experiments showed improved accuracy, repeatability and Hct-independency of the SIMPLE-DBS compared to the traditionally sub-punched DBS.

The second part of the work (encompassing **Chapter 5 - 7**) aimed at improving the efficacy and invasiveness of capillary blood collection. In this context, in **Chapter 5**, a finger-tourniquet procedure was proposed and validated to improve the obtained capillary blood volume. To measure this, a self-filling volume metering tool with maximal capacity of 200 µL was first developed. First, passive filling of blood into a microfluidic channel was enhanced by a Tween 20 coating, which resulted in an uptake of up to 140 µL of blood in only 2 minutes. Furthermore, the tools were shown to be accurate and repeatable. 18 healthy volunteers were then recruited to self-

sample capillary blood multiple times by both the traditional and finger-tourniquet methods and meter the obtained blood volume using these metering tools. In 81% of the sample collections, the collected capillary blood volume improved by finger-tourniquet application after lancet activation.

As an alternative to finger-pricking, the transition to using hollow microneedle arrays (HMNA) for sampling offers a promising approach to reduce the invasiveness of capillary blood sampling, thereby facilitating the development of integrated microsampling systems. To address the existing scarcity of practical HMNAs for blood sampling, the objective of **Chapter 6** was to fabricate these arrays in stainless steel, primarily with the intention to utilize them as a reusable research tool. In collaboration with Prof. Dominiek Reynaerts, a novel two-step fabrication approach by the combination of percussion laser drilling and micro-milling was adopted to meet the required length to reach the skin's blood capillaries. First, percussion laser drilling settings were optimized to achieve nearly straight microlumens with the required diameter and circularity. Then, 5x5 HMNAs were fabricated by subsequent milling. After the fabrication, water was flown through each individual needle of different HMNAs to assess their sampling capacity, which showed that the average pressure drops were < 10 kPa in 87% of the lumens. Next, the HMNAs were integrated in a self-powered microfluidic sampling device containing a SIMPLE pump which was shown to robustly generate negative pressure gradients up to 40.9 ± 1.8 kPa. At last, this sampling device was validated to consistently sample up to 40 µL of water and blood-mimicking glycerol solution from an open container, as well as 40 µL of water from a skin-mimicking agarose gel.

Although the stainless steel HMNAs served the purpose in the context of developing a proof-of-concept SIMPLE-based sampling patch, the material and fabrication techniques may lack scalability. To meet the requirements for HMNAs that can be mass produced and integrated into disposable microsampling devices, in **Chapter 7**, we delved deeper into their fabrication in polymer through micro-injection molding. This was done in collaboration

with Prof. Albert Van Bael and Prof. Sylvie Castagne. First, microneedle cavities with different lumen positions were successfully prepared by laser ablation. Then, the replication of the HMNAs showed that a high temperature, injection flow rate and melt temperature resulted in the best replication fidelity. Finally, the functionality of 3x3 HMNAs integrated on a chip containing a single microfluidic channel was proven by the successful injection of colored water into a skin-mimicking agarose gel with a constant pressure-time profile.

In conclusion, this dissertation focused on the main aspects required to realize the next generation of microsampling devices. These aspects are minimally invasive sample collection by the integration of microneedles, on the one hand, and further processing of the collected sample for collecting and storing high-quality samples, on the other hand. Hereto, a holistic approach was taken, not only to surpass the technical state of the art of self-powered capillary microfluidics and microfabrication, but also to make the solutions user-friendly and robust to be used by patients and personnel of the analytical laboratories. The reported results clearly show the opportunities to be combined into the direction of fully-integrated POC sampling devices.

8.2. Future perspectives

The next generation of POC microsampling devices are envisioned to become tools that only need a single finger-push to activate the sample collection and processing steps without any form of manual intervention. These tools could be in the form of patches that can be stuck onto the arm, cartridges by the size of a normal credit card or any other size-limited formats. Although, within this vision, some key elements were developed or further improved in this work, achieving it all will require further efforts and challenges to be overcome. In this regard, this final section summarizes some key aspects in further microfluidic development, clinical validation and exploitation of the technology.

8.2.1 Further development of the microfluidics

8.2.1.1 Integration of multiple microfluidic modules

In this dissertation, microfluidic modules were developed for capillary blood collection, metering and DBS loading. In the next step, they will be integrated into a stand-alone microneedle-based DBS collection patch, as schematically depicted in **Figure 8.1**. Although the microneedles stay into contact with skin during the complete process, only a discrete sample volume needs to be collected. Hence, the system needs to be fluidically disconnected after a certain time without the need for a manual intervention, e.g. by removing the microneedle patch. Hereto, a flow splitter will be implemented to stop collecting blood when an adequate volume has been obtained. This flow splitter will also avoid the backflow of on-chip stored reagents needed for the further processing of the sample. This will be an important milestone in developing fully-integrated POC sampling systems, and a starting point to implement additional sample processing modules.

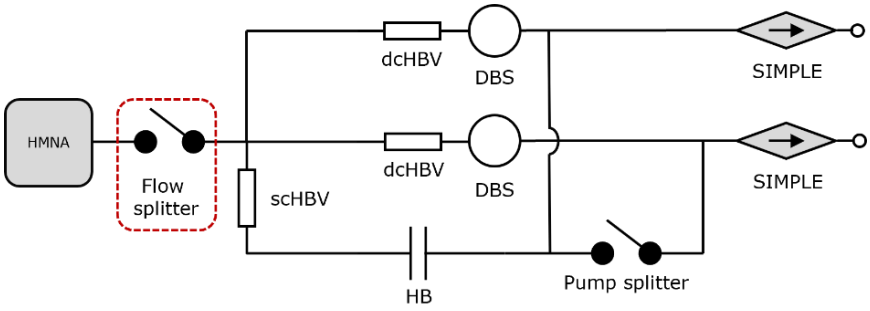

Figure 8.1: *Schematic drawing of the stand-alone microneedle-based DBS sampling device.*

While the primary focus of this dissertation was centered on dried sample storage, it is essential to acknowledge the limitations associated with this approach as well. For example, the sample extraction step to be carried out in the analytical laboratory leads to additional processing requirements and inherent sample dilution. For the applications where analysis of the samples can be conducted within a few days after self-sampling, microfluidic modules for liquid sample storage will be explored as alternative for the DBS. Potentially, both dried and

liquid microsampling could eventually be combined on one platform, e.g., to allow an extra sample to be biobanked for eventual *post forma* verification measurements.

8.2.1.2 Plasma separation

If haematological parameters are not of interest for the analysis, plasma can be separated from the cellular content, mostly red blood cells (RBC), before on-chip liquid or dried storage. The latter is referred to as dried plasma spots (DPS). As most blood-borne molecules are contained in the plasma fraction, plasma separation is a standard procedure for the majority of the blood samples that are being processed in analytical laboratories. It offers various advantages such as an improved sensitivity and specificity, as well as an increased accuracy by avoiding haemolysis to interfere with the bioassay[1]. The gold standard technique for plasma separation is centrifugation, which is unfortunately not compatible with POC applications. Alternative techniques that can be integrated with microfluidics are sedimentation and filtration[2]. In the Biosensors group, the latter has been adopted by integrating commercially available filter material at the inlet of a SIMPLE chip (**Figure 8.2A-B**)[3]. Although effective, as shown by the data in **Figure 8.2C**, the concept of SIMPLE-based plasma separation revealed some important challenges. First, if sample volumes become larger, the filter paper size becomes too small to effectively retain all RBCs. Second, downstream manipulation of the plasma sample, such as metering and DPS loading, requires splitting-off a discrete sample from the inlet. To solve these challenges, future work will focus on the enhancement and integration of the microfluidic plasma separation module.

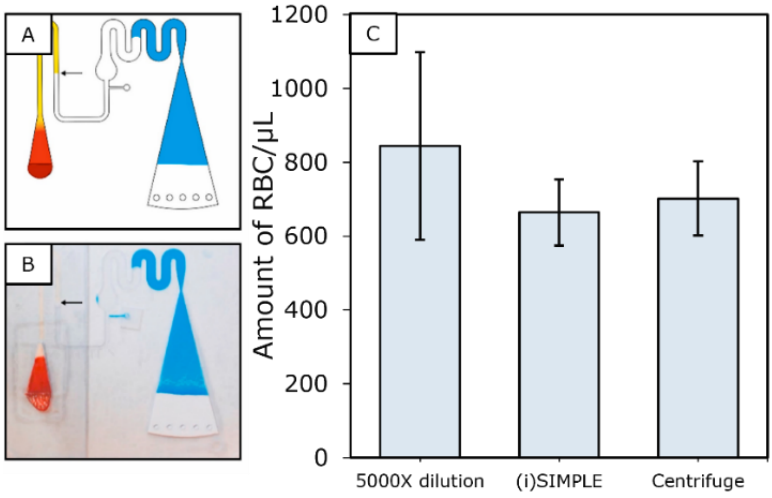

Figure 8.2: *(i)SIMPLE-based plasma separation module. A) Schematic representation of the working principle and B) the top view of the real-life equivalent. C) The comparison by RBC counting of plasma obtained by (i)SIMPLE to the gold standard (centrifugation) and 5000-times dilution.*

8.2.1.3 Sample stabilization

Plasma separation might also have a positive effect on the stability of the blood sample. However, the addition of certain reagents might still be required to optimally preserve the analytes, especially in the case of liquid storage. For example, a low concentration of nitric acid is often needed to enhance plasma sample stability for lithium analysis. Besides, plasma separation is not in all cases a relevant processing step. The sampling of whole blood might still be necessary for analysis, but its microfluidic manipulation might evoke coagulation (i.e. blood clotting) due to increased shear forces or contact with surfaces[4–6]. A full assessment of the risk for on-chip coagulation will only be possible by further validating SIMPLE-based microsampling with unstabilized capillary blood, obtained by finger-pricking or microneedles (see further). Nevertheless, the most plausible solution has already been anticipated for, which is on-chip addition of anticoagulants such as EDTA, heparin or citrate.

For mixing microsamples, substantial dilution ratios and large variabilities have to be avoided as they could lead to

inaccuracies due to the small sample sizes. Therefore, the reconstitution of coated or freeze-dried (lyophilized) anticoagulants is the preferred method that will be further explored. If this is not possible to achieve, alternative solutions for precisely adding liquid reagents to the sample can be developed as well. Moreover, it is of utmost importance to obtain a well-mixed sample in order to be effective. In this context, the advantage of the (i)SIMPLE technology is that it allows for additional complex liquid manipulations to be performed on-chip to carry out such extra sample stabilization and mixing steps.

8.2.1.4 Towards sample-in-result-out systems

(i)SIMPLE technology is not only limited to sample processing and storage, but it is also envisioned to transfer the pre-processed samples to integrated *in vitro* diagnostic assays for applications that require immediate results, like the detection of contagious viruses or sexual transmittable diseases. These assays can be as complex as enzyme-linked immunosorbent assays (ELISA) or isothermal nucleic acid amplification tests (NAATs), requiring complex steps such as timed incubation steps, cell lysis, prolonged heating for isothermal processes, etc. An (i)SIMPLE-based ELISA platform to detect adalimumab in plasma has recently been published by Ordutowski et al.[3]. Besides, we are also working on the integration of lateral flow assays (LFAs) with, among others, microneedle-based sampling, reagent addition, mixing and heating.

8.2.1.5 External liquid storage

The (i)SIMPLE technology relies on the wicking of a working liquid, and eventually, on-chip sample manipulation will also involve multiple reagents and buffers. Currently, the liquids are still manually pre-loaded into the microfluidic channels before use. However, this is not a feasible approach as the shelf-life of the devices would be critically reduced as a result of evaporation of liquids through the plastic layers. To confirm this, a storage experiment at room temperature resulted in a working liquid loss of more than 20 µL, which is detrimental for successful pump activation (**Figure 8.3A**). As a solution, liquids are preferentially

contained externally and pre-filled automatically on the spot. This can be done by blister pouches, which are inexpensive to produce (**Figure 8.3B**). Moreover, they are usually produced from flexible and contractible materials with low evaporation rates (e.g. aluminum). To activate the device, the user has to push on the blister to break the sealing foil and release the working liquid into the channel. Despite the effectiveness, they all have to be activated separately if multiple different liquids are involved. This would deviate from the demanded single-push concept. Therefore, we will further investigate innovative alternatives to blister pouches for the simultaneous release of multiple liquids.

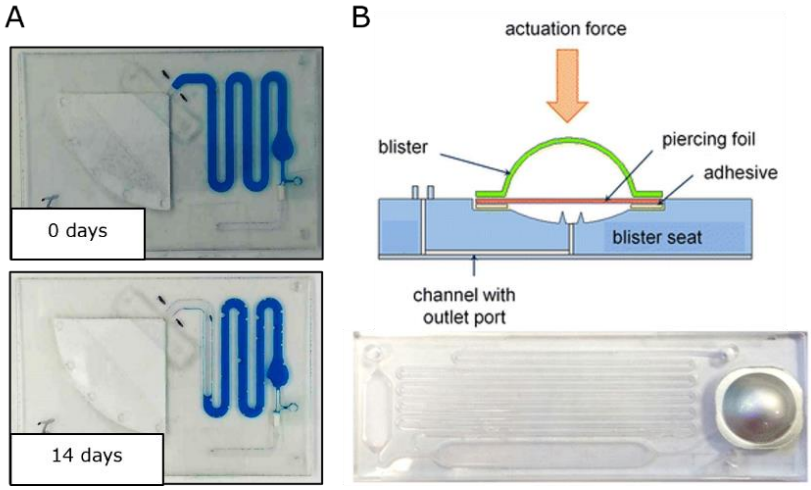

Figure 8.3: *A) Top view photos of the same chip at the beginning and after 14 days of a storage experiment at room temperature. During storage, the inlet and venting holes of the SIMPLE chip were sealed air-tight with sealing tape and contained inside of an aluminum pouch. B) Working principle and example of a blister pouch for external liquid storage [Adopted with permission from Smith et al.[7]].*

8.2.1.6 Alternative body fluids

Blood and its derivatives (plasma or serum) are essential to monitor health parameters, however, other body fluids are equally interesting for self-sampling applications (cf. Section 1.3.1.1 of Chapter 1). Among these, saliva is expected to become the most prominent alternative to blood. The opportunity to sample saliva non-invasively is, for instance, ideal for a large

population screening during contagious infections like Influenza or COVID-19. Besides, saliva is interesting for many other applications like cardiovascular diseases, systemic diseases, oral cancers, etc.[8,9]. Despite its broad applicability and user acceptance, saliva is a challenging sample matrix. The presence of mucins leads to a highly variable viscosity while its volume and composition may change depending on factors like the time of the day, diet or medication. Therefore, in future work, we will evaluate the fluid behaviour of saliva within the currently developed (i)SIMPLE microsampling system.

8.2.2 From laboratory to field validation

Besides technical characterization and *in vitro* validation in laboratory-controlled environments, it is key to challenge the developed systems to actual in-field clinical situations.

8.2.2.1 In-field validation of the SIMPLE-DBS device

In Chapters 3 and 4, the analytical performance of the SIMPLE-DBS device has been validated on *in vitro*, citrated blood samples. This allowed to challenge the device to a broad range of conditions. However, an *in vitro* validation does not allow to study the analytical performance of the device with non-stabilized finger-prick blood samples in real-life conditions. Furthermore, a holistic development approach requires the assessment of patient acceptance as soon as possible in the development process. Therefore, the next step is to perform a field study with real patients. To build further on the TDM application, Crohn's disease patients will be included in a longitudinal study.

8.2.2.2 Evaluation of the tourniquet finger-prick procedure

Chapter 5 reported the results of a first small-scale validation study to investigate the evidence of improving the bleeding intensity by applying a finger-tourniquet before activating the lancet. Although healthy volunteers were recruited for self-sampling multiple times, the sample size and age variation was relatively small. Furthermore, the experimental setup tested only for a single parameter, i.e. the influence of the finger-tourniquet.

Therefore, a large-scale validation study (including >200 subjects) is currently on-going in collaboration with Prof. M.D. Jan Verbakel to investigate additional parameters which are suspected to affect bleeding intensity: age of the patient, lancet length and warming-up hands before lancing. Based on these data, an optimal finger-pricking procedure will be considered to ensure the collection of an adequate amount of capillary blood.

To assess the quality of the obtained blood sample, haemolysis, dilution with ISF and the occurrence of inflammation biomarkers will be further studied by comparing the finger-tourniquet procedure with the traditional 'milking' procedure. Firstly, haemolysis can be assessed by measuring the amount of free haemoglobin inside of the blood sample. A preliminary experiment comparing excessive milking and finger-tourniquet showed evidence of this increase in haemolysis, as shown in **Figure 8.4**.

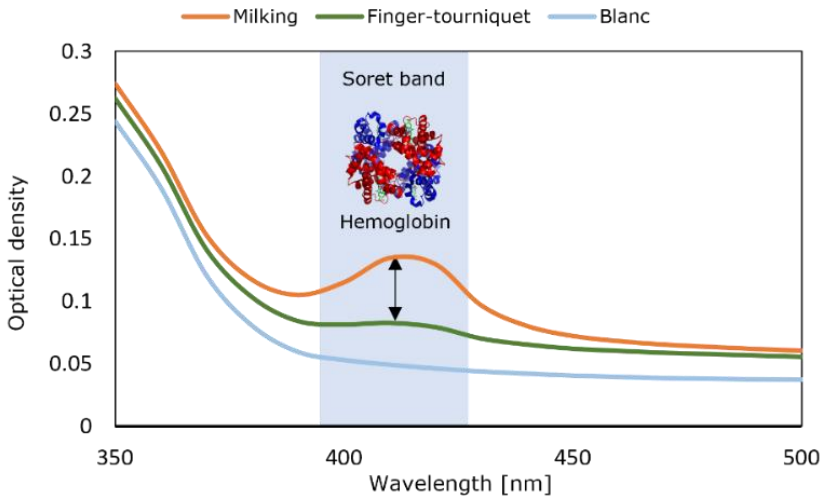

Figure 8.4: *Results of a preliminary spectrophotometric comparison of a capillary blood sample, 100 times diluted in PBS buffer, obtained by excessive milking (orange) and the finger-tourniquet method (green). The blanc measurement (blue) is measured on the PBS buffer.*

8.2.2.3 Microneedle-based capillary blood sampling

Upon the development of next-generation sampling tools, microneedle-based capillary blood collection will be key to substitute the finger-prickers used today. Although, this is still a relatively unexplored concept. In future work, this will be further studied both on *in vitro* and *in vivo* model systems. Firstly, multi-layered PDMS-based artificial skin model will be developed to mimic the skin's viscoelastic properties and the perfusion with a microcapillaries network. This simplified, yet realistic, model will allow to explore the basic principles of the interaction of microneedle arrays with skin tissue. Secondly, *in vivo* models will be adopted for pre-clinical studies. To understand the capillary blood sampling capability of microneedles in terms of obtained volume and sample quality, a study will be carried out on piglets as their skin is the closest equivalent to human skin[10]. Both single HMNs and HMNAs will be tested in different designs with the goal of collecting samples of minimally 50 µL without the occurrence of coagulation or haemolysis. Finally, it is anticipated that microneedle-based sampling is highly similar to pool feeding by mosquitoes, during which they use their fascicle to rupture multiple capillaries and to feed from the resulting pool[11]. This pool creation is also the expected result of using HMNAs where many needles rupture capillaries but only a part of the tips are at the right position to eventually collect the capillary blood from this pool. As a consequence, a certain degree of ISF dilution is expected. To assess this, another *in vivo* study is required, for which naked rats are easier to be used than piglets. This will be done similarly to Section 8.2.2.2 by inducing easy-to-measure analytes with a known correlation to capillary blood in the rats (e.g. through feeding).

8.2.3 Regulatory aspects toward the industry

Before clinical studies can be performed, it is important to understand the legal framework of the devices that are being developed. It is, first of all, a key element in applying for ethical approval to perform the experiments with real patients (samples). Furthermore, when thinking of commercializing the technology, it is essential that the right pre-market data is

collected to avoid future delays in product development and collection of the required documentation. This also includes the outlining of the relevant clinical studies.

Firstly, POC microsampling devices are defined as *in vitro* diagnostics (IVD) medical devices. These are governed under regulation (EU) 2017/746 of the European Parliament, more commonly known as the IVDR, which applies since 26 May 2022 to warrant the safety, performance and quality of the IVD products on the European market[12]. Since the SIMPLE-DBS device of Chapters 3 and 4 makes use of an external finger-pricker to collect a capillary blood sample, it is seen as a 'specimen receptacle'. In this regard, it is worth to mention that if additional manual handling steps are required (e.g. plasma separation, buffer addition, etc.), devices are intended for self-testing, which applies under a higher class of the IVDR. Hence, researching ways to reduce the risk for manual handling errors by inexperienced users also reflects in the classification of the device in a positive way. Secondly, if microneedles are integrated into the microsampling device, it also includes an invasive component which is governed under another regulation, i.e. regulation (EU) 2017/745 of the European Parliament, or Medical Device Regulation (MDR)[13]. While the IVD part of the microneedle-based device still needs to comply with the IVDR, the microneedle component is classified as 'surgically invasive device for transient use' according to the MDR. Even though microneedles are a minimally-invasive means to pierce the skin. In other words, the integration of microneedles within the POC sampling device slightly complicates the regulatory framework. Although the IVDR and MDR are similar at high level, not all medical devices are IVD devices and, therefore, need another framework.

The safety and performance requirements, which are described in the IVDR and MDR, are needed to eventually apply for CE marking. This is an obligatory step toward commercialization of a medical device. To guide organizations and companies in meeting these requirements, the independent international organization for standardization (ISO) defined some

industry standards applicable to POC sampling devices. These standards are also recognized by the regulatory bodies like EMA (Europe) and FDA (USA) and have the purpose to guide the development, production and testing of the devices. The most important standard in this case is ISO 13485:2016 on the implementation and maintenance of a quality management system.

8.3. References

1. Ji, J. Z. & Meng, Q. H. Evaluation of the interference of hemoglobin, bilirubin, and lipids on Roche Cobas 6000 assays. *Clinica Chimica Acta* 412, 1550–1553 (2011).
2. Wang, Y., Nunna, B. B., Talukder, N., Etienne, E. E. & Lee, E. S. Blood plasma self-separation technologies during the self-driven flow in microfluidic platforms. *Bioengineering* 8, (2021).
3. Ordutowski, H. *et al.* Next generation point-of-care test for therapeutic drug monitoring of adalimumab in patients diagnosed with autoimmune diseases. *Biosens Bioelectron* 208, 114189 (2022).
4. Hathcock, J. J. Flow effects on coagulation and thrombosis. *Arterioscler Thromb Vasc Biol* 26, 1729–1737 (2006).
5. Zhang, C. & Neelamegham, S. Application of microfluidic devices in studies of thrombosis and hemostasis. *Platelets* 28, 434–440 (2017).
6. Vogler, E. A. & Siedlecki, C. A. Contact activation of blood-plasma coagulation. *Biomaterials* 30, 1857–1869 (2009).
7. Smith, S., Sewart, R., Becker, H., Roux, P. & Land, K. Blister pouches for effective reagent storage on microfluidic chips for blood cell counting. *Microfluid Nanofluidics* 20, (2016).
8. Anizan, S. & Huestis, M. A. The potential role of oral fluid in antidoping testing. *Clin Chem* 60, 307–322 (2014).
9. Tripoliti, E. E. *et al.* Point-of-care testing devices for heart failure analyzing blood and saliva samples. *IEEE Rev Biomed Eng* 13, 17–31 (2020).
10. Jacobi, U. *et al.* Porcine ear skin: An in vitro model for human skin. *Skin Research and Technology* 13, 19–24 (2007).
11. Choumet, V. *et al.* Visualizing non Infectious and infectious anopheles gambiae blood feedings in naive and saliva-immunized mice. *PLoS One* 7, (2012).
12. European Commission. Regulation (EU) 2017/746 of the European parliament and of the council on in vitro diagnostic medical devices and repealing Directive 98/79/EC and Commission Decision 2010/227/EU. *Official Journal of the European Union* Preprint at (2017).
13. European Commission. Regulation (EU) 2017/745 of the European parliament and of the council of 5 April 2017 on medical devices, amending Directive 2001/83/EC, Regulation (EC) No 178/2002 and Regulation (EC) No 1223/2009 and repealing Council Directives 90/385/EEC and 93/42/EE. *Official Journal of the European Union* (2017).

Publication list

Articles in international reviewed journals

Van Hileghem, L., Kushwaha, S., Piovesan, A., Verboven, P., Nicolai, B., Reynaerts, D., . . . Lammertyn, J. (2023). Innovative Fabrication of Hollow Microneedle Arrays Enabling Blood Sampling with a Self-Powered Microfluidic Patch. Micromachines, 14(3), 15 pages. doi:10.3390/mi14030615

Joseph, M., **Van Hileghem, L.**, Postelmans, A., Lammertyn, J., Saeys, W. with Saeys, W. (corresp. author) (2023). Fabrication and characterization of porous tissue-mimicking optical phantoms as a tool for optical sensor validation. Journal Of Biophotonics, Art.No. e202200338. doi: 10.1002/jbio.202200338

Vloemans, D., **Van Hileghem, L.**, Verbist, W., Thomas, D., Dal Dosso, F., Lammertyn, J. with Vloemans, D. (joint first author), Van Hileghem, L. (joint first author), Lammertyn, J. (corresp. author) (2021). Precise sample metering method by coordinated burst action of hydrophobic burst valves applied to dried blood spot collection. Lab On A Chip, 1-10. doi: 10.1039/d1lc00422k

Evens, T., **Van Hileghem, L.**, Dal Dosso, F., Lammertyn, J., Malek, O., Castagne, S., Seveno, D., Van Bael, A. with Evens, T. (corresp. author) (2021). Producing Hollow Polymer Microneedles Using Laser Ablated Molds in an Injection Molding Process. Journal of Micro and Nano-Manufacturing, 9 (3), Art.No. 030902, 1-9. doi: 10.1115/1.4051456

Papers at international scientific conferences

Vloemans, D., **Van Hileghem, L.**, Dal Dosso, F., Lammertyn, J. (2022). Novel self-powered microfluidic platform for advanced remote microsampling applications. Presented at the 15th European Bioanalysis Forum Open Symposium, Barcelona, Spain, 16 Nov 2022-18 Nov 2022.

Vloemans, D., **Van Hileghem, L.**, Dal Dosso, F., Lammertyn, J. (2022). Direct sample extraction and advanced pre-processing on a self-powered microfluidic chip for lateral flow immunoassay automation. Presented at the The 26th International Conference on Miniaturized Systems for Chemistry and Life Sciences (μTAS 2022), Hangzhou, China, 23 Oct 2022-27 Oct 2022.

Van Hileghem, L., Vloemans, D., Verbist, W., Thomas, D., Dal Dosso, F., Lammertyn, J. (2021). From drop to spots: autonomous dried blood spot sampling device enabling decentralized monitoring of biologicals. Presented at the The 25th International Conference on Miniaturized Systems for Chemistry and Life Sciences (μTAS 2021), Palm Springs, California, USA.

Van Hileghem, L., Vloemans, D., Dal Dosso, F., Lammertyn, J. (2020). Precisely metered dried blood spots by using tunable hydrophobic burst valves. Presented at the The 24th International Conference on Miniaturized Systems for Chemistry and Life Sciences (MicroTAS 2020), Online, 05 Oct 2020-09 Oct 2020. Open Access

Van Hileghem, L., Bellotti, M., Kushwaha, S., Dal Dosso, F., Reynaerts, D., Lammertyn, J. (2020). Sampling made SIMPLE: a self-powered microfluidic platform with integrated microneedles for sampling blood from skin capillaries. Presented at the DIATECH 2020, Leuven (Belgium).

Vloemans, D., **Van Hileghem, L.**, Dal Dosso, F., Lammertyn, J. (2020). Enabling precise sample metering on passive microfluidic chip by simple fabrication of hydrophobic burst valves. Presented at the DIATECH 2020, University Hall, Naamsestraat 22, B-3000 Leuven.

Talks at international conferences

Van Hileghem, L., Kushwaha, S., Dal Dosso, F., Piovesan, A., Nicolaï, B., Reynaerts, D., Lammertyn, J. A self-powered sampling patch enabled by innovative hollow microneedle arrays and a microfluidic pump. MNE Eurosensors 2022 conference, Leuven, Belgium.

Van Hileghem, L., Vloemans, D., Verbist, W., Pollet, F., Thomas, D., Kushwaha, S., Reynaerts, D., Dal Dosso, F., Lammertyn, J. Self-powered microfluidic cartridge with integrated hollow microneedles for minimally invasive dried blood spot sampling. NanoBioTech-Montreux 2022, Montreux (Switzerland)

Patents

Lammertyn Jeroen, Vloemans Dries, **Van Hileghem Lorenz**, Dal Dosso Francesco and KU Leuven, Activation and Pressure Balancing Mechanism, WO 2022/058470 A1, Patent pending